2017-11-01

Pull-Out Strength of Fiberglass/Epoxy Composite RebarFabricated on a Three-Dimensional Braiding Machine

Tarisai Machanzi
Brigham Young University

Pull-Out Strength of Fiberglass/Epoxy Composite Rebar Fabricated on a Three-Dimensional Braiding Machine

Tarisai Machanzi

A thesis submitted to the faculty of
Brigham Young University
in partial fulfillment of the requirements for the degree of

Master of Science

David W. Jensen, Chair
Andrew George
Fernando Fonseca

Department of Civil and Environmental Engineering

Brigham Young University

ABSTRACT

Pull-Out Strength of Fiberglass/Epoxy Composite Rebar
Fabricated on a Three-Dimensional Braiding Machine

Tarisai Machanzi
Department of Civil and Environmental Engineering, BYU
Master of Science

The objective of this research was to explore and demonstrate the production and performance of fiber-reinforced polymer (FRP) rebar manufactured on a continuous three-dimensional braiding machine for use as reinforcement in concrete structures. Different configurations of fiberglass/epoxy composite cylindrical rebar rods were manufactured, embedded in concrete, and tested in axial tension to identify the relationships between manufacturing parameters and tensile pull-out strength of the rebar. The strength of the bond between concrete and FRP rebar was investigated using the pull-out test detailed by ACI 440.3R-12. The rebar was a No. 4 size and produced by combining multiple tows of fiberglass/epoxy prepreg to form the core of cylindrical rods which were consolidated using spirally-wound aramid consolidation fibers. The manufactured rebar was cured at 121°C (250°F) as specified by the material manufacturer, TCR Composites. Preliminary research performed on carbon/epoxy rebar guided the process of developing a test matrix based on multiple variables. Primary variables investigated included the nature of the consolidation fiber material (dry vs prepreg), and the use of sand coating as a secondary process. The rebar samples were cast in 200 mm x 200 mm x 200 mm (8.0 in x 8.0 in x 8.0 in) concrete cubes to investigate bond strength. A test fixture was designed and fabricated for use on a universal tensile testing machine. Standard 12.7 mm (0.5 in) diameter steel rebar and a commercially comparable fiberglass rebar were also tested to provide baseline values. Measurements were collected at both the free and loaded ends of the rebar with free-end results being a more accurate presentation of rebar bond stress.

Results showed that the bond strength was 6-13% higher for the free-end for rebar consolidated with a dry tow compared to prepreg tow consolidated rebar. When sand was added, dry tow consolidated sand-coated samples showed higher bond stress in the range of 15-26% for the free-end than samples consolidated with a dry tow but excluded sand coating. Samples consolidated with prepreg tow and coated with sand showed higher bond stress in the range of 43-58% for the free-end compared to prepreg tow no-sand coating samples. Overall, for the rebar manufactured on the 3-D braiding machine, the prepreg tow consolidated rebar samples recorded the highest bond strength values with a maximum average bond stress value of 15.2 MPa (2.26 ksi). The dry tow sand consolidated rebar recorded a maximum average bond stress value of 11.4 MPa (1.65 ksi). The rebar purchased from American Fiberglass Rebar recorded a maximum average bond stress of 12.0 MPa (1.74 ksi) while the maximum average bond stress of steel rebar was 13.1 MPa (1.90 ksi). Results demonstrated that quality composite rebar can be manufactured using the 3-D braiding machine and that consolidating the rebar with a prepreg tow and coating the surface with sand resulted in a rebar which bonded well with concrete compared to commercialized FRP and steel rebar.

Keywords: Fiberglass/epoxy, carbon/epoxy, prepreg tow, FRP, rebar, composite, sand

ACKNOWLEDGEMENTS

I would like to thank Sandy and Scott Clark who I dedicate this thesis to. They gave me the opportunity of a lifetime to attain higher education when I thought it was impossible. I will forever be indebted to them.

I would also like to thank all of the people who have supported me through this research process. The members of my committee for the time they spent reviewing and helping me to submit a high quality thesis. I'm sincerely grateful to Dr. David Jensen, my advisor, who took me in and guided me throughout this whole process; thank-you for teaching me to be a professional, for helping me not settle for less and above all for your patience with me. Your passion for the subject of composites guided me through my time at BYU. I gratefully acknowledge the technical support that I received from Dave Anderson, Rodney Mayo, and their lab assistants. I would like to thank Steve Erwing of Geneva Rock for the kind donation of concrete aggregates that I used in this research. I'm grateful to my fellow undergraduate colleagues who worked as research assistants: Robert Thompson, Braiden Green, Trenton Sparks and Jordan Wilson. I'm gratefully indebted to Mikale Williamson who helped me with professionally editing this thesis and assisting me in delivering quality work.

TABLE OF CONTENTS

LIST OF TABLES

LIST OF FIGURES

1 INTRODUCTION

The purpose of this study was to develop and demonstrate the functionality of a form of fiberglass/epoxy reinforcing bar (rebar) manufactured on a three-dimensional braiding machine for use in concrete structures. The functionality of this composite polymer rebar was validated by embedding the rebar in concrete and quantifying bond stress through pull-out testing.

Rebar manufactured from a composite polymer is commonly referred to as Fiber Reinforced Polymer (FRP) rebar. FRP rebar is made from advanced composite materials using fibers such as carbon, fiberglass, aramid, or basalt fibers, combined with resins such as epoxy, vinylester or polyester. Fiberglass preimpreginated with epoxy (prepreg tow) was used to produce the rebar described in this research. Fiberglass was preferred due to lower costs. Figure 1-1 shows a picture of the manufactured fiberglass/epoxy composite rebar.

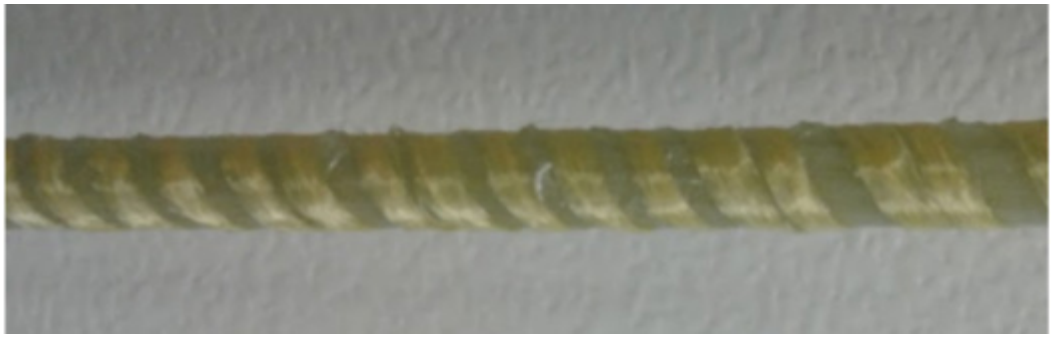

Figure 1-1: Manufactured Fiberglass\Epoxy Composite Rebar (Isorebar)

To assess the feasibility of manufacturing quality rebar on the three-dimensional braiding machine, preliminary exploratory research was performed using surplus carbon/epoxy from a previous study. Results from the preliminary study were used to develop the design and manufacturing process to produce FRP rebar, and to develop an appropriate test matrix to explore the influence of critical variables. Details on the preliminary research are explained in Chapter 2.

FRP rebar manufacturing was performed on a three-dimensional braiding machine primarily used for the manufacturing of IsoTruss®, IsoBeam™ and other isogrid structures. Consequentially, the manufactured rebar was nicknamed "isorebar". The prepreg that made up the core of the FRP rebar was consolidated using aramid fiber, in either a dry tow or prepreg tow form. The consolidation fibers also served the purpose of creating "ribs" or grooves to help the composite rebar bond to the concrete.

In some cases, sand coating was applied to the rebar samples to further improve surface roughness for bonding. The pull-out strength of the rebar embedded in concrete was investigated using ACI 440.3R-12 B.3.

1.1 Brief Description of the IsoTruss®

The IsoTruss® is a composite, lightweight structure that can be used as an alternative to steel, aluminum, wood, concrete and other structural materials. IsoTruss® structures provide structural integrity while minimizing weight. They are composed of longitudinal and helical members. Longitudinal members primarily carry axial loads while helical members carry torsional and shear loads. Figure 1-2 shows examples of the IsoTruss™ geometry. For a

detailed description of the IsoTruss™ and other isogrid structures, see Asay [1], Kesler [2]. Winkel [3], Scoresby [4], and McCune [5]

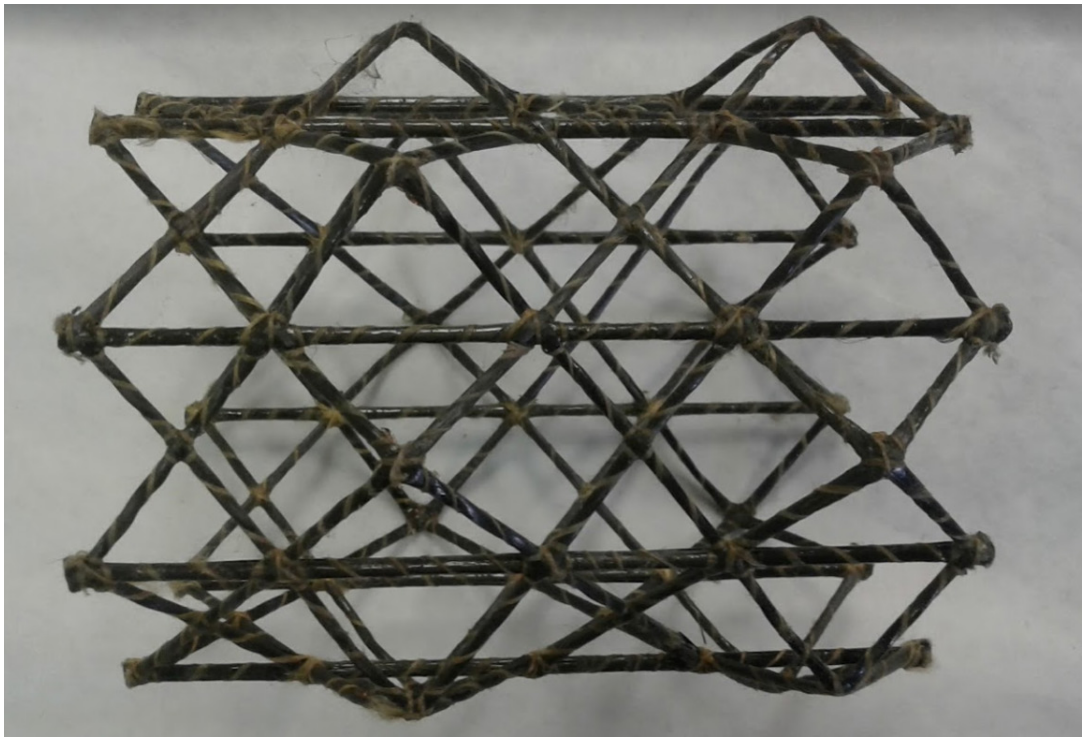

Figure 1-2: Photo of 6-Node IsoTruss® Structure

1.2 Research Background

Concrete, commonly used in construction, possesses very high compressive strength, but limited tensile strength. To enhance its tensile capabilities and increase its ductility, concrete is often reinforced with steel reinforcement bars. Steel rebar performs fairly efficiently and has the added advantage of being relatively affordable. There are, however, some disadvantages to using steel

When subjected to moisture, steel corrodes, making it less than ideal for use in structures exposed to water such as footings, foundations, piles, and bridge decks. Steel corrosion can also

occur when commonly used admixtures, such as chlorides and other salts, are added to the concrete mix design. The degradation of corroding steel rebar compromises its strength and can cause the concrete to crack, resulting in the reinforced structure losing its structural integrity. To counter the effects of corrosion, steel rebar is sometimes coated with non-corrosive materials such as epoxy. These measures are largely temporary, generally becoming ineffective over time.

By comparison, FRP rebar possesses corrosion-resistant advantages over steel rebar and is less susceptible to the effects of weathering and additives in concrete. Additionally, FRP rebar is comparatively weight efficient, providing the strength of steel at approximately one-quarter of the weight. Rebar manufactured from composite materials also eliminates the need for advanced fabrication processes such as welding or the use of cutting torches. It can also be manufactured with resins that are fire retardant, enhancing concrete protection against fire hazards.

1.3 Related Research

The use of fiber reinforced polymers as concrete reinforcement has been studied at Brigham Young University by Blake [6], Layne [7], and McCune [5] among others with a focus mainly directed toward advanced composite structures such as the IsoTruss®.

Blake tested IsoTruss® reinforced concrete specimens and concluded that under axial compression, steel reinforced specimens were stronger due to spalling of the concrete outside the IsoTruss®. When measured in bending, however, IsoTruss® reinforced concrete was superior to steel reinforced concrete. Blake [6] used a basic IsoTruss® geometry which was equivalent to a No.3 rebar and a double IsoTruss® configuration, which was equivalent to two No.3 steel bars.

Layne further expanded Blake's research by hypothesizing that upgraded manufacturing methods and better fiber consolidation of the double IsoTruss® configuration with longitudinal

members placed at the peaks of the IsoTruss® pyramids rather than the valleys would yield improved results. The results of the study showed trends similar to those previously published, but with increased strength values.

Cutting edge research has been and is still being conducted on the general performance of FRP rebar. Benmokrane [8], who investigated the durability of fiberglass rebar, stated that factors such as type of glass fibers used, resin content, and curing greatly affect the life of FRP rebar. Additionally, Achillided and Pilakoutas [9] discovered that there was no significant difference between the bond strengths developed by fiberglass FRP (GFRP) and carbon FRP (CFRP) bars. In other work, Cosenza [10] studied the development length of glass FRP and found a bond strength of 14.5 MPa (2.10 ksi) at a slip of 0.25 mm (0.01 in) using an embedment length of 10 times the diameter of the rebar. As far as surface roughness, Consenza, Manfield and Realfonzo [11] concluded that plain FRP rebar that lacks any surface roughness provides inadequate bonding strength.

Similarly, Dong [12] and his colleagues studied the bond durability of basalt fiber-reinforced polymer (BFRP) bars embedded in concrete under seawater conditions and the long-term bond strength prediction. Their intent was to determine measures to improve the durability performance of concrete structures in extreme corrosive environments using BFRP reinforcement bars. They concluded that the bond durability in salt water of composite bars with epoxy resin is generally better than that of bars with vinyl ester resin.

Akishin et al. [13] studied FRP rebar by modeling slippage using 3D finite element analysis. They modeled rebar with two and four longitudinal ribs, as well as without. The effect of different rib geometries on the maximal pull-out load was also investigated. Their studies concluded that the number of the longitudinal ribs significantly influences the pull-out load of

composite rebar in concrete. In the case of rebar with two longitudinal ribs, the pull-out load was 7% less than that for rebar with four ribs. They also demonstrated that increasing the height of the ribs increased the pull-out load for rebar with four ribs by about 4%. This was most likely due to the increased surface for bonding.

Abdeldjelil and Huanzi [14] investigated the bond-slip performance of commercially available FRP rods embedded in concrete reinforced with discrete randomly distributed polypropylene fibers under monotonic direct pull-out loading. They tested 27 pull-out samples, investigating characteristics such as short fibers, bar surface, and embedment length. Results showed that the addition of polypropylene fibers did not increase the ultimate bond strength, but provided enhanced ductile bond behavior. The authors also observed that bond strength increased with increasing rebar embedment length. Additionally, their studies showed that bond value corresponding to 0.050 mm (0.002 in) of free-end slip was recommended as the design bond strength.

In other work, Jong-Pil [15] and his colleagues studied the effect of synthetic and steel fibers in concrete on the bond properties of high-strength concrete and fiber-reinforced polymer (FRP) reinforcing bars. They performed direct bond tests to evaluate the bond performance of 9.0 mm (0.35 in) diameter CFRP and 13 mm (0.51 in) diameter GFRP reinforcing bars in three types of high-strength concrete with varying amounts of steel or synthetic fibers. Their research discovered that bond strength increased with the compressive strength of the high-strength concrete. The type and amount of fiber also affected the bond strength. The specimens with 40 kg/m^3 (2.5 lb/ft^3) steel fiber had the highest bond strength. The larger FRP bars tended to have stronger bonds, regardless of the strength of the concrete and type or amount of fiber, most likely due to the increased surface area.

Larralde and Silva-Rodriguez [16] compared FRP rebar to steel rebar under direct pull-out in concrete. From their experimental results, they concluded that the anchorage design for steel rebar was not directly applicable for FRP rebar. For the same test conditions, the average nominal bond stress at failure was greater for the steel rebar than for the FRP rebar. The slip of the rebar was greater for the FRP rebar than for the steel rebar.

Like steel rebar, sometimes FRP rebar is used to reinforce concrete structures subject to high temperatures. High temperatures, such as those due to fires or even those occurring in extremely hot climates may negatively affect the properties of FRP rebar. Katz, et al. [17] studied the effect of high temperature on the bond strength of FRP rebar. They investigated the bond properties of these reinforcing bars at temperatures ranging from room temperature 20°C (68°F) to high temperatures of up to 250°C (482°F). The rebar they studied were commercially produced and had different surface ‘‘treatments.’’ Test results showed a reduction of between 80 and 90% in the bond strength as the temperature increased from 20ºC to 250ºC. In comparison, ordinary deformed steel rebar showed a reduction of only 38% in the same temperature range. In addition, a reduction in the bond stiffness, which was determined from the slope of the ascending branch of the pullout load versus slip curve, was seen as the temperature increased. The post-peak bond strength decrease at elevated temperatures was gradual as compared with the instantaneous drop at room temperature. Greater sensitivity to high temperatures was seen in FRP rebar, in which the bond relies mainly on the polymer treatment at the surface of the rod.

One of the advantages of using steel rebar is its cost effectiveness. Steel is relatively inexpensive. Berg [18] and his colleagues performed a construction process and cost analysis on the use of FRP materials as reinforcements and formwork for a concrete highway bridge deck. They concluded that FRP rebar has higher initial costs, but these costs offset the potential long-

term durability and maintenance benefits of FRP rebar. The cost of using FRP rebar can further be reduced by optimization of FRP stay-in-place formwork such as IsoTruss® configurations.

1.4 Scope of Investigation

This research was directed at investigating the bond strength and performance of concrete rebar manufactured from fiberglass/epoxy. An exploratory preliminary research project was also performed with rebar manufactured from carbon/epoxy. The preliminary research was used primarily to determine research trends and variables that could affect FRP rebar strength for further detailed research. The FRP rebar was manufactured on a three-dimensional braiding machine. Bond strength was investigated using a pull-out test as detailed in ACI 440.3R-12 B.3. Two configurations of fiberglass rebar were devised by varying the type of consolidation used. These configurations involved the use of dry and resin impregnated aramid fiber for consolidating the fiberglass tows. As a secondary process, some samples of the FRP rebar were coated with sand to increase rebar surface roughness, creating a stronger bond between the concrete and the rebar. This research also focused on comparing fiberglass/epoxy rebar to steel rebar, and fiberglass rebar available commercially.

This research answers the following questions about fiberglass/epoxy rebar manufactured on the three-dimensional braiding machine:

- How is FRP rebar pull-out strength affected by the use of either dry or prepreg material for consolidation of the core composite tows?
- How effectively does the addition of a second process, such as sand coating, increase the bond strength of the currently manufactured FRP rebar?

- How does the pull-out strength of FRP rebar manufactured on the three dimensional braiding machine compare to FRP rebar already commercially available?
- How does the pull-out strength of FRP rebar manufactured on the three dimensional braiding machine compare to steel rebar with and without epoxy coating?

To answer these questions, unidirectional fiberglass/epoxy composite rods with different consolidation mechanisms and surface coating were fabricated, embedded in concrete, and tested for bond strength using a standard embedded rebar pull-out test. The unidirectional core samples were manufactured with an average diameter of 12 mm (0.49 in) and average length of 53 cm (21 in). The FRP rebar was embedded in concrete with 6.4 cm (2.5 in) in direct contact with the concrete representing approximately five times the diameter of the rebar. One group of rebar samples was consolidated with dry aramid fiber, while a second group of samples was consolidated using prepreg aramid fiber. These configurations were repeated with sand coating. Sand-coated samples had an increased diameter of 14 mm (0.56 in). Three additional sets of samples were acquired for comparison: 1) epoxy coated steel rebar with a diameter of 13 mm (0.50 in); 2) plain steel rebar with a diameter of 13 mm (0.50 in); and, 3) fiberglass rebar manufactured by American Fiberglass Rebar of Las Vegas, Nevada with a diameter of 15 mm (0.57 in).

1.5 Thesis Overview

This thesis contains eight chapters. Chapter 2 summarizes the preliminary research that was performed using carbon/epoxy as a prelude to explore design process and testing details. Chapter 3 details the fiberglass/epoxy composite rebar experimental approach and data reduction procedures. Test results are described in Chapter 4. Chapter 5 compares results across different

experimental variables. Chapter 6 discusses results and draws conclusions. Chapter 7 gives insights into the commercialization potential of manufacturing rebar using the three-dimensional braiding machine. Chapter 8 summarizes the conclusions and provides recommendations for further research.

2 PRELIMINARY RESEARCH ON CARBON/EPOXY REBAR

Fiberglass/epoxy rebar was the main focus of this research, however, a preliminary exploratory investigation of FRP rebar manufacturing using the three-dimensional braiding machine and testing of bond strength was performed using carbon/epoxy rebar. Carbon/epoxy was used for this preliminary research because it was readily available. The objective of the preliminary research was to assess the feasibility of manufacturing rebar on the three-dimensional braiding machine, and to explore variables that would affect FRP rebar bond strength. Results of this preliminary research were used to develop a research test matrix for the studying of bond strength using fiberglass/epoxy. The manufacturing process of fiberglass/epoxy rebar and carbon/epoxy rebar were generally identical, and a full description of the manufacturing process will be given in Chapter 3. The minor differences in the manufacturing and testing of the carbon/epoxy rebar are outlined in this chapter. Variables in the preliminary research were not strictly controlled and, therefore, results were not considered conclusive but were crucial in guiding the research of FRP rebar using fiberglass/epoxy.

2.1 Scope of FRP Rebar Preliminary Investigation

As many variables affect FRP rebar bond stress, this preliminary research explored and focused primarily on composite rebar manufacturing. The carbon/epoxy rebar was compared to

steel rebar and commercially purchased FRP rebar for measurement of composite rebar bond stress performance. The commercial FRP was purchased from American Fiberglass Rebar.

Specifically, this exploratory research was performed to answer the following questions about FRP rebar:

- Can FRP rebar manufactured using the three-dimensional machine have sufficient pull-out strength?
- How does FRP rebar manufactured using the three-dimensional pull-out strength compare to that of steel rebar and commercial FRP rebar?
- What variables affect the pull-out strength of FRP rebar manufactured on the three-dimensional braiding machine, and what should be included in a test matrix for the investigation of rebar bond strength using fiberglass/epoxy rebar?

To answer these questions, unidirectional carbon/epoxy composite rods with different consolidation mechanisms and surface coating were fabricated, embedded in concrete, and tested for bond strength using a pull-out test. Primary variables investigated included 1) the consolidation fiber material (aramid, fiberglass and basalt), 2) prepreg vs. dry consolidation tows, and 3) the number of tows used to consolidate the rebar (i.e., the size of tows used to consolidate the rebar).

Aramid fiber, both dry and resin impregnated, were used to consolidate the core fiberglass tows. Selected samples of the FRP rebar were coated with sand in an attempt to increase rebar surface roughness, creating a stronger bond between the concrete and the rebar.

2.2 Carbon/Epoxy Rebar Geometry and Manufacturing

The carbon/epoxy rebar was produced by combining multiple tows of carbon/epoxy prepreg to form the core of cylindrical rods. The tows were bound together and consolidated using various spirally-wound consolidation fibers. After consolidation, the rods were cured at 121°C (250°F). Details of the curing process are outlined in Chapter 3.

The consolidation tows also served the purpose of providing the rebar with ribs similar to those on steel rebar to improve FRP rebar bonding with concrete. Some consolidation tows were hand-braided together using three smaller tows to create thicker consolidating tows that gave the rebar larger ribs. Selected rebar samples were subsequently coated with sand to increase rebar surface roughness for improved bonding with concrete.

The carbon/epoxy rebar was manufactured with a diameter of 10.4 mm (0.41 in). This diameter was a result of using 119 tows of carbon-/epoxy prepreg tow. Each rebar specimen was 61cm (24 in) long. A 38 mm (1.5 in) doubler was incorporated to prevent crushing of the rebar core and induction of localized failure by the jaws of the pull-out testing when the rebar was gripped and pulled in tension during testing. Figure 2-1 shows a sample of the rebar.

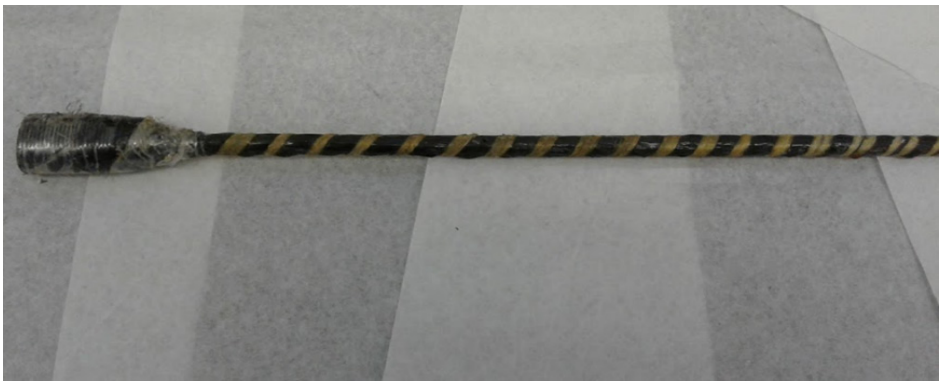

Figure 2-1: Carbon/Epoxy Rebar with Doubler on End for Gripping in Testing Machine

The unidirectional core was consolidated using either unidirectional dry or prepreg aramid tows. Table 2-1 shows the list of the materials making up the core, the manufacturer, and the type. Table 2-2 shows the nominal mechanical properties for the core material.

Table 2-1: Carbon/Epoxy Rebar Core Materials Specification

Material	Manufacturer	Material Specification	Filmament Diameter [in (μm)]	Filament Count per Tow
Carbon Fiber	Toray	T700SC-24K-50C	2.8E -04 (7.0)	24,000
Epoxy (Pre-Preg)	TCR Composites	UF3369-100	-	-

Table 2-2: Carbon/Epoxy Rebar Nominal Mechanical Properties

Material	Modulus of Elasticity [Msi (GPa)]	Tensile Strength [ksi (MPa)]	Compressive Strength [ksi (MPa)]
T700/UF3369 Carbon/Epoxy	20.0 (138)	370 (2551)	111 (765)

The sleeve created during the consolidation process was a half braid spiral wrap. Two bobbin carriers were used to create the sleeve. The rebar core was consolidated using aramid fiber. Aramid fiber was selected due to its high strength and resistance to fraying. Mechanical properties of Aramid fiber used for consolidation are discussed in Chapter 3. Fiberglass, which had the advantage of being inexpensive compared to aramid, was also explored as an option but resulted in significant fraying on the bobbin carrier. Basalt fiber was another option but, like fiberglass, it resulted in significant fraying. The biggest problem with fraying materials was that during the manufacturing process, the thread would break repeatedly. Figure 2-2 shows fraying fiberglass.

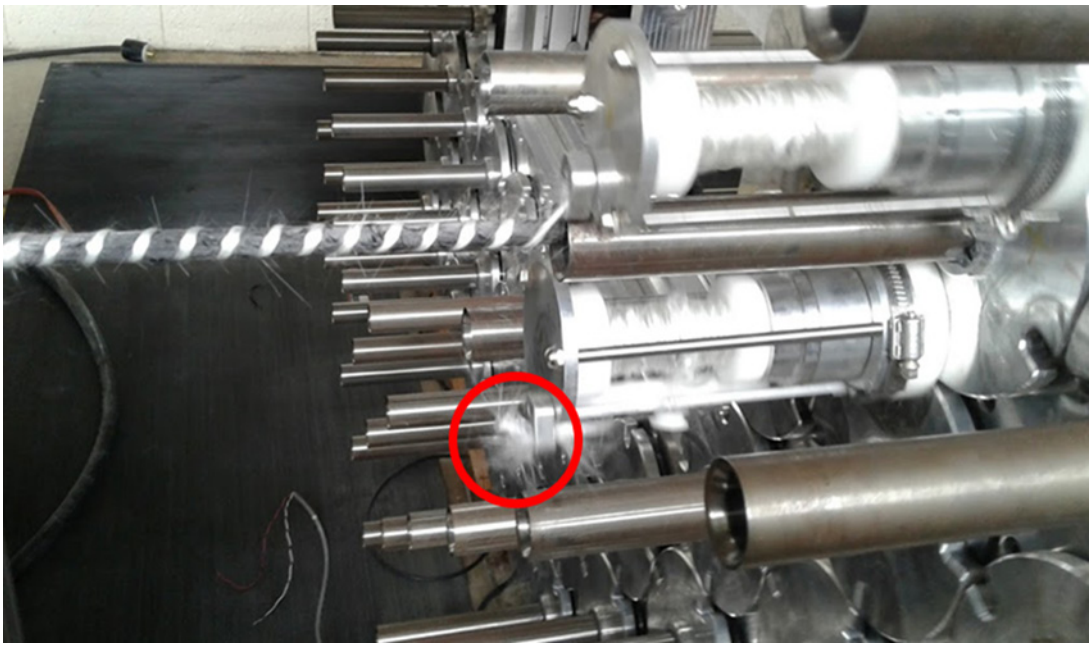

Figure 2-2: Fraying of Fiberglass at the Pay-Out Eye during Manufacturing of Carbon/Epoxy Core

Another consolidation option that was used was called the multi-tow consolidation method. In this consolidation type, three tows of the aramid fiber were braided together to create a thicker consolidation tow.

2.3 Carbon Epoxy Specimen Preparation

Using the three-dimensional braiding machine, the carbon/epoxy rods were manufactured in approximately 71 cm (2.3 ft.) lengths. This length of manufactured rebar was constrained by the length of the curing oven that was available at the time. A different curing oven described in Chapter 3 was fabricated to enable manufacturing of longer samples in the fiberglass/epoxy rebar research as the oven used in the preliminary research was discovered to be too small and had significant heat loss. After curing, the rebar rods were cut to lengths of 61 cm (2.0 ft.) using a

diamond-coated cutting blade. Sand coating was applied to selected samples using the procedure that will be described in section 3.5.4.

2.4 Concrete Mix Design and Casting

The concrete mix was designed using general guidelines from the American Concrete Institute's design guidelines. Local aggregates were used along with Type I cement. A mix design with a projected 28-day strength of 27.6 MPa (4000 psi) was used.

Rebar was cast in 200 mm x 200 mm x 200 mm (8.0 in x 8.0 in x 8.0 in) concrete cubes using a fixture specifically made to investigate bond strength. The fixture was made using steel and manufactured in a manner that was collapsible. Figure 2-3 shows a carbon/epoxy rebar cast in concrete.

Figure 2-3: Rebar Embedded in Concrete

2.5 Rebar Pull-Out Testing

Rebar pull-out testing was performed by using a standard tensile testing machine. A custom made testing fixture was manufactured to mount the concrete block onto the tensile machine apparatus. The testing fixture is described in detail in chapter 3. The set-up of the test is shown Figure 2-4. Load was applied at a rate of 1.5mm/min (0.06 in/min) and pull out testing was performed until maximum load was recorded. After peak load was registered, the test was left to run as the load ramped down until approximately 50% of the maximum load was reached.

Figure 2-4: Preliminary Test Set-up

The test was performed using guidelines specified in ACI 440.3R-12 B.3 to test for FRP rebar bond stress. These guidelines were not strictly followed as no deflection testing equipment was mounted to the concrete and rebar. Bond stress was calculated by dividing maximum load by the area of the rebar.

Along with the carbon/epoxy rebar manufactured on the three-dimensional braiding machine, standard 12.7 mm (0.5") diameter steel rebar and a commercially comparable fiberglass rebar were also tested for comparison.

2.6 Preliminary Study Results

Results (shown in Figure 2-5) showed that the bond strength was below 344 MPa (50 ksi) when dry winding was used, regardless of whether a single or a multiple tow consolidation bundle was used. Prepreg consolidation combined with sand resulted in a bond strength of 478 MPa (69 ksi), comparable to steel at 464 MPa (67 ksi). The results demonstrated that consolidating the rods with a prepreg tow resulted in a rebar which bonded better with concrete than using a dry tow. During testing, however, it was discovered that dry consolidating materials would easily strip off the FRP rebar due to poor bonding. Sand was shown to significantly increase the bond strength of the composite rebar by more than 30%. A prepreg multi-tow consolidating tow, which was made by hand braiding three tows together, recorded the highest bond stress when sand was added.

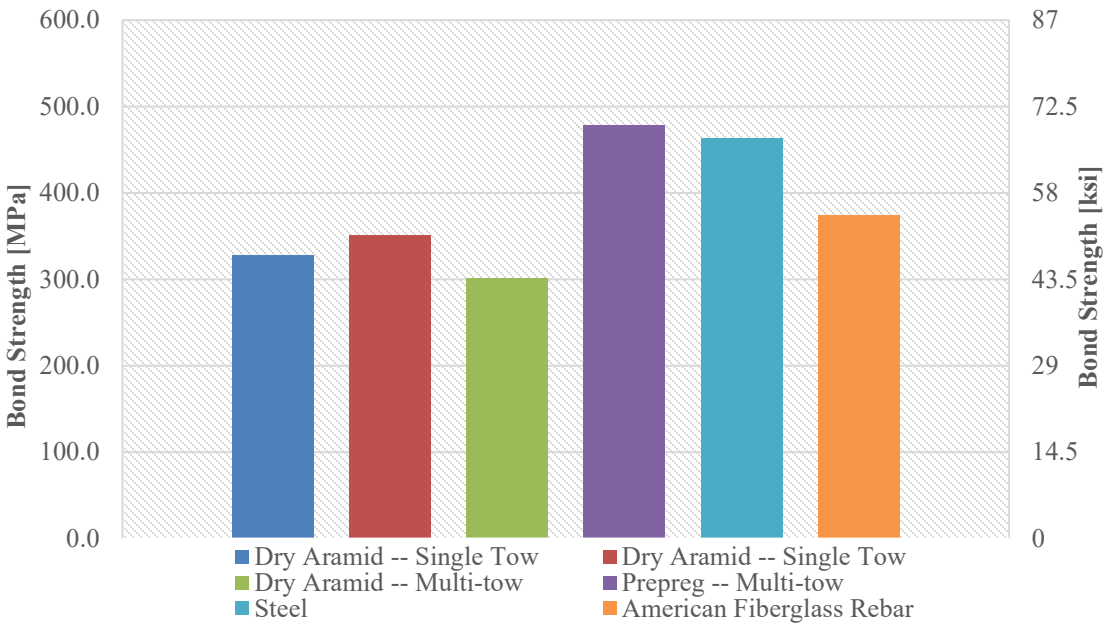

Figure 2-5: Carbon/Epoxy Test Results

2.7 Preliminary Study Summary

Using results from this preliminary study, a test matrix was set up where FRP rebar bond strength was investigated in detail using higher quality samples and more controlled parameters. Researchers felt that sufficient motive for investigating FRP rebar was established based on its varied strength due to the consolidation mechanisms tested, and specifically whether prepreg consolidation or dry consolidation was used. Bond strength also varied on whether sand coating was used.

Likewise, it was found that when manufactured correctly, FRP rebar has the ability to provide the same bond strength in concrete as conventional steel rebar. Considering its ability to resist corrosion among other advantages, FRP rebar can be used instead of steel rebar in appropriate situations. The use of different consolidation mechanisms and sand coating will be further explored in Chapter 3.

3 FIBERGLASS/EPOXY REBAR EXPERIMENTAL APPROACH

This chapter details the experimental variables, manufacturing process, specimen preparation, and procedure for testing the rebar.

3.1 Experimental Variables

Variables examined in this research included the nature of the consolidating material—either prepreg or dry, and rebar surface coating. Results from the preliminary research described in Chapter 2 were the basis of studying these variables.

3.1.1 Fiberglass/Epoxy Composite Rebar Geometry

The rebar was manufactured with a desired diameter of 12.7 mm (0.50 in). The average measured diameter of the rebar after manufacturing was 12.3 mm (0.49 in). This diameter corresponds to a No. 4 standard rebar. To achieve this diameter, 238 tows of unidirectional fiberglass filament were used. Each specimen was 53 cm (21 in) long and was reinforced with an end cap that was 3.8 cm (1.5 in) in diameter. The purpose of the reinforcement end cap was to prevent crushing of the rebar core when gripped by the jaws of the universal tensile testing machine during pull-out. Figure 3-1 shows a picture of a rebar sample.

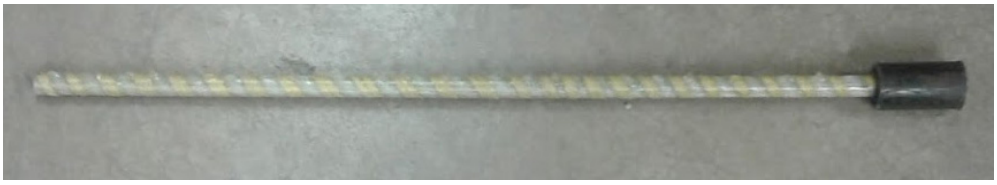

Figure 3-1: Rebar Sample with Reinforcement End-Cap for Gripping

3.1.2 Fiberglass/Epoxy Composite Rebar Core Material

Unidirectional fiberglass/epoxy prepreg tows were used for the manufacturing of the rebar core. Table 3-1 [19] shows the list of the materials making up the core with the manufacturer and the type. Tables 3-2 [20] and 3-3 [21] show the nominal mechanical properties for the core material. The resin content of the prepreg tow material was reported to be between 24.89 – 25.55% by TCR Composites.

Table 3-1: Fiberglass/Epoxy Core Material Specifications

Material	Manufacturer	Material Specification	Filament Diameter [µm (in)]	Filament Count per Tow
Fiberglass	Owens Corning	E-Glass 158B-AA-675	13.4 (5.3E -04)	2,000
Epoxy (Pre-Preg)	TCR Composites	UF3369-100	N/A	N/A

Table 3-2: Nominal Mechanical Properties of Fiberglass/Epoxy Tow Material Fibers

Material	Nominal Tensile Modulus [GPa (Msi)]	Tensile Strength [MPa (ksi)]
E-Glass 158B-AA-675	72.4 (10.5)	2350-2790 (341-404)

Table 3-3: Nominal Mechanical Properties of Fiberglass/Epoxy Tow Resin

Property	Cure Temperature of 121°C (250°F) for 90 minutes	Test Method
Tensile Modulus	3.1 GPa (445 ksi)	ASTM D638

3.1.3 Consolidation Sleeve Material

The rebar core was consolidated using either unidirectional dry tow or unidirectional prepreg aramid tow. The sleeve configuration created during the consolidation process was a half braid. Two bobbin carriers were used to create the braided sleeve. Figure 3-2 shows the two bobbins braiding the sleeve onto the core material.

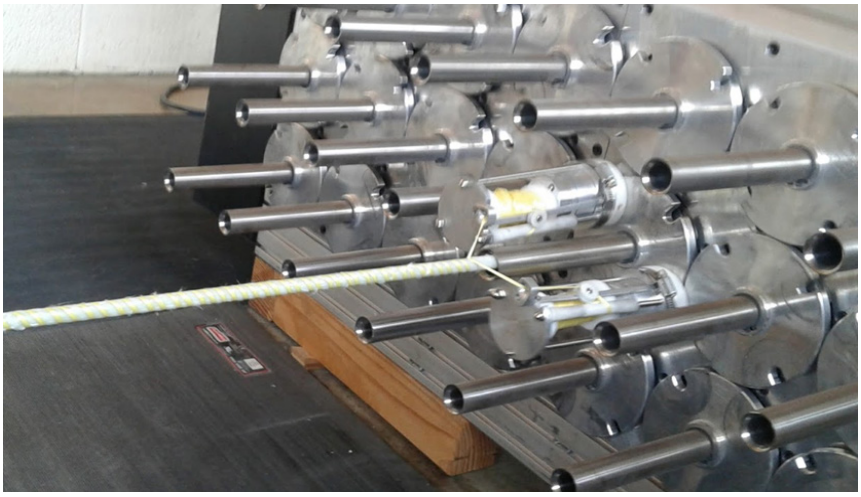

Figure 3-2: Two Bobbins Braiding a Sleeve on the Core for Consolidation

As shown in Figure 3-2, the aramid tow was yellow in color and its mechanical properties are described in Table 3-4. For prepreg aramid tow, the resin used was the same as that of the fiberglass/epoxy core whose properties are described in Table 3-3.

Table 3-4: Mechanical Properties of Aramid Fiber Used Consolidate the Fiberglass Core

Material	Modulus [GPa (Msi)]	Elongation at break %
TWARON 2200 8050 DTEX	60-80 (8.7 -11.6)	3.0 - 4.4

3.1.4 Test Matrix

Four different configurations of specimens were manufactured on the three-dimensional braiding machine. Two were consolidated with dry aramid. Of the two, one was later coated with sand. The other two samples were consolidated using prepreg aramid, with one of the samples being coated with sand. These four configurations were embedded in concrete and compared with steel rebar, plain and epoxy coated, as well as fiberglass rebar purchased from American Fiberglass Rebar. This resulted in seven unique configurations. Five samples of each configuration, for a total of 35 test specimens, were embedded in concrete and tested for pull-out. Table 3-5 shows the test matrix and naming notation of the different rebar configurations.

Table 3-5: Rebar Pull-Out Strength Test Matrix

Rebar Type	Consolidation Material	Secondary Process	Diameter		Configuration Name	Specimen Number
			mm	(in)		
Manufactured Fiberglass	Dry Aramid	None	12.3	0.49	D-N	1 to 5
Manufactured Fiberglass	Prepreg Aramid	None	12.3	0.49	P-N	1 to 5
Manufactured Fiberglass	Dry Aramid	Sand Coating	14.3	0.56	D-S	1 to 5
Manufactured Fiberglass	Prepreg Aramid	Sand Coating	14.3	0.56	P-S	1 to 5
American Fiberglass	N/A	Sand Coating	14.6	0.57	A-S	1 to 5
Plain Steel	N/A	None	12.7	0.50	S-N	1 to 5
Steel Epoxy Coated	N/A	Epoxy Coating	12.7	0.50	S-E	1 to 5

The samples cut from each manufactured specimen were assigned numerical values and a random number generator was used to select samples for sand coating. Samples with the same configuration were randomly assigned identification numbers 1 through 5. Each sample was named in the configuration; e.g., [P-S-3]. In this example "P" denotes prepreg consolidation, "S" denotes sand coating, and "3" denotes the third sample. Another example would be [D-N-1] where "D" denotes dry tow consolidation, "N" denotes no-sand coating and "1" denotes sample number 1. Randomness in selection and numbering of specimens was implemented to improve statistical validity.

The purchased rebar was identified in a similar manner to the manufactured rebar. For the steel rebar, the naming comprised of the rebar type, surface coating and sample number [S-E/S-N-#] with "S-E" representing steel epoxy coated, and "S-N" denoting steel with no-sand coating. An example would be [S-N-5], for steel non-coated Sample 5. The commercially purchased fiberglass rebar was named the configuration [A-S-#] with "A" representing American Fiberglass, the name of the company that manufactured the rebar and "S" denoting the sand coating on the rebar. An example would be [A-S-4], for American Fiberglass rebar sample 5.

Figures 3-3 through Figures 3-7 show photographs of the different configurations described in the test matrix. Photographically, it was difficult to see distinguishing features between the dry tow consolidated no-sand (D-N) and prepreg tow consolidated no-sand (P-N) samples. These samples are represented, therefore, in just one photograph, shown in Figure 3-3. The same was true for the dry tow consolidated sand (D-S) samples and prepreg tow consolidated sand (P-S) samples. The D-S and P-S samples are represented by Figure 3-4. Both the dry and prepreg consolidating aramid had the same color and resin on the prepreg had a clear color making visual distinction between the two difficult.

Figure 3-3: Photo of Non-Sand-coated Rebar Configurations

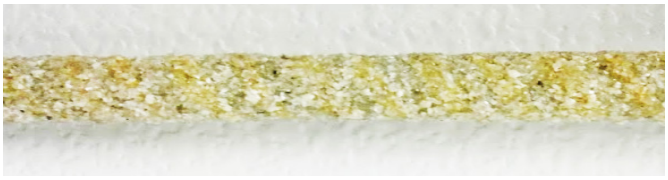

Figure 3-4: Photo of Sand-Coated Rebar Configurations

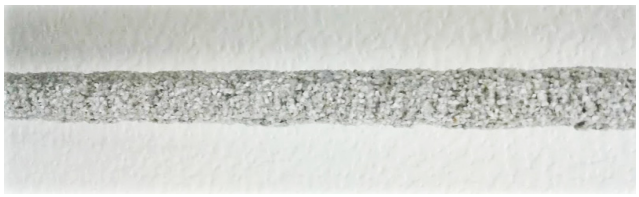

Figure 3-5: Photo of American Fiberglass Rebar Configuration

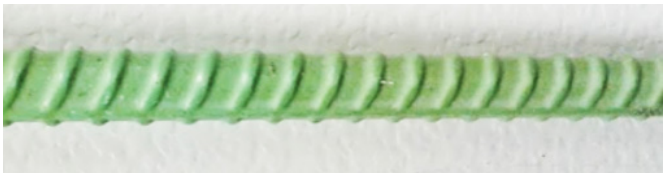

Figure 3-6: Photo of Steel-Epoxy Coated Rebar Configuration

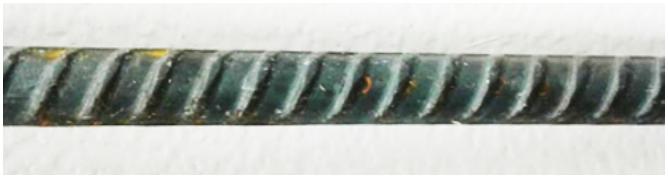

Figure 3-7: Photo of Plain Steel Rebar Configuration

3.2 Fiberglass/Epoxy Composite Rebar Manufacturing and Curing

Using the three-dimensional braiding machine shown in Figure 3-8, the fiberglass/epoxy prepreg tows were pulled in line using a pulley system. The tows which formed the core of the rebar were kept in tension as bobbins turned in a counterclockwise direction to perform consolidation. Once consolidation was finished, the rebar was cured in an inline oven, designed and built for this research, while still in tension. For a complete and detailed report outlining the basic three-dimensional manufacturing method, creation of sleeve patterns, and consolidation, refer to Allen [22].

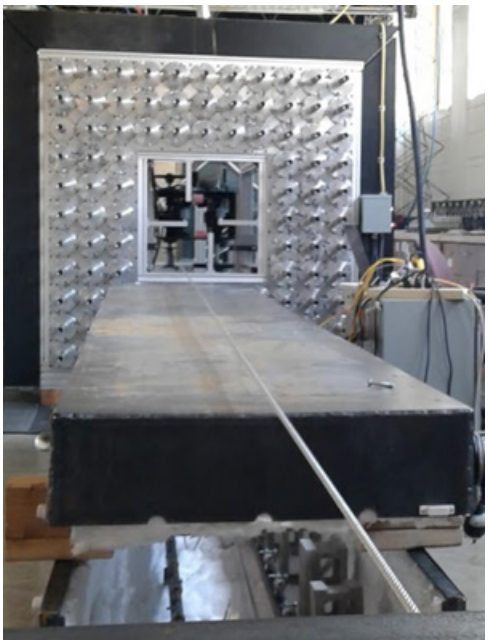

Figure 3-8: Rebar Manufacturing on Prototype IsoTruss Machine with Inline Oven

Four 3.8 m (12.5 ft) long specimens were manufactured and cured. Each sample took around 15 minutes to manufacture followed by curing at 121°C (250°F). The curing process comprised of three cycles. The first cycle was the temperature ramp up from room temperature to 121°C (250°F). This cycle took roughly two hours. The temperature was held at 121°C (250°F) for 90 minutes during the second cycle. The final cycle was the ramp down which was

advised to be for at least 30 minutes after the oven was turned off. All manufactured batches were left to ramp down overnight. The first two batches were manufactured using dry aramid fiber as the braiding method to create the consolidating sleeve, while the third and fourth samples used prepreg aramid fiber. Each sample was cut to 53 cm (21 in) long specimens.

3.3 Inline Oven

The oven used in this research was manufactured in-house primarily for this project. The original oven that was used for the preliminary research was only capable of curing rebar samples that were 71 cm (2.3 ft.) long. The in-house manufactured oven was 4.3 m (14 ft.) long and had a rectangular cross-section that measured 61 cm (2.0 ft.) wide by 46 cm (1.5 ft.) high. The oven was comprised of two sections, a top lid piece and bottom base piece. The base had a cross-sectional area of a 61 cm (2.0 ft.) wide by 30 cm (1.0 ft.) high, and the top piece was 61 cm (2.0 ft.) by 30 cm (0.5 ft.) high. There were three evenly spaced 25 cm (1.0 in.) diameter holes on the front and back of the oven. These holes allowed for three individual strands of consolidated tows of fiber to go through the front of the oven and out the back of the oven. For the rebar manufacturing discussed in this research, only the center hole was used as one strand of rebar was manufactured. During rebar manufacturing, the top lid would be lifted and fibers were pulled through the oven while maintaining tension. When consolidation was completed, the lid would be closed and oven turned on for curing. Manufacturing drawings of the oven are in Appendix C.

The oven was manufactured using steel. Angle iron and flat bars were used to create a frame. Figure 3-9 is an image showing pieces of the frame.

Figure 3-9: Top and Bottom Piece Oven Frames

12-gauge steel sheets were attached to the frame. Ceramic blanket insulation was attached to the inside walls of the oven to prevent heat loss. Steel heating element coils were placed at the bottom of the oven and two fans on opposite ends of the oven were installed to ensure heat circulation. Figure 3-10 shows the components of the inline oven.

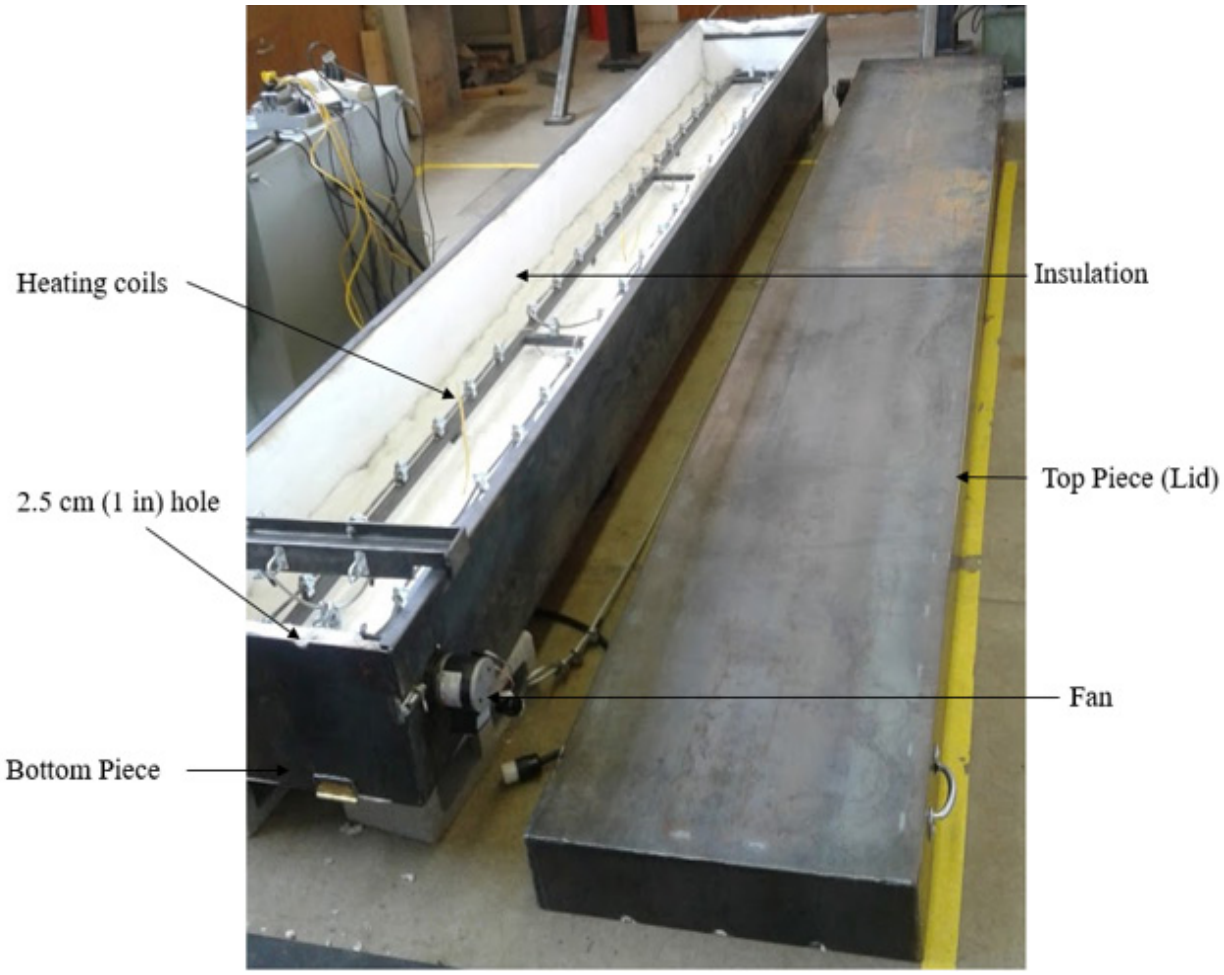

Figure 3-10: Rebar Manufacturing Inline Oven Components

The oven was manufactured with various specifications and fail-safe measures. It was operated using an electric source and was designed for a maximum heating capacity of 315°C (600°F). Sensors were installed that allowed the oven to only heat up when the top lid was shut. Other safety regulations were installed in accordance with standards specified by the Fire Marshall and Brigham Young University Safety Department.

3.4 Final Specimen Preparation

This section contains a summary of the specimen preparation procedure. Most of these steps were generally similar to research previously conducted by Allen [22], Sika [23], Embley [24] and Cahoon [25].

3.4.1 Specimen Cutting

The 3.80 m (12.5 ft) long fiberglass/epoxy rods were cut to samples that were 56 cm (22 in) in length using a cut-off saw with a diamond-coated cutting blade, as shown in Figure 3-11. A 25 mm (1.0 in) long sample was cut from each 56 cm (22 in) rod, polished, and used to investigate the consolidation quality of each rod.

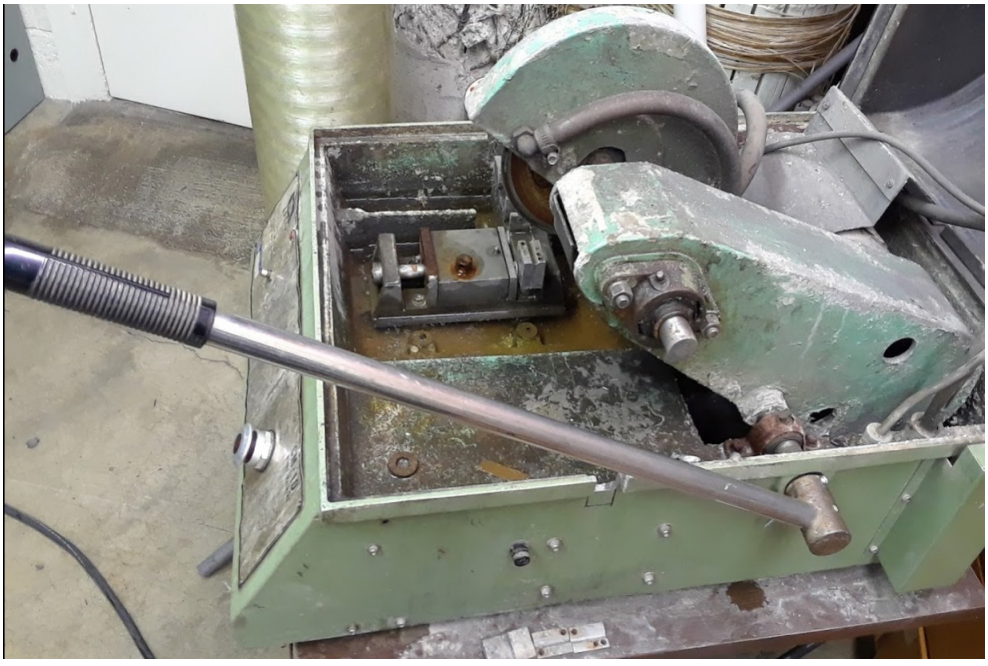

Figure 3-11: Cut-off Saw Jig with Diamond Coated Blade Specimen Polishing

The 25 mm (1.0 in) long samples were polished using the Leco CM-10 polishing machine (see Figure 3-12). Polishing instructions and procedures were as follows:

1. Prepare the samples based on the preferred method of polishing, either fitting into the provided fixture or hand polishing. Preparation instructions for hand polishing or using the machine fixture are provided in the machine handbook.
2. On the machine, insert the polishing discs and put the sandpaper on the machine using the instructions provided in the machine handbook.
3. Wet the surface of the disc with water and insert the provided ring to hold the sand paper in place.
4. Use the screen monitor to change speeds, pressure and disc rotation direction.
5. Set the pressure to 27 N (6 lbs), and the rotation to CCW.
6. Wet the top of the sandpaper, and keep the water on while sanding.
7. The entire machine top can rotate, so after positioning it, push down the black handle located towards the upper right of the sandpaper fixture. For detailed instructions on machine polishing, see machine instructions handbook.
8. Use the following sandpaper grit procession, disc rotation speed, and times in this order:
    1) 120 grit, 50 rpm, 30 seconds.
    2) 600 grit, 250 rpm, 2 min.
    3) 800 grit, 250 rpm, 5 min.
    4) 1200 grit, 275 rpm, 20 min.

9. After the 1200 grit, switch to diamond paste polishing using these instructions:

    1) Fit the cloth pad onto the ring—use the wider rings.

    2) Spray diamond paste as instructed by the manufacturer.

    3) Soak the pad with oil.

    4) Run the machine, and spray oil occasionally.

Trial samples were polished first to ensure that the polishing procedure was perfected before polishing the actual samples.

Figure 3-12: Photograph of Leco CM-10 Polishing Machine

3.4.2 End Cap Reinforcement Manufacturing

The purpose of the end cap reinforcement on the rebar, like the doubler in the preliminary research with carbon/epoxy described in Chapter 2, was to provide extra strength in the area and

prevent local failure in the area that was gripped in the jaws of the testing machine. The end reinforcement was a hollow steel pipe with 5.1 cm (2.0 in) outside diameter, and an inside diameter of 4.45 cm (1.75 in). The length of the end reinforcement was 5.1 cm (2.0 in). The rebar samples were wrapped in a 1.9 cm (0.75 in) weaved prepreg fabric tape and inserted into the end reinforcement. Resin was poured into the end cap reinforcement and cured following the same procedures and cure cycle described in Section 3.2 for the rebar manufacturing cure. The end cap reinforcement resin curing occurred along with the curing of the sand coating resin. The sand coating procedure is described in Section 3.3.4. Trial testing showed that the end cap reinforcement had a capacity of 76 kN (17 kips) when tension was applied before failure.

3.4.3 Sand Coating

The sand coating process involved the use of finely graded silica sand and epoxy/resin to coat the rebar. Silica sand was chosen due to its fine grains and availability in the laboratory. The silica sand was sieved and very specific sized sand grains were used for the coating. Grains that could pass through a No. 16 sieve but were retained on a No. 20 sieve were employed since these were similar to the observed and estimated grain size of the sand used on the commercial rebar. Coating the manufactured rebar with sand increased the surface diameter of the rebar from an average of 12.3 mm (0.49 in) to 14.3 mm (0.52 mm).

The sand coating process followed is listed below:

1. A sand layer of approximately 6.35 mm (0.25 in) thick was spread evenly on a flat surface.
2. A piece of rebar was dipped in a container containing Proset INF-114 epoxy/resin. Table 3-6 [26] shows the properties of Proset INF-114.

3. The rebar was rolled on the sand layer until uniform consistency was achieved.

Once coated with sand, the rebar was cured, along with the end reinforcement resin using the curing cycle described in Section 3.2. Trial samples made earlier during the preliminary research had shown that curing the sand coating resin at room temperature was not effective as sand could easily be rubbed off. After oven curing, sand-coated samples were left to cure at room temperature for three weeks while preparations for concrete casting were being made.

Table 3-6: Mechanical Properties of Sand Coating Resin

Property of Proset INF-114	Cure Temperature of 22°C(77°F) x 4 weeks	Test Method
Tensile Modulus, GPa (psi)	3.61 (5.24E+5)	ASTM D638
Hardness, Type D	86	ASTM D2240
Compressive Yield, MPa (psi)	101 (14,700)	ASTM D695

3.5 Concrete Mix Design

The concrete mix design implemented in this research complied with general guidelines specified by the American Concrete Institute. The mix was designed for ¾ m^3 (1 yd^3) of concrete. Tables 3-7 and 3-8 show the concrete mix design ingredients and parameters. The ingredients were Portland Type I cement purchased from a local cement distributor, and the air entrainer used was DARAVAIR® AT60. Coarse and fine aggregates meeting ASTM C 33 (Standard Specification for Concrete Aggregates) were obtained from Geneva Rock, a local ready mix concrete company for utilization in the concrete mixture. Design parameters and dosage of ingredients were determined from concrete trail batches and standards obtained from the American Concrete Institute. Once the ¾ m^3 (1 yd^3) mix was designed, the ingredients were scaled to produce a batch size that was 0.08 m^3 (0.1 yd^3).

Table 3-7: Concrete Mix Design Main Ingredients and Description

Ingredient	Description
Cement	Portland Type I
Air Entrainer	DARAVAIR® AT60
Sand	2.4 mm (0.10 in)
Aggregate	19 mm (0.75 in)

Table 3-8: Concrete Mix Design Parameters

Parameter	Value
Cement	6 bags
Slump	10 +/- 2.5 cm (4.0 +/- 1.0 in)
Water-Cement Ratio	0.51
Air Entrainment	6.0 +/- 1.0 %
Strength	27.5 MPa (4000 psi)

A concrete casting metal form, shown in Figure 3-13 was designed and manufactured to allow six identical concrete cubes with 203 mm (8 in) sides to be cast simultaneously. Each cube was embedded with a different rebar type from the test matrix.

Figure 3-13: Metallic Forms/Casting Fixture

When the casting fixture was manufactured, the original test matrix considered only six rebar types. To accommodate the seventh rebar type with only six forms that required five

repetitions, concrete batching and casting were performed six times instead of five, with one rebar option being omitted on each specific casting. Table 3-9 shows the rebar that was cast on each day from a batch.

Table 3-9: Samples Cast from Each Batch

Batch No.	Specimens Cast						
	D-N	P-N	D-S	P-S	A-S	S-N	S-E
1	1	1	1	1	1	-	1
2	2	2	2	2	2	2	-
3	3	3	3	3	-	3	3
4	4	-	4	4	4	4	4
5	5	5	5	-	5	5	5
6	-	4	-	5	3	1	2

In addition to the concrete material needed for each of the six cubes in a batch, sufficient additional material was prepared to allow casting of three 10 cm (4.0 in) diameter cylinders, each 20 cm (8.0 in) in height. Each batch size was also increased by 10 percent to accommodate potential losses of material during casting. This resulted in each batch having a total of 0.08 m^3 (0.10 yd^3) of concrete. The quantities of materials common to all batches are shown in Table 3-10.

Table 3-10: Concrete Mix Design

Ingredient	Specific Gravity	Design Weight per 3/4 m^3 (1 yd^3)		Measured Weight Per Batch	
		[kg	(lb)]	[kg	(lb)]
Free Water	1.00	157	(346)	14.8	(32.7)
Cement	3.15	277	(610)	26.1	(57.6)
Coarse Aggregate	2.56	741	(1633)	70.0	(154)
Fine Aggregate	2.58	505	(1114)	47.8	(105)
Air Entrainment	1.00	-	-	27 ml	(0.91) oz
Total		1680	(3703)	158.7	(349)

The specified amounts of both coarse aggregate and fine aggregate are given as oven-dry weights. To ensure that the aggregates were 'bone dry', both the gravel and sand were dried in pans in a conventional oven at 60ºC (140º F) for 24 hours to achieve their oven dry weight.The gradation and additional properties of both the coarse and fine aggregates are listed in Appendix B.

Following the guidelines adapted from Pinkerton [27], trial batches were made multiple times to determine the order in which materials combined and the lengths of successive mixing times. Like Pinkerton [27], the resulting mixing procedures are described in the following steps:

Step 1. Before any material was added to the drum mixer, the inside surface of the mixer was sprayed with water. The walls of the mixer were moistened before each batch to prevent the mixer from absorbing a portion of the free water in the concrete mix. Excess water was poured out of the mixer.

Step 2. Once the walls of the concrete mixer were sufficiently moistened, the first 75% of the total water needed was placed into the mixer.

Step 3. Once the initial allotment of water was added, all of the aggregates for the mix were also added. The mixer was allowed to rotate while the aggregates were being added.

Step 4. After all of the aggregates were added, the aggregates and water were mixed together for one additional minute.

Step 5. In order for the oven-dried aggregates to approach the Saturated Surface Dry (SSD) condition, the mixer was stopped, and the mixture of aggregates and water was allowed to sit for 15 minutes. To prevent any loss of water through evaporation, the opening of the mixer was covered with a piece of plastic during this period.

Step 6. After the aggregate and water mixture equilibrated for 15 minutes, 27 ml (0.91 oz.) of DARAVAIR AT60 air entrainer was added with 0.9 kg (2.0 lbs) of water. The mixer was allowed to rotate while the solution of air entrainer and water was added.

Step 7. The mixer was rotated for one additional minute after the air entrainer was added.

Step 8. The cement and all remaining water was added to the mix. To facilitate adequate mixing of the cement with the aggregate, the mixer was allowed to rotate while the cement and water were added.

Step 9. After all the materials for the mix were added, final mixing was performed. The mixer was run for three minutes, stopped to let the mix sit covered for three minutes, and finally run for one additional minute. A waiting period was provided to allow the cement to absorb the water.

Step 10. After mixing was complete, tests were performed to check for the appropriate slump and air entrainment. Slump was tested in accordance with ASTM C 143 (Standard Test Method of Slump for Hydraulic Cement Concrete) [28], and entrained air was tested in accordance with ASTM C 231 (Standard Test Method for Air Content of Freshly Mixed Concrete by the Pressure Method) [29]. Results for these tests are tabulated in Chapter 4.

Following this process, the concrete was distributed to the prepared specimen molds using a dry wheelbarrow. The rebar was placed in the 203 mm x 203 mm (8 in x 8 in) mold through a PVC pipe that was 14 mm (5.5 in) long as shown in Figure 3-14. This allowed for 6.4 mm (2.5 in) of the rebar to bond with concrete. The concrete was placed in the forms in two equal volume lifts. After each lift, consolidation was performed by rodding the concrete 25 times using a 3.0 mm (1/8 in) diameter steel rod, and tapping the sides of the form 10-15 times. Care

was taken not to strike the reinforcement. Figure 3-14 shows the layout of the rebar during casting.

Figure 3-14: Rebar Positioning and PVC in Form

The concrete was finished using a wooden trowel. After 24 hours, the specimens were removed from the forms and placed in air tight plastic bags for curing. Figure 3-15 shows two specimens that have been cast and are ready to be stripped for curing. Plastic bags aided in trapping moisture and enhancing concrete curing. In addition to the forms, four concrete

cylinders were also cast from each batch. The cylinders were also stripped from their molds after 24 hours and placed in the same bags as the specimens.

Figure 3-15: Concrete Specimens Cast into Forms and Ready for Stripping

Figure 3-16: Curing of Concrete Specimens in Plastic Bags

3.6 Test Procedures

This section summarizes the microscope imaging, concrete compressive strength, and rebar pull-out test procedures. The microscope image scanning procedure was conducted similarly to the research of Cahoon [25]. The test for concrete compressive testing was performed according to ASTM C39 (Standard Test Method for Compressive Strength of Cylindrical Concrete Specimens) [30]. The pull-out testing was performed following the guidelines in ACI 440.3R-13-B.3.

3.6.1 Length and Weight Measurements

Rebar samples from each configuration were measured for length and weight. Table 3-11 shows average lengths and weights of each of the rebar configurations. The lengths and weights of each sample are shown in Appendix B.

Table 3-11: Sample Lengths and Weights

Sample	Length		Weight	
Configuration	cm	(in)	g/cm	(lbs./in)
D-N	54.2	(21.4)	2.37	(0.013)
P-N	54.4	(21.4)	2.35	(0.013)
D-S	54.3	(21.4)	3.09	(0.017)
P-S	54.4	(21.4)	3.06	(0.017)
A-S	61.0	(24.0)	3.00	(0.017)
S-N	61.0	(24.0)	9.42	(0.053)
S-E	61.0	(24.0)	9.64	(0.054)

3.6.2 Microscope Imaging Procedure

To investigate the quality of the consolidation of the rods, specimens cut from the ends of each rod were viewed under a Leco Olympus GX51 model microscope. Microscope images were viewed and analyzed using Pax-it software.

3.6.3 Concrete Compressive Strength Testing

After 28 days, the three cast cylinders from each concrete batch were tested to determine the compressive strength. The specimens were capped according to ASTM C617 (Standard Practice for Capping Cylindrical Concrete Specimens) [31] prior to strength testing. The strength of the cured cylinders was measured following ASTM C39 [30]. Average compressive concrete strength and standard deviation from each batch was calculated from three cylinders. Compressive strength results are summarized in Chapter 4.

3.6.4 Fiber Volume Measurements

The void ratio and fiber volume percentages of the fiberglass/epoxy composite rebar were measured optically using the Leco Olympus GX51 microscope and Pax-it software. Table 4-7 summarizes the void ratios and average fiber volumes for each consolidation type. Tables summarizing the areas and fiber volume for each rebar sample in each configuration are in Appendix A.

Table 3-12: Void Ratio and Average Fiber Volume Fractions

Configuration	Void Ratio [%]	Fiber Volume Fraction [%]
D-N/D-S	0.09	74.6
P-N/P-S	0.09	71.4
A-S	0.08	71.9

Figures 3-18 through 3-20 show pictures of sample microscope images. The 50X magnification was used to calculate void ratio while the 200X magnification was used to calculate fiber volume measurements. The 100X and 500X magnifications are also shown to

illustrate the composite rebar fiberglass and epoxy matrix. Microscope images of each sample are in Appendix B.

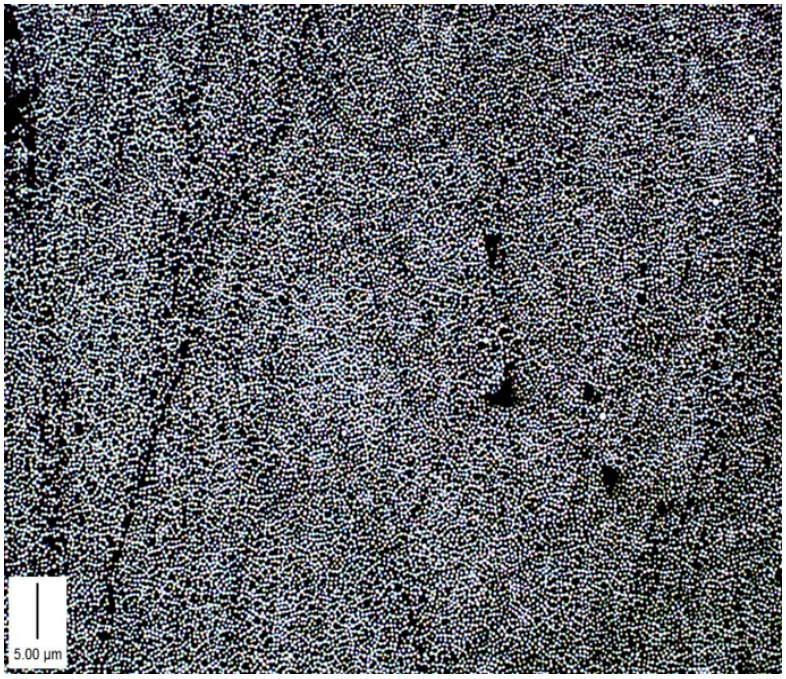

Figure 3-17: 50X Magnification of Polished Fiberglass/Epoxy Rebar

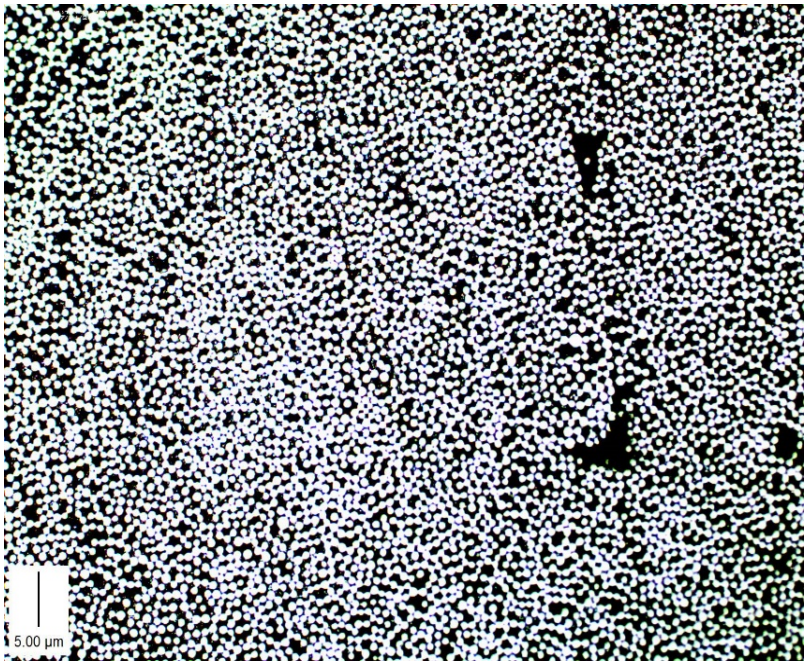

Figure 3-18: 100X Magnification of Polished Fiberglass/Epoxy Rebar

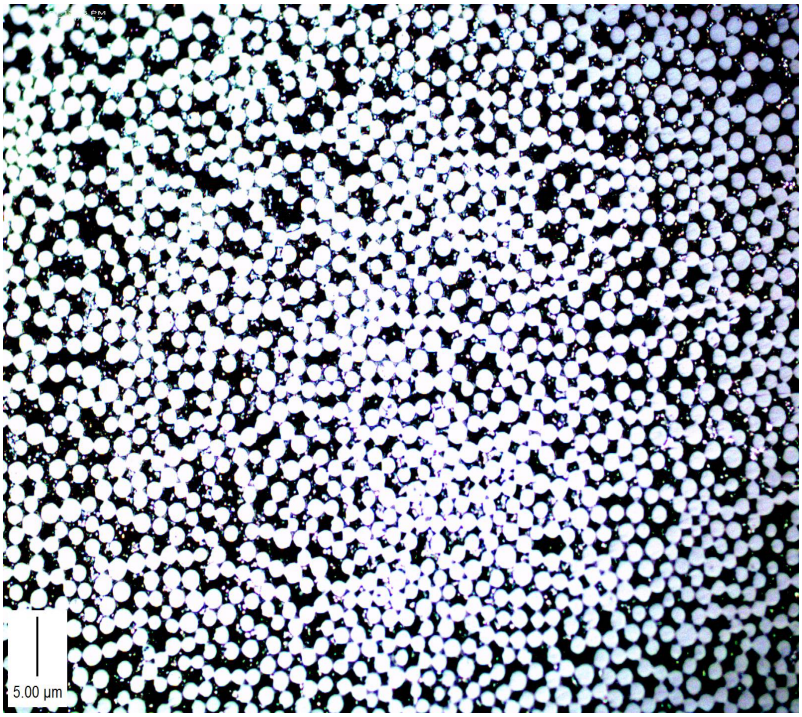

Figure 3-19: 200X Magnification of Polished Fiberglass/Epoxy Rebar

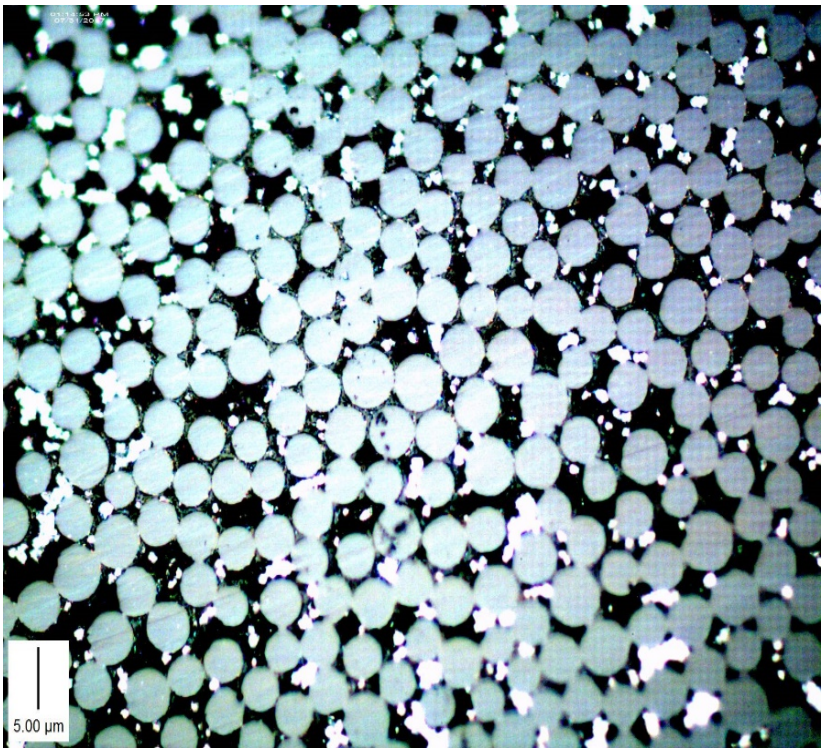

Figure 3-20: 500X Magnification of Polished Fiberglass/Epoxy Rebar

3.6.5 Rebar Preparation for Pull-Out Testing

A custom pull-out testing fixture was designed and manufactured specifically for specimens in this research. The fixture was made of steel and used four bolts that allowed the concrete specimens to fit tightly, as shown in Figure 3-21.

Figure 3-21: Photograph of Testing Fixture for Rebar Pull-Out Testing

3.6.6 Fiberglass/Epoxy Rebar Pull-Out Testing Procedure

The fixture and block were mounted on an 89 kN (20 kip) Instron Model universal testing machine (Figure 3-21). The end cap reinforcement on the rebar was fixed into the upper jaws of the machine, while the bottom of the fixture was fixed into the lower jaws. The upper jaws moved up while the lower jaws remained stationary. This set-up was inspired by guidelines from ACI 440.3R-13-B.3.

Pull-out testing was performed by applying load on to the head of the rebar at a rate of 1.2 mm/min (0.05 in/min).Load was applied until failure, which was defined as the maximum load required to break the rebar concrete bond. Once maximum load was reached and the rebar-concrete bond had failed, the loading on the tensile testing machine would begin to ramp down. The testing was completed when the load ramp down after failure was below 65% of the maximum recorded load.

Along with load, deflection data was collected using spring potentiometers and an extensometer. Four string potentiometers were used to measure relative deflection between the composite rebar and concrete. Two string potentiometers were mounted at the top, and two at the bottom of the rod. Each set of spring potentiometers was mounted with the spring potentiometers located opposite sides of each other. An extensometer was also mounted on the rebar to measure local strain in order to simultaneously determine the elastic modulus of the rebar. Figure 3-22 shows the complete set-up right before testing. Figures 3-23 and 3-24 show a close up of the Loaded-End potentiometers and extensometer, and free-end potentiometers, respectively.

Figure 3-22: Photograph of Test Set-up for Rebar Pull-Out Testing

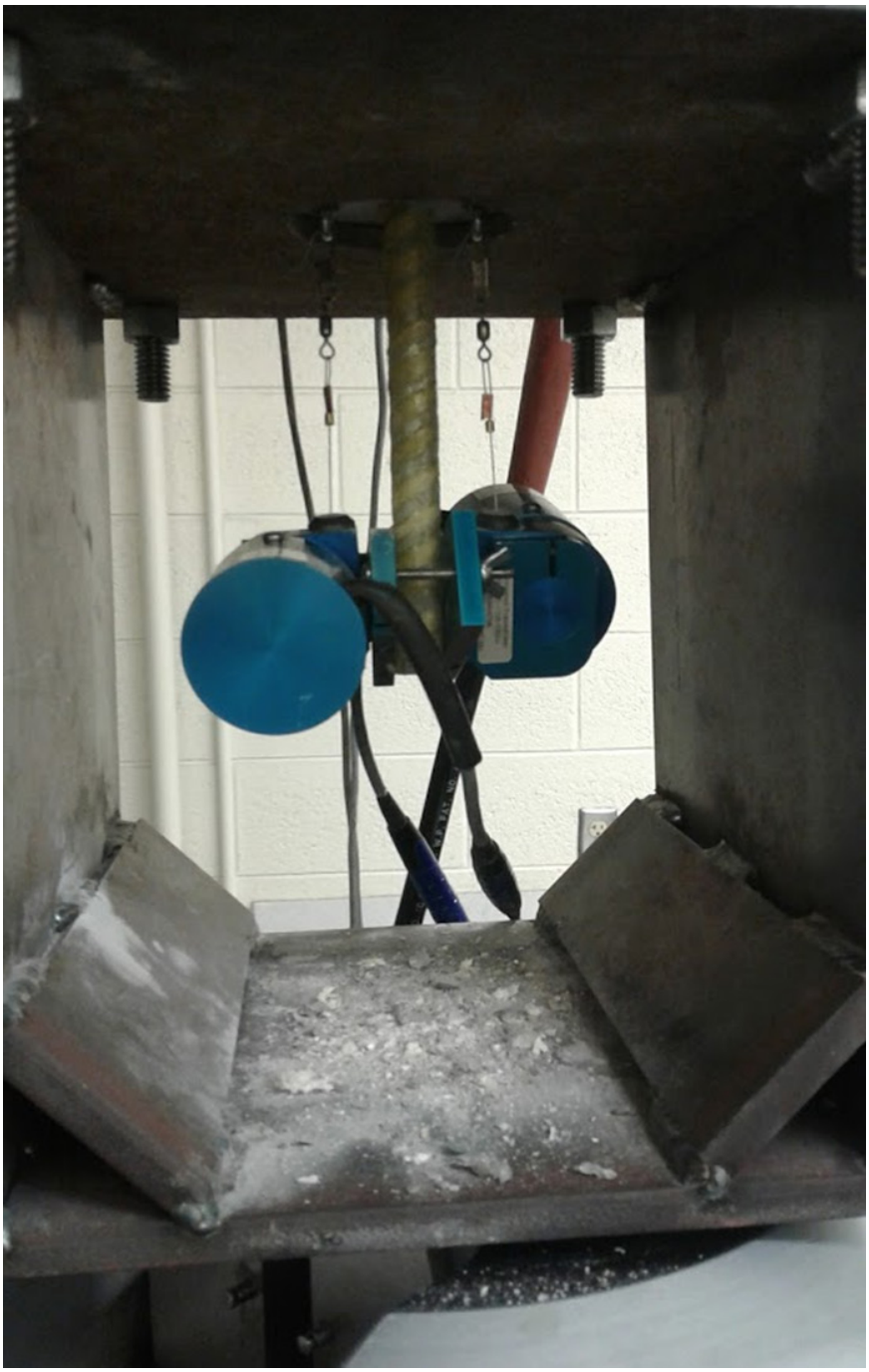

Figure 3-23: Photograph of Free-End String Potentiometers Mounted on Lower End of Rebar

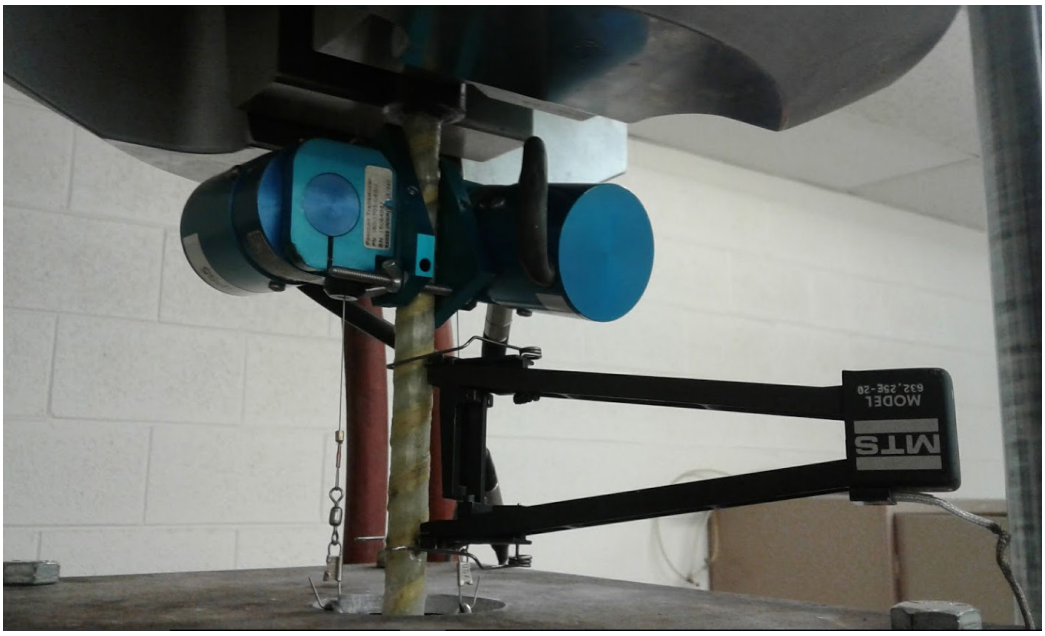

Figure 3-24: Photograph of Loaded-End String Potentiometers and Extensometer Mounted on Upper End of Rebar

3.7 Data Reduction and Analysis

Data reduction involved calculating and plotting the deflections measured by the loaded-end and free-end string potentiometers against load. The strain in the rebar recorded by the extensometer was used to calculate Young's modulus. Average bond stress was calculated using Equation 3-1 (Equation B.3.8.1 from ACI 440.3R-12 B.3);

$$\tau = \frac{F}{C_b l} \qquad \text{Equation 3-1}$$

Where:

F = tensile load, N

C_b = π times the effective diameter of the rebar

l = bonded length of concrete to the rebar

For the free-end, the average bond stress was plotted against slippage which was the average of the free-end displacements. For the loaded-end, slippage was calculated where the elongation of the bar between the point of attachment loaded-end spring potentiometers and the beginning of the rebar bonded zone was subtracted from the average of the loaded-end spring potentiometer measurement.

4 FIBERGLASS/EPOXY REBAR EXPERIMENTAL RESULTS

This chapter details the results for concrete strength tests along with the fiberglass epoxy rebar pull-out test. Deflection, stress-strain curves and slip graphs are illustrated together with tables summarizing average values. The cross-sectional areas of each specimen are also recorded in tables. Areas were calculated using a microscope and Pax-It software. In the stress-strain and bond stress-slip curves, an average is shown along with upper and lower bounds curves to signify any probable outliers. The upper and lower bounds curves were calculated using Chauvenet's Criterion [32].

After pull-out failure which was achieved at maximum load, the specimens were allowed to ramp down to 50% of the maximum load. Some specimens ramped down to 50% as anticipated, but others, particularly those coated in sand, did not achieve this mark. This was attributed to sand grains getting caught in the concrete, contributing to specimens gaining or maintaining load which was not relevant as failure had already occurred. In such cases the tests were terminated after over 3,000 data points were collected. Several specimens ramped down to half the load quickly while others took longer times resulting in different lengths of curves. A common algorithm of 65% of the maximum load or stress value was used to determine the termination point of the curves.

4.1 Concrete Strength Results

This section summarizes the properties of each concrete mix prepared and discusses the test results along with a statistical analysis.

4.1.1 Concrete Properties

Table 4-1 summarizes the slump, entrained air content, mean compressive strength, and standard deviations of the compressive strength of each of the concrete batches. The slump and air content were measured during casting while the compressive strength was determined after 28-days, the same day the pull-out tests were performed. Mix compressive strength values were the average of three concrete cylinders. The individual strength of each concrete cylinder from the different batches is tabulated in Appendix A.

Table 4-1: Summary of Concrete Properties

Batch Mix		Measured Slump		Entrained Air	Average Compressive Strength			
					Mean		Std. Dev.	
		cm	(in)	%	MPa	(psi)	MPa	(psi)
1		16.5	(6.5)	7	22.3	(3230)	1.37	(199)
2		16.5	(6.5)	6	24.7	(3584)	1.25	(182)
3		16.5	(6.5)	7	27.4	(3987)	1.23	(178)
4		14.0	(5.5)	7	25.3	(3671)	0.01	(14)
5		16.5	(6.5)	7	26.6	(3851)	0.93	(135)
6		16.5	(6.5)	7	25.4	(3681)	0.61	(88)
Average		16.1	(6.3)	7	25.3	(3667)	0.9	(133)
Std. Dev		0.93	(0.4)	0.4	1.61	(236)	0.47	(65)
Chauvenet's	Upper	17.7	(7.0)	7	28.1	(4076)	1.72	(244)
Limit	Lower	14.5	(5.7)	6	22.5	(3258)	0.08	(21)

4.1.2 Discussion of Concrete Properties

The goal of the mix designs was to produce concrete whose average strength was 27.6 +/- 1.37 MPa (4000 +/- 200 psi) for each mix design. Two out of the six batches were able to attain this concrete margin. All batches except batches 1 & 2 were, however, within 90% of the goal strength. It was interesting to note from the results that Batch 4, which had the lowest slump value had the lowest compressive strength standard deviation. Even though the mix designs appeared typical for a standard "six-bag" mix concrete, the below average strength of the concrete could be credited to the fact that the mix design was prepared based on 7-day cured concrete trial batches rather full 28-day concrete trial batch. The 28-day strength was projected from results the 7-day strength tests. The strength of the concrete, however, did not derail from the goal of the research, which was to compare FRP rebar to steel rebar. Having lower strength concrete in some of the batches allowed for comparison between failures modes when rebar was embedded in different strength concrete.

4.2 Fiberglass/Epoxy Composite Rebar Pull-Out Test Results

4.2.1 Dry Consolidation Tow with No-sand Coating (D-N) Results

The D-N configuration consisted of rebar samples that were consolidated with dry aramid tow without sand coating. Table 4-2 presents a summary of the D-N rebar configuration properties. Figure 4-3 show the stress-strain curves of the configurations.

Table 4-2 Fiberglass/Epoxy Rebar Properties for Dry Consolidation Tow with No-Sand Coating (D-N)

Specimen I.D.		Cross Section Area [mm^2]	(in^2)]	Young's modulus [GPa]	(Msi)]
D-N-1		112	(0.174)	46.3	(6.72)
D-N-2		114	(0.176)	46.3	(6.72)
D-N-3		119	(0.185)	48.3	(7.00)
D-N-4		126	(0.195)	48.3	(7.00)
D-N-5		126	(0.196)	48.7	(7.06)
D-N Average		119	(0.185)	47.6	(6.90)
Std. Dev.		5.93	(0.009)	1.04	(0.15)
Chauvenet's Limit	Upper	129	(0.200)	49.3	(7.15)
	Lower	110	(0.170)	45.9	(6.65)

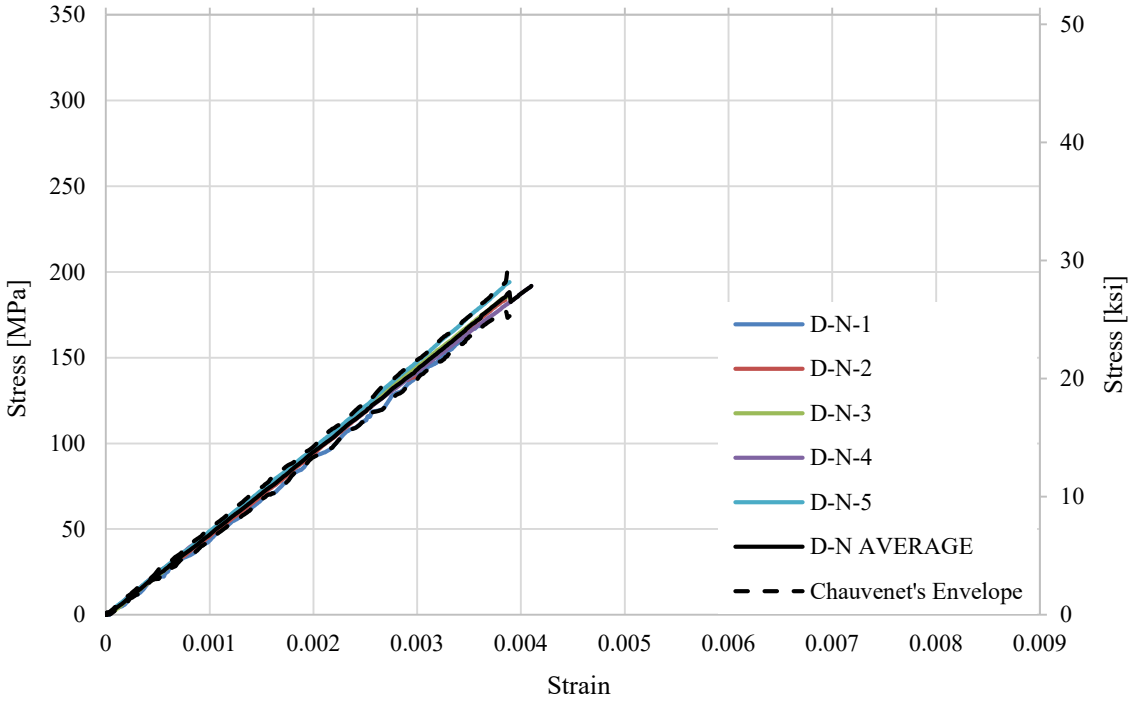

Figure 4-1: Stress-Strain Plots for Dry Consolidation Tow With No-sand Coating (D-N)

As shown in Table 4-2, the average Young's modulus for the D-N samples was 47.6 GPa (6.90 Msi). The average nominal diameter of the specimens was 119 mm^2 (0.185 in^2). All stress-strain curves were within Chauvenet's limits of statistical acceptability.

Figure 4-2, Table 4-3 and Figure 4-3 show the free-end deflection against load, bond stress data, and bond stress against slip of the free-end, respectively. Sample D-N-1 did not record free-end data, and therefore is not included in the reported data.

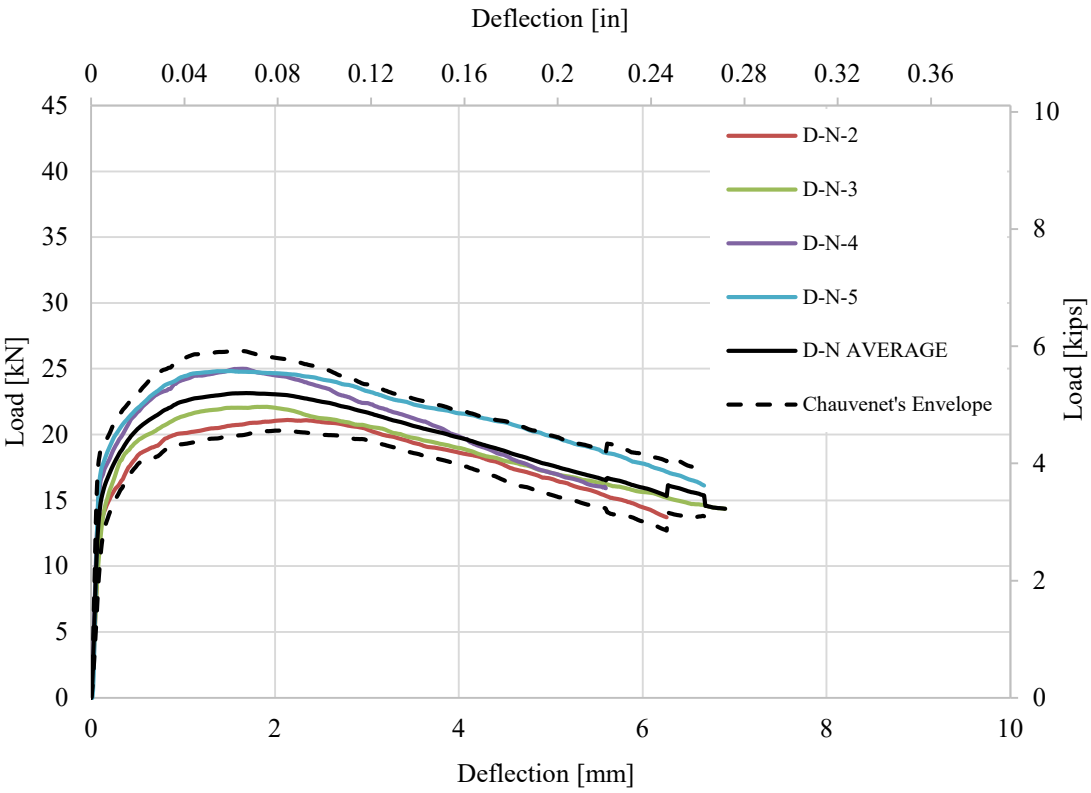

Figure 4-2: Free-End Deflections for Dry Consolidation Tow With No-sand Coating (D-N)

Table 4-3: Free-End Bond Stress for Dry Consolidation Tow with No-sand Coating (D-N)

Specimen I.D.	Bond Stress Corresponding to Slip Length of 0.05 mm (0.002 in)		0.1 mm (0.004 in)		0.25 mm (0.01 in)		Maximum Bond Stress	
	[MPa	(ksi)]	[MPa	(ksi)]	[MPa	(ksi)]	[MPa	(ksi)]
D-N-1	-	-	-	-	-	-	-	-
D-N-2	3.9	(0.56)	5.4	(0.79)	6.6	(0.95)	8.8	(1.27)
D-N-3	3.5	(0.51)	5.3	(0.77)	6.9	(1.00)	9.0	(1.30)
D-N-4	5.8	(0.83)	6.6	(0.96)	7.5	(1.08)	9.9	(1.44)
D-N-5	5.8	(0.84)	6.9	(1.00)	7.9	(1.14)	9.8	(1.42)
D-N Average	4.7	(0.69)	6.1	(0.88)	7.2	(1.04)	9.4	(1.36)
Std. Dev.	1.0	(0.15)	0.7	(0.10)	0.5	(0.07)	0.5	(0.07)
Chauvenet's Upper	6.3	(0.92)	7.2	(1.04)	8.0	(1.16)	10.1	(1.47)
Limit Lower	3.1	(0.46)	5.0	(0.72)	6.4	(0.93)	8.6	(1.25)

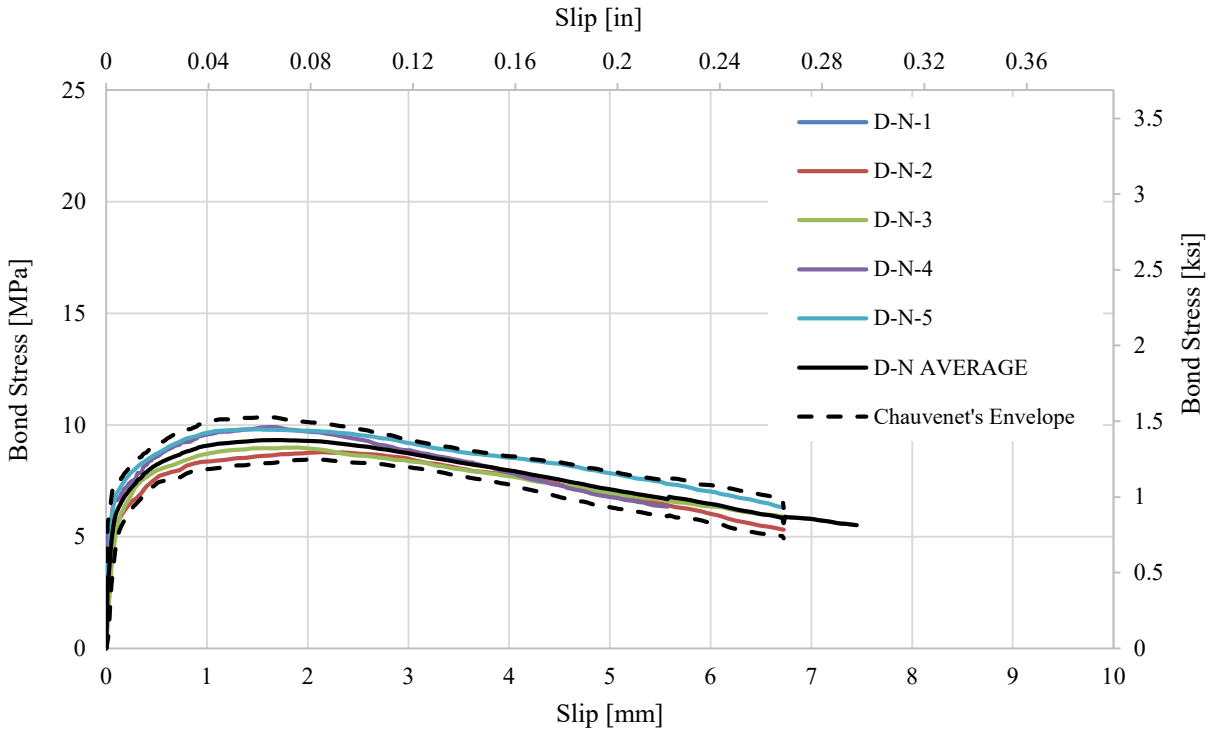

Figure 4-3: Free-End Slip for Dry Consolidation Tow with No-sand Coating (D-N)

As shown in Table 4-3, the average bond stress for the free-end causing slippage of 0.05 mm (0.002 in), 0.1 mm (0.004 in), and 0.25 mm (0.01 in) were 4.7 MPa (0.69 ksi), 6.1 MPa (0.88 ksi), and 7.2 MPa (1.0 ksi), respectively. The average maximum bond stress for the D-N configuration was 9.4 MPa (1.36 ksi). Figure 4-3 shows slippage curves for the free-end. Sample D-N-5 recorded the highest maximum bond stress and Sample D-N-2 the lowest.

Figure 4-4, Table 4-4 and Figure 4-5 show plots of the loaded-end deflection against load, bond stress data and bond against slip of the loaded-end, respectively.

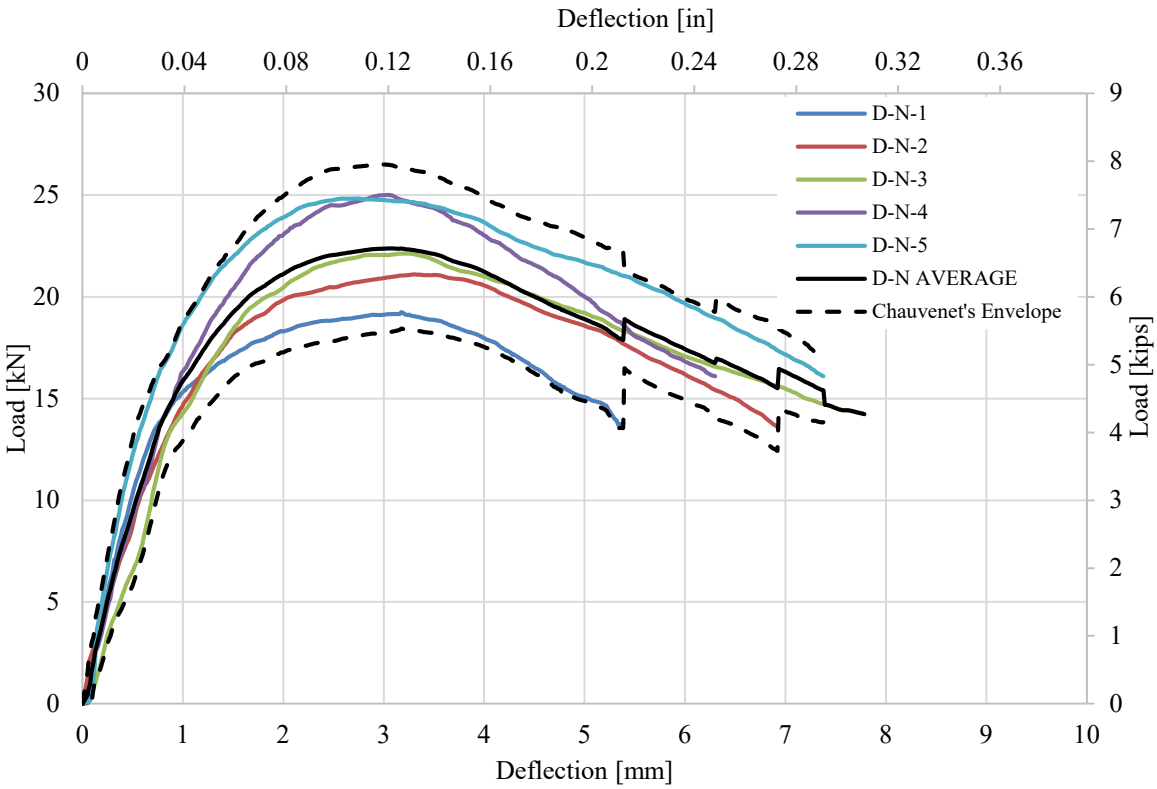

Figure 4-4: Loaded-End Deflections for Dry Consolidation Tow With No-sand Coating (D-N)

Table 4-4: Loaded-End Bond Stress for Dry Consolidation Tow with No-sand Coating (D-N)

Specimen I.D.		Bond Stress Corresponding to Slip Length of 0.05 mm (0.002 in) [MPa]	(psi)]	0.1 mm (0.004 in) [MPa]	(ksi)]	0.25 mm (0.01 in) [MPa]	(ksi)]	Maximum Bond Stress [MPa]	(ksi)]
D-N-1		3.3	(0.48)	4.5	(0.65)	5.6	(0.82)	7.6	(1.10)
D-N-2		2.9	(0.42)	3.9	(0.56)	5.6	(0.81)	8.8	(1.27)
D-N-3		2.1	(0.30)	2.9	(0.43)	4.9	(0.71)	9.0	(1.30)
D-N-4		5.8	(0.83)	6.6	(0.96)	7.5	(1.08)	9.9	(1.44)
D-N-5		5.3	(0.77)	6.0	(0.87)	7.2	(1.04)	9.8	(1.42)
D-N Average		3.9	(0.56)	4.8	(0.69)	6.1	(0.89)	9.0	(1.31)
Std. Dev.		1.4	(0.21)	1.4	(0.20)	1.0	(0.15)	0.8	(0.12)
Chauvenet's	Upper	6.2	(0.90)	7.0	(1.02)	7.8	(1.13)	10.4	(1.51)
Limit	Lower	1.5	(0.22)	2.5	(0.37)	4.5	(0.65)	7.6	(1.11)

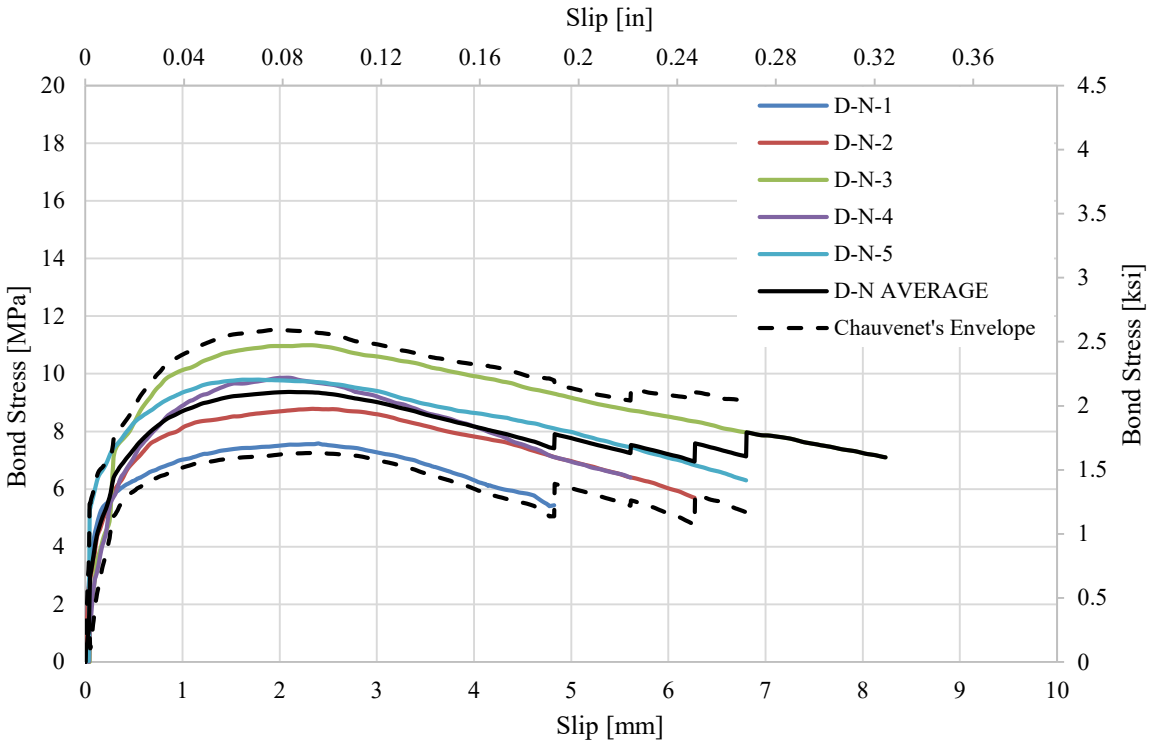

Figure 4-5: Loaded-End Slip for Dry Consolidation Tow with No-sand Coating (D-N)

As shown in Table 4-4, the average bond stress for the loaded-end causing slippage of 0.05 mm (0.002 in), 0.1 mm (0.004 in), and 0.25 mm (0.01 in) were 3.88 MPa (0.56 ksi), 4.79 MPa (0.69 ksi), and 6.14 MPa (0.89 ksi) respectively. The average maximum bond stress was 9.01 MPa (1.31 ksi). Figure 4-5 show slippage graphs for the loaded-end. Sample D-N-3 recorded the highest maximum bond stress and Sample D-N-1 the lowest.

4.2.2 Prepreg Consolidation Tow with No-sand Coating (P-N) Results

The P-N configuration consisted of rebar samples that were consolidated with prepreg aramid tow without sand coating. Table 4-5 presents a summary of the rebar configuration properties showing the measured results from each specimen that was tested along with the combined overall average of the samples consisting this configuration.

Table 4-5: Rebar Properties for Prepreg Consolidation Tow with No-sand Coating (P-N)

Specimen I.D.		Cross Section Area		Young's modulus	
		[mm^2	(in^2)]	[GPa	(Msi)]
P-N-1		132	(0.204)	49.4	(7.16)
P-N-2		128	(0.199)	51.6	(7.48)
P-N-3		112	(0.174)	48.2	(6.99)
P-N-4		112	(0.173)	48.3	(7.00)
P-N-5		122	(0.189)	48.0	(6.96)
P-N Average		121	(0.188)	49.1	(7.12)
Std. Dev.		8.15	(0.013)	1.34	(0.19)
Chauvenet's Limit	Upper	135	(0.209)	51.3	(7.44)
	Lower	108	(0.167)	46.9	(6.80)

Figure 4-6 show the stress-strain curves of the configurations. These stress-strain curves indicate Young's modulus for each individual specimen in the P-N configuration along with an average and Chauvenet's envelope for lower and upper limits.

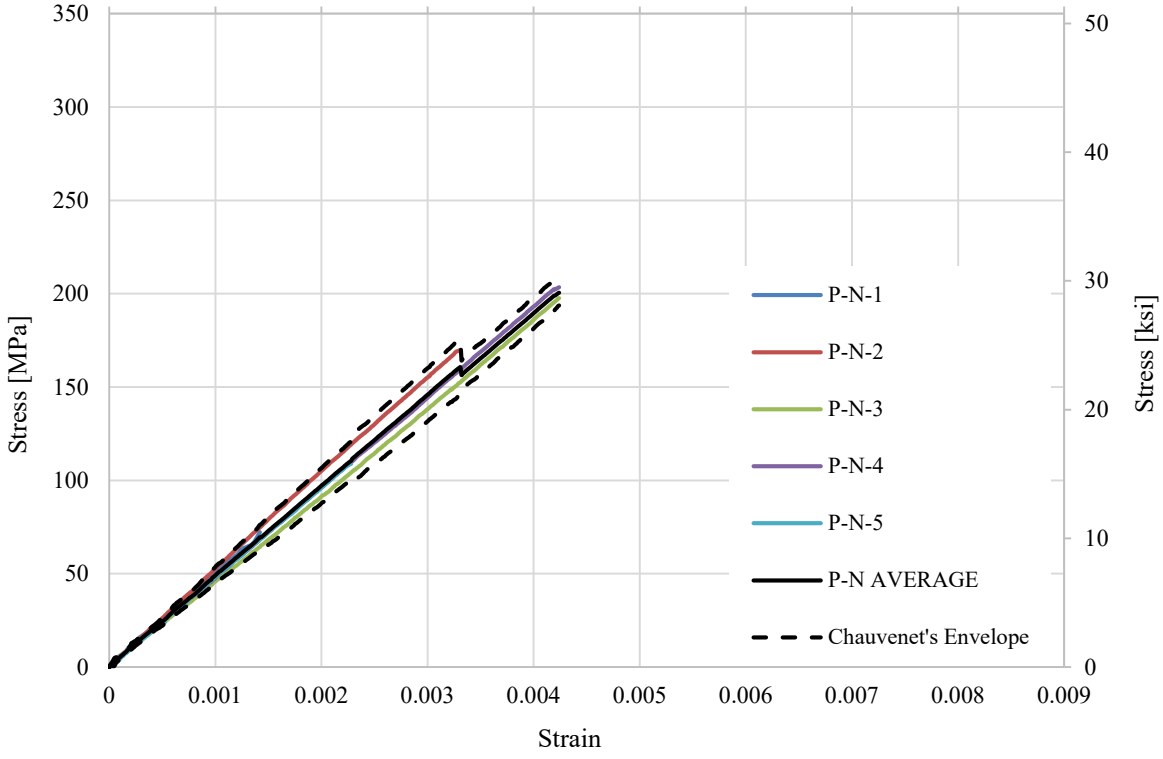

Figure 4-6: Stress-Strain Plots for Prepreg Consolidation Tow With No-sand Coating (P-N)

As shown in Table 4-5 and Figure 4-6, the average Young's modulus for the P-N samples was 49.1 GPa (7.12 Msi). The average nominal diameter of the specimens was 122 mm^2 (0.188 in^2).

Figure 4-7 and Table 4-6 show the free-end deflection against load, bond stress data respectively. Figure 4-8 show curves of bond stress against slip of the free-end.

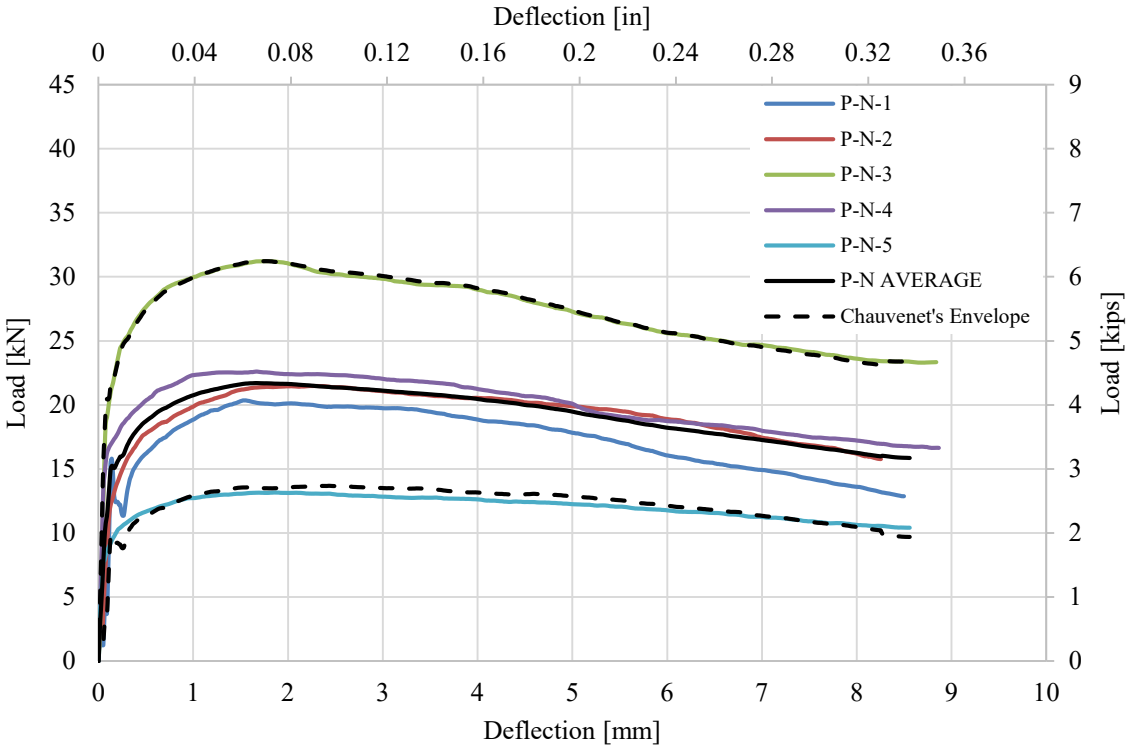

Figure 4-7: Free-End Deflections for Prepreg Consolidation Tow With No-sand Coating (P-N)

Table 4-6 Free-End Bond Stress for Prepreg Consolidation Tow with No-sand Coating (P-N)

Specimen I.D.		Bond Stress Corresponding to Slip Length of 0.05 mm (0.002 in)		0.1 mm (0.004 in)		0.25 mm (0.01 in)		Maximum Bond Stress	
		[MPa	(ksi)]	[MPa	(ksi)]	[MPa	(ksi)]	[MPa	(ksi)]
P-N-1		4.0	(0.58)	4.7	(0.68)	5.7	(0.83)	7.9	(1.14)
P-N-2		1.5	(0.21)	4.0	(0.58)	5.9	(0.86)	8.5	(1.23)
P-N-3		7.1	(1.04)	8.9	(1.29)	10.6	(1.53)	13.1	(1.90)
P-N-4		5.6	(0.82)	7.0	(1.01)	7.7	(1.12)	9.5	(1.38)
P-N-5		2.4	(0.34)	3.6	(0.52)	4.2	(0.62)	5.3	(0.77)
P-N Average		4.1	(0.60)	5.6	(0.81)	6.8	(0.99)	8.8	(1.28)
Std. Dev.		2.1	(0.30)	2.0	(0.29)	2.2	(0.31)	2.5	(0.37)
Chauvenet's	Upper	7.5	(1.09)	8.9	(1.29)	10.4	(1.51)	13.0	(1.89)
Limit	Lower	0.7	(0.10)	2.3	(0.34)	3.3	(0.47)	4.7	(0.68)

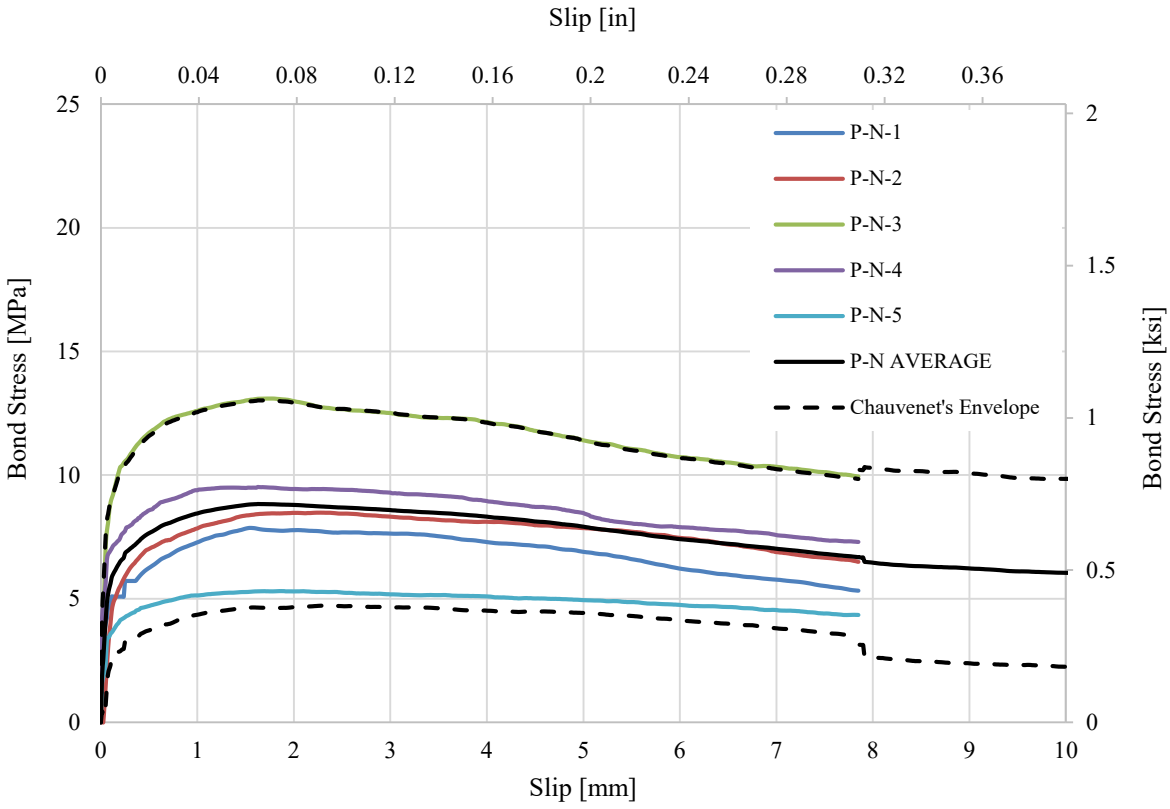

Figure 4-8: Free-End Slip for Prepreg Consolidation Tow With No-sand Coating (P-N)

As shown in Table 4-6, the average bond stress for the free-end causing slippage of 0.05 mm (0.002 in), 0.1 mm (0.004 in), and 0.25 mm (0.01 in) were 4.12 MPa (0.60 ksi), 5.61 MPa (0.81 ksi), and 6.83 MPa (0.99 ksi) respectively. The average maximum bond stress was 8.85 MPa (1.28 ksi). Figure 4-8 shows slippage curves for the free-end. Sample P-N-3 recorded highest maximum bond stress and Sample P-N-5 the lowest.

Deflection plots of the loaded-end are shown in Figure 4-9 along with Chauvenet's envelop signifying both the upper and lower limits of the curves. Table 4-7 and Figure 4-10 show bond stress data, and bond stress graphs for the loaded-end respectively.

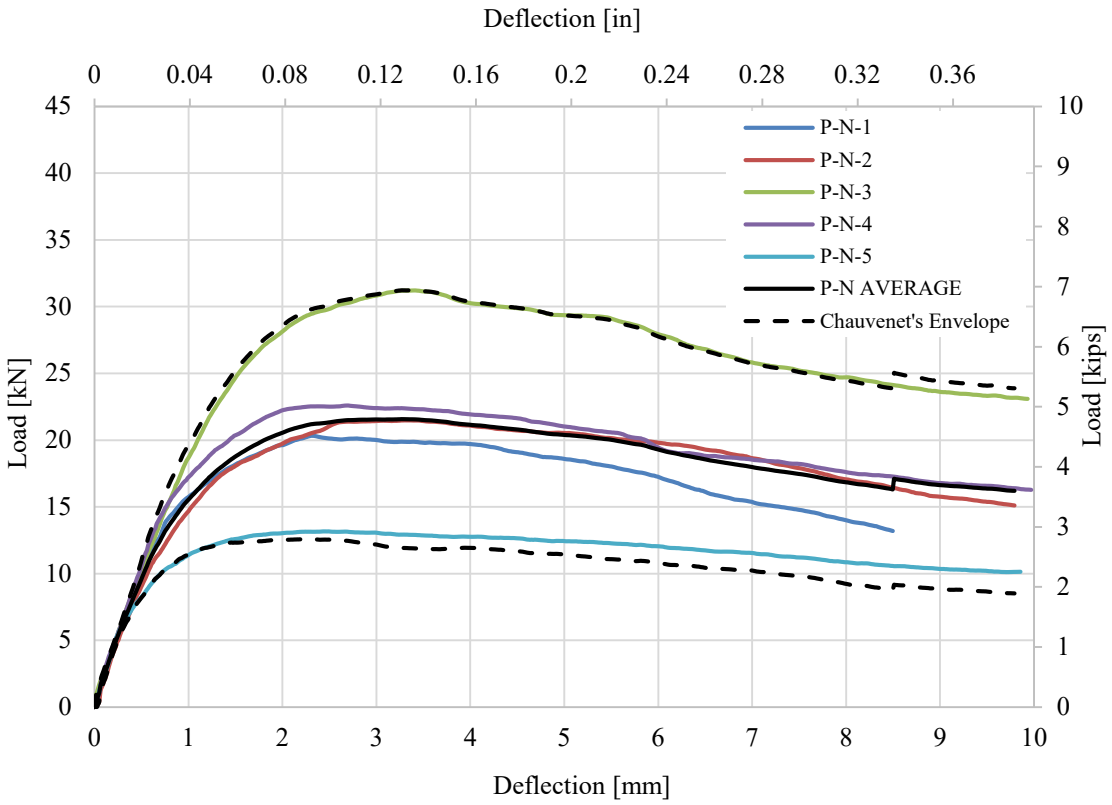

Figure 4-9: Loaded-End Deflections for Prepreg Consolidation Tow With No-sand Coating (P-N)

Table 4-7: Loaded-End Bond Stress for Prepreg Consolidation Tow with No-sand Coating (P-N)

Specimen I.D.		Bond Stress Corresponding to Slip Length of 0.05 mm (0.002 in)		0.1 mm (0.004 in)		0.25 mm (0.01 in)		Maximum Bond Stress	
		[MPa	(ksi)]	[MPa	(ksi)]	[MPa	(ksi)]	[MPa	(psi)]
P-N-1		1.9	(0.28)	2.9	(0.42)	5.3	(0.77)	7.9	(1.14)
P-N-2		2.3	(0.34)	3.4	(0.49)	5.0	(0.73)	8.5	(1.23)
P-N-3		3.6	(0.51)	5.1	(0.74)	7.9	(1.15)	12.3	(1.79)
*P-N-4**		*6.1*	*(0.89)*	*6.7*	*(0.96)*	7.5	(1.09)	9.5	(1.38)
P-N-5		2.5	(0.36)	2.9	(0.43)	3.8	(0.55)	5.2	(0.75)
P-N Average		3.3	(0.48)	4.2	(0.61)	5.9	(0.86)	8.7	(1.26)
Std. Dev.		1.5	(0.22)	1.5	(0.21)	1.6	(0.23)	2.3	(0.34)
Chauvenet's	Upper	5.8	(0.84)	6.6	(0.96)	8.5	(1.23)	12.5	(1.81)
Limit	Lower	0.8	(0.11)	1.8	(0.26)	3.3	(0.48)	4.9	(0.71)
P-N Average	Revised	2.6	(0.37)	3.6	(0.52)	5.5	(0.80)	8.7	(1.26)
Std. Dev.		0.6	(0.09)	0.9	(0.13)	1.6	(0.23)	2.3	(0.34)

*Specimen eliminated using Chauvenet's criterion; data not included in revised average or standard deviation

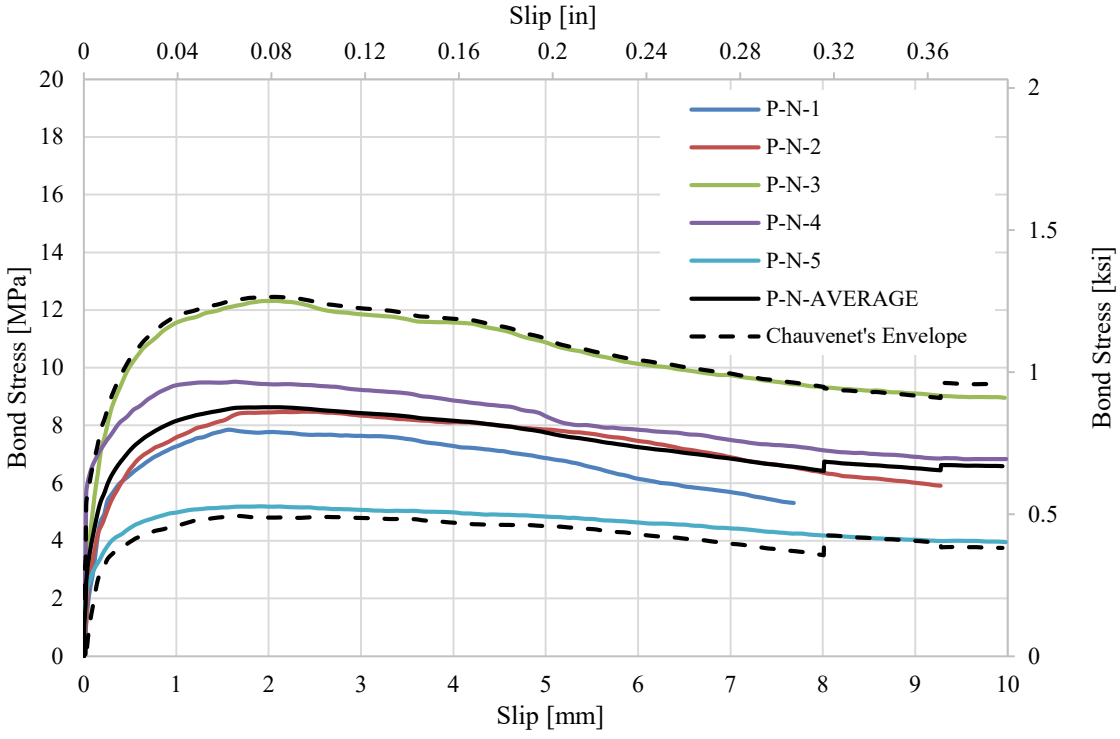

Figure 4-10: Loaded-End Slip for Prepreg Consolidation Tow With No-sand Coating (P-N)

As shown in Table in 4-7, the average bond stresses for the loaded-end causing slippage of 0.05 mm (0.002 in), 0.1 mm (0.004 in), and 0.25 mm (0.01 in) were 2.57 MPa (373 Psi), 3.59 MPa (0.52 ksi), and 5.91 MPa (0.86 ksi) respectively. Average maximum bond stress was 8.67 MPa (1.26 ksi). Sample P-N-4 fell out of the Chauvenet's limits for bond stress values corresponding to slip lengths of 0.05 mm (0.002 in) and 0.1 mm (0.004 in). The average bond stress values were recalculated excluding P-N-4. Figure 4-10 show slippage graphs for the loaded-end. Sample P-N-3 recorded the highest maximum bond stress and Sample P-N-5 the lowest.

4.2.3 Dry Consolidation Tow with Sand Coating (D-S) Results

The D-S configuration consisted of rebar samples that were consolidated with dry aramid tow with sand coating. Table 4-8 presents a summary of the rebar configuration properties showing the measured results from each specimen that was tested along with the combined overall average of the samples consisting this configuration.

Table 4-8 Rebar Properties for Dry Consolidation Tow with Sand Coating (D-S)

Specimen I.D.		Cross Section Area		Young's modulus	
		[mm^2	(in^2)]	[GPa	(Msi)]
D-S-1		126	(0.196)	48.3	(7.00)
D-S-2		128	(0.198)	47.7	(6.92)
D-S-3		129	(0.200)	43.8	(6.35)
D-S-4		130	(0.201)	42.6	(6.17)
D-S-5		128	(0.198)	47.6	(6.90)
D-S Average		128	(0.199)	46.0	(6.67)
Std. Dev.		1.12	(0.002)	2.34	(0.34)
Chauvenet's Limit	Upper	130	(0.201)	49.8	(7.22)
	Lower	126	(0.196)	42.1	(6.11)

Figure 4-11 show the stress-strain curves of the configurations. These stress-strain curves indicate Young's modulus for each individual specimen in the D-S configuration along with an average and Chauvenet's envelope for lower and upper limits.

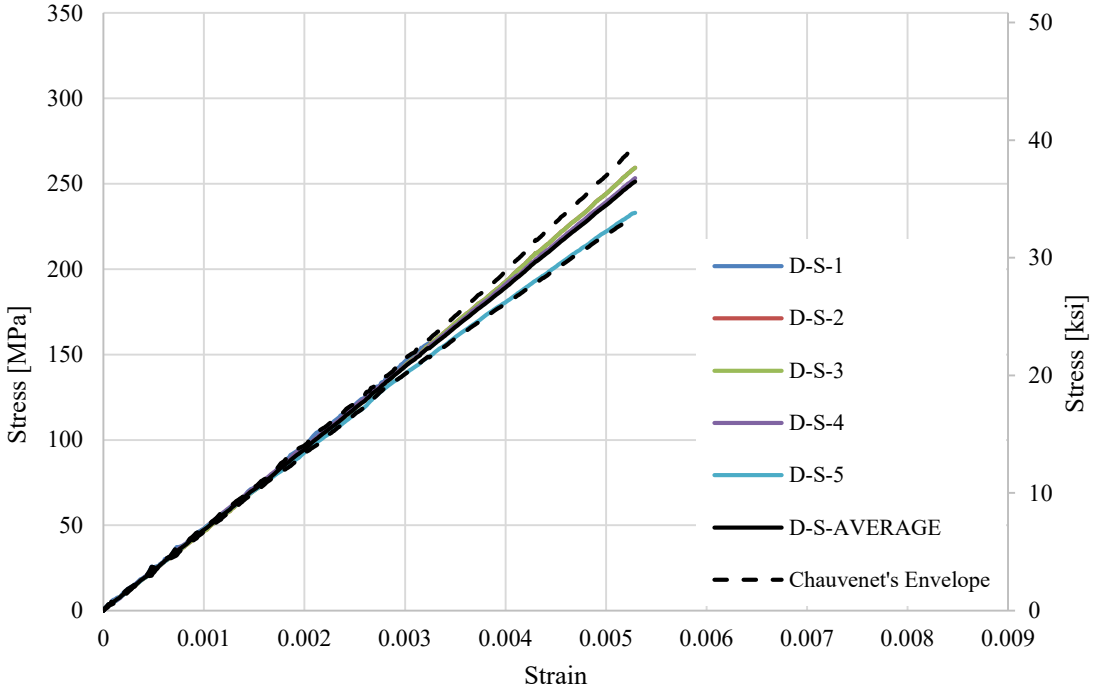

Figure 4-11: Stress-Strain Plots for Dry Consolidation Tow with Sand Coating (D-S)

As shown in Table 4-8 and Figure 4-11, the average Young's modulus for the D-S samples was 46.0 GPa (6.67 Msi). The average nominal diameter of the specimens was 122 mm^2 (0.199 in^2).

Figure 4-12 show curves of the free-end deflection against load for the dry tow consolidated with no sand samples, while Table 4-9 and Figure 4-13 show bond stress and slippage data of the free-end respectively.

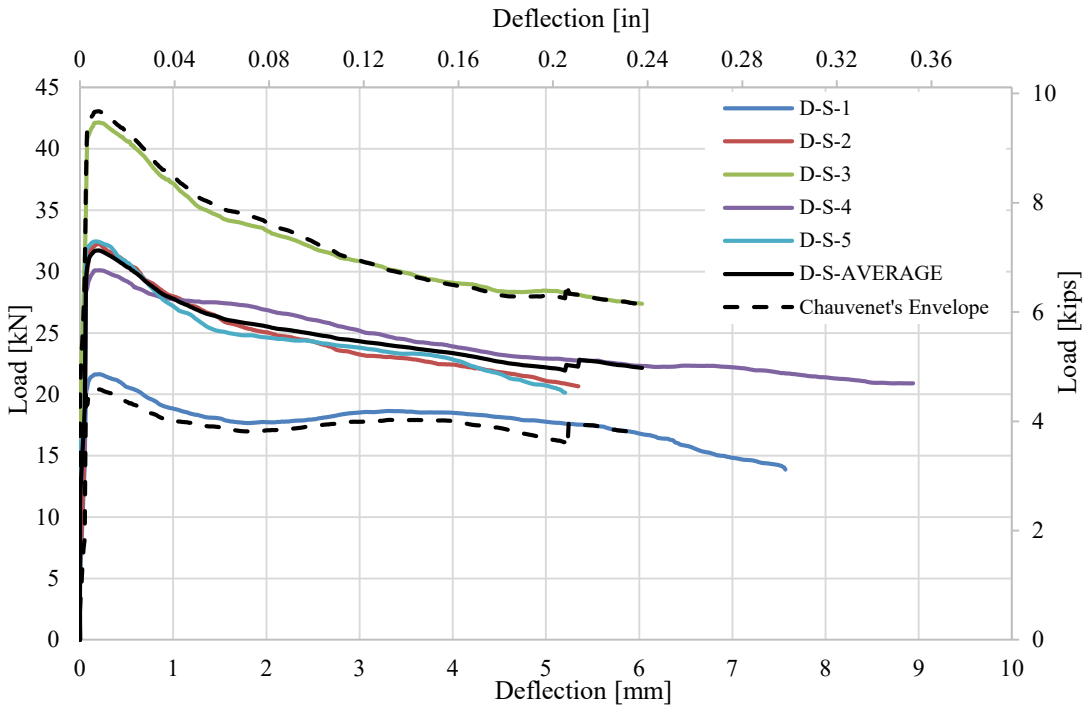

Figure 4-12: Free-End Deflections for Dry Consolidation Tow with Sand Coating (D-S)

Table 4-9: Free-End Bond Stress for Dry Consolidation Tow with Sand Coating (D-S)

Specimen I.D.		Bond Stress Corresponding to Slip Length of 0.05 mm (0.002 in) [MPa	(ksi)]	0.1 mm (0.004 in) [MPa	(ksi)]	0.25 mm (0.01 in) [MPa	(ksi)]	Maximum Bond Stress [MPa	(ksi)]
D-S-1		7.03	(1.02)	7.97	(1.16)	8.1	(1.18)	8.2	(1.18)
D-S-2		10.5	(1.52)	12.0	(1.74)	12.3	(1.78)	12.4	(1.80)
*D-S-3**		*17.5*	*(2.54)*	*18.3*	*(2.65)*	*18.6*	*(2.70)*	*18.7*	*(2.71)*
D-S-4		11.2	(1.62)	12.3	(1.78)	12.6	(1.82)	12.7	(1.84)
D-S-5		11.6	(1.68)	12.1	(1.75)	12.1	(1.76)	12.2	(1.76)
D-S Average		11.6	(1.68)	12.5	(1.82)	12.7	(1.85)	12.8	(1.86)
Std. Dev.		3.39	(0.49)	3.31	(0.48)	3.4	(0.49)	3.4	(0.49)
Chauvenet's Limit	Upper	17.2	(2.49)	18.0	(2.60)	18.3	(2.65)	18.4	(2.66)
	Lower	5.99	(0.87)	7.08	(1.03)	7.2	(1.05)	7.3	(1.05)
D-S Average	Revised	10.1	(1.46)	11.1	(1.61)	11.3	(1.64)	11.4	(1.65)
Std. Dev.		9.6	(0.70)	5.01	(0.73)	5.1	(0.74)	5.1	(0.74)

*Specimen eliminated using Chauvenet's criterion; data not included in final average or standard deviation

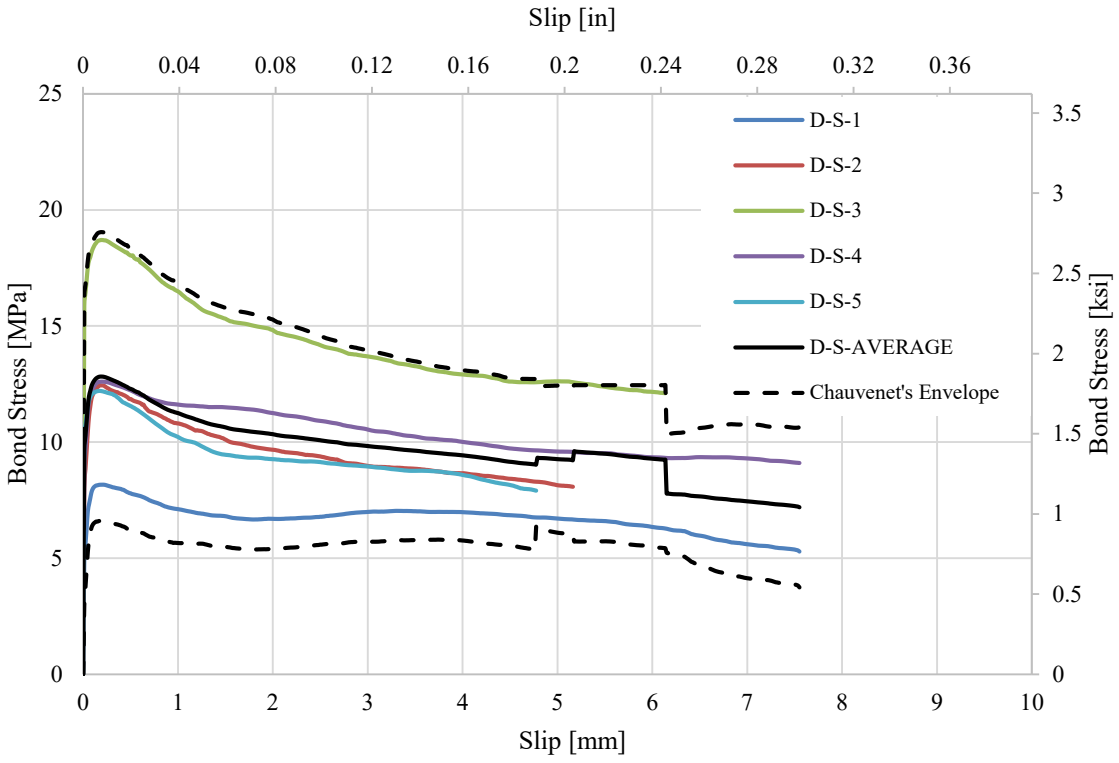

Figure 4-13: Free-End Slip for Dry Consolidation Tow with Sand Coating (D-S)

As shown in Table 4-9, the average bond stresses for the free-end causing slippage of 0.05 mm (0.002 in), 0.1 mm (0.004 in), and 0.25 mm (0.01 in) were 10.1 MPa (1.50 psi), 11.1 MPa (1.61 psi), and 11.3 MPa (1.64 ksi), respectively. The maximum average bond stress was 11.4 MPa (1.65 ksi). Sample D-S-3 fell out of the Chauvenet's limits, and the average bond stress values were recalculated excluding P-N-4. Figure 4-13 shows slippage curves for the free-end. Sample D-S-3 recorded highest maximum bond stress and Sample D-S-1 the lowest.

Deflection curves, bond stress data, and bond stress graphs for the loaded-end are shown in Figure 4-14, Table 4-10 and Figure 4-15, respectively.

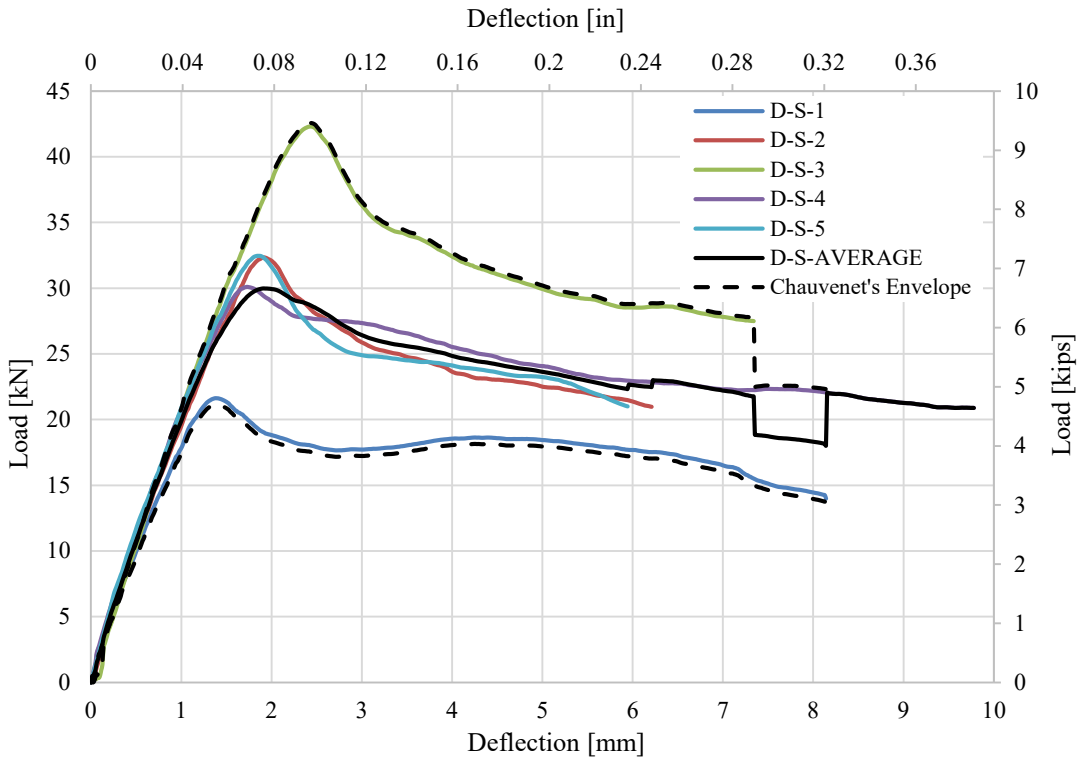

Figure 4-14: Loaded-End Deflections for Dry Consolidation Tow with Sand Coating (D-S)

Table 4-10: Loaded-End Bond Stress for Dry Consolidation Tow with Sand Coating (D-S)

Specimen I.D.		Bond Stress Corresponding to Slip Length of 0.05 mm (0.002 in)		0.1 mm (0.004 in)		0.25 mm (0.01 in)		Maximum Bond Stress	
		[MPa	(ksi)]	[MPa	(ksi)]	[MPa	(ksi)]	[MPa	(ksi)]
D-S-1		2.3	(0.34)	3.2	(0.47)	5.7	(0.83)	8.2	(1.18)
D-S-2		2.3	(0.34)	4.2	(0.61)	7.7	(1.11)	12.8	(1.86)
D-S-3		6.7	(0.98)	9.0	(1.31)	9.3	(1.35)	14.7	(2.13)
D-S-4		5.9	(0.86)	8.1	(1.17)	11.2	(1.62)	12.6	(1.83)
D-S-5		5.4	(0.79)	6.7	(0.98)	10.6	(1.54)	12.8	(1.86)
D-S Average		4.6	(0.66)	6.3	(0.91)	8.9	(1.29)	12.2	(1.77)
Std. Dev.		1.9	(0.27)	2.2	(0.32)	2.0	(0.29)	2.2	(0.31)
Chauvenet's	Upper	7.6	(1.10)	9.9	(1.43)	12.2	(1.77)	15.8	(2.29)
Limit	Lower	1.5	(0.22)	2.6	(0.38)	5.6	(0.81)	8.6	(1.25)

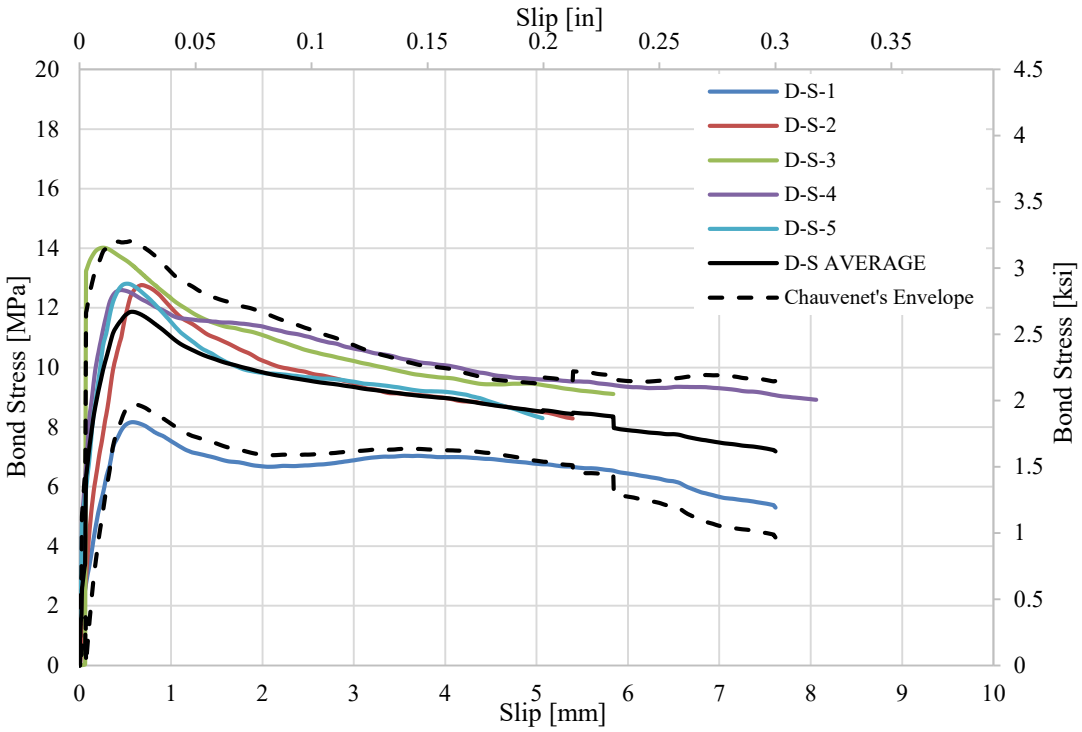

Figure 4-15: Loaded-End Slip for Dry Consolidation Tow with Sand Coating (D-S)

As shown in Table in 4-10, the average bond stresses for the loaded-end causing slippage of 0.05 mm (0.002 in), 0.1 mm (0.004 in), and 0.25 mm (0.01 in) were 4.55 MPa (0.66 ksi), 6.25 MPa (0.91 Ksi), and 8.90 MPa (1.29 ksi) respectively. The average maximum bond stress was 12.2 MPa (1771 Ksi). Figure 3-15 show slippage graphs for the loaded-end. Sample D-S-3 recorded the highest maximum bond stress and Sample D-S-1 the lowest.

4.2.4 Prepreg Consolidation Tow with Sand Coating (P-S) Results

The P-S configuration consisted of rebar samples that were consolidated with prepreg aramid tow with sand coating. Table 4-11 presents a summary of the rebar configuration properties showing the measured results from each specimen that was tested along with the combined overall average of the samples consisting this configuration.

Table 4-11: Rebar Properties for Prepreg Consolidation Tow with Sand Coating (D-S)

Specimen I.D.		Cross Section Area		Young's modulus	
		[mm^2	(in^2)]	[GPa	(Msi)]
P-S-1		126	(0.196)	47.2	(6.85)
P-S-2		125	(0.194)	47.9	(6.95)
P-S-3		122	(0.189)	48.5	(7.03)
P-S-4		122	(0.189)	48.4	(7.01)
P-S-5		128	(0.199)	47.0	(6.82)
P-S Average		125	(0.193)	47.8	(6.93)
Std. Dev.		2.44	(0.004)	0.60	(0.09)
Chauvenet's Limit	Upper	129	(0.200)	48.8	(7.07)
	Lower	121	(0.187)	46.8	(6.79)

Figure 4-16 show the stress-strain curves of the configurations. These stress-strain curves indicate Young's modulus for each individual specimen in the P-S configuration along with an average and Chauvenet's envelope for lower and upper limits.

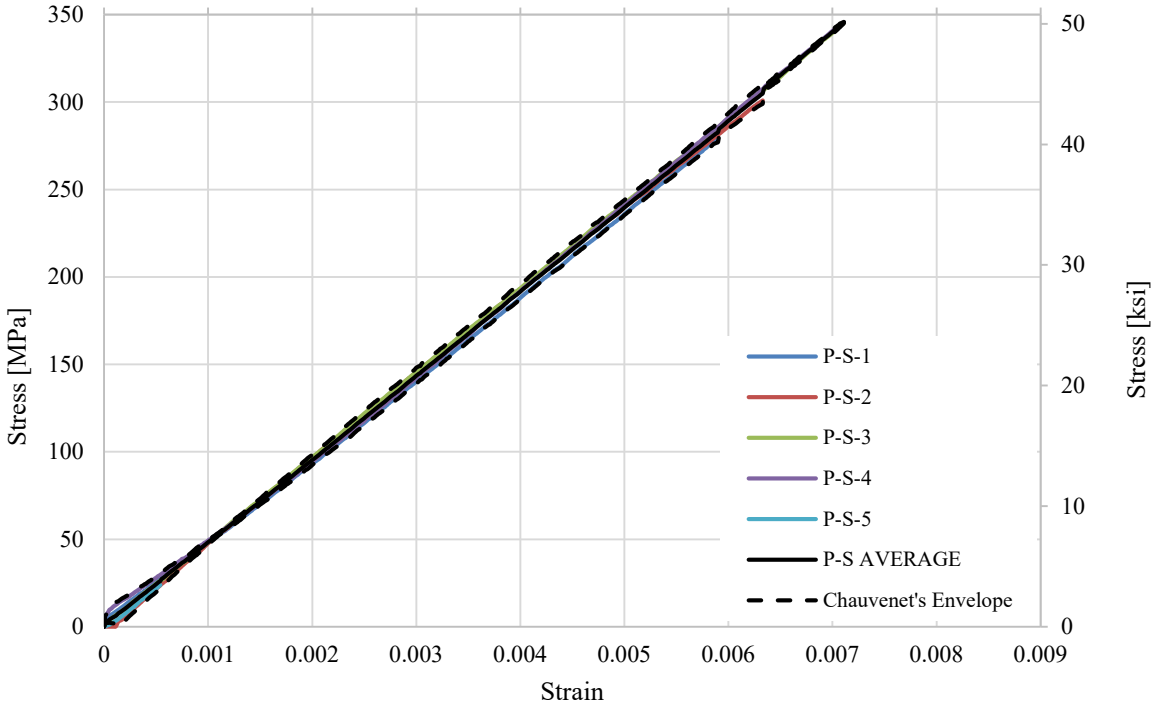

Figure 4-16: Stress-Strain Plots for Prepreg Consolidation Tow with Sand Coating (D-S)

As shown in table 4-11 and Figure 4-16, the average Young's modulus for the P-S samples was 47.8 GPa (6.93 Msi). The average nominal diameter of the specimens was 125 mm^2 (0.193 in^2).

Figures 4-17, Table 4-12 and Figure 4-18 show the deflection against load, bond stress data and bond against slip of the free-end, respectively.

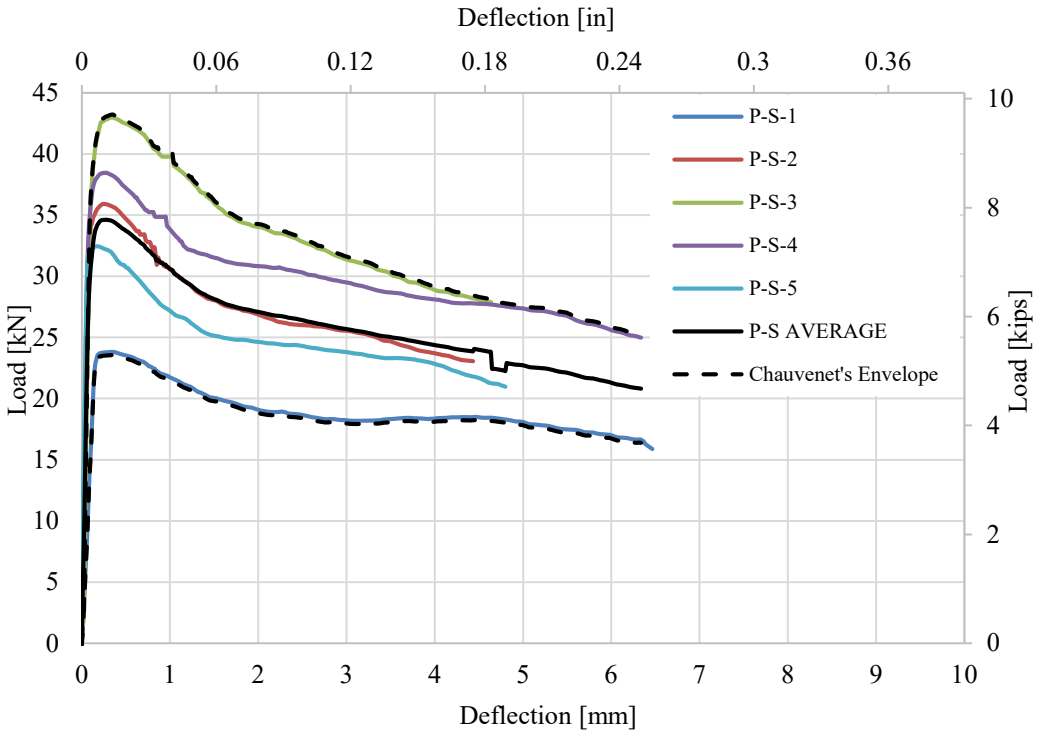

Figure 4-17: Free-End Deflections for Prepreg Consolidation Tow with Sand Coating (P-S)

Table 4-12: Free-End Bond Stress for Prepreg Consolidation Tow with Sand Coating (P-S)

Specimen I.D.		Bond Stress Corresponding to Slip Length of 0.05 mm (0.002 in) [MPa	(ksi)]	0.1 mm (0.004 in) [MPa	(ksi)]	0.25 mm (0.01 in) [MPa	(ksi)]	Maximum Bond Stress [MPa	(ksi)]
P-S-1		7.1	(1.03)	12.3	(1.78)	12.4	(1.79)	12.4	(1.80)
P-S-2		8.9	(1.29)	13.8	(2.01)	14.6	(2.12)	14.6	(2.12)
*P-S-3		11.9	(1.72)	20.1	(2.92)	23.9	(3.47)	24.0	(3.48)
P-S-4		10.9	(1.58)	15.0	(2.18)	16.2	(2.35)	16.2	(2.35)
P-S-5		10.4	(1.52)	12.3	(1.79)	19.2	(2.79)	19.2	(2.79)
P-S Average		9.8	(1.43)	14.7	(2.14)	17.3	(2.50)	17.3	(2.50)
Std. Dev.		1.7	(0.24)	2.9	(0.42)	4.0	(0.58)	4.0	(0.58)
Chauvenet's	Upper	11.8	(1.71)	19.5	(2.83)	23.8	(3.46)	23.9	(3.46)
Limit	Lower	7.1	(1.03)	10.0	(1.45)	10.7	(1.55)	10.7	(1.55)
P-S Average	Revised	9.3	(1.35)	13.4	(1.94)	15.6	(2.26)	15.6	(2.26)
Std. Dev.		1.5	(0.21)	1.1	(0.17)	2.5	(0.36)	2.5	(0.36)

*Specimen eliminated using Chauvenet's criterion; data not included in final average or standard deviation

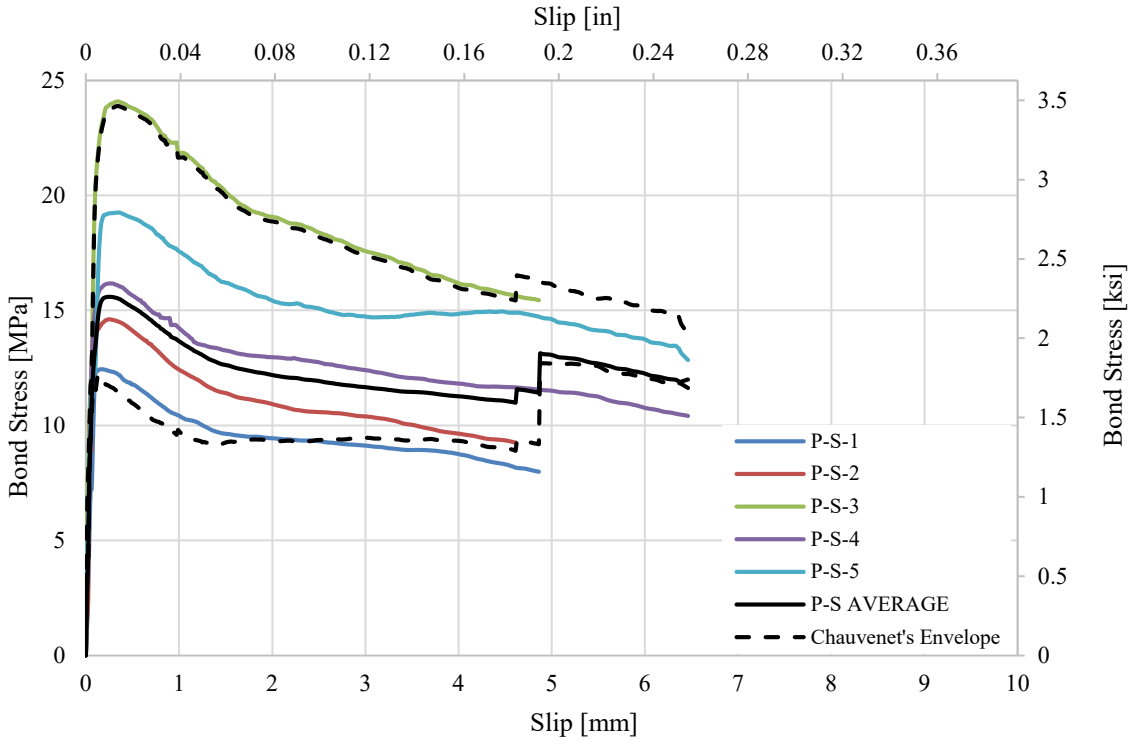

Figure 4-18: Free-End Slip for Prepreg Consolidation Tow with No-sand Coating (P-N)

As shown in table 4-12, the average bond stresses for the free-end causing slippage of 0.05 mm (0.002 in), 0.1 mm (0.004 in), and 0.25 mm (0.01 in) were 9.3 MPa (1.35 ksi), 13.4 MPa (1.94 ksi), and 15.6 MPa (2.26 ksi) respectively. Average maximum bond stress was 15.6 MPa (2.26 ksi).Figure 4-18 show slippage graphs for the free-end. Sample P-S-3 recorded the highest maximum bond stress and Sample P-S-1 the lowest.

Deflection plots, bond stress data, and bond stress graphs for the loaded-end are shown in Figure 4-19, Table 4-13 and Figure 4-20, respectively.

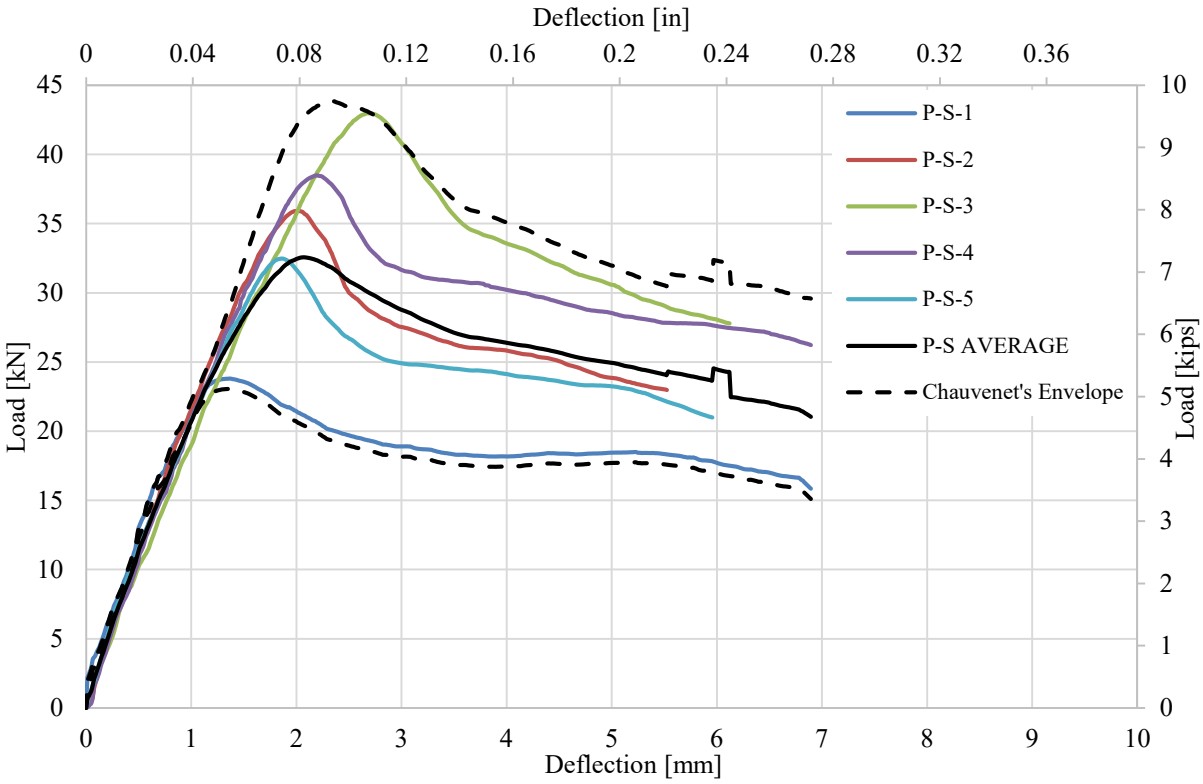

Figure 4-19: Loaded-End Deflections for Prepreg Consolidation Tow With Sand Coating (P-S)

Table 4-13: Loaded-End Bond Stress for Prepreg Consolidation Tow With Sand Coating (P-S)

Specimen I.D.		Bond Stress Corresponding to Slip Length of 0.05 mm (0.002 in)		0.1 mm (0.004 in)		0.25 mm (0.01 in)		Maximum Bond Stress	
		[MPa	(ksi)]	[MPa	(ksi)]	[MPa	(ksi)]	[MPa	(ksi)]
P-S-1		5.2	(0.76)	7.0	(1.01)	8.3	(1.20)	8.4	(1.22)
P-S-2		6.5	(0.95)	8.6	(1.25)	11.7	(1.70)	12.6	(1.83)
P-S-3		4.4	(0.63)	6.8	(0.98)	12.1	(1.75)	17.9	(2.60)
P-S-4		3.3	(0.48)	6.0	(0.87)	11.3	(1.64)	15.2	(2.20)
P-S-5		4.0	(0.58)	5.3	(0.77)	8.7	(1.26)	12.8	(1.86)
P-S Average		4.7	(0.68)	6.7	(0.98)	10.4	(1.51)	13.4	(1.94)
Std. Dev.		1.1	(0.16)	1.1	(0.16)	1.6	(0.23)	3.1	(0.46)
Chauvenet's	Upper	6.5	(0.94)	8.6	(1.24)	13.0	(1.89)	18.6	(2.69)
Limit	Lower	2.9	(0.41)	4.9	(0.71)	7.8	(1.13)	8.2	(1.19)

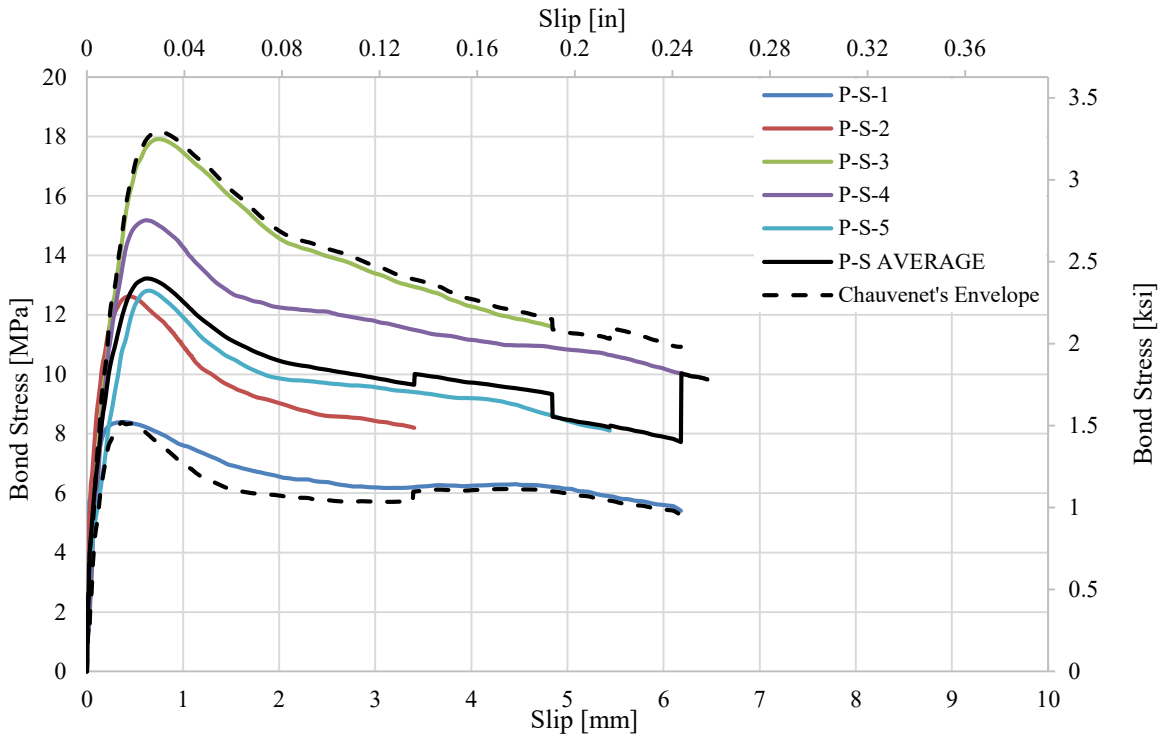

Figure 4-20: Loaded-End Slip for Prepreg Consolidation Tow with Sand Coating (P-S)

As shown in table in 4-13, the average bond stresses for the loaded-end causing slippage of 0.05 mm (0.002 in), 0.1 mm (0.004 in), and 0.25 mm (0.01 in) were 4.7 MPa (0.68 ksi), 6.74 MPa (0.98 ksi), and 10.4 MPa (1.51 ksi) respectively. Average maximum bond stress was 13.4 MPa (1.94 ksi). Sample P-S-3 recorded the highest maximum bond stress and Sample P-S-1 the lowest.

4.2.5 American Fiberglass Rebar, Sand-coated (A-S), Configuration

The A-S configuration consisted fiberglass/epoxy rebar purchased from American Fiberglass Rebar. The samples were coated with sand. Table 4-14 presents a summary of the rebar configuration properties showing the measured results from each specimen that was tested along with the combined overall average of samples consisting this configuration.

Table 4-14: Rebar Properties for American Fiberglass with Sand Coating (A-S)

Specimen I.D.		Cross Section Area		Young's modulus	
		[mm^2	(in^2)]	[GPa	(Msi)]
A-S-1		165	(0.255)	47.1	(6.83)
A-S-2		148	(0.229)	47.1	(6.83)
A-S-3		139	(0.216)	47.1	(6.82)
*A-S-4		137	(0.212)	44.2	(6.41)
A-S-5		132	(0.204)	49.0	(7.11)
A-S Average		144	(0.223)	46.9	(6.80)
Std. Dev.		11.5	(0.018)	1.54	(0.22)
Chauvenet's Limit	Upper	163	(0.253)	49.4	(7.17)
	Lower	125	(0.194)	44.4	(6.43)
A-S Average	Revised	146	(0.226)	47.6	(6.90)
Std. Dev.		12.2	(0.019)	0.83	(0.12)

*Specimen eliminated using Chauvenet's criterion; data not included in final average or standard deviation

Figure 4-21 show the stress-strain curves of the configurations. These stress-strain curves indicate Young's modulus for each individual specimen in the A-S configuration along with an average and Chauvenet's envelope for lower and upper limits.

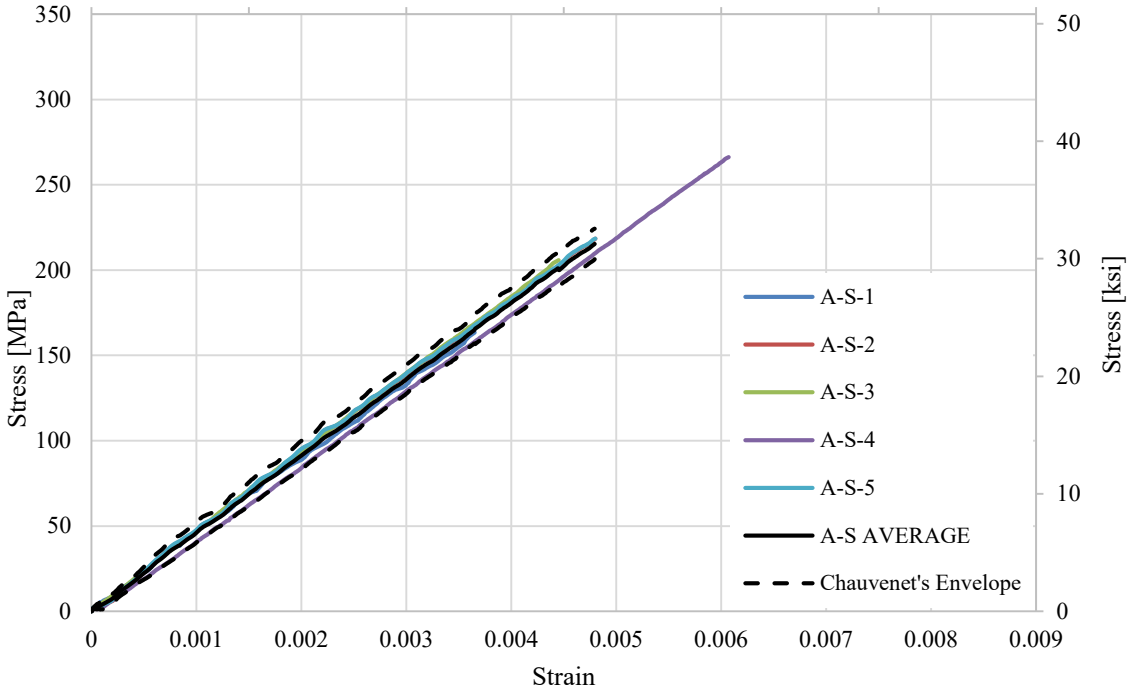

Figure 4-21: Stress-Strain plots for American Fiberglass Rebar Specimens

As shown in Table 4-14 and Figure 4-21, the average Young's modulus for the A-S samples was 47.6 GPa (6.90 Msi). The average nominal diameter of the specimens was 123 mm^2 (0.223 in^2).

Plots of deflection against load, bond stress data and bond stress against slip of the free-end are shown in Figure 4-22, Table 4-15 and Figure 4-23, respectively.

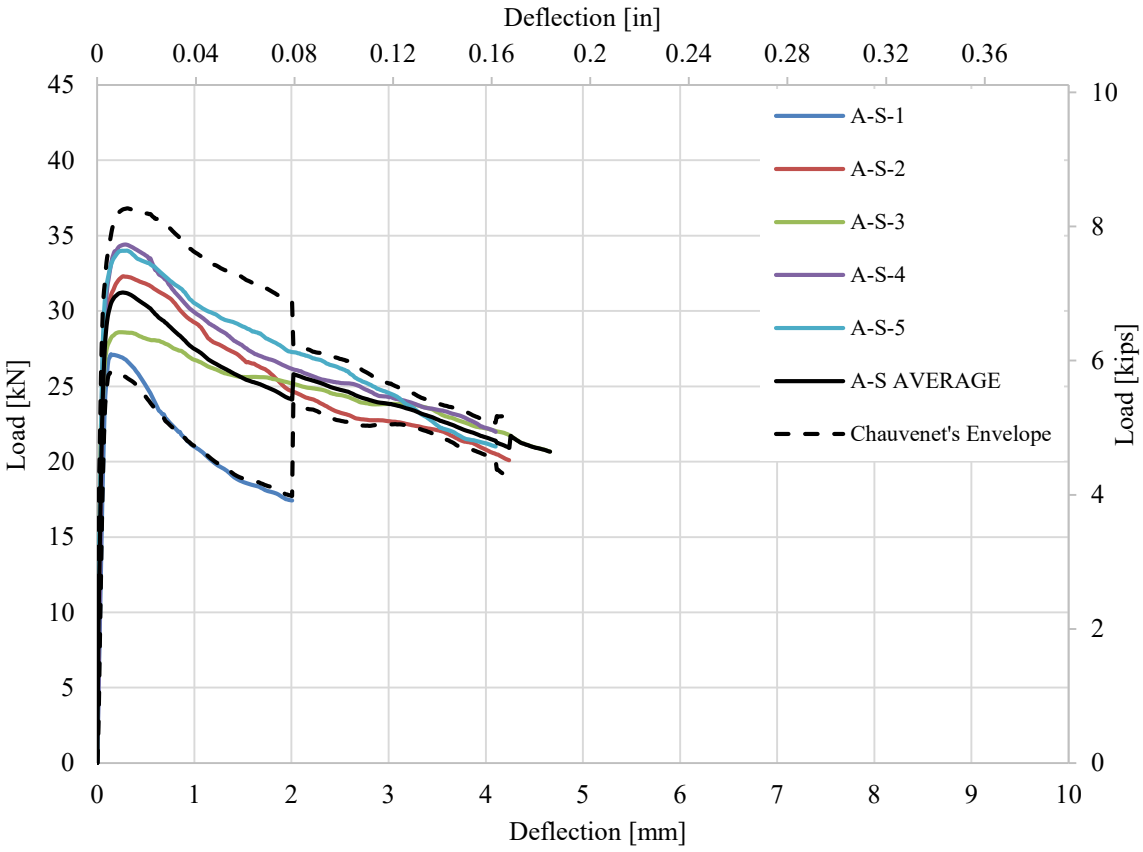

Figure 4-22: Free-End Deflections for American Fiberglass Rebar With Sand Coating (A-S)

Table 4-15: Free-End Bond Stress for American Fiberglass Rebar with Sand Coating (A-S)

Specimen I.D.		Bond Stress Corresponding to Slip Length of 0.05 mm (0.002 in) [MPa]	(ksi)]	0.1 mm (0.004 in) [MPa]	(ksi)]	0.25 mm (0.01 in) [MPa]	(ksi)]	Maximum Bond Stress [MPa]	(ksi)]
*A-S-1**		*5.9*	*(0.85)*	9.0	(1.31)	9.3	(1.35)	9.4	(1.36)
A-S-2		9.6	(1.4)	10.9	(1.58)	11.8	(1.71)	11.8	(1.71)
A-S-3		10.3	(1.5)	10.4	(1.51)	10.7	(1.55)	10.7	(1.55)
A-S-4		7.8	(1.1)	13.7	(1.99)	14.8	(2.15)	14.8	(2.15)
A-S-5		10.5	(1.5)	12.3	(1.78)	13.2	(1.91)	13.2	(1.91)
A-S Average		8.8	(1.28)	11.3	(1.63)	12.0	(1.74)	12.0	(1.74)
Std. Dev.		1.8	(0.25)	1.6	(0.23)	1.91	(0.28)	1.89	(0.27)
Chauvenet's Limit	Upper	11.7	(1.70)	13.9	(2.02)	15.1	(2.19)	15.08	(2.19)
	Lower	5.9	(0.86)	8.6	(1.25)	8.83	(1.28)	8.88	(1.29)
A-S Average	Revised	9.6	(1.39)	-	-	-	-	-	-
Std. Dev.		1.0	(0.15)	-	-	-	-	-	-

*Specimen eliminated using Chauvenet's criterion; data not included in final average or standard deviation

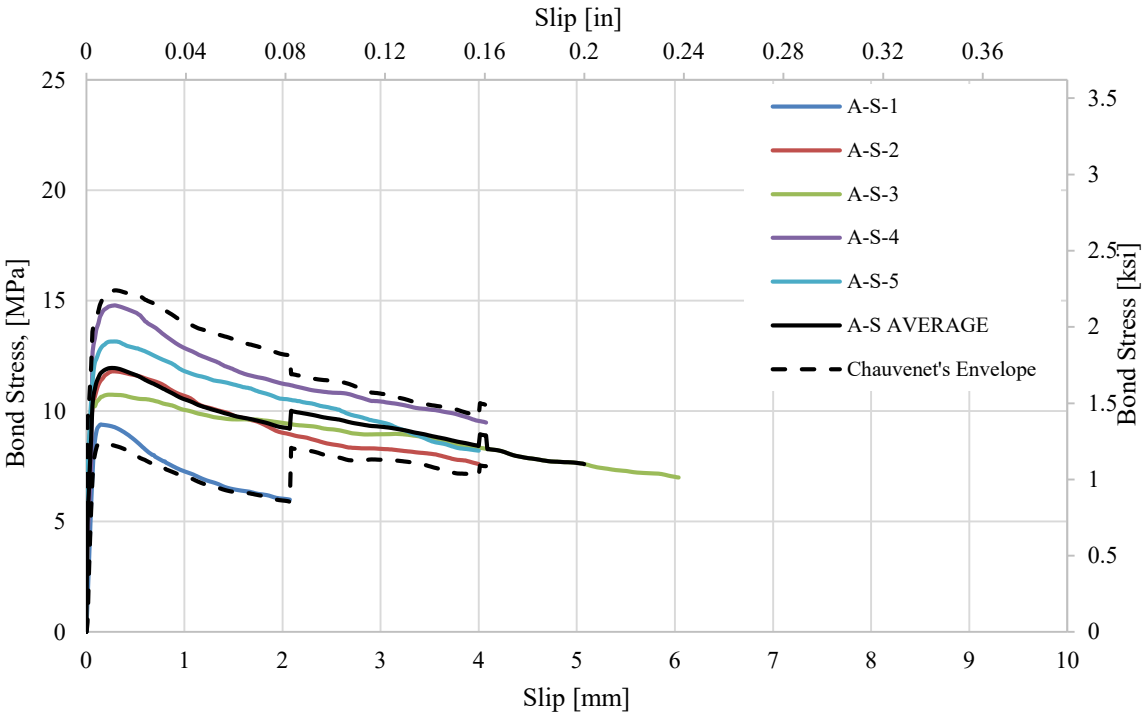

Figure 4-23: Free-End Slip for American Fiberglass Rebar with Sand Coating (A-S)

As shown in Table 4-15, the average bond stresses for the free-end causing slippage of 0.05 mm (0.002 in), 0.1 mm (0.004 in), and 0.25 mm (0.01 in) were 9.56 MPa (1.39 ksi), 11.3 MPa (1.63 ksi), and 12.0 MPa (1.74 ksi) respectively. Average maximum bond stress was 12.0 MPa (1.74 ksi).

Figure 4-23 show slippage graphs for the free-end. Sample A-S-4 recorded the highest maximum bond stress and Sample A-S-1 the lowest.

Deflection plots, bond stress data, and bond stress graphs for the loaded-end are shown in Figure 4-24, Table 4-16 and Figure 4-25, respectively.

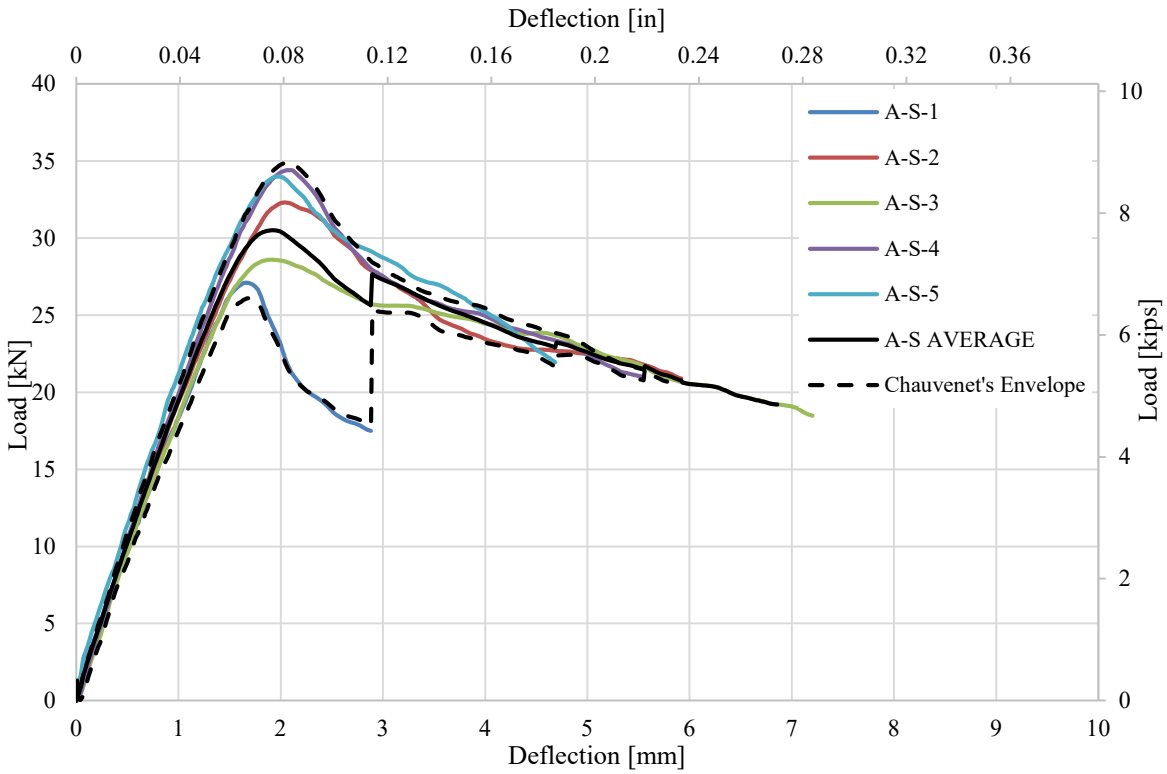

Figure 4-24: Loaded-End Deflections for American Fiberglass Rebar With Sand Coating (A-S)

Table 4-16: Loaded-End Bond Stress for American Fiberglass Rebar with Sand Coating (A-S)

Specimen I.D.		Bond Stress Corresponding to Slip Length of 0.05 mm (0.002 in)		0.1 mm (0.004 in)		0.25 mm (0.01 in)		Maximum Bond Stress	
		[MPa	(ksi)]	[MPa	(ksi)]	[MPa	(ksi)]	[MPa	(ksi)]
A-S-1		3.4	(0.49)	5.2	(0.76)	9.2	(1.33)	10.9	(1.58)
A-S-2		2.8	(0.41)	5.1	(0.74)	9.5	(1.37)	12.7	(1.84)
A-S-3		1.5	(0.22)	3.8	(0.55)	7.6	(1.10)	11.3	(1.64)
A-S-4		1.5	(0.21)	3.3	(0.48)	7.2	(1.04)	13.1	(1.90)
A-S-5		3.6	(0.53)	5.5	(0.80)	9.6	(1.39)	13.2	(1.91)
A-S Average		2.6	(0.37)	4.6	(0.67)	8.6	(1.25)	12.2	(1.78)
Std. Dev.		0.9	(0.13)	0.9	(0.13)	1.0	(0.14)	1.0	(0.14)
Chauvenet's	Upper	4.1	(0.59)	6.0	(0.87)	10.2	(1.48)	13.8	(2.00)
Limit	Lower	1.1	(0.15)	3.1	(0.46)	6.9	(1.01)	10.7	(1.55)

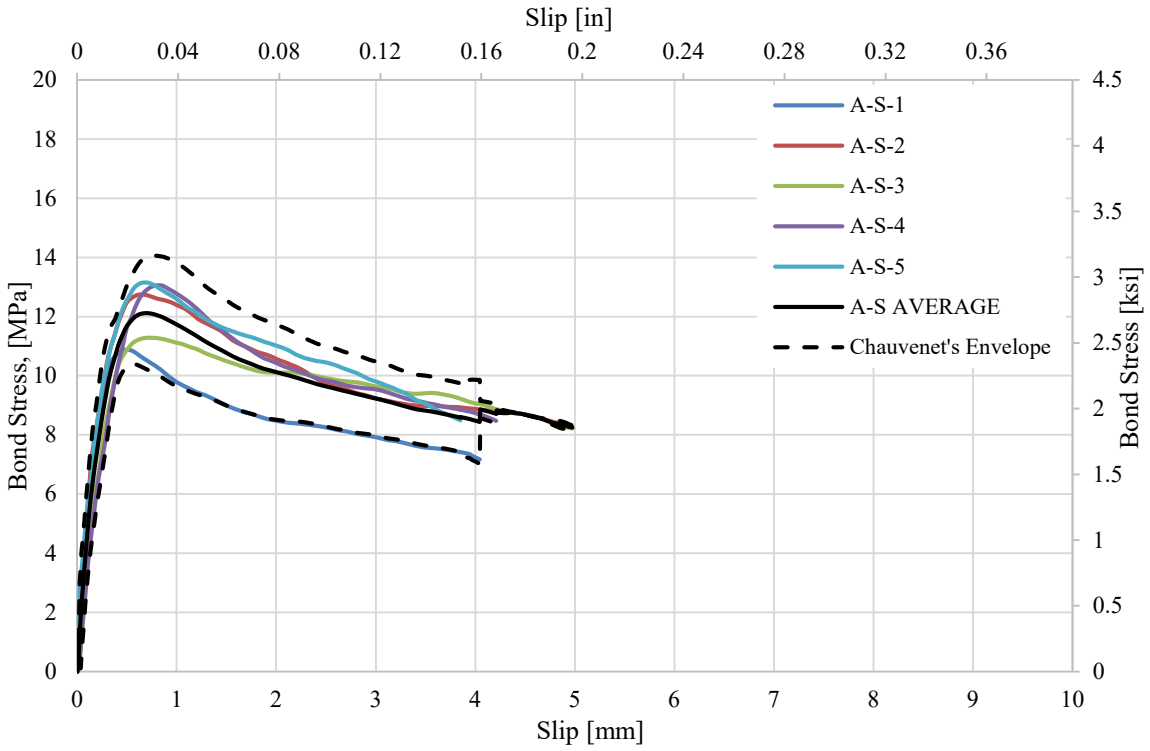

Figure 4-25: Loaded-End Slip for American Rebar Fiberglass with Sand Coating (A-S)

As shown in Table in 4-16, the average bond stresses for the loaded-end causing slippage of 0.05 mm (0.002 in), 0.1 mm (0.004 in), and 0.25 mm (0.01 in) were 2.56 MPa (0.37 ksi), 4.59 MPa (0.67 ksi), and 8.59 MPa (1.25 ksi) respectively. Average maximum bond stress was 12.2 MPa (1.78 ksi). Figure 4-25 show slippage graphs for the loaded-end. Sample A-S-5 recorded the highest maximum bond stress and Sample A-S-1 the lowest.

4.2.6 Plain Steel (S-N) Configuration

The S-N rebar configuration was one of the rebar configuration that was purchased. It comprised of plain steel rebar. Table 4-17 is a summary of the rebar configuration properties showing the measured results from each specimen that was tested along with the combined overall average of samples consisting this configuration.

Table 4-17 Properties for Plain Steel Rebar (S-N)

Specimen I.D.		Cross Section Area		Young's modulus	
		[mm^2	(in^2)]	[GPa	(Msi)]
S-N-1		126	(0.196)	189	(27.3)
S-N-2		126	(0.196)	190	(27.6)
S-N-3		126	(0.196)	224	(32.5)
S-N-4		126	(0.196)	194	(28.2)
S-N-5		126	(0.196)	193	(28.0)
S-N Average		126	(0.196)	198	(28.7)
Std. Dev.		0.00	(0.000)	13.2	(1.91)
Chauvenet's Limit	Upper	126	(0.196)	220	(31.9)
	Lower	126	(0.196)	176	(25.6)

Figure 4-26 show the stress-strain curves of the S-N configuration. These stress-strain curves indicate Young's modulus for each individual specimen in the S-N configuration along with an average and Chauvenet's envelope for lower and upper limits.

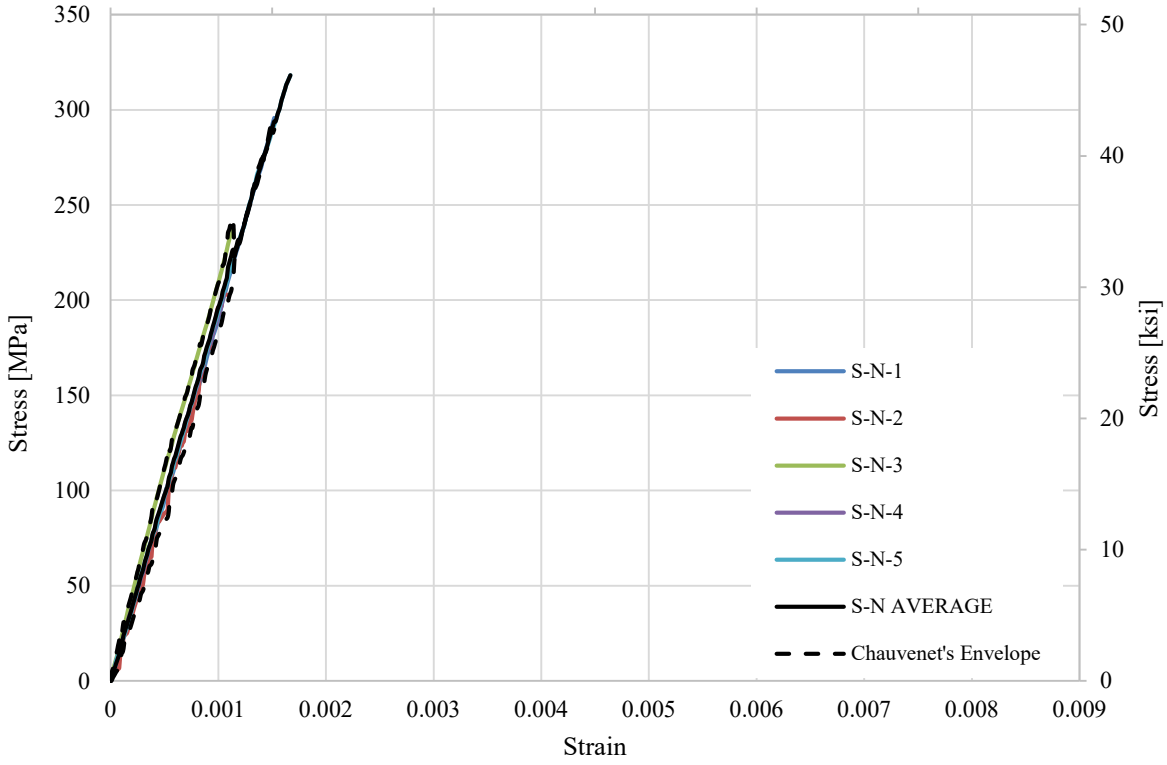

Figure 4-26: Stress-Strain Plots for Plain Steel Rebar

As shown in Table 4-17 and Figure 4-26, the average Young's modulus for the S-N samples was 198 GPa (28.7 Msi). The average area of the specimens was 126 mm^2 (0.196 in^2).

Figures 4-27, Table 4-18 and Figure 4-28 show the deflection against load, bond stress data and bond against slip of the free-end, respectively.

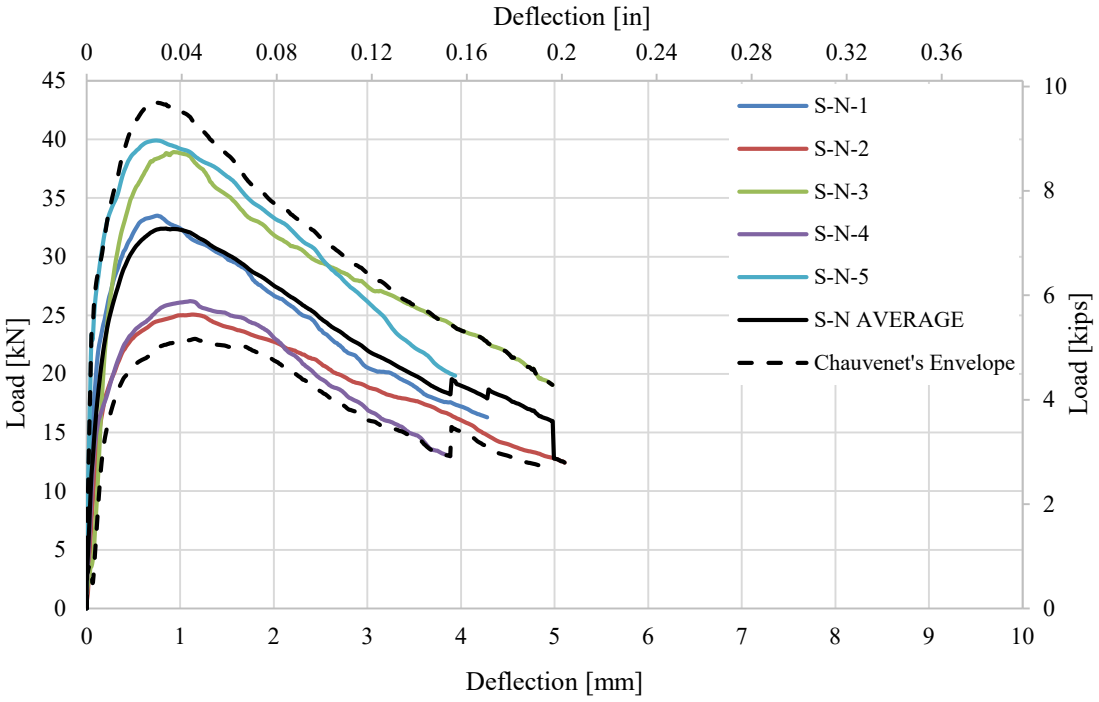

Figure 4-27: Free-End Deflections for Plain Steel Rebar (S-N)

Table 4-18: Free-End Bond Stress for Plain Steel Rebar (S-N)

Specimen I.D.		Bond Stress Corresponding to Slip Length of 0.05 mm (0.002 in) [MPa	(ksi)]	0.1 mm (0.004 in) [MPa	(ksi)]	0.25 mm (0.01 in) [MPa	(ksi)]	Maximum Bond Stress [MPa	(ksi)]
S-N-1		5.2	(0.75)	8.4	(1.21)	11.2	(1.62)	13.9	(2.02)
S-N-2		2.9	(0.42)	5.3	(0.77)	7.8	(1.12)	10.1	(1.46)
S-N-3		3.2	(0.46)	6.0	(0.87)	9.8	(1.42)	12.9	(1.87)
S-N-4		3.5	(0.50)	5.8	(0.84)	7.5	(1.09)	10.3	(1.49)
S-N-5		7.9	(1.14)	10.7	(1.55)	13.4	(1.94)	15.8	(2.29)
S-N Average		4.5	(0.65)	7.2	(1.05)	9.9	(1.44)	12.6	(1.83)
Std. Dev.		1.9	(0.27)	2.0	(0.29)	2.2	(0.32)	2.2	(0.31)
Chauvenet's	Upper	7.6	(1.10)	10.6	(1.53)	13.5	(1.96)	16.2	(2.35)
Limit	Lower	1.4	(0.21)	3.9	(0.56)	6.3	(0.92)	9.03	(1.31)

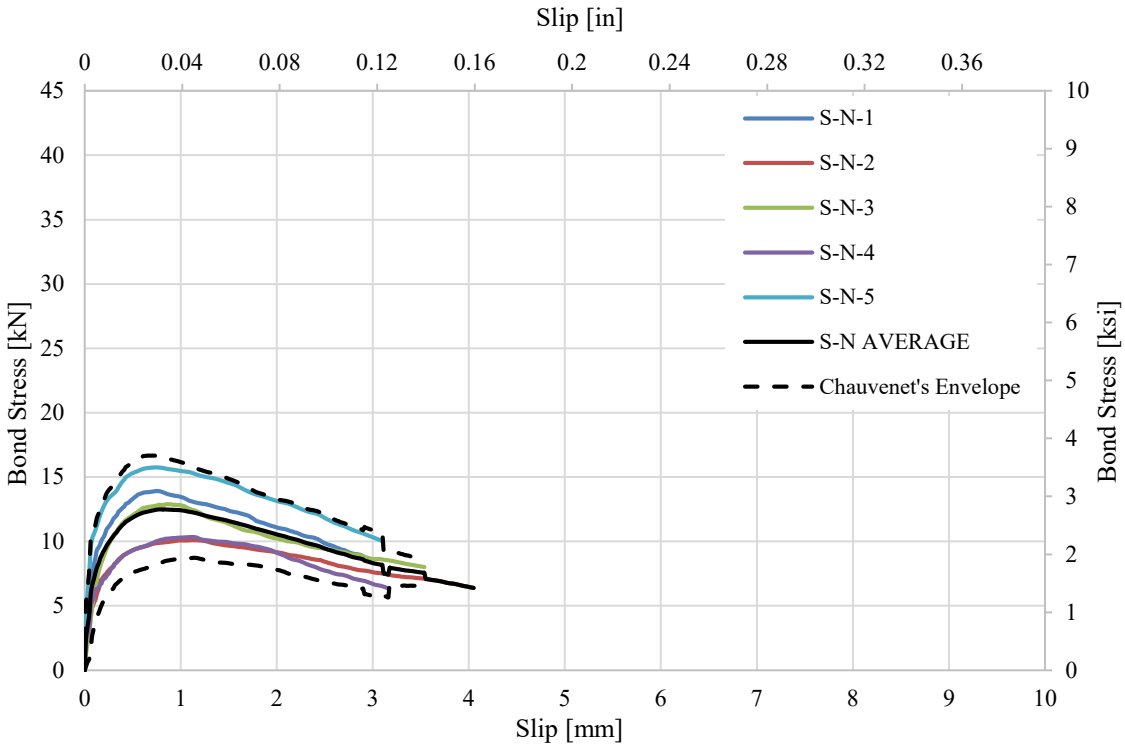

Figure 4-28: Free-End Slip for Plain Steel Rebar (S-N)

As shown in Table 4-18, the average bond stresses for the free-end causing slippage of 0.05 mm (0.002 in), 0.1 mm (0.004 in), and 0.25 mm (0.01 in) were 4.51 MPa (0.65 Msi), 7.23 MPa (1.05 Msi), and 9.92 MPa (1.44 Msi) respectively. Average maximum bond stress was 12.6 MPa (1.83 Msi).

Figure 4-28 show slippage graphs for the free-end. Sample S-N-3 recorded the highest maximum bond stress and Sample S-N-2 the lowest.

Deflection plots, bond stress data, and bond stress graphs for the loaded-end are shown in Figure 4-29, Table 4-19 and Figure 4-30, respectively.

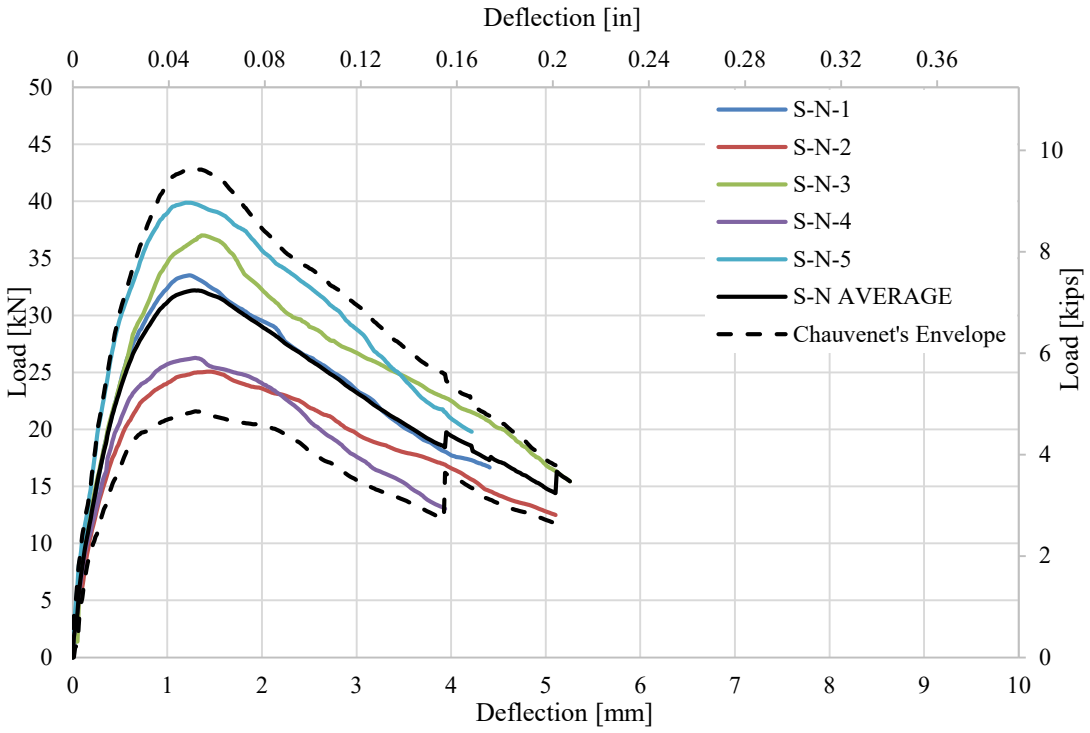

Figure 4-29: Loaded-End Deflections for Plain Steel Rebar (S-N)

Table 4-19: Loaded-End Bond Stress for Plain Steel Rebar (S-N)

Specimen I.D.		Bond Stress Corresponding to Slip Length of 0.05 mm (0.002 in)		0.1 mm (0.004 in)		0.25 mm (0.01 in)		Maximum Bond Stress	
		[MPa	(ksi)]	[MPa	(ksi)]	[MPa	(ksi)]	[MPa	(ksi)]
S-N-1		4.05	(0.59)	5.70	(0.83)	9.32	(1.35)	13.2	(1.92)
S-N-2		2.94	(0.43)	4.51	(0.65)	6.90	(1.00)	9.90	(1.44)
S-N-3		3.07	(0.45)	5.22	(0.76)	8.51	(1.23)	15.2	(2.20)
S-N-4		3.84	(0.56)	4.82	(0.70)	7.76	(1.13)	10.4	(1.51)
S-N-5		5.72	(0.83)	8.36	(1.21)	12.00	(1.74)	15.7	(2.28)
S-N Average		3.92	(0.57)	5.72	(0.83)	8.90	(1.29)	12.88	(1.87)
Std. Dev.		0.99	(0.14)	1.38	(0.20)	1.75	(0.25)	2.39	(0.35)
Chauvenet's	Upper	5.56	(0.81)	7.99	(1.16)	11.77	(1.71)	16.8	(2.44)
Limit	Lower	2.29	(0.33)	3.46	(0.50)	6.03	(0.87)	8.96	(1.30)

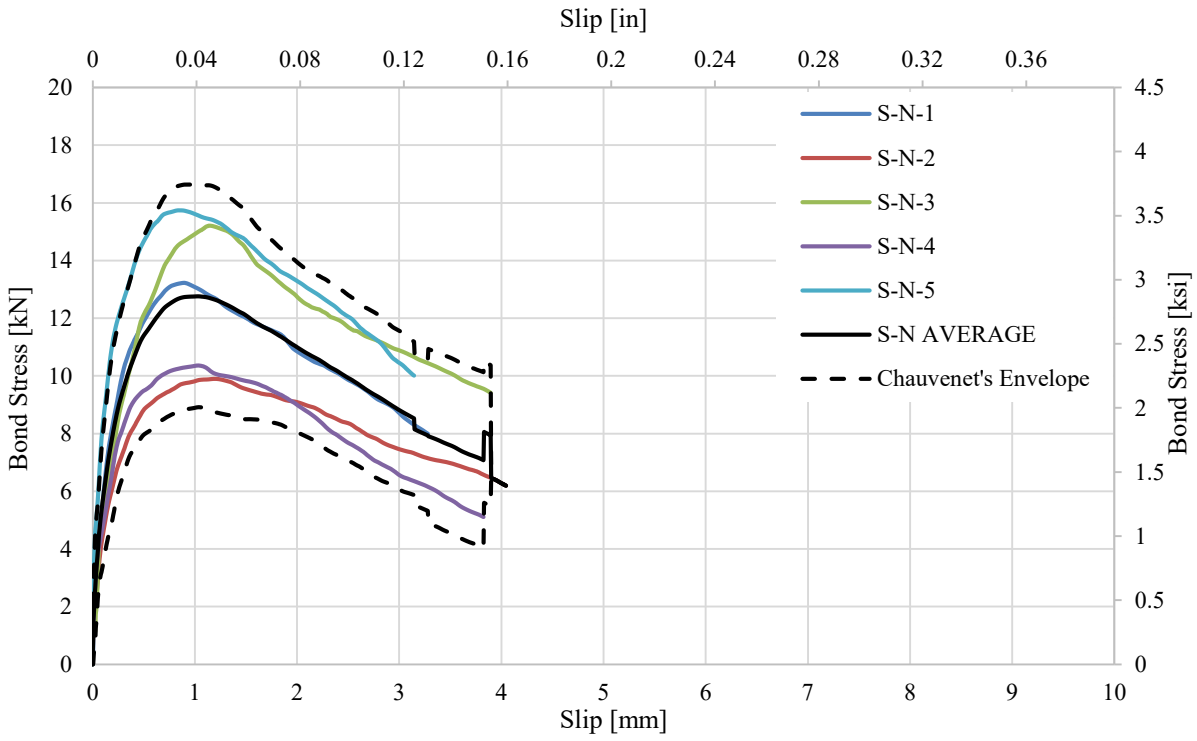

Figure 4-30: Loaded-End Slip for Plain Steel Rebar (S-N)

As shown in Table in 4-19, the average bond stresses for the loaded-end causing slippage of 0.05 mm (0.002 in), 0.1 mm (0.004 in), and 0.25 mm (0.01 in) were 3.92 MPa (0.57 Msi), 5.72 MPa (0.83 Msi), and 8.90 MPa (1.29 Msi), respectively. Average maximum bond stress was 12.9 MPa (1.87 Msi). Figure 4-30 show slippage graphs for the loaded-end. Sample S-N-3 recorded the highest maximum bond stress and Sample S-N-2 the lowest.

4.2.7 Epoxy-Coated Steel (S-E) Configuration

The S-E configuration was one of the rebar type that was purchased. This rebar configuration was manufactured of steel and coated with epoxy. Table 4-20 is a summary of the rebar configuration properties showing the measured results from each specimen that was tested along with the combined overall average of samples consisting this configuration.

Table 4-20: Rebar Properties for Steel Epoxy Coated Rebar (S-E)

Specimen I.D.		Cross Section Area		Young's modulus	
		[mm^2	(in^2)]	[GPa	(Msi)]
S-E-1		126	(0.196)	225	(32.7)
S-E-2		126	(0.196)	187	(27.1)
S-E-3		126	(0.196)	242	(35.0)
S-E-4		126	(0.196)	191	(27.7)
S-E-5		126	(0.196)	196	(28.5)
S-E Average		126	(0.196)	208	(30.2)
Std. Dev.		0.00	(0.000)	21.5	(3.11)
Chauvenet's Limit	Upper	126	(0.196)	244	(35.32)
	Lower	126	(0.196)	173	(25.08)

Figure 4-31 show the stress-strain curves of the configurations. These stress-strain curves indicate Young's modulus for each individual specimen in the S-E configuration along with an average and Chauvenet's envelope for lower and upper limits.

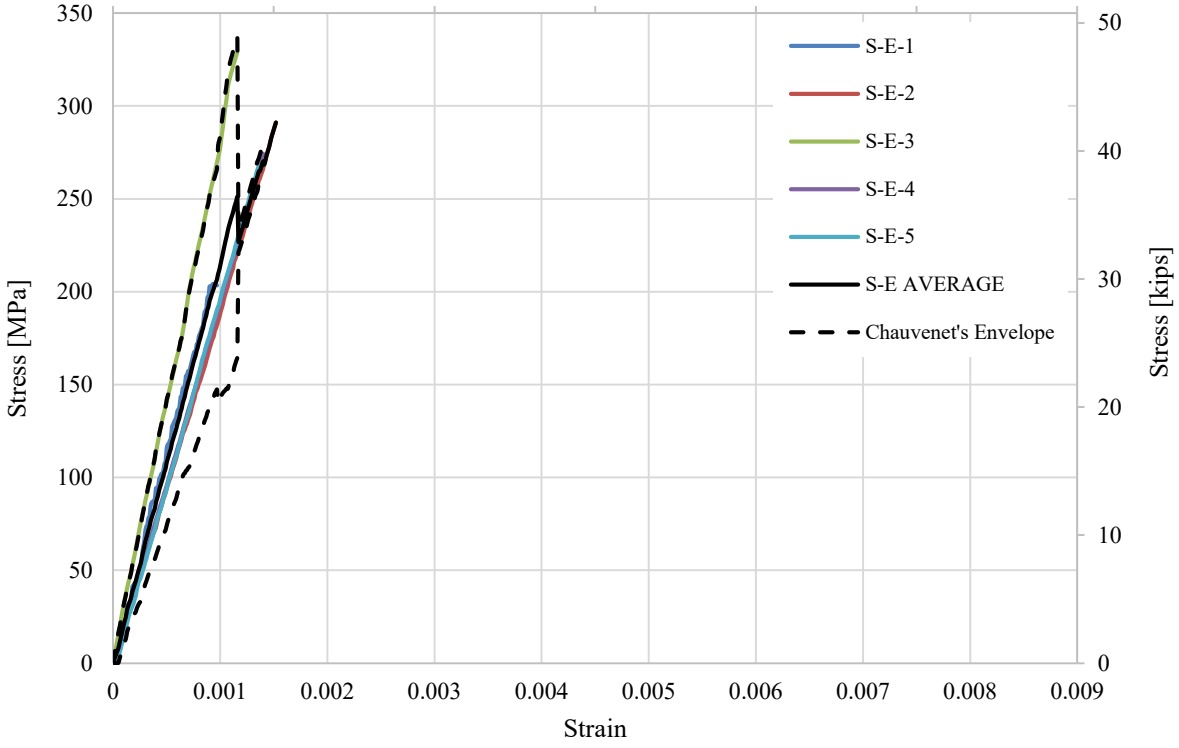

Figure 4-31: Stress-Strain Plots for Steel Epoxy Coated Rebar (S-E)

As shown in Table 4-20 and Figure 4-31, the average Young's modulus for the S-E samples was 208 GPa (30.2 Msi). The average area of the specimens was 126 mm^2 (0.196 in^2).

Figures 4-32 and Table 4-21 and Figure 4-33 show the deflection against load, bond stress data, and bond against slip of the free-end, respectively. Sample S-E-1 did not record free-end data, and therefore is not included in the reported data.

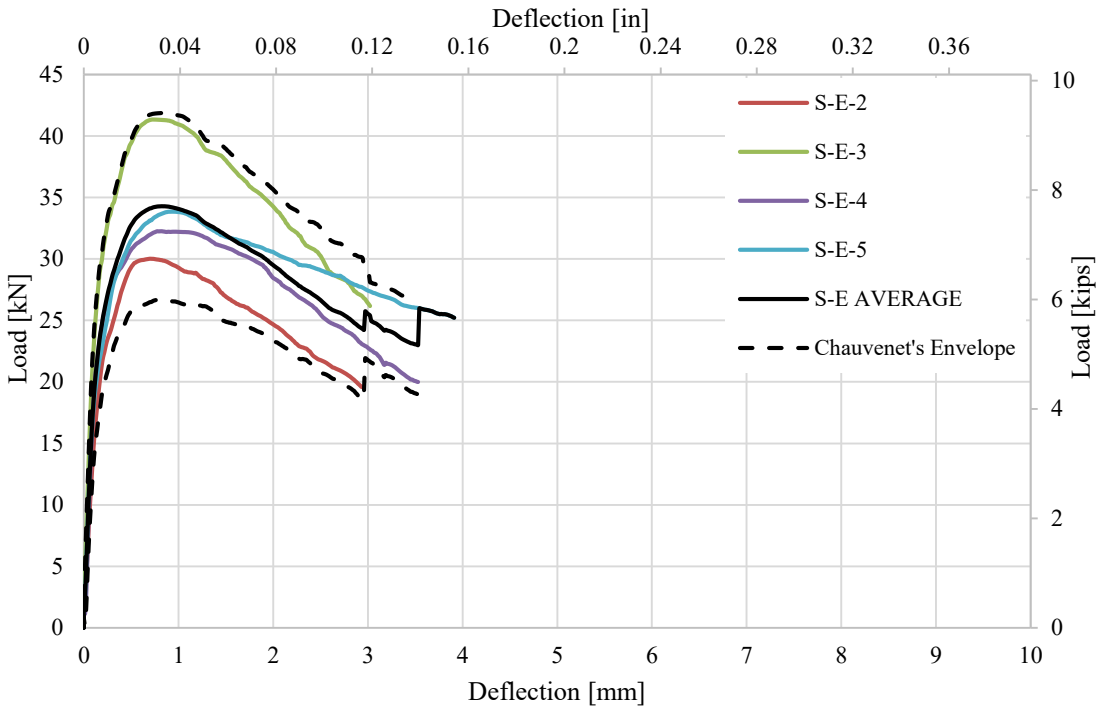

Figure 4-32: Free-End Deflections for Steel Epoxy Coated Rebar (S-E)

Table 4-21: Free-End Bond Stress for Steel Epoxy Coated Rebar Specimens

Specimen I.D.		Bond Stress Corresponding to Slip Length of 0.05 mm (0.002 in) [MPa	(ksi)]	0.1 mm (0.004 in) [MPa	(ksi)]	0.25 mm (0.01 in) [MPa	(ksi)]	Maximum Bond Stress [MPa	(ksi)]
S-E-1		-	-	-	-	-	-	-	-
S-E-2		3.10	(0.45)	5.68	(0.82)	9.27	(1.34)	11.9	(1.73)
S-E-3		5.28	(0.77)	8.81	(1.28)	13.0	(1.89)	16.3	(2.36)
S-E-4		3.50	(0.51)	7.19	(1.04)	10.5	(1.52)	12.7	(1.84)
S-E-5		4.16	(0.60)	6.97	(1.01)	9.99	(1.45)	13.40	(1.94)
S-E Average		4.01	(0.58)	7.16	(1.04)	10.69	(1.55)	13.58	(1.97)
Std. Dev.		0.83	(0.12)	1.11	(0.16)	1.40	(0.20)	1.66	(0.24)
Chauvenet's	Upper	5.28	(0.77)	8.87	(1.29)	12.84	(1.86)	16.12	(2.34)
Limit	Lower	2.74	(0.40)	5.46	(0.79)	8.54	(1.24)	11.03	(1.60)

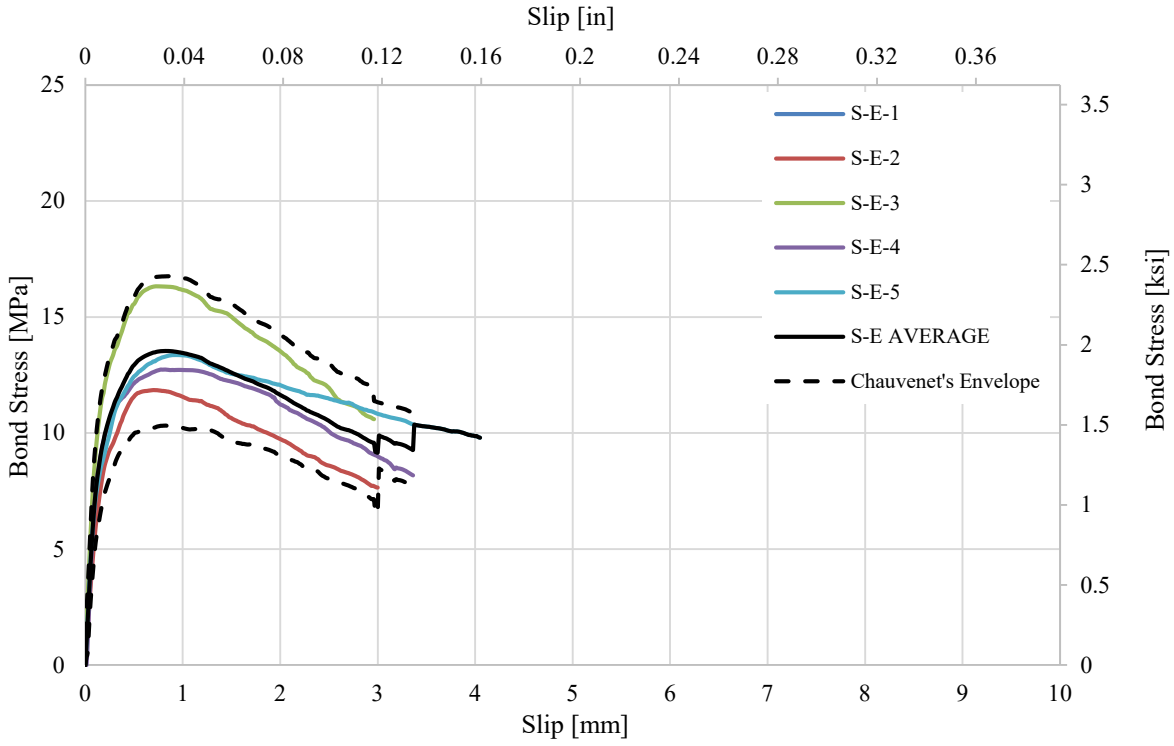

Figure 4-33: Free-End Slip for Steel Epoxy Coated Rebar Specimens

As shown in table 4-21, the average bond stresses for the free-end causing slippage of 0.05 mm (0.002 in), 0.1 mm (0.004 in), and 0.25 mm (0.01 in) were 4.01 MPa (582 Ksi), 7.16 MPa (1.04 ksi), and 10.7 MPa (1.55 ksi) respectively. Average maximum bond stress was 13.6 MPa (1.97 ksi). Figure 4-33 show slippage graphs for the free-end. Sample S-E-3 recorded the highest maximum bond stress and Sample S-E-2 the lowest.

Deflection plots, bond stress data, and bond stress graphs for the loaded-end are shown in Figure 4-34, Table 4-22 and Figure 4-35, respectively.

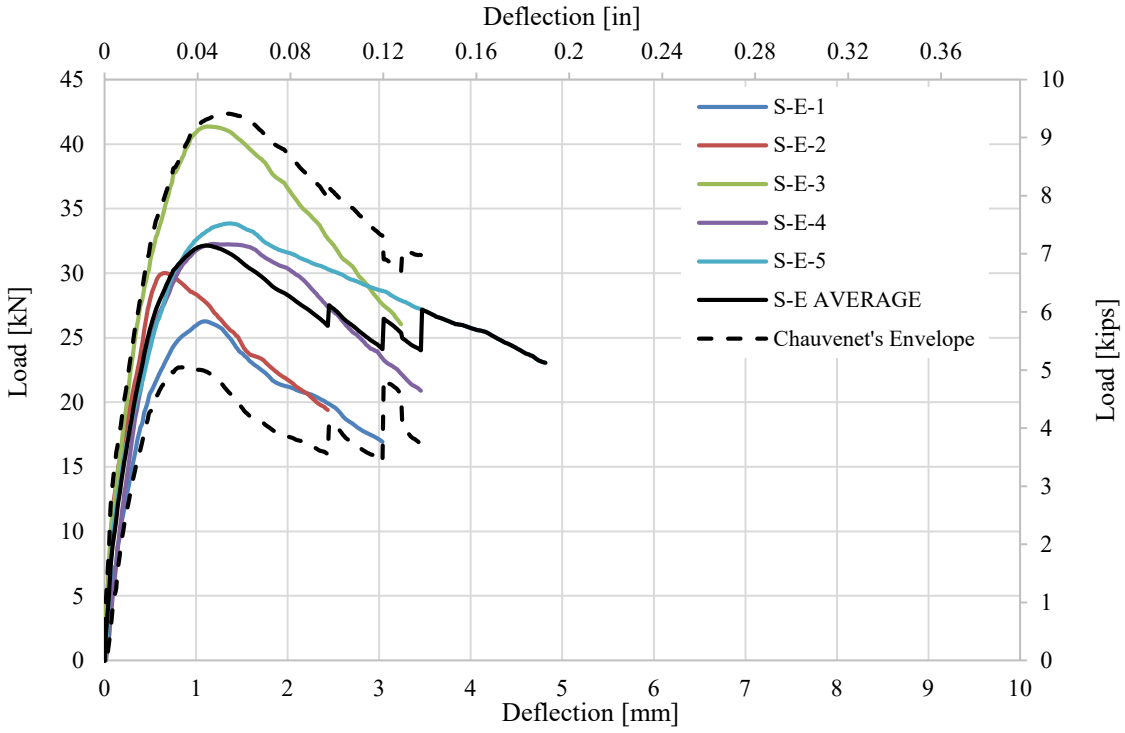

Figure 4-34: Loaded-End Deflections for Steel Epoxy Coated Rebar (S-E)

Table 4-22: Loaded-End Bond Stress for Steel Epoxy Coated Rebar (S-E)

Specimen I.D.		Bond Stress Corresponding to Slip Length of 0.05 mm (0.002 in)		0.1 mm (0.004 in)		0.25 mm (0.01 in)		Maximum Bond Stress	
		[MPa	(ksi)]	[MPa	(ksi)]	[MPa	(ksi)]	[MPa	(ksi)]
S-E-1		2.92	(0.42)	4.36	(0.63)	7.30	(1.06)	10.4	(1.50)
S-E-2		8.46	(1.23)	9.98	(1.45)	11.8	(1.72)	11.8	(1.72)
S-E-3		6.21	(0.90)	8.10	(1.17)	11.8	(1.71)	16.3	(2.37)
S-E-4		3.48	(0.50)	6.31	(0.92)	10.3	(1.49)	13.1	(1.90)
S-E-5		6.10	(0.89)	7.15	(1.04)	9.48	(1.37)	13.4	(1.94)
S-E Average		5.43	(0.79)	7.18	(1.04)	10.1	(1.47)	13.0	(1.89)
Std. Dev.		2.02	(0.29)	1.86	(0.27)	1.69	(0.24)	1.97	(0.29)
Chauvenet's	Upper	8.75	(1.27)	10.2	(1.49)	12.91	(1.87)	16.2	(2.36)
Limit	Lower	2.12	(0.31)	4.11	(0.60)	7.37	(1.07)	9.76	(1.41)

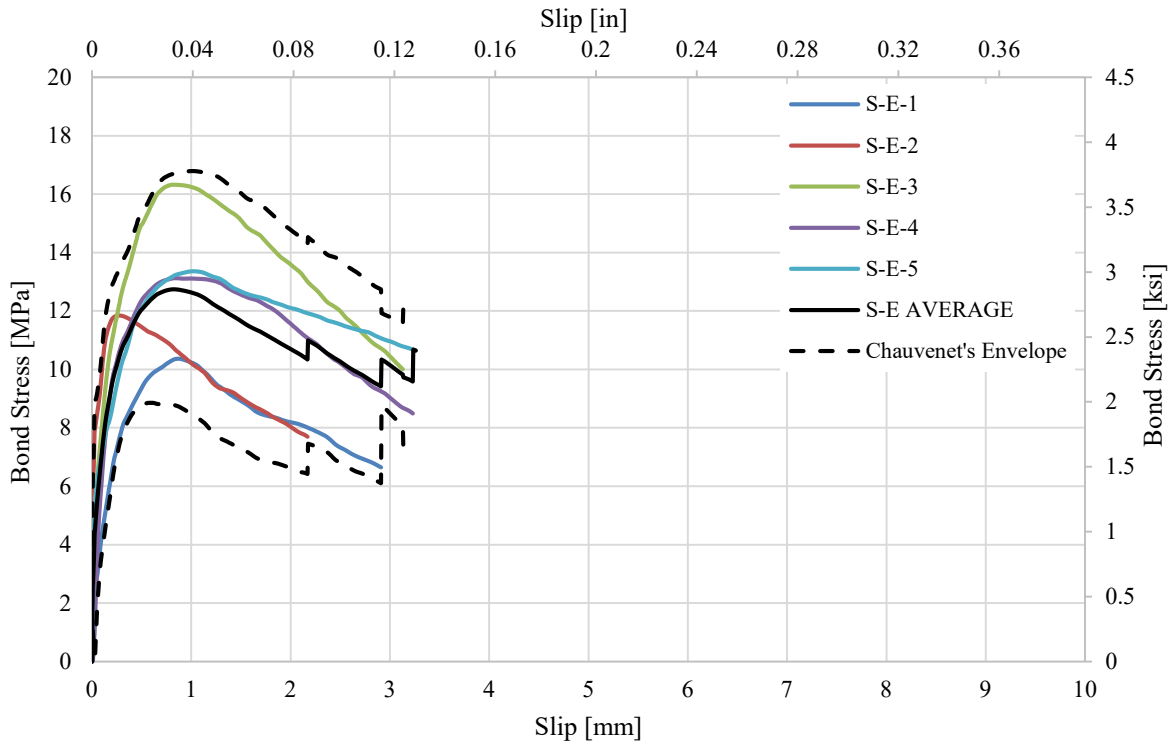

Figure 4-35: Loaded-End Slip for Steel Epoxy Coated Rebar Specimens

As shown in Table 4-22, the average bond stresses for the loaded-end causing slippage of 0.05 mm (0.002 in), 0.1 mm (0.004 in), and 0.25 mm (0.01 in) were 5.43 MPa (0.79 ksi), 7.18 MPa (1.04 ksi), and 10.1 MPa (1.47 ksi) respectively. Average maximum bond stress was 13.0 MPa (1.89 ksi). Figure 3-30 show slippage graphs for the loaded-end. Sample S-E-3 recorded the highest maximum bond stress and Sample S-E-1 the lowest.

4.3 Failure Modes

Investigation of the rebar and concrete blocks after pull-out testing showed how slippage had occurred during pull-out testing as well as described the manner in which the rebar-concrete bond had failed. It was observed that failure from rebar pull-out testing occurred as either concrete shearing or rebar surface failure.

For concrete whose compressive strength was greater than 25 MPa (3626 Psi), the bond failure interface occurred at the surface of the rebar. Failure images shown in Figures 4-36 through 4-39 show stripping of the rebar coatings or outside layers.

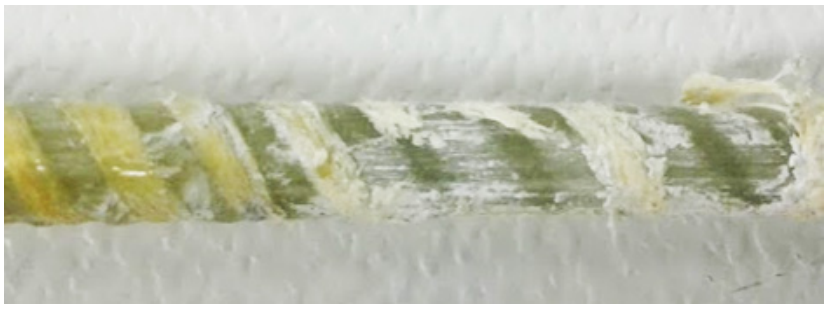

Figure 4-36: Rebar Surface Failure on Manufactured Non-Sand-coated Specimens

Figure 4-37 Rebar Surface Failure on Manufactured Sand-coated Specimens

Figure 4-38: Rebar Surface Failure on American Fiberglass Sand-coated Specimens

Figure 4-39: Rebar Surface Failure on Steel Epoxy Coated Rebar

For concrete whose compressive strength was below 25 MPa (3625 ksi), i.e. concrete batches 1 and 2, the failure mode was shearing of the concrete matrix. Bond strength for this mode of failure seemed to be related to the shear area. Influence of shear area is discussed Chapter 6. Figures 4-40 through 4-42 show photographs of shear failure.

Figure 4-40: Concrete Shear Failure on American Fiberglass Sand-coated Rebar

Figure 4-41: Concrete Shear Failure on Steel Epoxy Coated Rebar

Figure 4-42: Concrete Shear Failure on Manufactured Sand-coated Rebar

These two failure modes were also observed on the concrete blocks. Figure 4-43 shows rebar surface failure, while Figure 4-44 shows failure of the concrete. Failure of the rebar surfaces was observed by rebar coatings left on the concrete. Shear failure of the concrete was observed by a smooth surface excluding any rebar coating being left on the concrete.

Figure 4-43: Rebar Coatings Left on the Concrete after Pull-Out

Figure 4-44: Shear Failure of the Concrete as Observed by a Smooth Surface Being Left on the Concrete

5 COMPARISON OF RESULTS

This chapter discusses the significance of the pull-out results and compares experimental results of the different configurations. To quantitatively compare the bond strength of the different rebar configurations, averages from each configuration were assembled and compared to other configurations.

5.1 Comparison of Stress-Strain Behavior

To compare Young's modulus across configurations, Table 5-1 and Figure 5-1 were created. Data in Table 5-1 and Figure 5-1 were the overall averages of each configuration calculated from individual sample data in each configuration.

Table 5-1 represents the average Young's modulus of each configuration.

Table 5-1 Average Young's modulus for All Rebar Configurations

Configuration	Young's modulus	
	[GPa	(Msi)]
D-N	47.6	(6.90)
P-N	49.1	(7.12)
D-S	46.0	(6.67)
P-S	47.8	(6.93)
A-S	47.6	(6.90)
S-E	208	(30.2)
S-N	198	(28.7)

Figure 5-1 show curves of the average Young's modulus of each configuration.

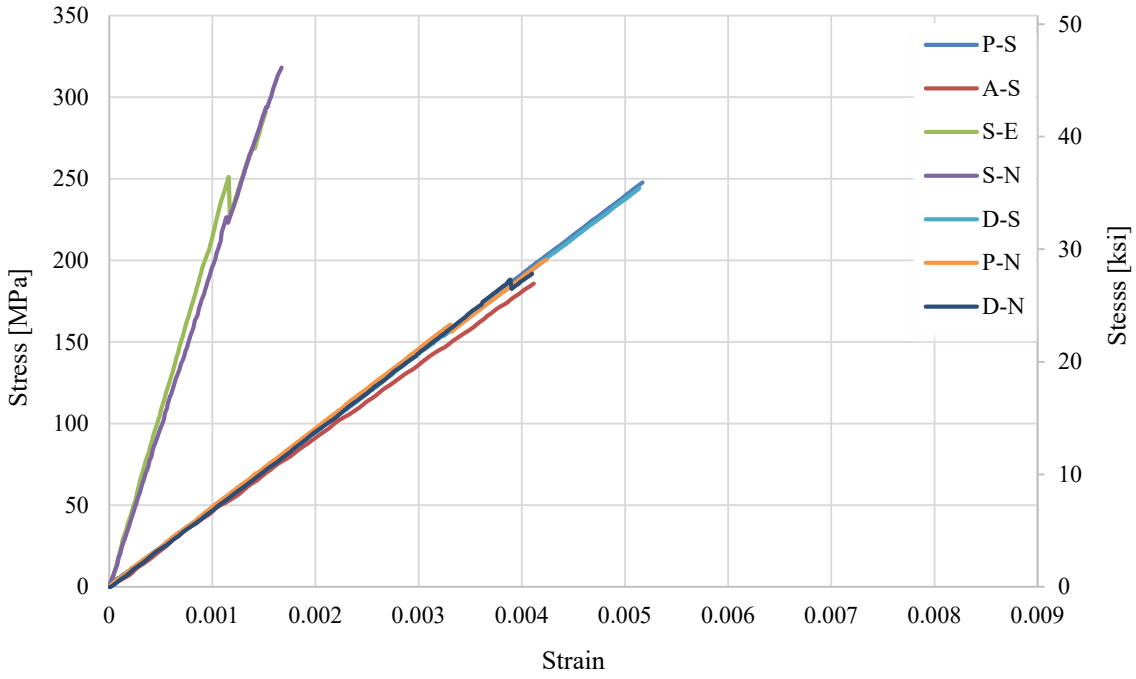

Figure 5-1: Stress-Strain Curves for All Rebar Configurations

The average Young's modulus for the in-house manufactured fiberglass/epoxy rebar was 47.6 MPa (6.90 Msi) with the prepreg no-sand configuration recording the highest Young's modulus which was 49.1 MPa (7.12 Msi), and the dry no-sand configurations recording the lowest value of 46.0 MPa (6.67 Msi). American Fiberglass Rebar recorded an average stiffness of 47.6 MPa (6.90 Msi) similar to the average of all the in-house manufactured FRP. Steel epoxy and plain steel recorded average Young's modulus values of 208 MPa (30.2 Msi) and 198 MPa (28.7 Msi), respectively.

5.2 Comparison of Free-End Bond Stress Behavior

To compare the results of free-end bond stress across configurations, Table 5-2 and Figure 5-2 were created combining results of all the configurations.

Table 5-2: Average Free-End Bond Stress for All Rebar Configurations

Specimen I.D.	Bond Stress Corresponding to Slip Length of						Maximum Bond Stress	
	0.05 mm (0.002 in)		0.1 mm (0.004 in)		0.25 mm (0.01 in)			
	MPa	(ksi)]	[MPa	(ksi)]	[MPa	(ksi)]	[MPa	(ksi)]
D-N	4.7	(0.69)	6.1	(0.88)	7.2	(1.04)	9.4	(1.36)
P-N	4.1	(0.60)	5.6	(0.81)	6.8	(0.99)	8.8	(1.28)
D-S	10.1	(1.46)	11.1	(1.61)	11.3	(1.64)	11.4	(1.65)
P-S	9.3	(1.35)	13.4	(1.94)	15.6	(2.26)	15.6	(2.26)
A-S	9.6	(1.39)	11.3	(1.63)	12.0	(1.74)	12.0	(1.74)
S-N	4.5	(0.65)	7.2	(1.05)	9.9	(1.44)	12.6	(1.83)
S-E	4.0	(0.58)	7.2	(1.04)	10.7	(1.55)	13.6	(1.97)

For bond stress corresponding to a slip length of 0.05 mm (0.002 in), the D-S configuration recorded the highest bond stress of 10.1 MPa (1.46 ksi). The A-S configuration recorded the second highest bond stress value which was 95% of the D-S configuration. The S-E and S-N samples recorded the lowest bond stress values of 4.01 MPa (0.58 ksi) and 4.51 MPa (0.65 ksi) which were 40% and 45% of the D-S configuration.

For bond stress corresponding to a slip length of 0.1 mm (0.004 in), the P-S configuration recorded the highest bond stress of 13.4 MPa (1.94 ksi). The A-S configuration recorded the highest second bond stress value which was 84% of the P-S configuration. The P-N and D-N samples recorded the lowest bond stress values of 5.61 MPa (0.81 ksi) and 6.07 MPa (0.88 ksi) which were 42% and 45% of the P-S configuration.

For bond stress corresponding to slip length of 0.25 mm (0.01 in) the P-S configuration recorded the highest bond stress of 15.6 MPa (2.26 ksi). The A-S configuration recorded the second highest bond stress value which was 77% of the P-S configuration. The P-N and D-N samples recorded the lowest bond stress values of 7.20 MPa (1.04 ksi) and 6.83 MPa (0.99 ksi), which were 46% and 44% of the P-S configuration.

The P-S configuration recorded the highest maximum bond stress of 15.6 MPa (2.26 ksi). The lowest bond stress, which was 56% of the highest, was 8.8 MPa (1.28 ksi) recorded by the P-N configuration. Figure 5-2 shows the plots for bond stress against slip.

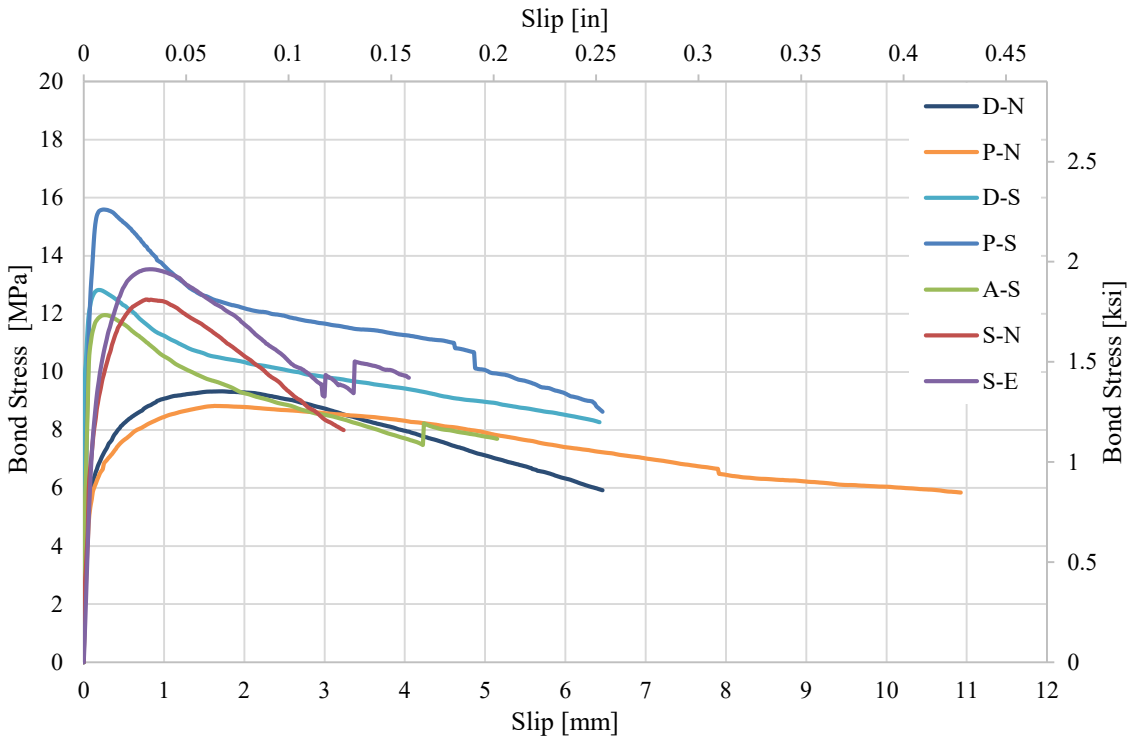

Figure 5-2 Average Free-End Bond Stress vs Slip for All Rebar Configurations

5.3 Comparison of Loaded-End Bond Stress Behavior

To compare the results of loaded-end bond stress across configurations, Table 5-3 and Figure 5-3 were created combining results of all the configurations.

Table 5-3: Average Loaded-End Bond Stress for All Rebar Configurations

Specimen I.D.	Bond Stress Corresponding to Slip Length of						Maximum Bond Stress	
	0.05 mm (0.002 in)		0.1 mm (0.004 in)		0.25 mm (0.01 in)			
	[MPa	(ksi)]	[MPa	(ksi)]	[MPa	(ksi)]	[MPa	(ksi)]
D-N	3.9	(0.56)	4.8	(0.69)	6.1	(0.89)	9.0	(1.31)
P-N	2.6	(0.37)	3.6	(0.52)	5.5	(0.80)	8.7	(1.26)
D-S	4.6	(0.66)	6.3	(0.91)	8.9	(1.29)	12.2	(1.77)
P-S	4.7	(0.68)	6.7	(0.98)	10.4	(1.51)	13.4	(1.94)
A-S	2.6	(0.37)	4.6	(0.67)	8.6	(1.25)	12.2	(1.78)
S-N	3.9	(0.57)	5.7	(0.83)	8.9	(1.29)	12.9	(1.87)
S-E	5.4	(0.79)	7.2	(1.04)	10.1	(1.47)	13.0	(1.89)

For bond stress corresponding to slip length of 0.05 mm (0.002 in) the S-E configuration recorded the highest bond stress of 5.43 MPa (0.78 ksi). The P-S configuration recorded the second highest bond stress value which was 87% of the S-E configuration. The P-N and A-S configurations recorded the lowest bond stresses of 2.57 MPa (0.37 ksi) and 2.56 MPa (0.37 ksi) which were 47% of the D-S configuration.

For bond stress corresponding to slip length of 0.1 mm (0.004 in) the S-E configuration recorded the highest bond stress of 7.18 MPa (1.04 ksi). The P-S configuration recorded the highest second bond stress value which was 94% of the P-S configuration. The P-N and A-S configurations recorded the lowest bond stress values which were 3.59 MPa (0.520 ksi) and 4.59 MPa (0.67 ksi) which were 50% and 64% of the P-S configuration.

For bond stress corresponding to slip length of 0.25 mm (0.01 in) the P-S configuration recorded the highest bond stress of 10.4 MPa (1.51 ksi). This bond stress value was 19% higher

than the average and over the upper limit by 2.9%. The S-E configuration recorded the second highest bond stress value of 10.1 MPa (1.47 ksi) which was 97% of the P-S configuration. The P-N and D-N samples recorded the lowest bond stress values of 6.14 MPa (0.89 ksi) and 5.91 MPa (0.86 ksi) which were 59% and 57% of the P-S configuration.

The P-S configuration recorded the maximum bond stress of 13.4 MPa (1.94 ksi). The lowest bond stress, which was 65% of the highest, was 8.67 MPa (1.26 ksi) recorded by the P-N configuration. The Average maximum bond stress was 11.6 MPa (1.69 ksi). Figure 5-3 shows the plots for the loaded-end bond stress against slip.

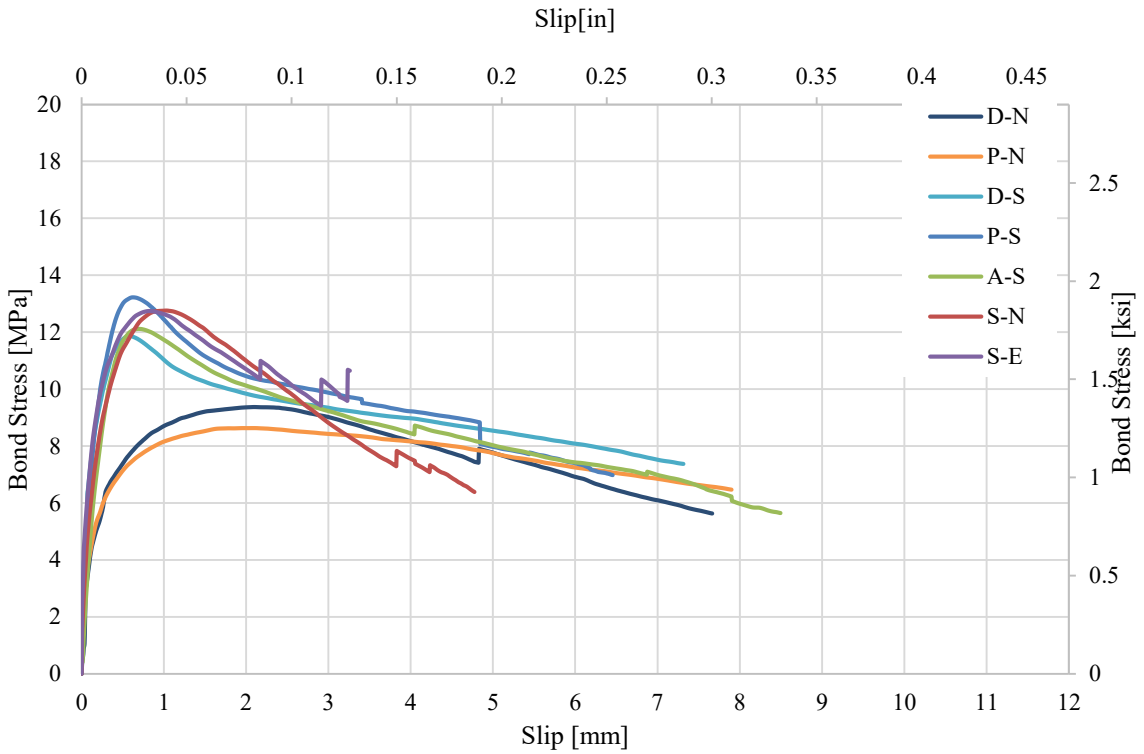

Figure 5-3 Average Loaded-End Bond Stress vs Slip for All Rebar Configurations

6 DISCUSSION OF RESULTS

This chapter compares various aspects and configurations of the rebar described in this thesis and draws conclusions on rebar bond strength based on test results. Rebar configurations are compared based on the percentage of differences in bond stress.

6.1 Influence of Prepreg Tow Consolidation

To illustrate the effect of resin impregnation on consolidation tow, Tables 6-1 and 6-2 were created by combining the average bond stress of the dry tow no-sand configuration (D-N) and average bond stress of the prepreg tow no-sand configuration (P-N). This combination approach allows for comparison of the effects of consolidating the core of the rebar with prepreg tow versus dry fiber. The prepreg tow no-sand configuration recorded the lowest bond stress values. For the free-end bond stress, the prepreg tow no-sand configuration average bond stress values were 13%, 7%, 5%, and 6% lower than the dry tow no-sand configuration for bond stress corresponding to slip values of 0.05 mm (0.002 in), 0.10 mm (0.004 in), 0.25 mm (0.01 in), and maximum bond stress, respectively. For the loaded-end bond, the prepreg tow no-sand configuration average bond stress was 34%, 25%, 10%, and 4% lower than the dry tow no-sand configuration for bond stress corresponding to slip values of 0.05 mm (0.002 in), 0.1 mm (0.004 in), 0.25 mm (0.01 in), and maximum bond stress, respectively. The bond stress-slip curves shown in Figures 6-1 and 6-2 indicate that for both the free-end and loaded-end respectively, the dry tow no-sand configuration recorded the maximum bond stress. Once maximum bond stress

was attained, the dry tow no-sand configuration quickly lost load and slipped significantly while the prepreg samples slipped slowly. The differences in bond stress, with the dry tow no-sand configuration exhibiting higher bond stress, are likely due to the slippery surface of the prepreg wound samples. Consolidating the fiberglass composite rebar with a prepreg tow increased the resin content on the surface of the rebar, thereby increasing the smoothness and slippery behavior of the rebar. In summary, samples consolidated with dry tow showed higher bond stress in the range of 6 - 13% for the free-end and 4 - 34% for the loaded-end than those consolidated with a prepreg tow when embedded in concrete directly without any secondary processes such as sand coating.

Table 6-1: Average Free-End Bond Stress Values of D-N and P-N Configuration

Configuration	Average Bond Stress Corresponding to Slip Length of						Maximum Bond Stress	
	0.05 mm (0.002 in)		0.1 mm (0.004 in)		0.25 mm (0.01 in)			
	[MPa	(ksi)]	[MPa	(ksi)]	[MPa	(ksi)]	[MPa	(ksi)]
D-N Average	4.7	(0.69)	6.1	(0.88)	7.2	(1.04)	9.4	(1.36)
P-N Average	4.1	(0.60)	5.6	(0.81)	6.8	(0.99)	8.8	(1.28)
Difference	13%		7%		5%		6%	

Table 6-2: Average Loaded-End Bond Stress Values of D-N and P-N Configuration

Configuration	Average Bond Stress Corresponding to Slip Length of						Maximum Bond Stress	
	0.05 mm (0.002 in)		0.1 mm (0.004 in)		0.25 mm (0.01 in)			
	[MPa	(ksi)]	[MPa	(ksi)]	[MPa	(ksi)]	[MPa	(ksi)]
D-N Average	3.9	(0.56)	4.8	(0.69)	6.1	(0.89)	9.0	(1.31)
P-N Average	2.6	(0.37)	3.6	(0.52)	5.5	(0.80)	8.7	(1.26)
Difference	34%		25%		10%		4%	

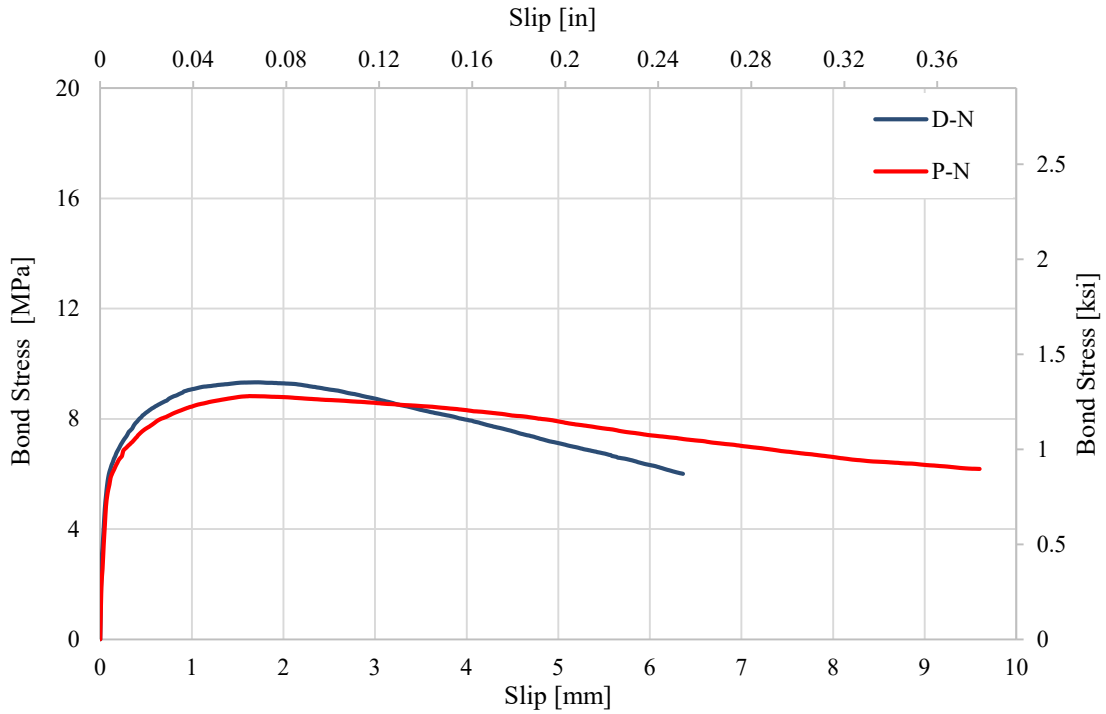

Figure 6-1: Average Free-End Slippage of D-N and P-N Configurations

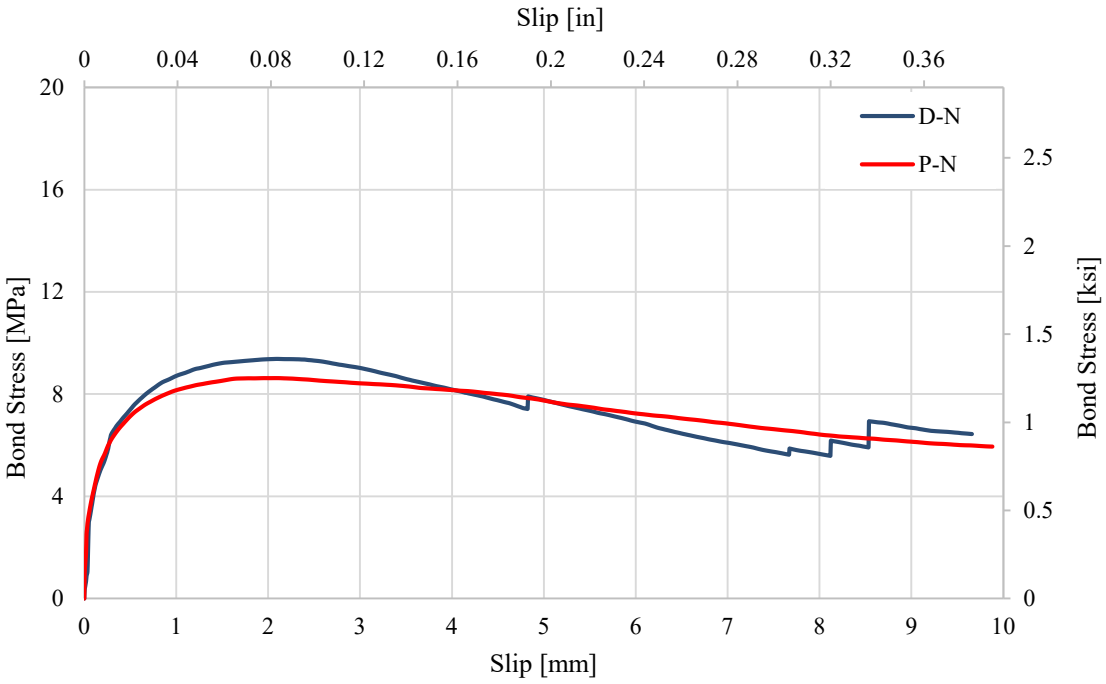

Figure 6-2: Average Loaded-End Slippage of D-N and P-N Configurations

6.2 Influence of Sand Coating

To examine the influence of sand coating, samples from the dry tow no-sand configuration (D-N) were compared to the dry tow sand-coated configuration (D-S), while samples from the prepreg tow no-sand configuration (P-N) were compared to samples from the prepreg tow sand configuration (P-S).

6.2.1 Influence of Sand-Coating on Dry Tow Consolidated Samples

The average bond stress for the two configurations consolidated with dry tow, which were the dry tow no-sand (D-N), and dry tow with sand coating (D-S), were compared to illustrate the effect of sand coating on rebar bond stress as illustrated in Tables 6-3 and 6-4. Dry tow samples prepared with no-sand coating recorded the lowest bond stress values. For the free-end bond stress, the dry tow no-sand configuration average bond stress was 53%, 45%, 36%, and 17% lower than the dry tow with sand coating configuration for bond stress corresponding to slip of 0.05 mm (0.002 in), 0.10 mm (0.004 in), 0.25 mm (0.01 in), and maximum bond stress, respectively. For the loaded-end bond, the dry tow no-sand configuration average bond stress was 15%, 23%, 31%, and 26% lower than the dry tow with sand configuration for bond stress corresponding to slip of 0.05 mm (0.002 in), 0.10 mm (0.004 in), 0.25 mm (0.01 in), and maximum bond stress, respectively. The bond stress slip curves shown in Figures 6-3 and 6-4 indicate the free-end and loaded-end data for these two configurations showing dry tow with sand coating configuration having higher bond stress than the dry tow, no-sand configuration for corresponding slip values.

Overall, samples consolidated with dry tow and coated with sand showed higher bond stress in the range of 15-26% for the free-end and 17-53% for the loaded-end than the samples consolidated with dry tow and excluded sand coating. This behavior was attributed to sand grains which increased the surface roughness of the rebar, and thereby enhanced the capacity of the rebar to bond to the concrete.

Table 6-3: Average Free-End Bond Stress Values of D-N and D-S Configuration

Configuration	Average Bond Stress Corresponding to Slip Length of						Maximum Bond Stress	
	0.05 mm (0.002 in)		0.1 mm (0.004 in)		0.25 mm (0.01 in)			
	[MPa	(ksi)]	[MPa	(ksi)]	[MPa	(ksi)]	[MPa	(ksi)]
D-N Average	4.7	(0.69)	6.1	(0.88)	7.2	(1.04)	9.4	(1.36)
D-S Average	10.1	(1.46)	11.1	(1.61)	11.3	(1.64)	11.4	(1.65)
Difference	53%		45%		36%		17%	

Table 6-4: Average Loaded-End Bond Stress Values of D-N and D-S Configuration

Configuration	Average Bond Stress Corresponding to Slip Length of						Maximum Bond Stress	
	0.05 mm (0.002 in)		0.1 mm (0.004 in)		0.25 mm (0.01 in)			
	[MPa	(ksi)]	[MPa	(ksi)]	[MPa	(ksi)]	[MPa	(ksi)]
D-N Average	3.9	(0.56)	4.8	(0.69)	6.1	(0.89)	9.0	(1.31)
D-S Average	4.6	(0.66)	6.3	(0.91)	8.9	(1.29)	12.2	(1.77)
Difference	15%		23%		31%		26%	

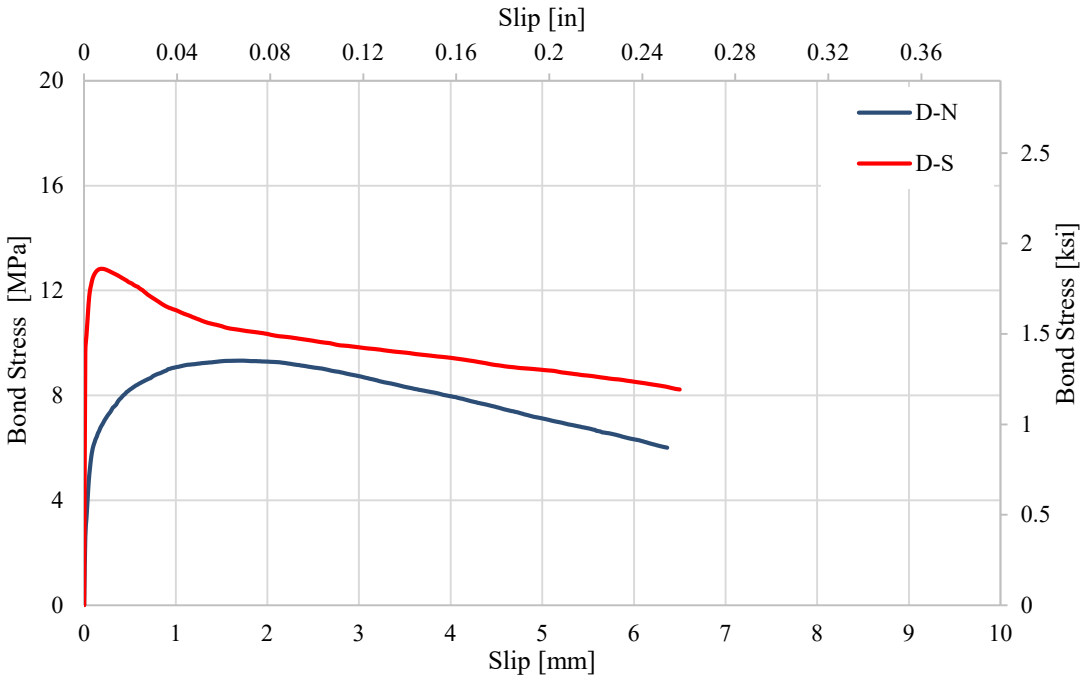

Figure 6-3: Average Free-End Slippage of D-N and D-S Configurations

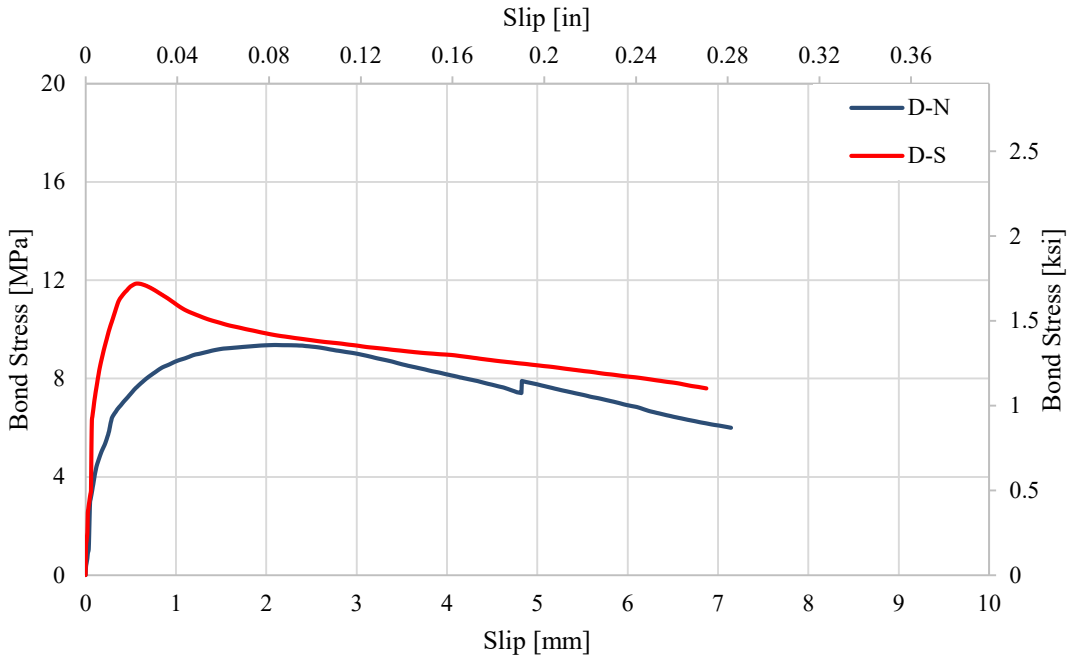

Figure 6-4: Average Loaded-End Slippage of D-N and D-S Configurations

6.2.2 Influence of Sand Coating on Prepreg Tow Consolidated Samples

The average bond stress for the two configurations consolidated with prepreg tow, prepreg tow no-sand (P-N) and prepreg tow with sand coating (P-S) were compared to illustrate the effect of sand coating on rebar bond stress as illustrated in Tables 6-5 and 6-6. Prepreg tow samples prepared with no-sand coating recorded the lowest bond stress values. For the free-end bond stress, the prepreg tow no-sand configuration average bond stress was 56%, 58%, 46% and 43% lower than the prepreg tow with sand coating configuration for bond stress corresponding to slip of 0.05 mm (0.002 in), 0.10 mm (0.004 in), 0.25 mm (0.01 in), and maximum bond stress, respectively. For the loaded-end bond, the prepreg tow no-sand configuration average bond stress was 45%, 47%,47% and 35% lower than the prepreg tow with sand configuration for bond stress corresponding to slip of 0.05 mm (0.002 in), 0.10 mm (0.004 in), 0.25 mm (0.01 in), and maximum bond stress, respectively. The bond stress-slip curves shown in Figures 6-5 and 6-6 indicate the free-end and loaded-end data for these two configurations showing prepreg tow with sand coating configuration having higher bond stress than the prepreg tow no-sand configuration for corresponding slip values.

Overall, samples consolidated with prepreg tow and coated with sand showed higher bond stress in the range of 43% – 58% for the free-end and 35 – 47% for the loaded-end than the samples consolidated with prepreg tow and excluded sand coating. As observed with dry tow samples, sand grains on sand-coated rebar improved the surface roughness of the rebar, and thereby enhancing the bond capabilities of the rebar to concrete.

Table 6-5: Average Free-End Bond Stress of P-N and P-S Configurations

Configuration	Average Bond Stress Corresponding to Slip Length of						Maximum Bond Stress	
	0.05 mm (0.002 in)		0.1 mm (0.004 in)		0.25 mm (0.01 in)			
	[MPa	(ksi)]	[MPa	(ksi)]	[MPa	(ksi)]	[MPa	(ksi)]
P-N Average	4.1	(0.60)	5.6	(0.81)	6.8	(0.99)	8.8	(1.28)
P-S Average	9.3	(1.35)	13.4	(1.94)	15.6	(2.26)	15.6	(2.26)
Difference	56%		58%		56%		43%	

Table 6-6: Average Loaded-End Bond Stress of P-N and P-S Configurations

Configuration	Average Bond Stress Corresponding to Slip Length of						Maximum Bond Stress	
	0.05 mm (0.002 in)		0.1 mm (0.004 in)		0.25 mm (0.01 in)			
	[MPa	(ksi)]	[MPa	(ksi)]	[MPa	(ksi)]	[MPa	(ksi)]
P-N Average	2.6	(0.37)	3.6	(0.52)	5.5	(0.80)	8.7	(1.26)
P-S Average	4.7	(0.68)	6.7	(0.98)	10.4	(1.51)	13.4	(1.94)
Difference	45%		47%		47%		35%	

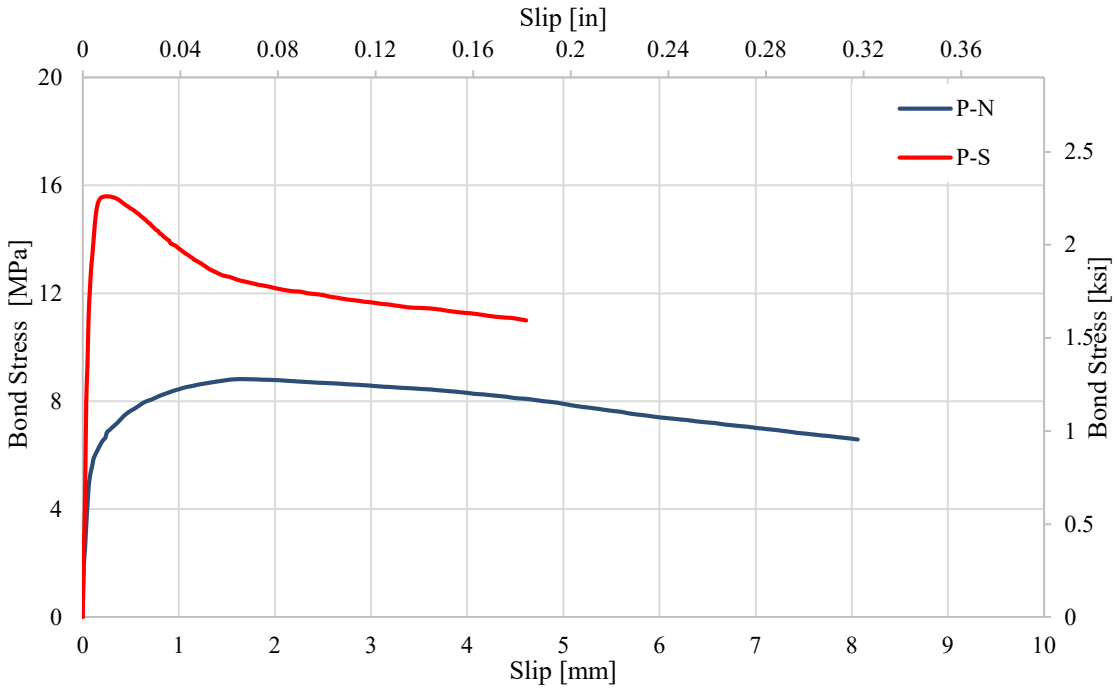

Figure 6-5: Average Free-End Slippage of P-N and P-S Configurations

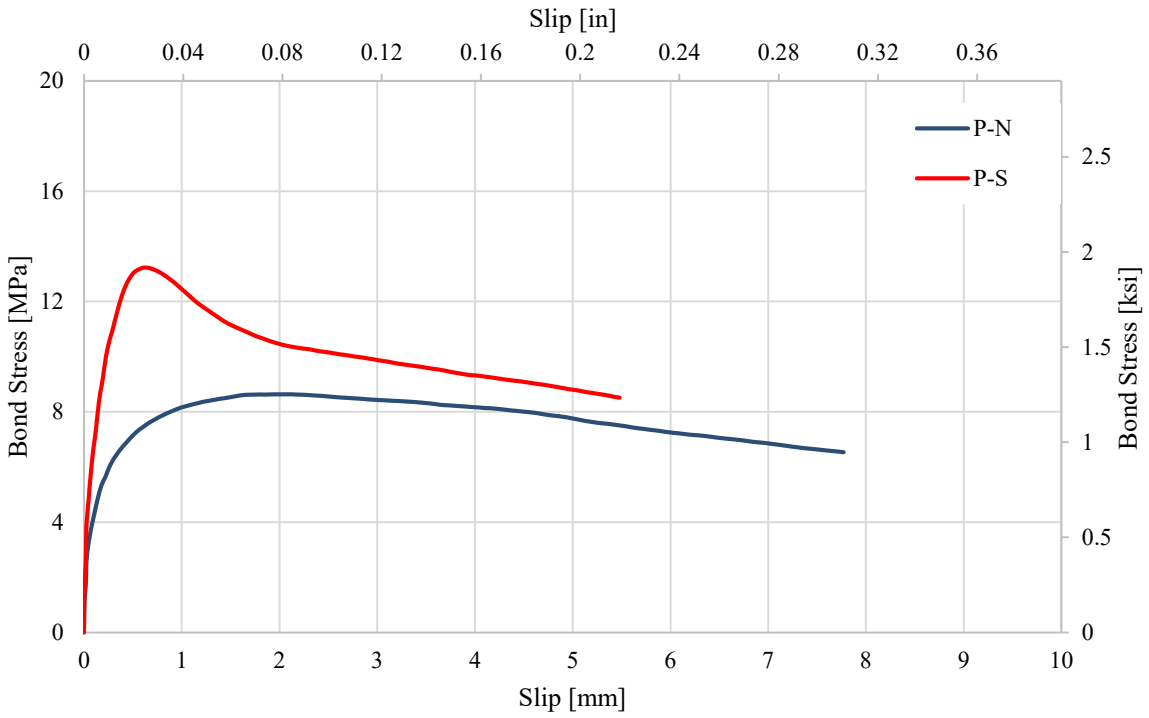

Figure 6-6: Average Loaded-End Slippage of P-N and P-S Configurations

6.2.3 Summary on Influence of Sand Coating

For both the dry tow and prepreg tow consolidation, the addition of sand on the surface of the fiberglass composite epoxy increased the surface roughness of the rebar, which significantly improved the bond of the composite rebar to the concrete.

6.3 Assessment of Dry and Prepreg Tow Consolidation on Sand Coated Samples

As discussed in Sections 6.1 and 6.2 and shown in Table 6-7, when directly embedded without any sand coating, samples consolidated with prepreg tow recorded lower bond stress values than those consolidated with dry tow. When sand was added, however, it was observed that prepreg samples recorded higher bond stress values.

Table 6-7: Summary of Average Differences

Configuration	Free-End	Loaded-End
D-N vs P-N	6 - 13%	4 - 34 %
D-S vs D-N	15 - 26%	17 - 53%
P-S vs P-N	43 - 58%	35 - 47%

To examine the differences between the dry tow sand-coated configuration (D-S) and the prepreg tow sand-coated configuration (P-S), Tables 6-8 and 6-9 were created from the averages of the two samples. For the free-end bond stress, the dry tow sand-coated configuration recorded an 8% higher bond stress than the prepreg tow sand-coated configuration for slip corresponding to 0.05 mm (0.002 in). For the slip corresponding to (0.002 in), 0.10 mm (0.004 in), 0.25 mm (0.01 in), and maximum bond stress, however, the prepreg tow sand configuration recorded average bond stress values that were 17%, 28%, and 27% higher than the dry tow respectively. For the loaded-end bond, the dry tow sand configuration average bond stress was 3%, 7%, 14%, and 9% lower than the prepreg tow sand configuration for bond stress corresponding to slip values of 0.05 mm (0.002 in), 0.10 mm (0.004 in), 0.25 mm (0.01 in), and maximum bond stress, respectively. Bond stress-slip curves of these two configurations are shown in Figures 6-7 and 6-8. These results are not consistent with trends recorded between the dry tow no-sand configuration and the prepreg no-sand configuration. The increase in bond strength when sand was added to the prepreg samples was possibly due to the fact that the resin on the prepreg tow provided a better bonding surface for the sand than the dry tow. In summary, a considerable increase in bond stress was observed for the prepreg tow sand-coated configuration compared to the dry tow sand-coated configuration.

Table 6-8: Average Free-End Bond Stress of D-S and P-S Configurations

Configuration	Average Bond Stress Corresponding to Slip Length of						Maximum Bond Stress	
	0.05 mm (0.002 in)		0.1 mm (0.004 in)		0.25 mm (0.01 in)			
	[MPa	(ksi)]	[MPa	(ksi)]	[MPa	(ksi)]	[MPa	(ksi)]
D-S Average	10.1	(1.46)	11.1	(1.61)	11.3	(1.64)	11.4	(1.65)
P-S Average	9.3	(1.35)	13.4	(1.94)	15.6	(2.26)	15.6	(2.26)
Difference	8%		17%		28%		27%	

Table 6-9: Average Loaded-End Bond Stress of D-S and P-S Configurations

Configuration	Average Bond Stress Corresponding to Slip Length of						Maximum Bond Stress	
	0.05 mm (0.002 in)		0.1 mm (0.004 in)		0.25 mm (0.01 in)			
	[MPa	(ksi)]	[MPa	(ksi)]	[MPa	(ksi)]	[MPa	(ksi)]
D-S Average	4.6	(0.66)	6.3	(0.91)	8.9	(1.29)	12.2	(1.77)
P-S Average	4.7	(0.68)	6.7	(0.98)	10.4	(1.51)	13.4	(1.94)
Difference	3%		7%		14%		9%	

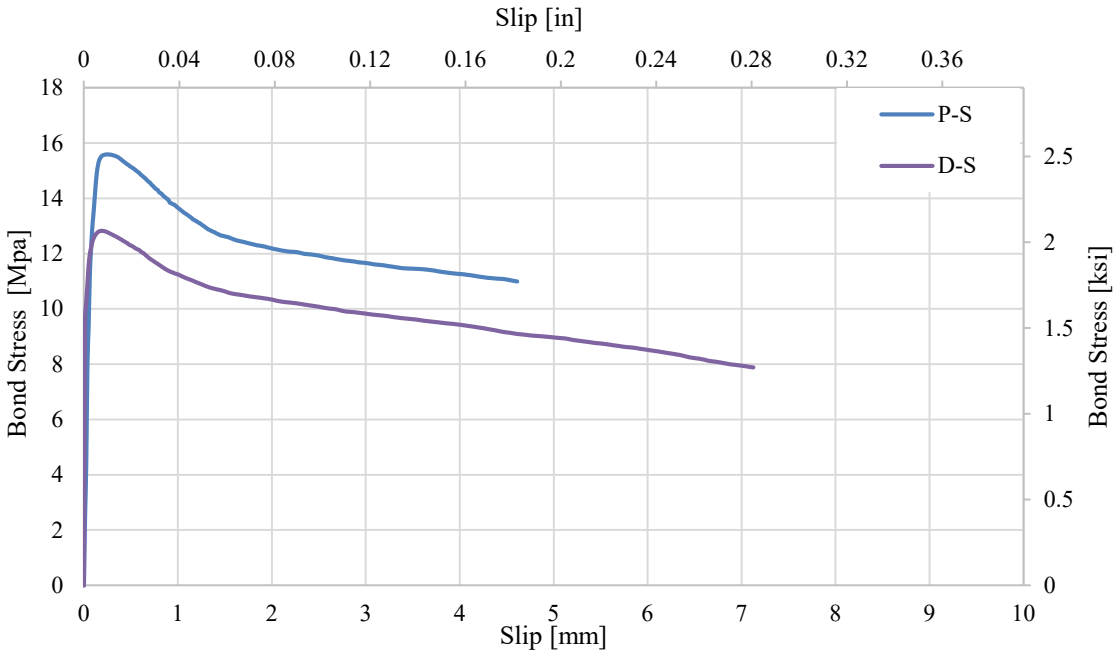

Figure 6-7: Average Free-End Slippage of D-S and P-S Configurations

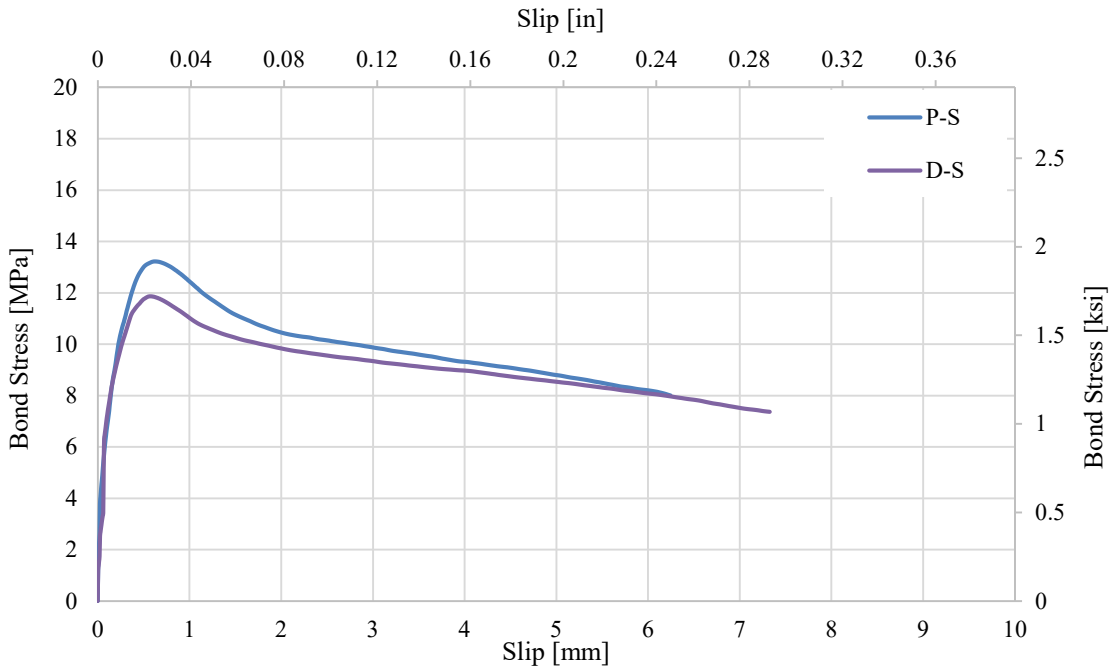

Figure 6-8: Average Loaded-End Slippage of D-S and P-S Configurations

6.4 Influence of Shear Area on Bond Strength

To illustrate the effect of the different diameters of the rebar configurations on bond stress, the bond stress of each configuration was calculated using maximum load at failure and the shear area. Shear area was calculated from the bond length, which was 63.5 mm (2.50 in) for all specimens, and a nominal circumference based on the measured diameter for specimens in each configuration. Shear diameter was measured again to account for the change in diameter due to rebar bonding with concrete and being pulled out. The shear area was calculated using Equation 6-1:

$$\boldsymbol{A = \pi l d} \qquad \textbf{Equation 6-1}$$

where:

l = bonded length

d = diameter of rebar measured after pull-out

Individual shear areas of specimens in each configuration were used to calculate bond stress using specimen maximum load. Averages were compiled for each configuration and compared with other configurations. The average shear area and bond stress is summarized in Table 6-10, while a chart of the configurations and bond stresses is shown in Figure 6-9. The prepreg sand-coated configuration (P-S) exhibited the highest bond stress, totaling 3% and 4% higher than the plain steel (S-N) and steel epoxy (S-E) configurations, respectively. The dry tow sand-coated configuration (D-S) and American Fiberglass sand-coated configuration (A-S) recorded bond stresses that were 6% and 9% lower than the P-S configurations. The weakest bond stresses were recorded by the dry tow no-sand (D-N) and prepreg tow no-sand (P-N) configurations which had the smallest shear areas. The largest shear area was recorded by the American Fiberglass sand-coated configuration.

In summary, when shear area was considered to account for slightly bigger diameters on some of the rebar configurations, the prepreg sand-coated configuration still recorded the highest bond stress values.

Table 6-10: Average Bond Stress at Maximum Load and Average Shear Area

Configuration	Average Maximum Bond Stress		Average Shear Area	
	MPa	(psi)	mm^2	(in^2)
D-N	9.08	(1320)	2480	(3.84)
P-N	8.92	(1290)	2437	(3.78)
D-S	12.0	(1740)	2774	(4.30)
P-S	12.6	(1820)	2782	(4.31)
A-S	11.2	(1620)	2800	(4.34)
S-N	12.3	(1790)	2606	(4.04)
S-E	12.4	(1800)	2637	(4.09)

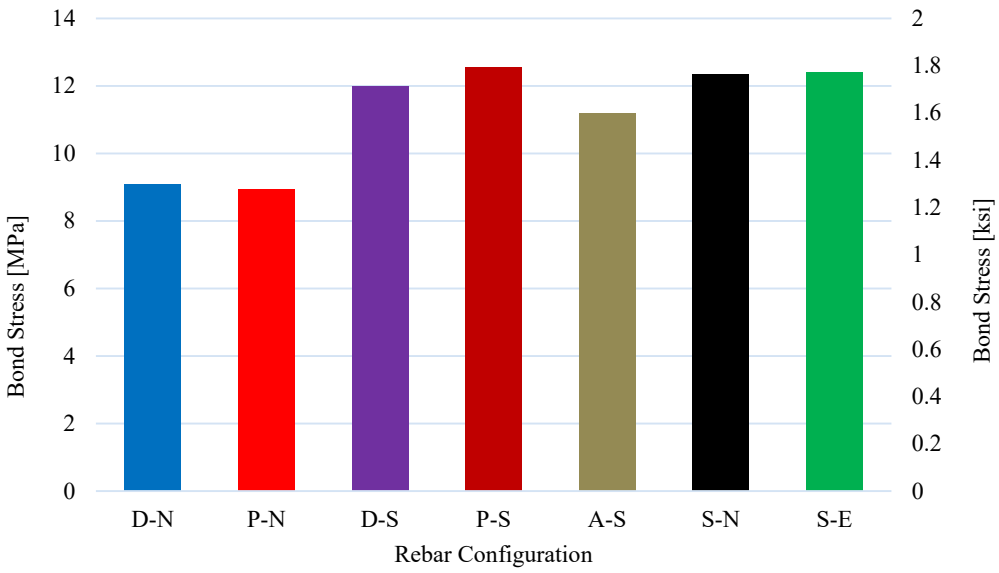

Figure 6-9: Average Bond Stress at Maximum Load Calculated from Shear Area after Pull-Out

6.5 Comparison of 3-D Braiding Machine Manufactured Fiberglass/Epoxy Rebar to Commercial Composite and Steel Rebar

This section compares the rebar manufactured for this study to the rebar from American Fiberglass Rebar as well as steel rebar.

6.5.1 Sand-Coated Rebar Compared to American Fiberglass Rebar

To illustrate the differences between the prepreg tow sand-coated configuration (P-S) and the American Fiberglass sand-coated configuration (A-S), Tables 6-11 and 6-12 were created with the average bond stress of the two configurations. For the free-end bond stress, the American Fiberglass sand-coated configuration recorded a 3% higher bond stress than the prepreg tow sand-coated configuration for slip corresponding to 0.05 mm (0.002 in). For the slip corresponding to (0.002 in), 0.10 mm (0.004 in), 0.25 mm (0.01 in), and maximum bond stress,

however, the prepreg tow sand configuration recorded average bond stress values that were 13%, 23%, and 23% higher than the American Fiberglass sand-coated configurations, respectively. For the loaded-end bond, the American Fiberglass sand-coated configuration average bond stress was 10%, 32%, 17%, and 9% lower than the prepreg tow sand configuration, for bond stress corresponding to slip values of 0.05 mm (0.002 in), 0.10 mm (0.004 in), 0.25 mm (0.01 in), and maximum bond stress, respectively. Bond stress-slip curves of these two configurations are shown in Figures 6-10 and 6-11.

Overall, the prepreg tow sand-coated configuration showed bond stress in the range of 3% - 23% higher for the free-end, and 9% - 32% higher for the loaded-end as compared with the American Fiberglass sand-coated rebar. The goal to manufacture rebar that had an equal or higher bond strength than FRP rebar currently sold on the commercial market was achieved.

Table 6-11: Average Free-End Bond Stress of P-S and A-S Configurations

Configuration	Average Bond Stress Corresponding to Slip Length of						Maximum Bond Stress	
	0.05 mm (0.002 in)		0.1 mm (0.004 in)		0.25 mm (0.01 in)			
	[MPa	(ksi)]	[MPa	(ksi)]	[MPa	(ksi)]	[MPa	(ksi)]
P-S Average	9.3	(1.35)	13.4	(1.94)	15.6	(2.26)	15.6	(2.26)
A-S Average	9.6	(1.39)	11.3	(1.63)	12.0	(1.74)	12.0	(1.74)
Difference	-3%		16%		23%		23%	

Table 6-12: Average Loaded-End Bond Stress of P-S and A-S Configurations

Configuration	Average Bond Stress Corresponding to Slip Length of						Maximum Bond Stress	
	0.05 mm (0.002 in)		0.1 mm (0.004 in)		0.25 mm (0.01 in)			
	[MPa	(ksi)]	[MPa	(ksi)]	[MPa	(ksi)]	[MPa	(ksi)]
P-S Average	4.7	(0.68)	6.7	(0.98)	10.4	(1.51)	13.4	(1.94)
A-S Average	4.2	(0.37)	4.6	(0.67)	8.6	(1.25)	12.2	(1.78)
Difference	10%		32%		17%		9%	

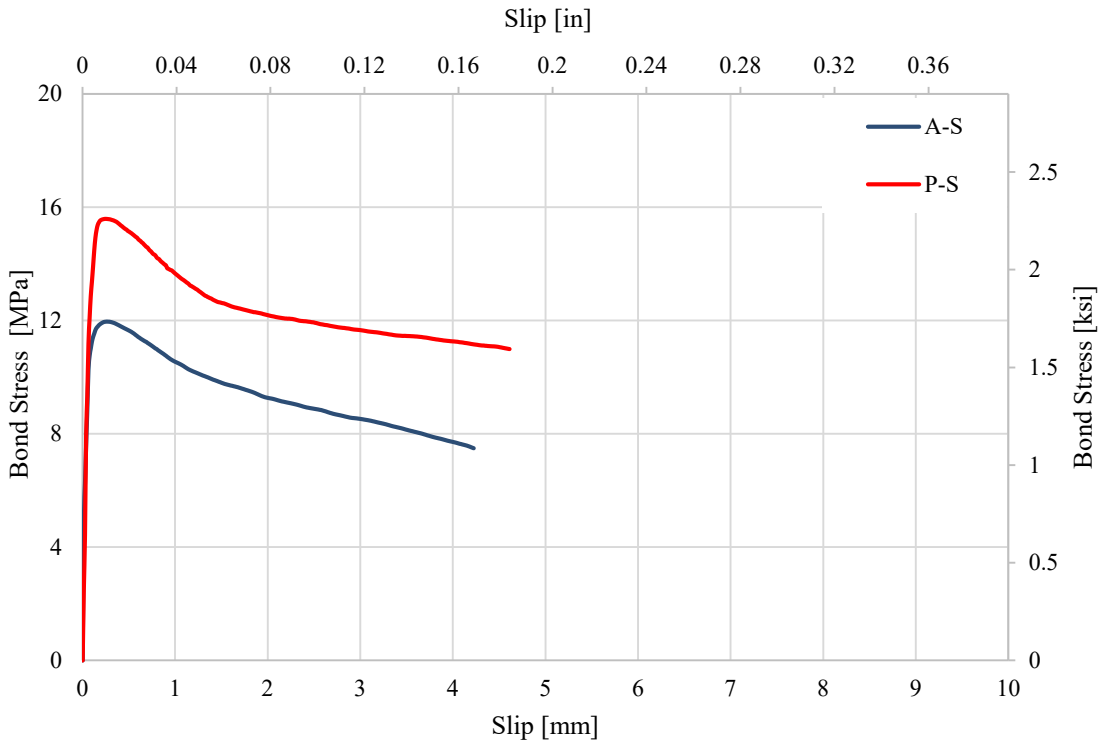

Figure 6-10: Average Free-End Slippage of A-S and P-S Configurations

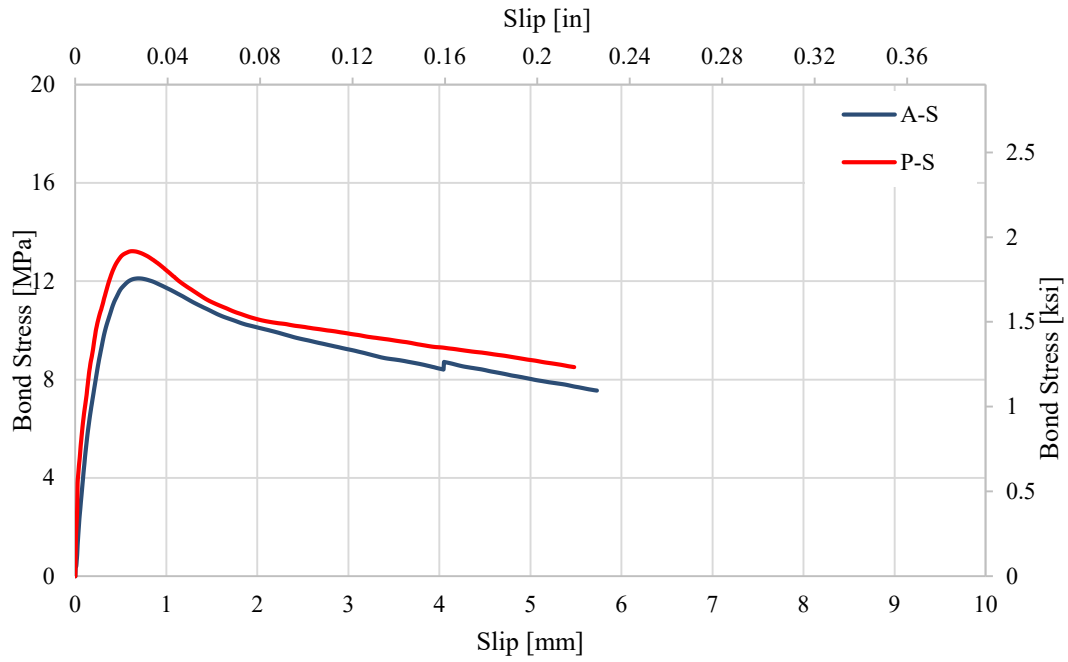

Figure 6-11: Average Loaded-End Slippage of A-S and P-S Configurations

6.5.2 Sand-Coated Rebar Compared to Steel Rebar

To illustrate the differences between the prepreg tow sand-coated configuration (P-S) and the steel configurations, Tables 6-13 and 6-14 were created to compare bond stress. As bond stress behavior exhibited by the plain steel configuration (S-N) was roughly the same as the steel epoxy configuration (S-E), the average of the plain steel configuration and the steel epoxy configuration was compared to the prepreg tow sand-coated (P-S) configuration. For the free-end bond stress, the steel average bond stress was 8%, 30%, 34% and 16% lower than the prepreg tow sand configuration, for slip corresponding to 0.05 mm (0.002 in), 0.10 mm (0.004 in), 0.25 mm (0.01 in), and maximum bond stress, respectively. For the loaded-end bond, there was no difference in bond stress of slip corresponding to 0.05 mm (0.002 in). For slip corresponding to 0.10 mm (0.004 in), 0.25 mm (0.01 in), and maximum bond stress, the steel bond stress was 4%, 3% and 9% lower than the prepreg tow sand-coated configuration, respectively. Bond stress-slip curves of these two configurations are shown in Figures 6-12 and 6-13. Overall, the prepreg tow sand configuration showed a bond stress in the range of 8% – 34% higher than the steel rebar for the free-end, and 0%–9% higher than the steel rebar for the loaded-end. In summary, the goal to manufacture rebar that possessed bond strength properties compatible to steel rebar was achieved.

Table 6-13: Average Free-End Bond Stress of P-S and Steel Configurations

Configuration	Average Bond Stress Corresponding to Slip Length of						Maximum Bond Stress	
	0.05 mm (0.002 in)		0.1 mm (0.004 in)		0.25 mm (0.01 in)			
	[MPa	(ksi)]	[MPa	(ksi)]	[MPa	(ksi)]	[MPa	(ksi)]
P-S Average	9.3	(1.35)	13.4	(1.94)	15.6	(2.26)	15.6	(2.26)
Steel Average	8.6	(0.62)	9.4	(1.04)	10.3	(1.49)	13.1	(1.90)
Difference	8%		30%		34%		16%	

Table 6-14: Average Loaded-End Bond Stress of P-S and Steel Configurations

Configuration	Average Bond Stress Corresponding to Slip Length of						Maximum Bond Stress	
	0.05 mm (0.002 in)		0.1 mm (0.004 in)		0.25 mm (0.01 in)			
	[MPa	(ksi)]	[MPa	(ksi)]	[MPa	(ksi)]	[MPa	(ksi)]
P-S Average	4.7	(0.68)	6.7	(0.98)	10.4	(1.51)	13.4	(1.94)
Steel Average	4.7	(0.68)	6.5	(0.94)	9.5	(1.38)	12.9	(1.88)
Difference	0%		4%		9%		3%	

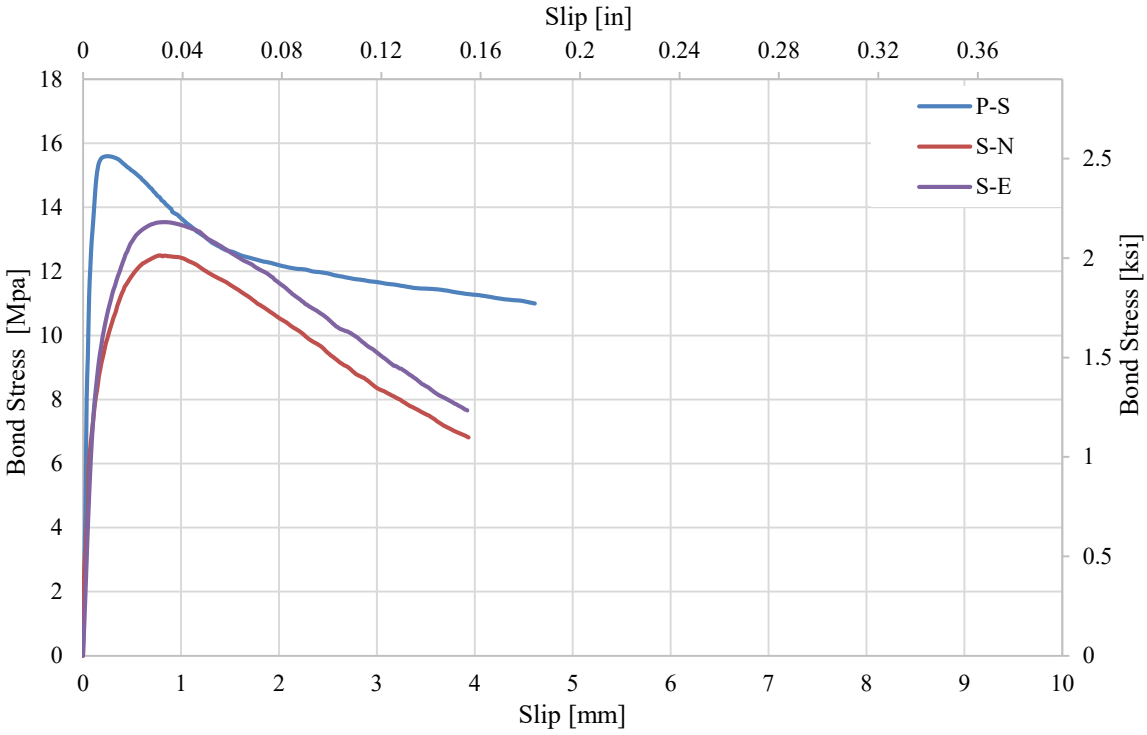

Figure 6-12 Average Free-End Slippage of P-S and Steel Configurations

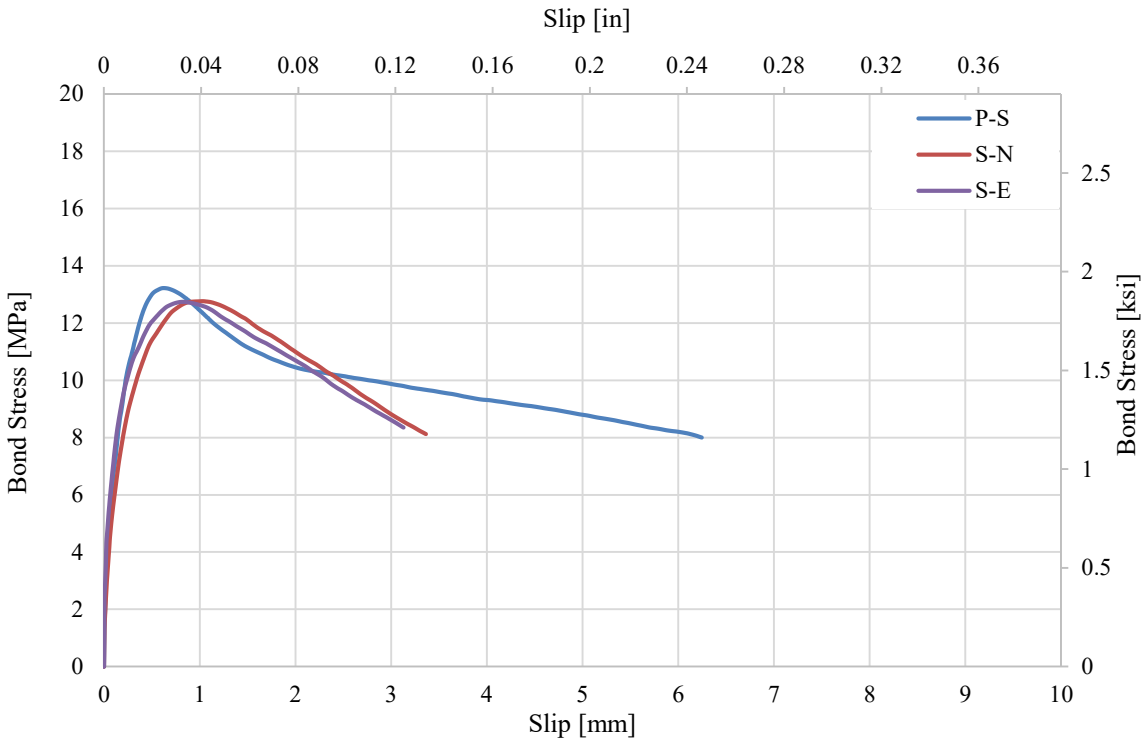

Figure 6-13: Average Loaded-End Slippage of P-S and Steel Configurations

6.6 Comparison of Free-End vs Load End Measurements

Results discussed in this thesis focused on both the free and loaded ends measurements as illustrated in ACI 440.3R-12. In this research, the free-end bond stress results, however, are a more accurate indication of bond stress compared to the loaded-end results. Displacement measuring instrumentation for the free-end were mounted at the bottom of the rebar while displacement measuring instrumentation for the loaded-end were mounted at the top of the rebar where load was applied. The loaded-end results factored in the elongation of the rebar, along with rebar slippage, which varied across samples due to different stiffness values even among samples of the same configuration. The free-end bond stress results were calculated from measurements that involved displacement data that excluded rebar elongation but only rebar movement of the rebar due to de-bonding with concrete.

7 COMMERCIALIZATION POTENTIAL FOR 3-D BRAIDED FIBER REINFORCE POLYMER REBAR

This chapter presents a simple analysis of the potential manufacturing capability of the AN1 three-dimensional braiding machine to continuously produce FRP rebar commercially on a large scale. The AN1 machine was originally designed and constructed by Atlus Poles LLc for Novatek Inc. The machine was modified in-house at Brigham Young University.

7.1 Description of AN1 3D Braiding Machine Used in this Research

The AN1 3D Braiding machine is a composite filament winding machine that is comprised of a creel with approximately 400 spools of prepreg tows under tension, a braiding wall with rotating horn gears, a gear and cable system to pull the prepreg tows. In the rebar manufacturing described in this thesis, the prepreg tow fibers were pulled from the creel through the horn gears. Bobbins that consolidate the fibers are driven by the horn gears. The creel is usually covered with plastic sheathing to prevent dust particles from contaminating the prepreg tow fibers.

The components of the AN1 3D Braiding machine are described through pictures in Figures 7-1 through 7-5. These pictures illustrate the setup of the machine using examples of how the rebar in described in this thesis was manufactured.

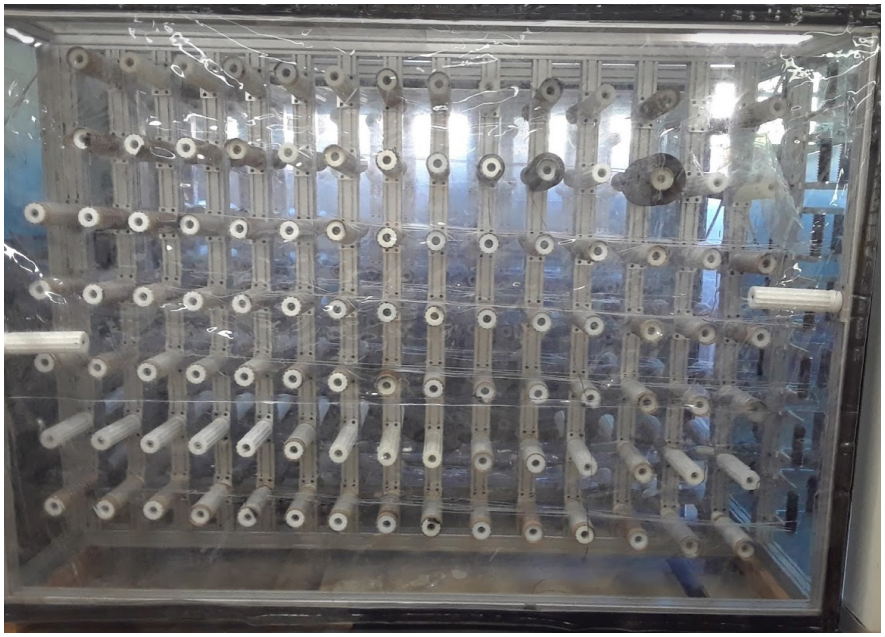

Figure 7-1: AN1 3D Braiding Machine Creel System with Spools of Prepreg Tow

Figure 7-2 Prepreg Tows Being Pulled From the Creel

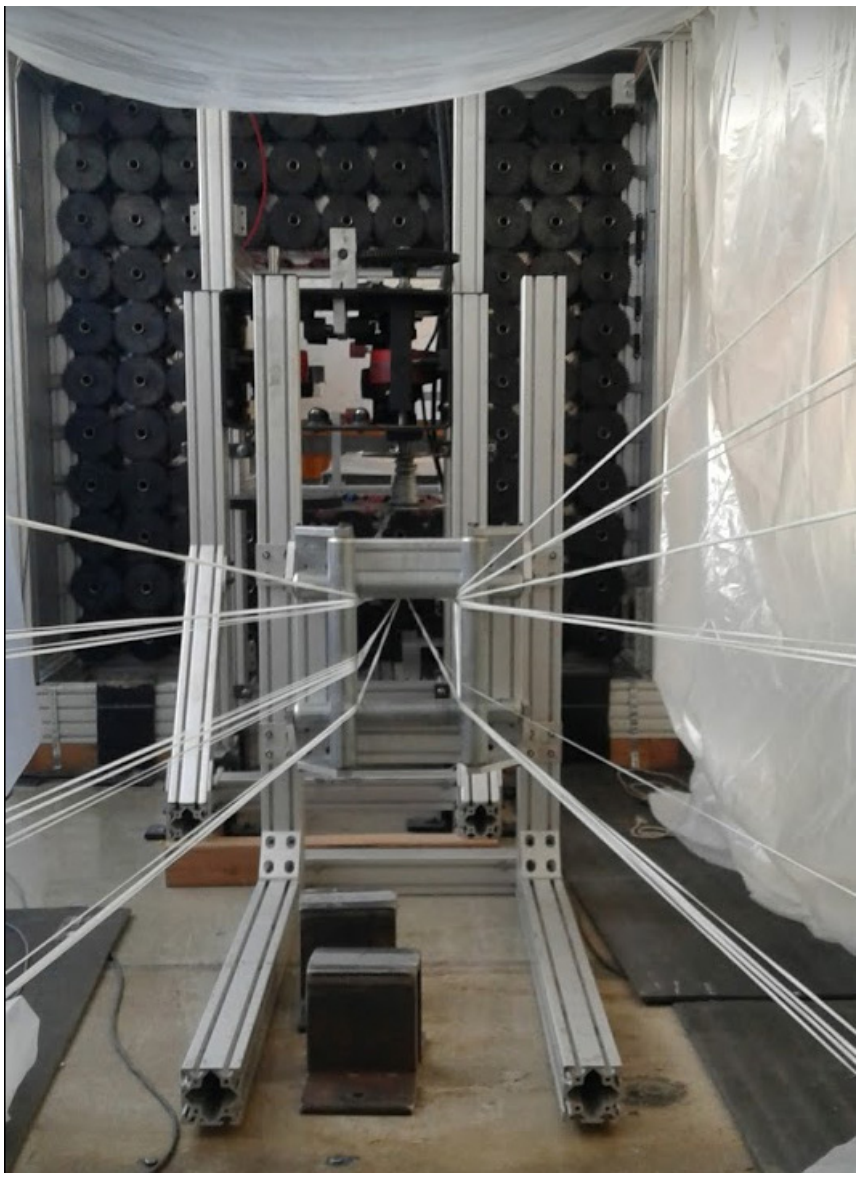

Figure 7-3: Back view of AN1 3-D Braiding Machine Showing Tows Passing through Center of Horn Gears

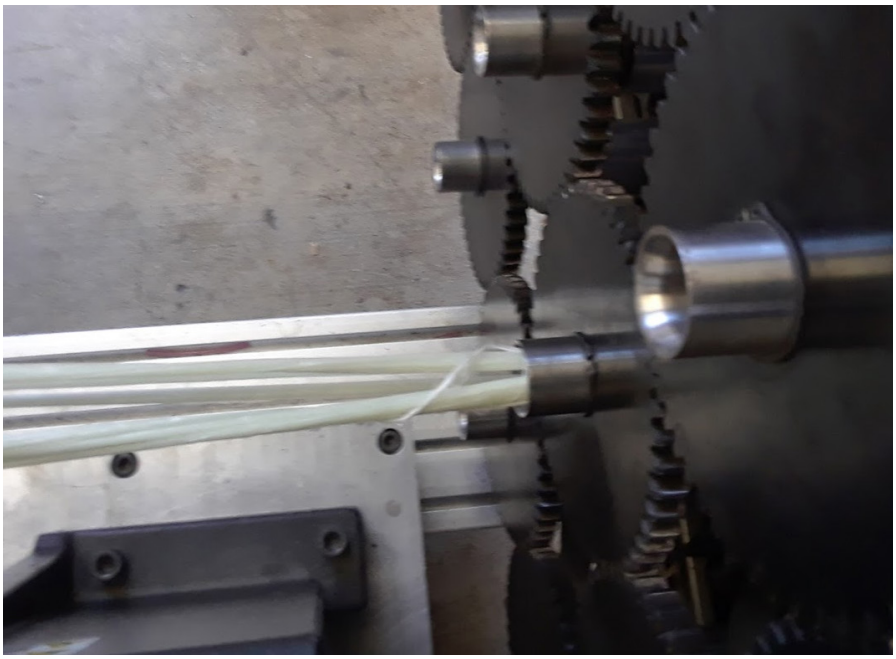

Figure 7-4: Close-Up View of Prepreg Tows Coming through Shaft in Center of Horn Gear

Figure 7-5: Fiberglass/Epoxy Rebar Comprising Prepreg Tows Being Consolidated by Bobbins on Braiding Wall

A cable and pulley system attached to an external frame was used to pull the prepreg tows through the horn gears and keep the tows under tension while they were being consolidated on the braiding wall, cured in an inline oven. Figure 7-6 shows the inline oven in front of the braiding wall. Figure 7-7 is a photo of the inline oven and the pulley system external frame. A pulley cable tied to the prepreg tows was used to pull the prepreg tows through the oven. As the prepreg tows were being pulled through the horn gear, consolidation was performed at the braiding wall. Once enough length of prepreg tow was completed, the machine was paused and the consolidated fibers were cured under tension, following the manufacture's recommended cure cycle as described in Chapter 3.

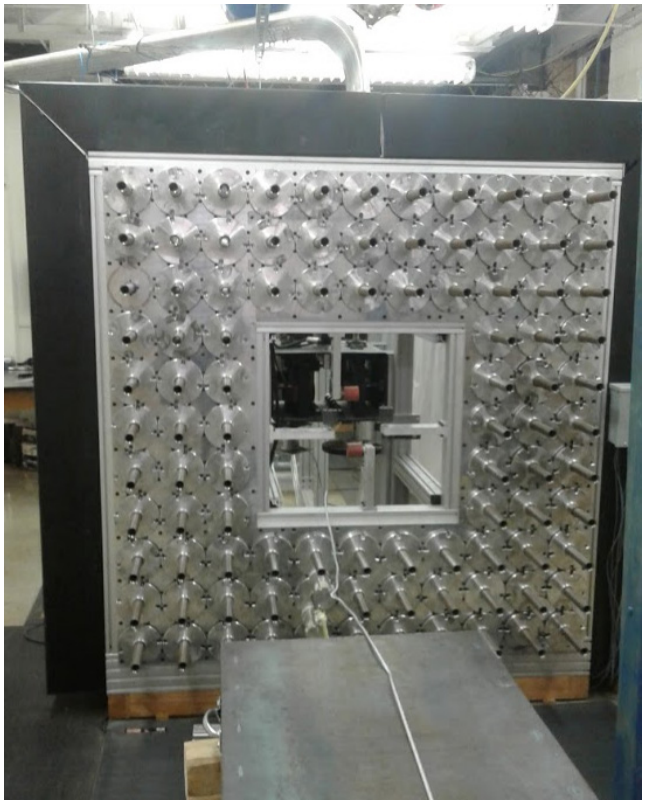

Figure 7-6: Front of 3-D Braiding Machine with Braiding Wall and Inline Oven

Figure 7-7: Inline Oven and Pulley Frame System for Pulling Small Numbers of Rebar

7.2 Modifications of AN1 3D Braiding Machine Required for Commercial Production

In the research performed, only one horn gear and one pulling cable were used to manufacture fiberglass rebar. The AN1 machine can, however, be modified to manufacture 96 rebar simultaneously using the entire braiding wall. To ensure full scale production of 96 simultaneous rebar, a roller system will be required that would ensure the pulling of prepreg tow. The current creel system has a total of 420 spools, each with a capacity to withstand 22 N (5.0 lbs) of tension force. Additional creels can be installed to increase production.

The No. 4 rebar size described in this research was manufactured using 238 tows of E-Glass 158B-AAA-675 unidirectional fiberglass filament obtained from TCR Composites. This fiberglass had 2,000 filaments per tow, as detailed in section 3.1. The manufacturer, however, is capable of increasing the tow size by a factor of at least up to 15. Using a bigger tow size would

be ideal for large scale production as it would reduce the number of individual tows required for a specific size of rebar and ensure faster production. In this case, that translates to 30,000 filaments per tow, requiring no more than 16 spools on the creel for a single 12.7 mm (0.5 in.) rebar. Without even using larger tows, the creel system will have to be quadrupled to use the full capacity of the braiding wall.

The AN1 machine has a manufacturing speed of 0.9 m/min (3.0 ft/ min). Therefore, in one minute, 86 meters (288 ft) of rebar can be manufactured. During the rebar manufacturing for this research, production was slowed mainly by rebar curing. For commercial production, tow impregnated with ultraviolet (UV) curing resin or another rapid curing resin would greatly accelerate rebar production time. Rebar curing should be performed when the consolidated tows are under tension. The UV light can be used for a preliminary cure that will allow the rebar to gain stiffness. After this preliminary cure, the rebar can be moved away from the production line and post cured using an oven, if necessary. The interim time between the preliminary and post cure can also be used for a secondary process of sand coating of the rebar, as results from this research showed that sand coating is required for manufacturing of rebar with compatible bond strength to steel rebar.

Sand coating can also be applied during braiding before any curing. To ensure the possibility of applying sand during braiding, the prepreg tows can be twisted while being pulled. If sand is dropped onto the rebar using gravity, the twisting will facilitate the rebar getting fully covered around its circumference rather than only on the side facing up. One advantage of using this sand coating approach is that it would eliminate a secondary process for sand coating. The rebar can afterwards be cured using UV light or infrared or thermal heating. The efficiency of the curing process employed would dictate the need for a post-cure using an oven. A mechanism

is required to cut the rebar during production. An ideal cut-off saw would be one that does not disrupt the production line. The saw will need to cut through 96 pieces of rebar. A water jet would be a compatible option as well.

8 CONCLUSIONS AND RECOMMENDATIONS

This chapter presents general conclusions reached and describes recommendations for future research. Pull-out strength tests were completed to quantify the bond strength of fiber epoxy composite rods consolidated with aramid fiber. Test variables include nature of consolidation material, secondary process, and comparison with baseline rebar types of commercial FRP and steel rebar.

8.1 General Conclusions

1. Rebar consolidated with dry tow showed higher bond stress in the range of 6% to 13% higher for the free-end and 4% to 34% higher for the loaded-end than rebar consolidated with a prepreg tow when embedded in concrete directly without any secondary processes such as sand coating. Therefore, in the absences of sand coating, consolidating FRP rebar with a dry tow compared to a prepreg tow yields rebar with better bonding capacity.
2. For both the dry tow and prepreg tow consolidation, the addition of sand bonded onto the surface of the fiberglass/epoxy composite rebar increased the surface roughness of the rebar, which considerably improved the bond of the composite rebar to the concrete. Therefore, for better concrete rebar, sand coating or another form of surface roughness should be employed during the manufacturing of FRP rebar.

3. The prepreg sand-coated configuration recorded the highest bond stress values compared to all the other configurations discussed in this research, leading to the conclusion that a combination of prepreg tow consolidation and sand coating is the most effective way of manufacturing fiberglass/epoxy rebar.
4. The goal to manufacture rebar on the three-dimensional braiding machine that had an equal or higher bond strength than FRP rebar currently sold on the commercial market was achieved. Therefore, AN1 three-dimensional braiding machine can be used for the manufacturing of commercial FRP rebar.
5. The goal to manufacture rebar on the three-dimensional braiding machine that possessed bond strength properties compatible to steel rebar was achieved and therefore FRP rebar should be used over steel in appropriate situations, such as when corrosion is most likely to degrade steel rebar.
6. With modifications to accommodate large scale production, the three-dimensional braiding machine can be used to manufacture quality FRP rebar.

8.2 Recommendations for Future Research

1. This research should be expanded to studying the behavior of FRP rebar in bending.
2. The results between the prepreg sand-coated configuration and dry sand-coated configuration should be studied further with the research focused primarily on these two configurations.
3. To allow for consistency, the concrete mix design in this research should be revised and trial batches be mixed and tested for 28-days for a better projection and estimation of the concrete 28-day strength.

4. Other measures to introduce ribs on the surface of the rebar must be investigated. For example, shrink tape may be used to introduce rebar ribs.
5. The bobbins should be modified to improve the fiber release mechanism. The tension on the current bobbins would increase causing the braiding fibers to be tangled or to break periodically, slowing down the manufacturing process and causing the braided sleeves to be inconsistent.

REFERENCES

[1] Asay, B.(2015), "Bending Behavior of Carbon/Epoxy Composite IsoBeam Structures" M.S Thesis, Brigham Young University, Provo, Utah

[2] Kesler, S. (2006), "Consolidation and Interweaving of Composite Members by a Continuous Manufacturing Process," M.S. Thesis, Brigham Young University, Provo, Utah.

[3] Winkel, L. (2001), "Parametric Investigation of IsoTruss™ Geometry Using Linear Finite Element Analysis," M.S. Thesis, Brigham Young University, Provo, Utah.

[4] Scoresby, B. (2003), "Low Velocity Longitudinal and Radial Impact of IsoTruss™ Grid Structures," M.S. Thesis, Brigham Young University, Provo, Utah.

[5] McCune, A. (2001), "Tension and Compression of Carbon/Epoxy IsoTruss™ Grid Structures," M.S. Thesis, Brigham Young University, Provo, Utah.

[6] Blake, R. (1998), "Compression and Flexure of Graphite/Epoxy IsoTruss-Reinforced Concrete." M.S. Thesis, Brigham Young University, Provo, Utah.

[7] Layne Jones. (2000), "Flexural Behavior of Spirally-Consolidated Double IsoTruss Reinforced Concrete Beams." M.S. Thesis, Brigham Young University, Provo, Utah

[8] Brahim Benmokraine. (2002), "Durability of Glass Fiber-Reinforced Polymer Reinforcing Bars in Concrete Environment." Journal of Composites for Construction, Vol 6 Issue 3, August 2002

[9] Zenon Achillides, and Kypros Pilakoutas. (2004), "Bond Behavior of Fiber Reinforced Polymer Bars under Direct Pullout Conditions." Journal of Composites for Construction, Vol 8 Issue 2. April 2004

[10] Cosenza, E., Manfredi, G., Pecce, M., and Realfonzo, R. (1999), "Bond between Glass Fiber Rebar Reinforced Plastic Reinforcing Bars and Concrete." *ACI* SP-188, 1999

[11] Cosenza, E., Manfredi, G., Pecce, M., and Realfonzo, R. (1997), "Behavior and Modeling of Bond of FRP Rebars to Concrete." Journal of Composites for Construction, Vol 1 Issue 2. May 1997

[12] Zhiqiang Dong, GangWu, Bo Xu, Xin Wang, and Luc Taerwe. (2014), "Bond durability of BFRP bars embedded in concrete under seawater conditions and the long-term bond strength prediction." ELSEVIER, December 2015

[13] Pavel Akishin, Andrejs Kovalovs, Vladimir Kulakov, Alexander Arnautov. (2014), "Finite Element Modelling of Slipage Between FRP Rebar and Concrete in Pull-Out Test." Proceedings of the International Conference, Innovative Materials, Structures and Technologies,10.7250/iscconstrs.2014.01. August 2014

[14] Abdeldjelil Belarbi, and Huanzi Wang. (2012). "Bond Durability of FRP Bars Embedded in Fiber-Reinforced Concrete." Journal of Composites for Construction, Volume 16 Issue 4 - August 2012

[15] Jong-Pil Won, Chan-Gi Park, Hwang-Hee Kim, Sang-Woo Lee, Chang-Il Jang. (2007). "Effect of fibers on the bonds between FRP reinforcing bars and high-strength concrete." ELSEVIER, December 2007

[16] J. Larralde, Associate Member, ASCE, and R. Silva-Rodriguez. (1993). "Bond and Slip of FRP Rebar in Concrete." Journal of Materials in Civil Engineering, Vol 5 Issue 1, February 1993

[17] Ammon Katz, Neta Berman, and Lawrence C. Bank (1999). "Effect of High Temperature on Bond Strength of FRP Rebar. Journal of Composites for Construction, Vol 3, Issue 2 May 1999

[18] Adam C. Berg, Lawrence C. Bank, Michael G. Oliva, Jeffrey S. Russell (2005). "Construction and cost analysis of an FRP reinforced concrete bridge deck." ELSEVIER, April 2005.

[19] Owens Corning® (1999). "158B Type 30® Roving." http://www.owenscorning.com.cn/Form_Up/Images/17111-D.pdf

[20] TCR Composites (2013). "UF3369 TCRTM Resin Technical Data Sheet," Revision 13 http://www.tcrcomposites.com/pdfs/resindata/uf3369_v11_912.pdf

[21] Teijin Aramid (2012). "Twaron – a versatile high-performance fiber." http://www.teijinaramid.com/wp-content/uploads/2016/07/Product-Brochure Twaron.pdf

[22] Allen, D. (2011), "Damage Tolerance of Unidirectional Basalt Composites Encased in an Aramid Sleeve," M.S. Thesis, Brigham Young University, Provo, Utah

[23] Sika, C. (2012), "Damage Tolerance of Unidirectional Carbon and Fiberglass Composites with Aramid Sleeves," M.S. Thesis, Brigham Young University, Provo, Utah.

[24] Embley, M. (2011), “Damage Tolerance of Buckling-Critical Unidirectional Carbon, Fiberglass, and Basalt Fiber Composites in Co-Cured Aramid Sleeves,” M.S. Thesis, Brigham Young University, Provo, Utah.

[25] Cahoon, L. (2016), “Micro-CT Inspection of Impact Damage in Carbon/Epoxy Rods,” M.S. Thesis, Brigham Young University, Provo, Utah.

[26] Pro-Set (2015). “Technical Data INF-114 INF 211”. http://www.prosetepoxy.com/wp-content/uploads/INF-114_INF-211.pdf

[27] Pinkerton, T. (2007), “Sensitivity of Half-Cell Potential Measurements to Properties of Concrete Bridge Decks,” M.S. Thesis, Brigham Young University, Provo, Utah.

[28] ASTM C143 / C143M-15a, Standard Test Method for Slump of Hydraulic-Cement Concrete, ASTM International, West Conshohocken, PA, 2015, www.astm.org

[29] ASTM C231 / C231M-17a, Standard Test Method for Air Content of Freshly Mixed Concrete by the Pressure Method, ASTM International, West Conshohocken, PA, 2017, www.astm.org

[30] ASTM C39 / C39M-17b, Standard Test Method for Compressive Strength of Cylindrical Concrete Specimens, ASTM International, West Conshohocken, PA, 2017, www.astm.org

[31] ASTM C617 / C617M-15, Standard Practice for Capping Cylindrical Concrete Specimens, ASTM International, West Conshohocken, PA, 2015, www.astm.org

[32] Mansfield, M (2012). “A TEXTBOOK ON THE METHOD OF LEAST SQUARES. 8TH ED., REV,” Indiana: Repressed Publishing LLC, 2012

APPENDIX A. MIX DESIGN AND CONCRETE PROPERTIES

A.1 Coarse and Fine Aggregate Properties

A.1.1 Coarse Aggregate Properties

Table A-1 and Table A-2 were provided and used by of permission of Charles Robinson of Geneva Rock.

Table A-1: Properties of Coarse Aggregate

Aggregate Submittal			
Report of Physical Properties			
GRP Material Description: Washed, Concrete Rock		Report Date: February 24, 2017	
GRP Material Code: ROCA		Reviewed by: Victor Johnson	
Source Location/Code: Point of the Mtn/525		Report No.: 525ROCA00117	
Test Results			
Standard	Physical Properties		Result
ASTM C 29 AASHTO T19	Unit Weight	Unit Weight, lbs/cu.ft Voids, % ○ Jigged ○ Loose ● Rodded	96 39
ASTM C131 AASHTO T96	L.A. Abrasion	Small Coarse Loss, % Grading/Revolutions	23 B/500
ASTM C 127 AASHTO T85	Coarse Specific Gravity & Absorbtion	Bulk Specific Gravity (dry) Bulk Specific Gravity, SSD Apparent Specific Gravity Absorbtion, %	2.520 2.563 2.634 1.7
ASTM C 88 AASHTO T104	Soundness	Coarse Soundness Loss, % Sodium Sulfate No. Of Cycles	1 5
ASTM C40 AASHTO T21	Organic Impurities	Coarse Aggregate, %	Lighter Plate #1
ASTM C142 AASHTO T112	Clay/Friable Impurities	Coarse Aggregate, %	0
ASTM C123 AASHTO T113	Lightweight Pieces	Coarse Aggregate, %	0
ASTM D5821	Fractured Face	1 or 2 Faces Fractured Face, %	1 = 100 2 = 99

Table A-2: Coarse Aggregate Sieve Analysis

Coarse Aggregate Sieve Analysis		
Sieve Size	% Passing	
25.0 mm (1")	100	
19.0 mm (3/4")	98	
12.5 mm (1/2")	65	
9.5 mm (3/8")	34	
4.75 mm (No. 4)	2	
2.36 mm (No. 8)	1	
0.075 mm (No. 200)	0.4	
ASTM D4791	Ratio	5:1
	Flat & Elongated %	0

A.1.2 Fine Aggregate Properties

Table 3 and Table 4 below were provided and used by of permission of Charles Robinson of Geneva Rock.

Table A-3: Properties of Fine Aggregate

Geneva Rock Aggregate Submittal ASTM C-33 Report of Physical Properties **Geneva Rock** GRP Material Description: Washed, Concrete Sand GRP Material Code: SAND Source Location/Code: Point of the Mtn/533		Report Date: Januay 31, 2017 Reviewed by: Victor Johnson ASTM C-33 Report No.: 533SAND00216	
Test Results			
Standard	Physical Properties		Result
ASTM C 29 AASHTO T19	Unit Weight	Unit Weight, lbs/cu.ft Voids, %	104 35
		○ Jigged ○ Loose ● Rodded	
ASTM D4318 AASHTO T89/90	Liquid Limit Plastic Limit Plasticity Index	Liquid Limit Plastic Limit Plasticity Index	0 0 NP
ASTM C 128 AASHTO T84	Fine Specific Gravity & Absorbtion	Bulk Specific Gravity (dry) Bulk Specific Gravity, SSD Apparent Specific Gravity Absorbtion, %	2.549 2.580 2.631 1.2
ASTM C 88 AASHTO T104	Soundness	Fine Soundness Loss, % Sodium Sulfate No. Of Cycles	2 5
ASTM C 1252 AASHTO T304	Fine Aggregate Singularity	Uncompacted Voids, % Method C (as received material)	46.3
ASTM C40 AASHTO T21	Organic Impurities	Fine Aggregate, %	Lighter Plate #1
ASTM C142 AASHTO T112	Clay/Friable Impurities	Fine Aggregate, %	0
ASTM C123 AASHTO T113	Lightweight Pieces	Fine Aggregate, %	0

Table A-4: Fine Aggregate Sieve Analysis

Sand Sieve Analysis	
Sieve Size	% Passing
4.75 mm (No. 4)	100
2.36 mm (No. 8)	85
1.18 mm (No. 16)	64
0.600 mm (No. 30)	47
0.300 mm (No. 50)	25
0.150 mm (No. 100)	5
0.075 mm (No. 200)	1.0

A.2 Concrete Mix Design Properties

Table A-5: Batch 1 Cylinder Test results

Cylinder	Load		Compressive Strength	
	[kN	(lbs)]	[MPa	(psi)]
1	173	(38875)	21.34	(3095)
2	172	(38740)	21.27	(3084)
3	196	(44110)	24.21	(3512)
Average	181	(40575)	22.27	(3230)
Std.Dev	11	(2500)	1.37	(199)

Table A-6: Batch 2 Cylinder Test Results

Cylinder	Load		Compressive Strength	
	[kN	(lbs)]	[MPa	(psi)]
1	213	(47885)	26.29	(3813)
2	200	(44895)	24.64	(3574)
3	188	(42280)	23.21	(3366)
Average	200	(45020)	24.71	(3584)
Std.Dev	10	(2290)	1.26	(182)

Table A-7: Batch 3 Cylinder Test Results

Cylinder	Load		Compressive Strength	
	[kN	(lbs)]	[MPa	(psi)]
1	222	(49885)	27.38	(3972)
2	211	(47430)	26.04	(3776)
3	235	(52915)	29.05	(4213)
Average	223	(50077)	27.49	(3987)
Std.Dev	10.0	(2243)	1.23	(179)

Table A-8: Batch 4 Cylinder Test Results

Cylinder	Load		Compressive Strength	
	[kN	(lbs)]	[MPa	(psi)]
1	205	(46100)	25.31	(3670)
2	204	(45910)	25.20	(3655)
3	206	(46335)	25.44	(3689)
Average	205	(46115)	25.31	(3672)
Std.Dev	0.80	(174)	0.10	(14)

Table A-9: Batch 5 Cylinder Test Results

Cylinder	Load		Compressive Strength	
	[kN	(lbs)]	[MPa	(psi)]
1	213	(47890)	26.29	(3813)
2	207	(46595)	25.58	(3710)
3	225	(50655)	27.81	(4033)
Average	215	(48380)	26.56	(3852)
Std.Dev	8.00	(1693)	0.93	(135)

Table A-10: Bach 6 Cylinder Test Results

Cylinder	Load		Compressive Strength	
	[kN	(lbs)]	[MPa	(psi)]
1	206	(46185)	25.35	(3677)
2	200	(44920)	24.66	(3576)
3	212	(47615)	26.14	(3791)
Average	206	(46240)	25.38	(3682)
Std.Dev	5.00	(1101)	0.60	(88)

Table A-11: Weight Amounts of Each Ingredient

Batch	Coarse Aggregate		Fine Aggregate		Water		Cement		Air Entrainer		Slump	
	[kg	(lbs)]	[kg	(lbs)]	[kg	(lbs)]	[kg	(lbs)]	[ml	(oz)]	[cm	(in)]
1	70.0	(154.3)	47.8	(105.3)	14.8	(32.7)	26.1	(57.6)	27.0	(0.91)	16.5	(6.5)
2	70.0	(154.4)	47.8	(105.4)	14.8	(32.7)	26.1	(57.6)	27.0	(0.91)	17.8	(7.0)
3	69.9	(154.2)	47.7	(105.2)	14.8	(32.6)	26.1	(57.6)	26.8	(0.91)	14.0	(5.5)
4	69.9	(154.2)	47.7	(105.2)	14.8	(32.7)	26.1	(57.6)	27.0	(0.91)	16.5	(6.5)
5	69.9	(154.2)	47.7	(105.2)	14.8	(32.7)	26.1	(57.6)	26.0	(0.88)	16.5	(6.5)
6	69.9	(154.2)	47.7	(105.2)	14.8	(32.7)	26.1	(57.6)	26.0	(0.88)	15.9	(6.3)

APPENDIX B. FIBERGLASS/EPOXY REBAR GEOMETRY PROPERTIES

B.1 Weights and Unit Length

Table B-1: Dry Tow No-sand Configuration Length and Unit Weight

Sample I.D	Length		Unit Weight	
	cm	In	g/cm	lb/in
D-N-1	55.0	(21.7)	2.36	(0.013)
D-N-2	54.4	(21.4)	2.38	(0.013)
D-N-3	54.2	(21.3)	2.38	(0.013)
D-N-4	53.8	(21.2)	2.37	(0.013)
D-N-5	53.7	(21.1)	2.36	(0.013)
Average	54.2	(21.3)	2.37	(0.013)
Std. Dev	0.47	(0.18)	0.01	(0.000)

Table B-2: Prepreg Tow No-sand Configuration Length and Unit Weight

Sample I.D	Length		Unit Weight	
	cm	In	g/cm	lb/in
P-N-1	55.0	(21.7)	2.37	(0.013)
P-N-2	54.2	(21.3)	2.36	(0.013)
P-N-3	53.8	(21.2)	2.34	(0.013)
P-N-4	54.9	(21.6)	2.32	(0.013)
P-N-5	54.3	(21.4)	2.38	(0.013)
Average	54.4	(21.4)	2.35	(0.013)
Std. Dev	0.45	(0.18)	0.02	(0.000)

Table B-3: Dry Tow Sand Configuration Length and Unit Weight

Sample I.D	Length		Unit Weight	
	cm	In	g/cm	lb/in
D-S-1	55.1	(21.7)	2.92	(0.016)
D-S-2	53.7	(21.1)	3.07	(0.017)
D-S-3	54.5	(21.5)	3.21	(0.018)
D-S-4	53.8	(21.2)	3.11	(0.017)
D-S-5	54.3	(21.4)	3.17	(0.018)
Average	54.3	(21.4)	3.09	(0.017)
Std. Dev	0.51	(0.20)	0.10	(0.001)

Table B-4: Prepreg Tow Sand Configuration Length and Unit Weight

Sample I.D	Length		Unit Weight	
	cm	In	g/cm	lb/in
P-S-1	55.2	(21.7)	3.07	(0.017)
P-S-2	54.8	(21.6)	3.02	(0.017)
P-S-3	54.0	(21.3)	3.06	(0.017)
P-S-4	54.6	(21.5)	3.08	(0.017)
P-S-5	53.4	(21.0)	3.07	(0.017)
Average	54.4	(21.4)	3.06	(0.017)
Std. Dev	0.63	(0.25)	0.02	(0.000)

Table B-5: American Fiberglass Configuration Length and Unit Weight

Sample I.D	Length		Unit Weight	
	cm	In	g/cm	lb/in
A-S-1	61.0	(24.0)	3.04	(0.017)
A-S-2	61.0	(24.0)	2.96	(0.017)
A-S-3	61.0	(24.0)	2.99	(0.017)
A-S-4	61.0	(24.0)	3.00	(0.017)
A-S-5	61.0	(24.0)	3.00	(0.017)
Average	61.0	(24.0)	3.00	(0.017)
Std. Dev	0.00	(0.00)	0.03	(0.000)

Table B-6: Plain Steel Configuration Length and Unit Weight

Sample I.D	Length		Unit Weight	
	cm	In	g/cm	lb/in
S-N-1	61.0	(24.0)	9.40	(0.053)
S-N-2	61.0	(24.0)	9.42	(0.053)
S-N-3	61.0	(24.0)	9.47	(0.053)
S-N-4	61.0	(24.0)	9.44	(0.053)
S-N-5	61.0	(24.0)	9.41	(0.053)
Average	61.0	(24.0)	9.43	(0.053)
Std. Dev	0.00	(0.00)	0.02	(0.000)

Table B-7: Steel Epoxy Configuration Length and Unit Weight

Sample I.D	Length		Unit Weight	
	cm	In	g/cm	lb/in
S-E-1	61.0	(24.0)	9.65	(0.054)
S-E-2	61.0	(24.0)	9.59	(0.054)
S-E-3	61.0	(24.0)	9.68	(0.054)
S-E-4	61.0	(24.0)	9.63	(0.054)
S-E-5	61.0	(24.0)	9.69	(0.054)
Average	61.0	(24.0)	9.65	(0.054)
Std. Dev	0.00	(0.00)	0.04	(0.000)

B.2 Void Ratio and Fiber Volume Fraction

Table B-8: Dry Tow No-sand Configuration Void Ratio and Fiber Volume Fraction

Specimen I.D.	Void Ratio	Fiber Volume Fraction %
D-N-1	0.09	77.1
D-N-2	0.09	76.3
D-N-3	0.09	73.3
D-N-4	0.09	73.9
D-N-5	0.09	73.8
Average	0.09	74.9
std.dev	0.00	1.52

Table B-9: Prepreg Tow No-sand Configuration Void Ratio and Fiber Volume Fraction

Specimen I.D.	Void Ratio	Fiber Volume Fraction %
P-N-1	0.09	73.0
P-N-2	0.09	73.5
P-N-3	0.09	73.1
P-N-4	0.09	71.6
P-N-5	0.09	68.9
Average	0.09	72.0
std.dev	0.00	1.68

Table B-10: Dry Tow Sand Configuration Void Ratio and Fiber Volume Fraction

Specimen I.D.	Void Ratio	Fiber Volume Fraction %
D-S-1	0.09	75.0
D-S-2	0.09	73.9
D-S-3	0.09	74.1
D-S-4	0.09	74.1
D-S-5	0.09	74.1
Average	0.09	74.3
std.dev	0.00	0.39

Table B-11: Prepreg Tow Sand Configuration Void Ratio and Fiber Volume Fraction

Specimen I.D.	Void Ratio	Fiber Volume Fraction %
P-S-1	0.09	68.8
P-S-2	0.09	73.6
P-S-3	0.09	73.3
P-S-4	0.09	72.5
P-S-5	0.09	73.5
Average	0.09	72.3
std.dev	0.00	1.79

Table B-12: American Fiberglass Configuration Void Ratio And Fiber Volume Fraction

Specimen I.D.	Void Ratio	Fiber Volume Fraction %
C-1	0.08	75.1
C-3	0.08	72.1
C-2	0.08	71.0
C-4	0.08	69.9
C-5	0.08	71.4
Average	0.08	71.9
std.dev	0.00	1.74

B.3 Microscope Images

B.3.1 Dry Tow No-sand Configuration (D-N) Images

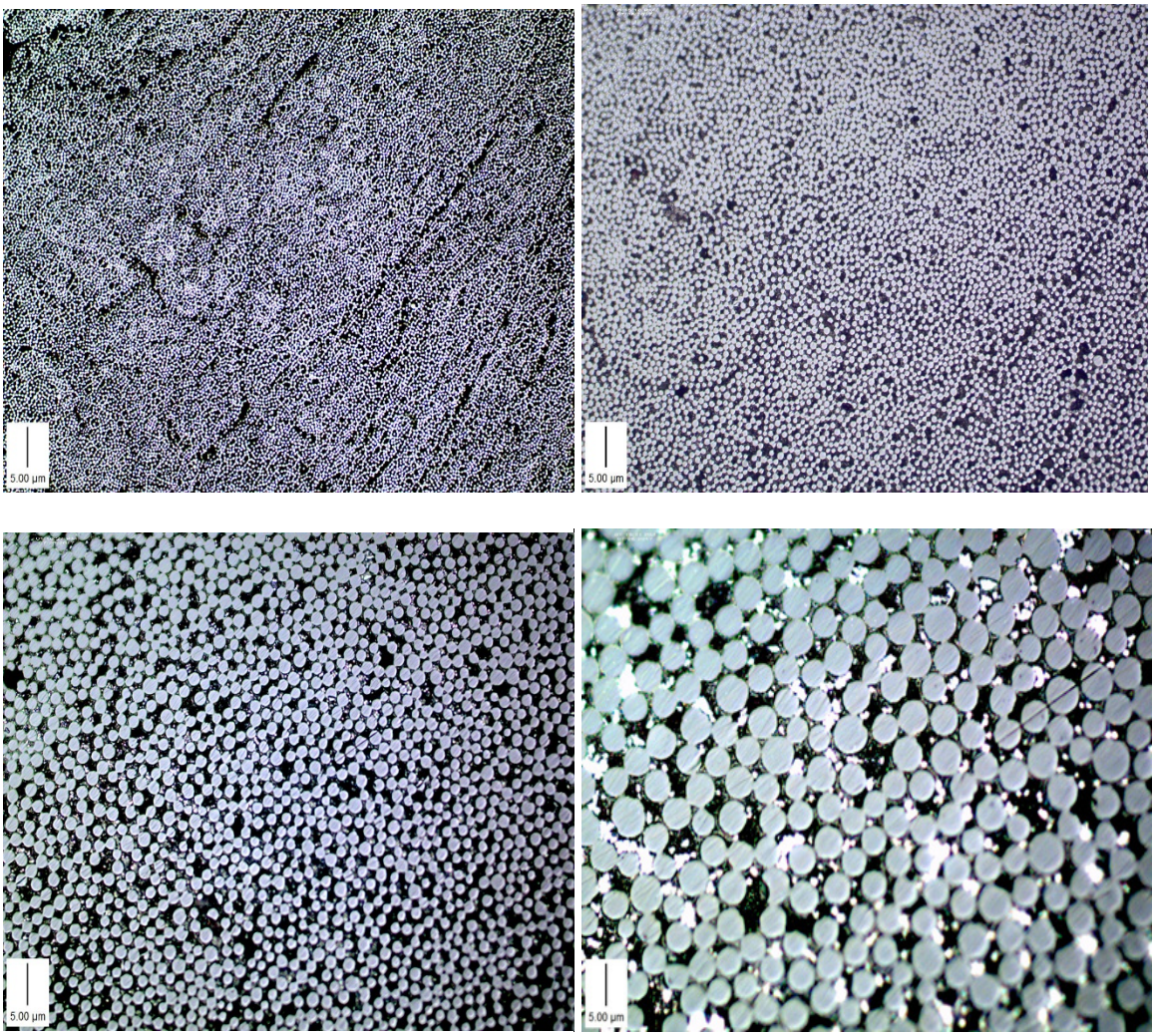

Figure B-13: D-N-1 x50 Magnification (top left); x100 Magnification (top right); x200 Magnification (bottom left); x500 Magnification (bottom right)

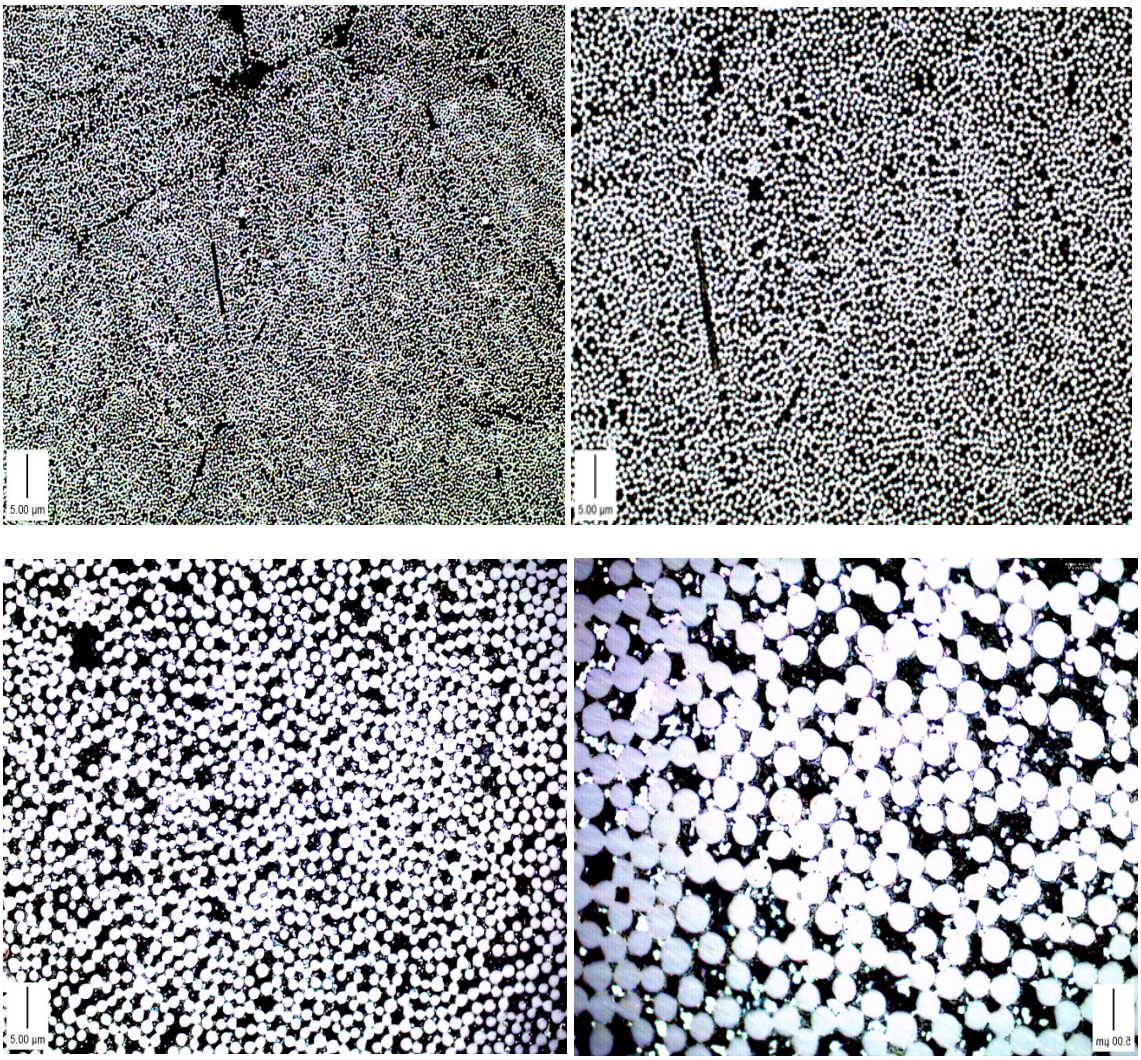

Figure B-14: D-N-2 x50 Magnification (top left); x100 Magnification (top right); x200 Magnification (bottom left); x500 Magnification (bottom right)

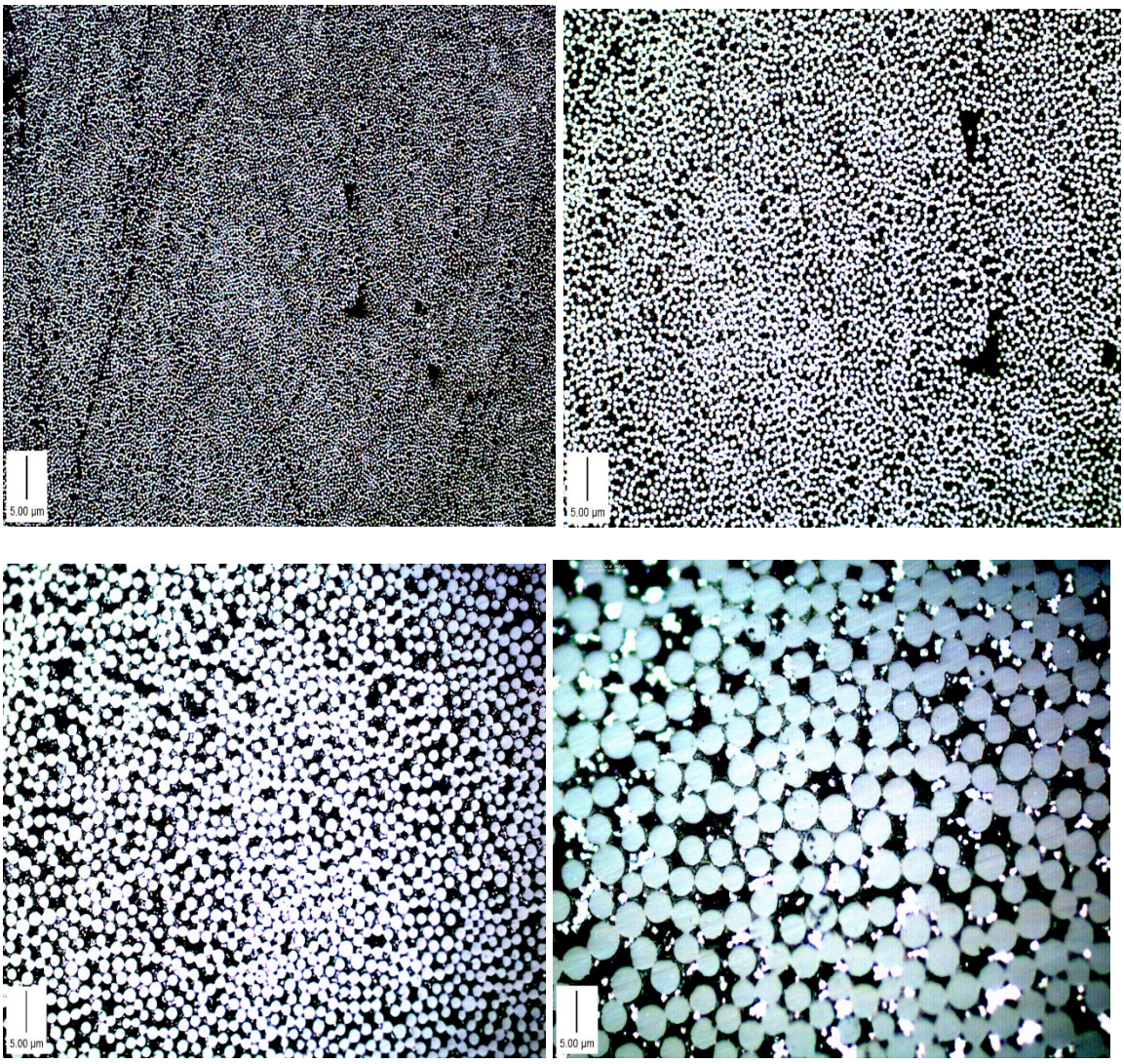

Figure B-15: D-N-3 x50 Magnification (top left); x100 Magnification (top right); x200 Magnification (bottom left); x500 Magnification (bottom right)

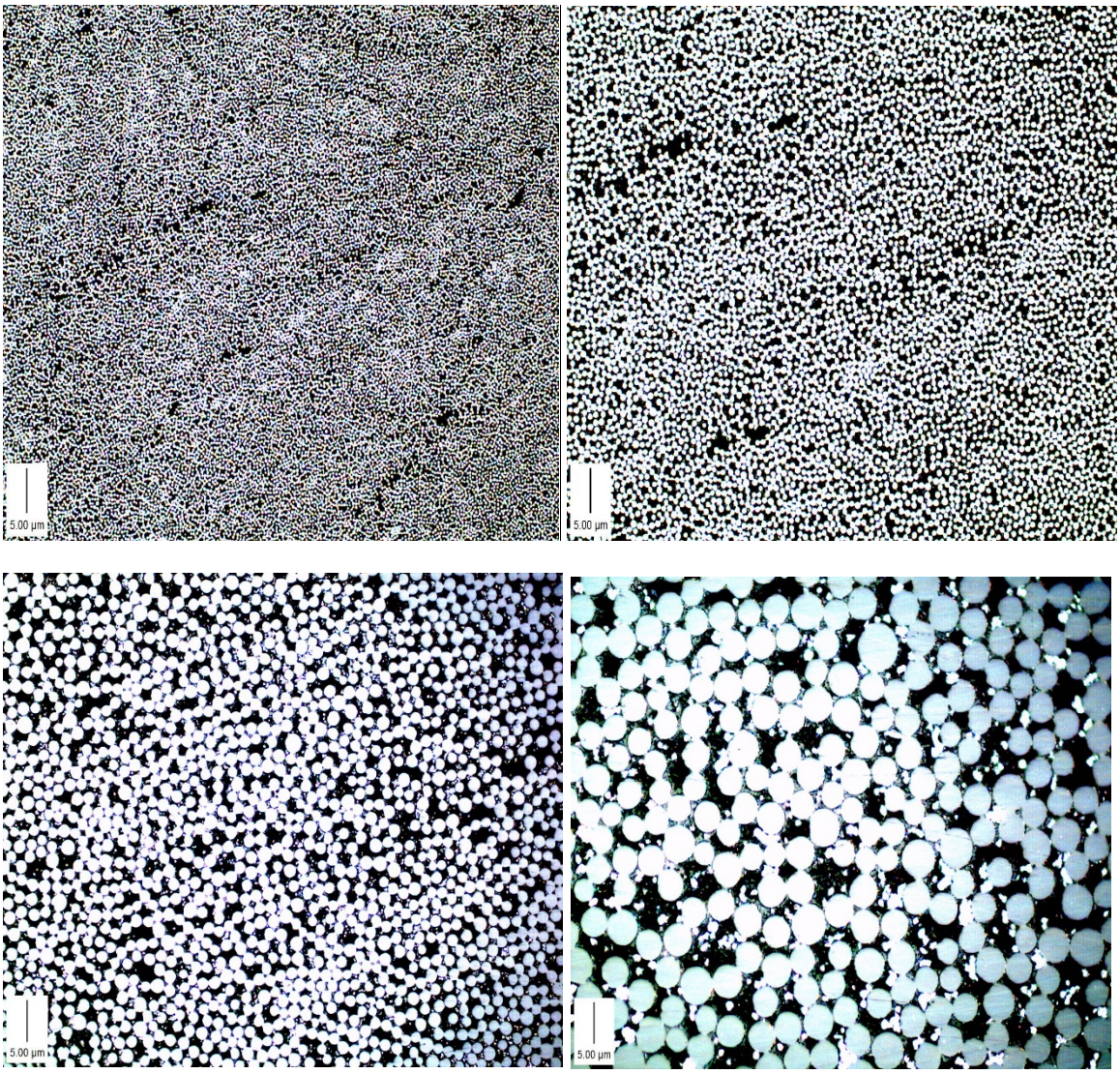

Figure B-16: D-N-4 x50 Magnification (top left); x100 Magnification (top right); x200 Magnification (bottom left); x500 Magnification (bottom right)

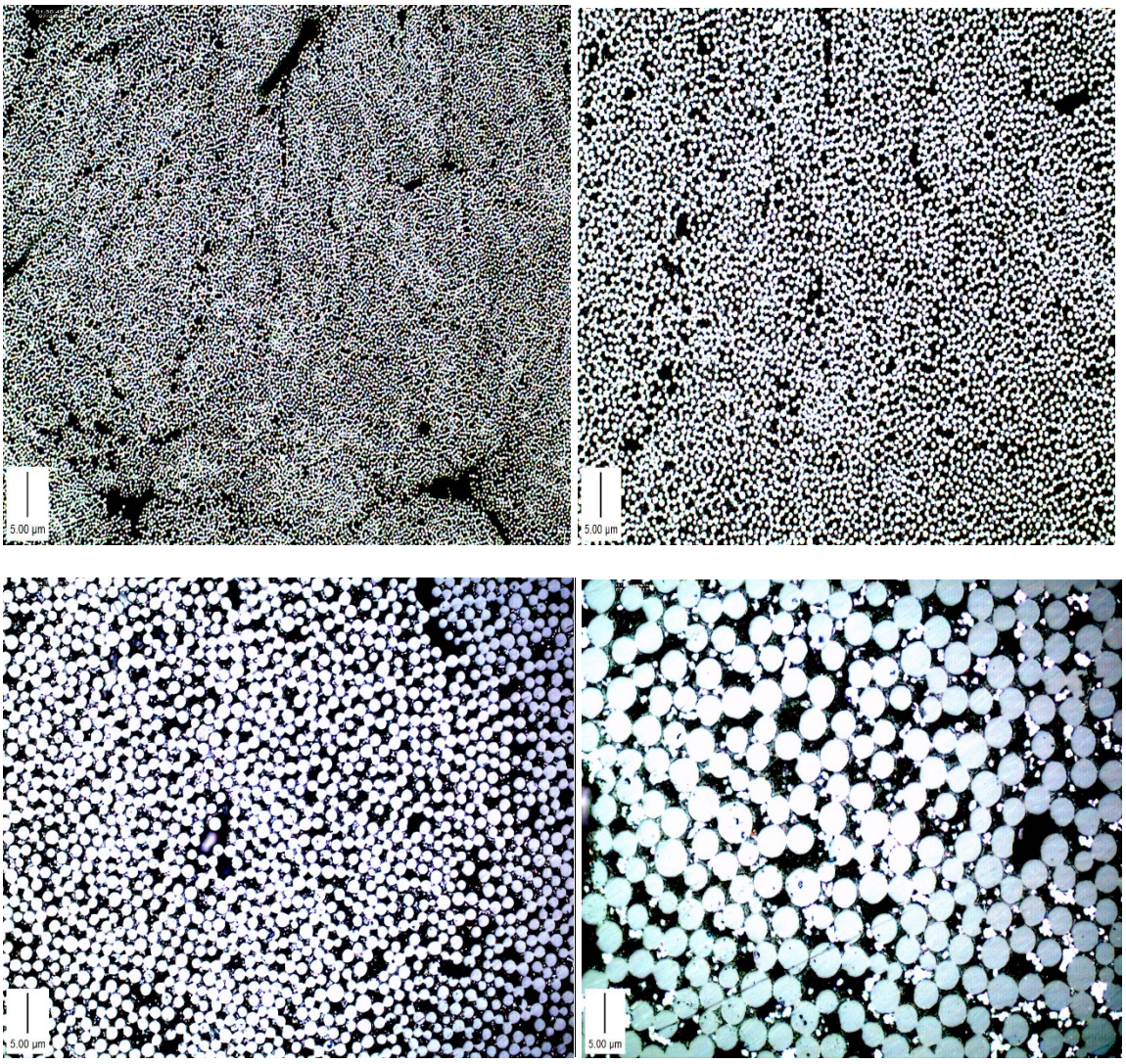

Figure B-17: D-N-5 x50 Magnification (top left); x100 Magnification (top right); x200 Magnification (bottom left); x500 Magnification (bottom right)

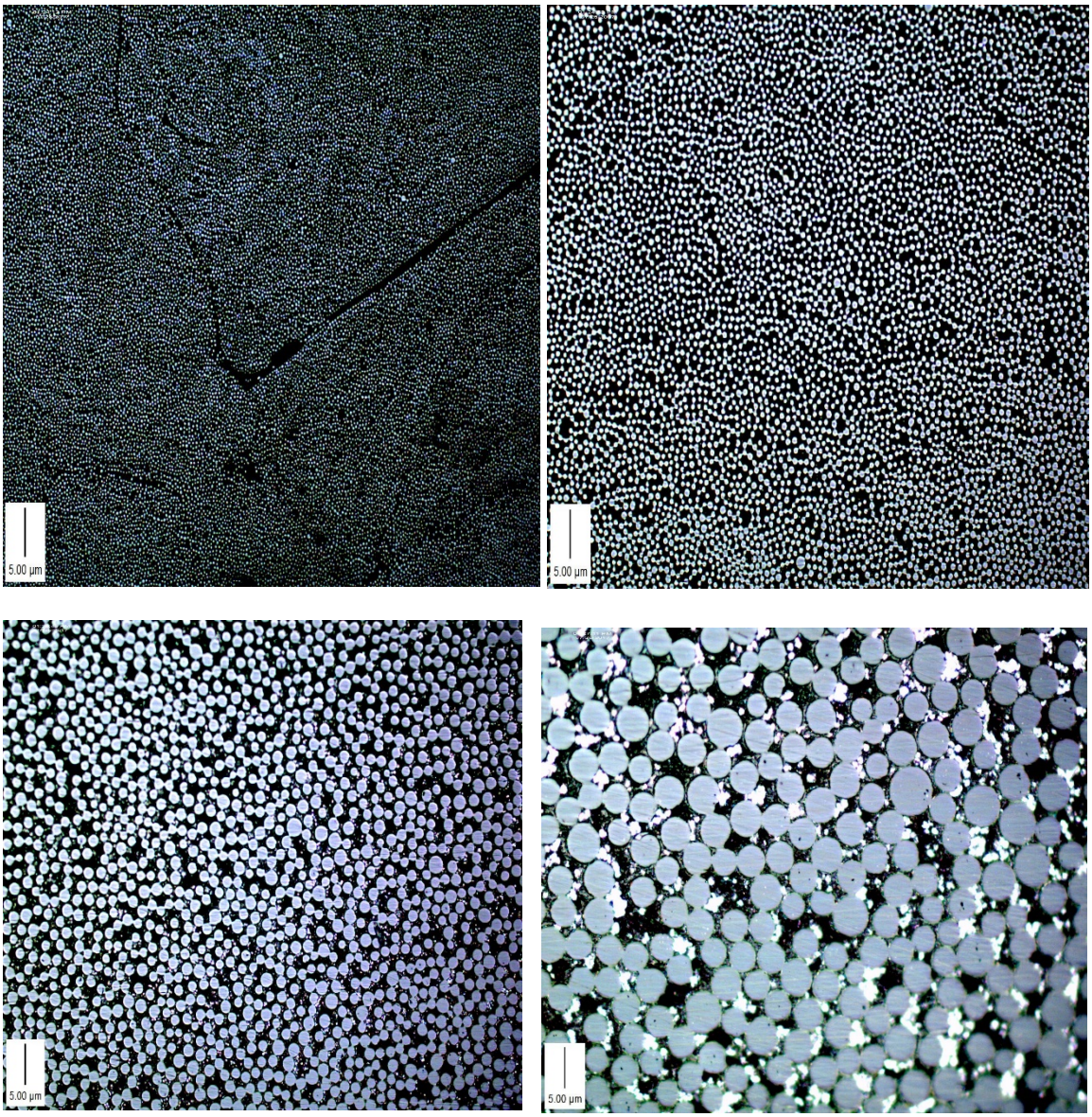

Figure B-18: P-N-1 x50 Magnification (top left); x100 Magnification (top right) x200 Magnification (bottom left), x500 Magnification (bottom right)

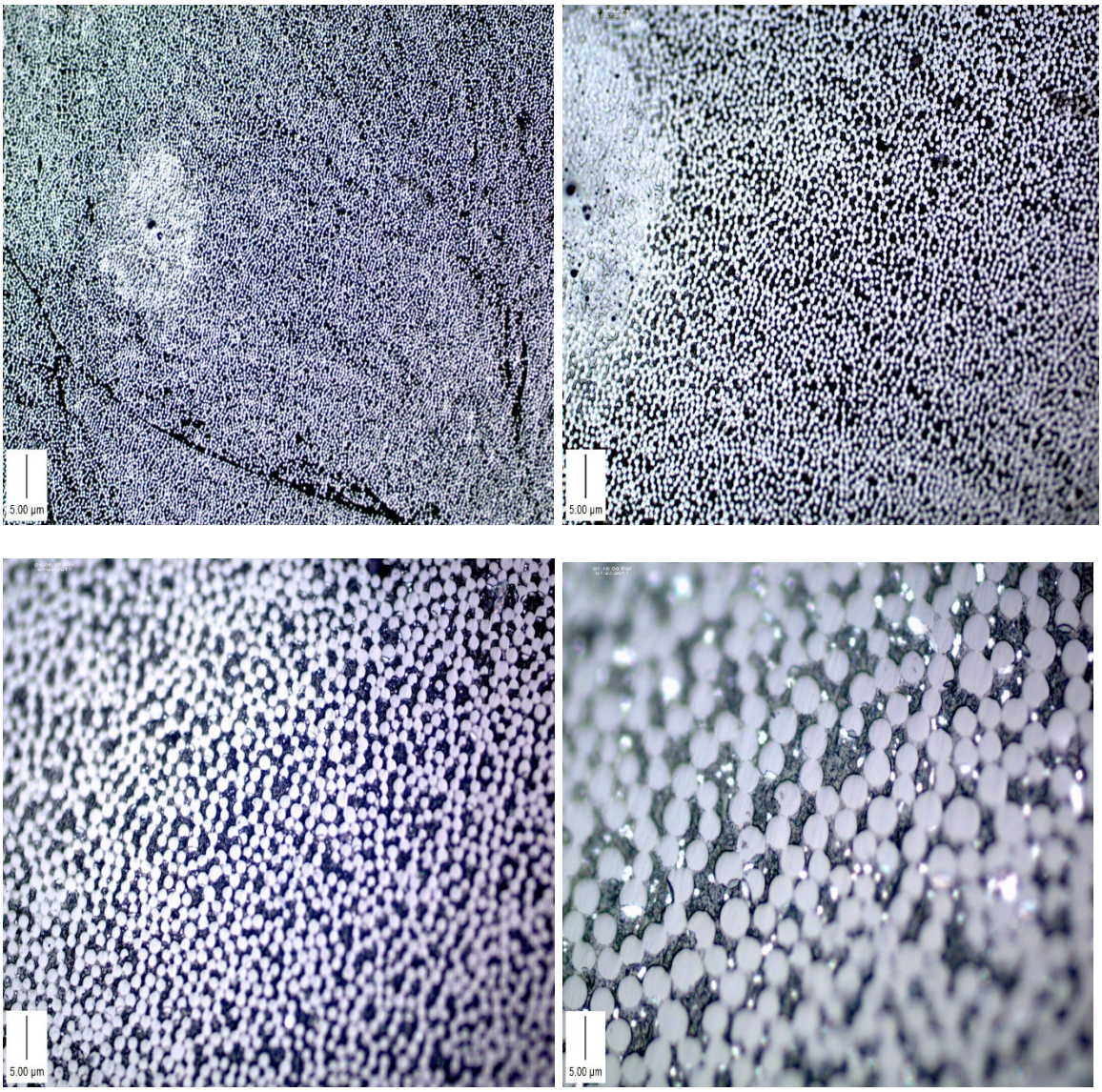

Figure B-19: P-N-2 x50 Magnification (top left); x100 Magnification (top right) x200 Magnification (bottom left), x500 Magnification (bottom right)

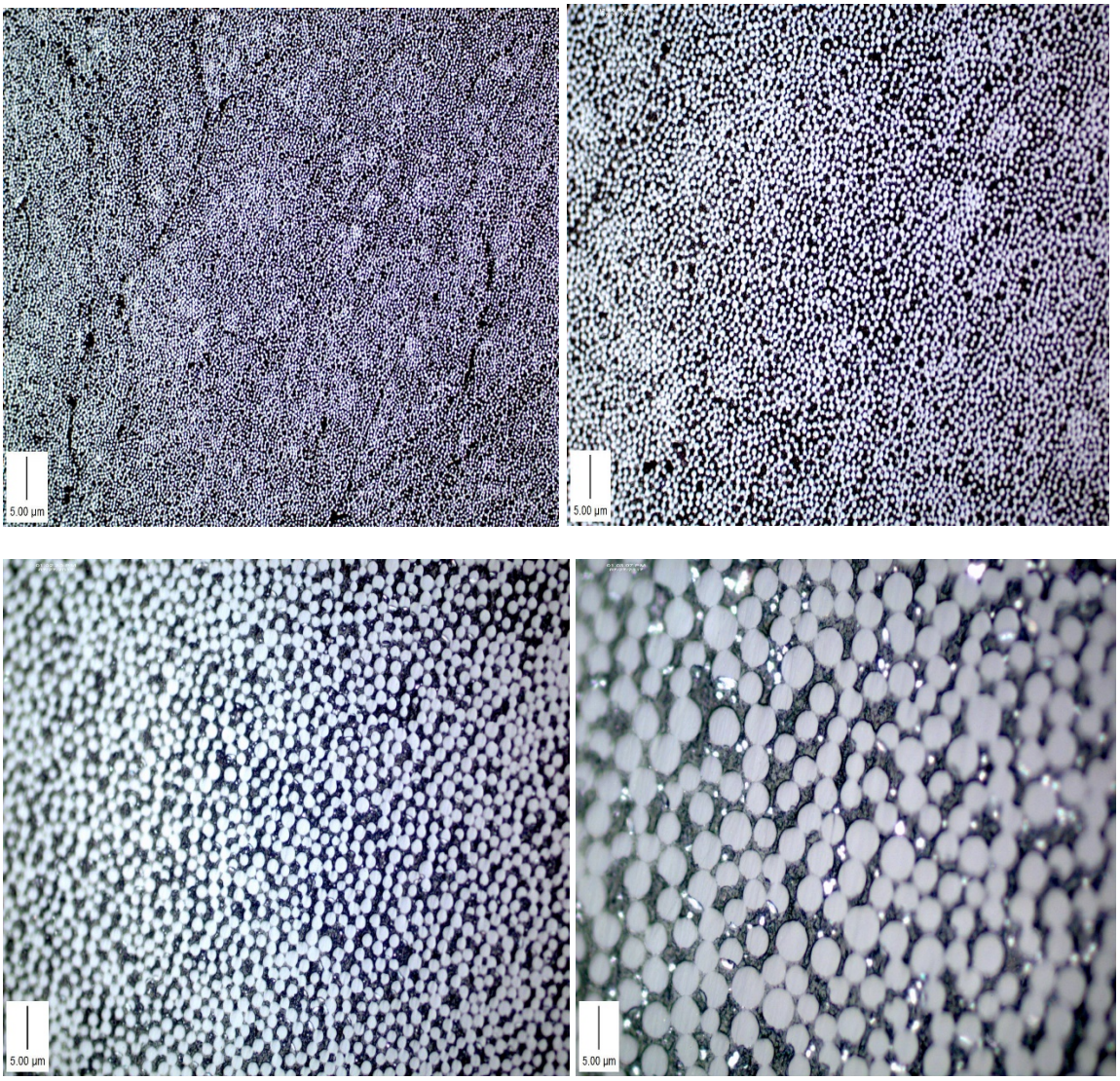

Figure B-20: P-N-3 x50 Magnification (top left). x100 Magnification (top right) x200 Magnification (bottom left), x500 Magnification (bottom right)

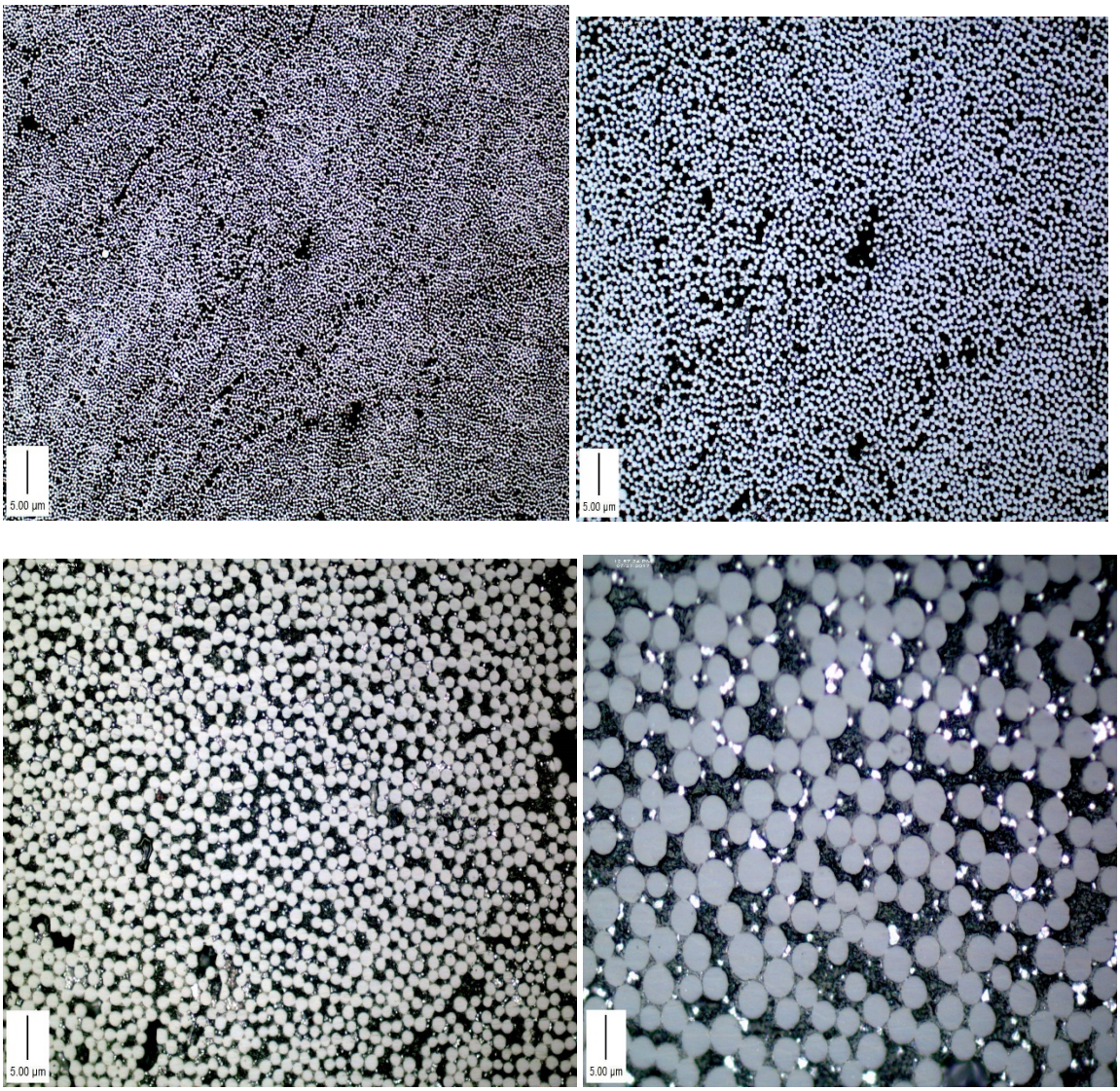

Figure B-21: P-N-4 x50 Magnification (top left). x100 Magnification (top right) x200 Magnification (bottom left), x500 Magnification (bottom right)

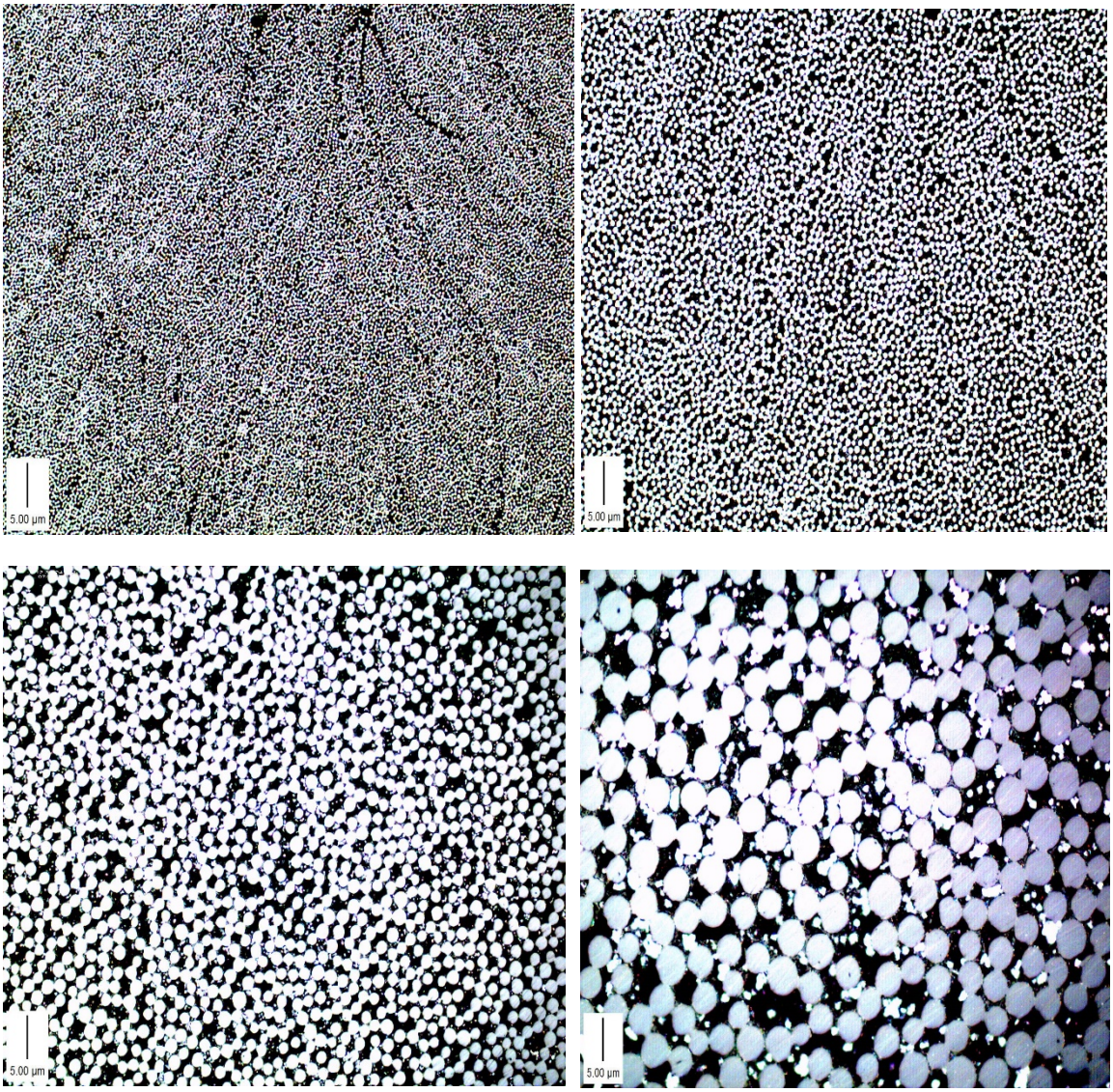

Figure B-22: P-N-5 x50 Magnification (top left). x100 Magnification (top right) x200 Magnification (bottom left), x500 Magnification (bottom right)

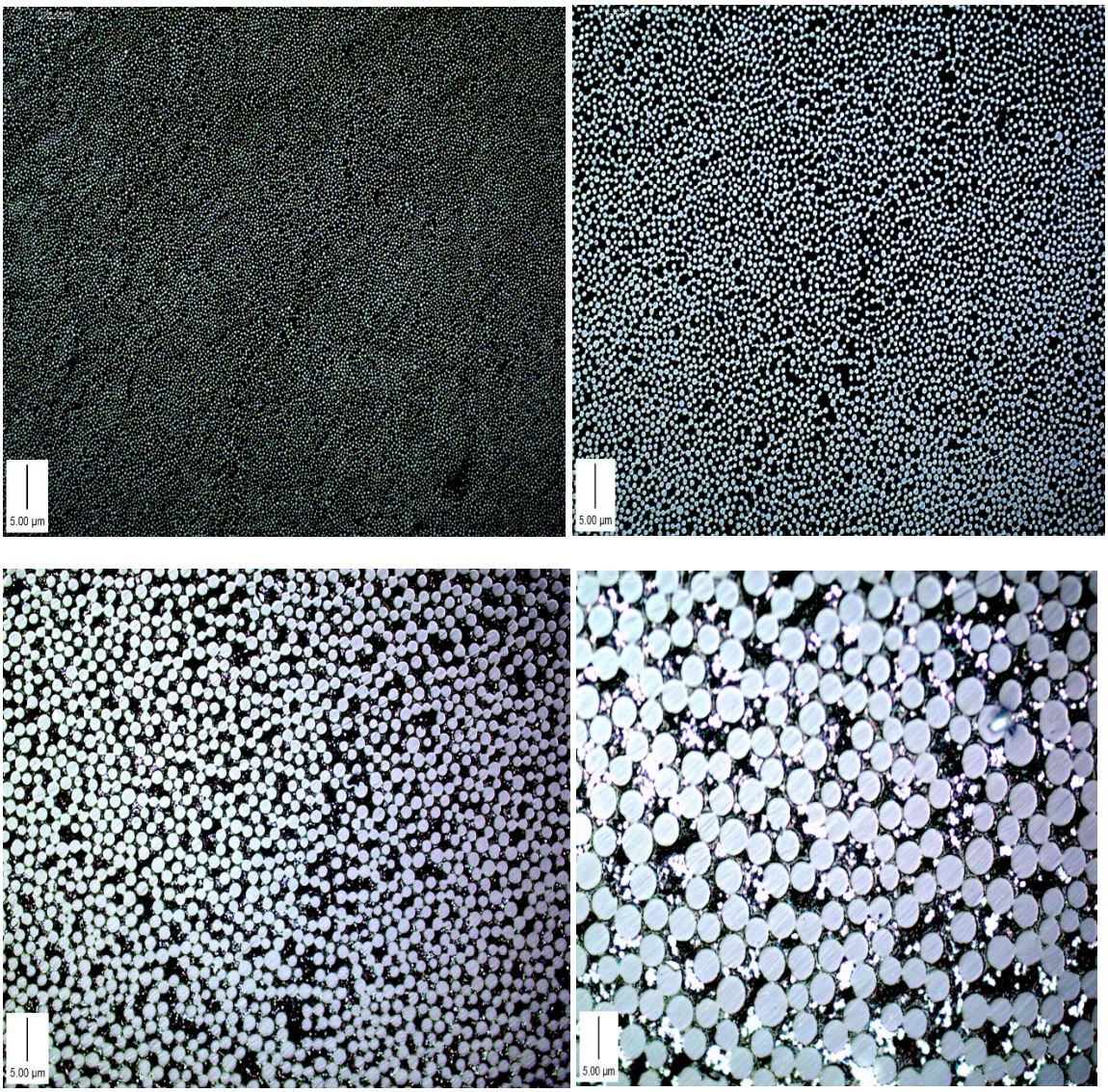

Figure B-23: D-S-1 x50 Magnification (top left). x100 Magnification (top right) x200 Magnification (bottom left), x500 Magnification (bottom right)

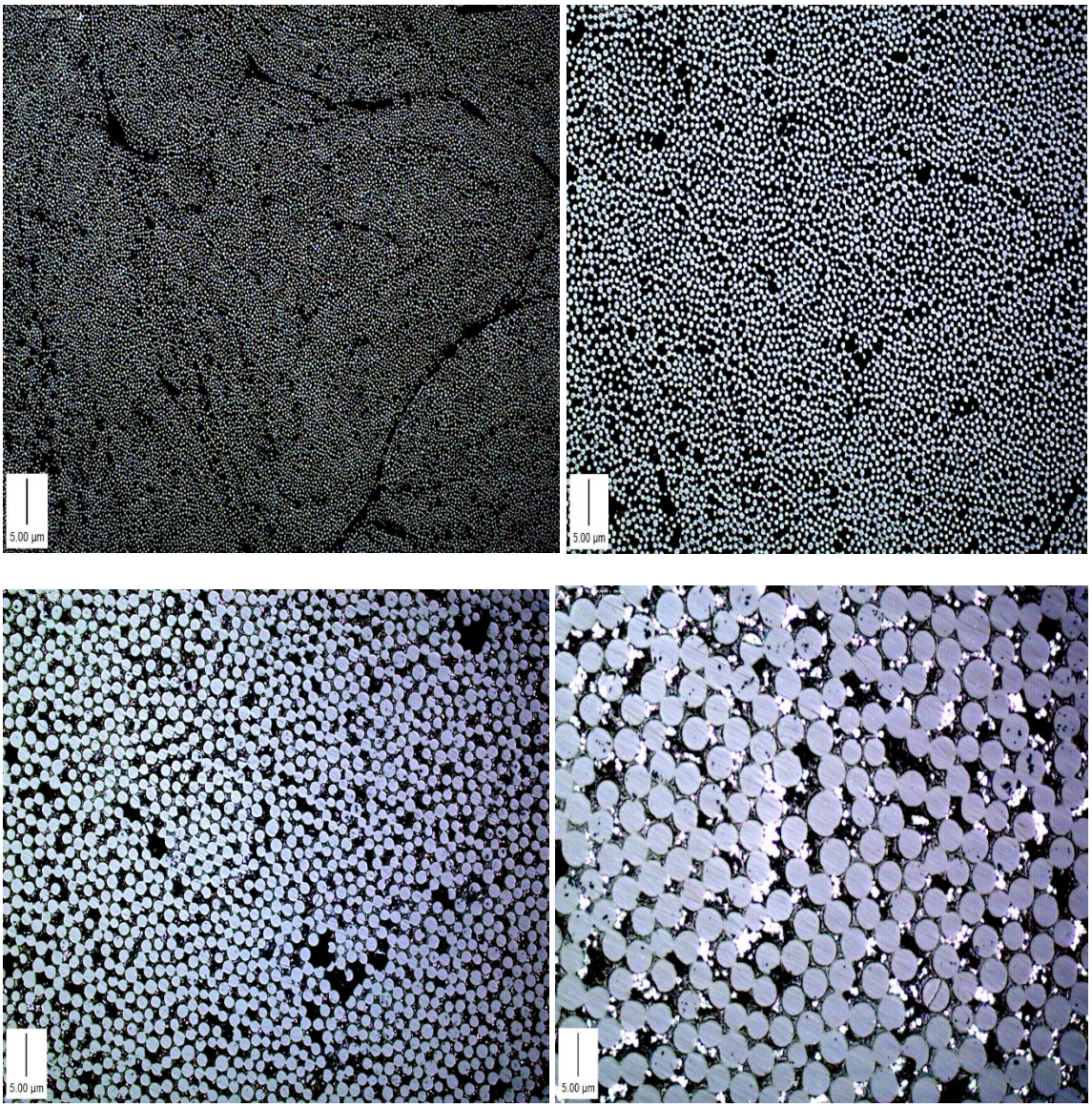

Figure B-24: D-S-2 x50 Magnification (top left). x100 Magnification (top right) x200 Magnification (bottom left), x500 Magnification (bottom right)

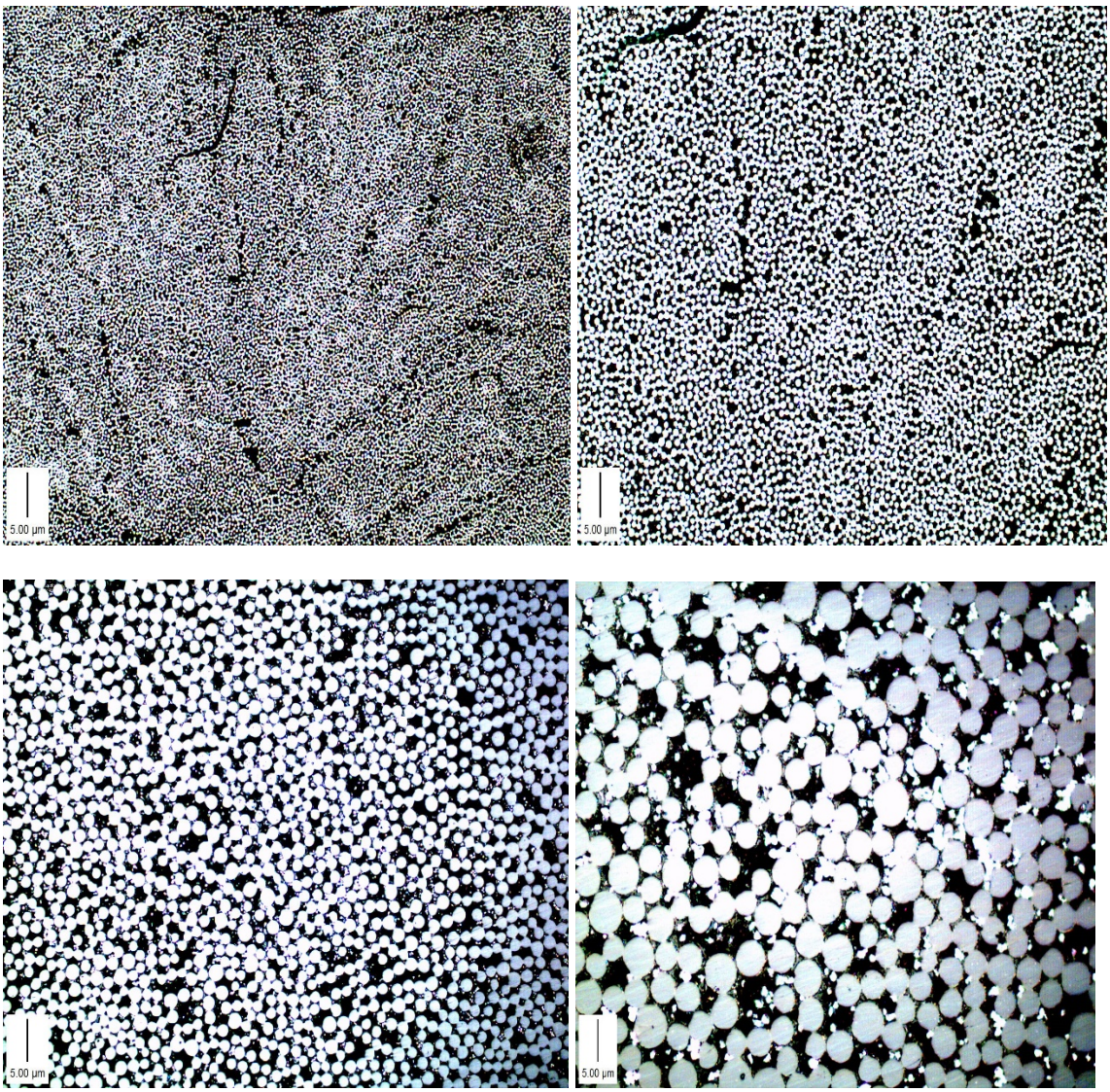

Figure B-25: D-S-3 x50 Magnification (top left). x100 Magnification (top right) x200 Magnification (bottom left), x500 Magnification (bottom right)

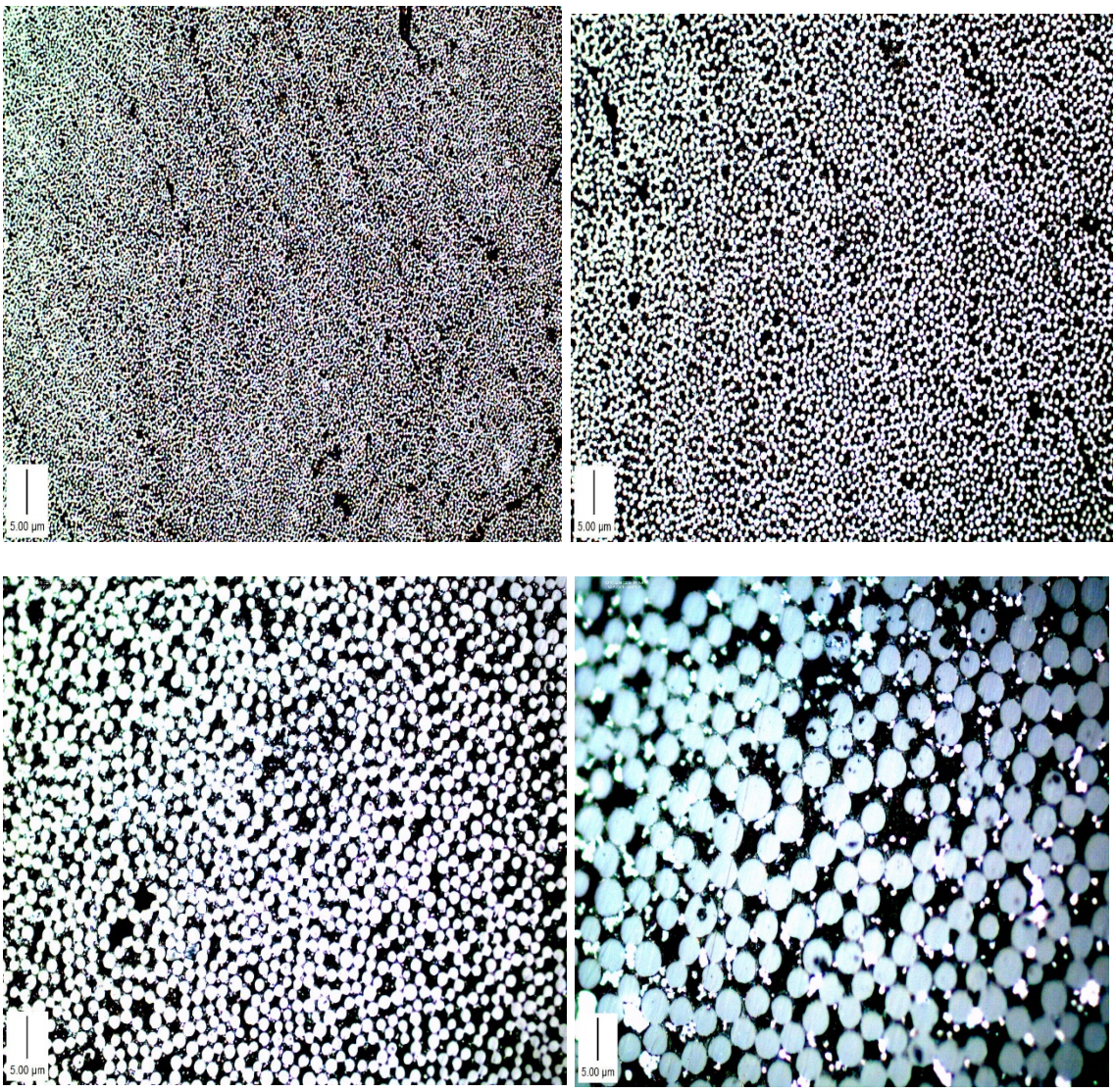

Figure B-26: D-S-4 x50 Magnification (top left). x100 Magnification (top right) x200 Magnification (bottom left), x500 Magnification (bottom right)

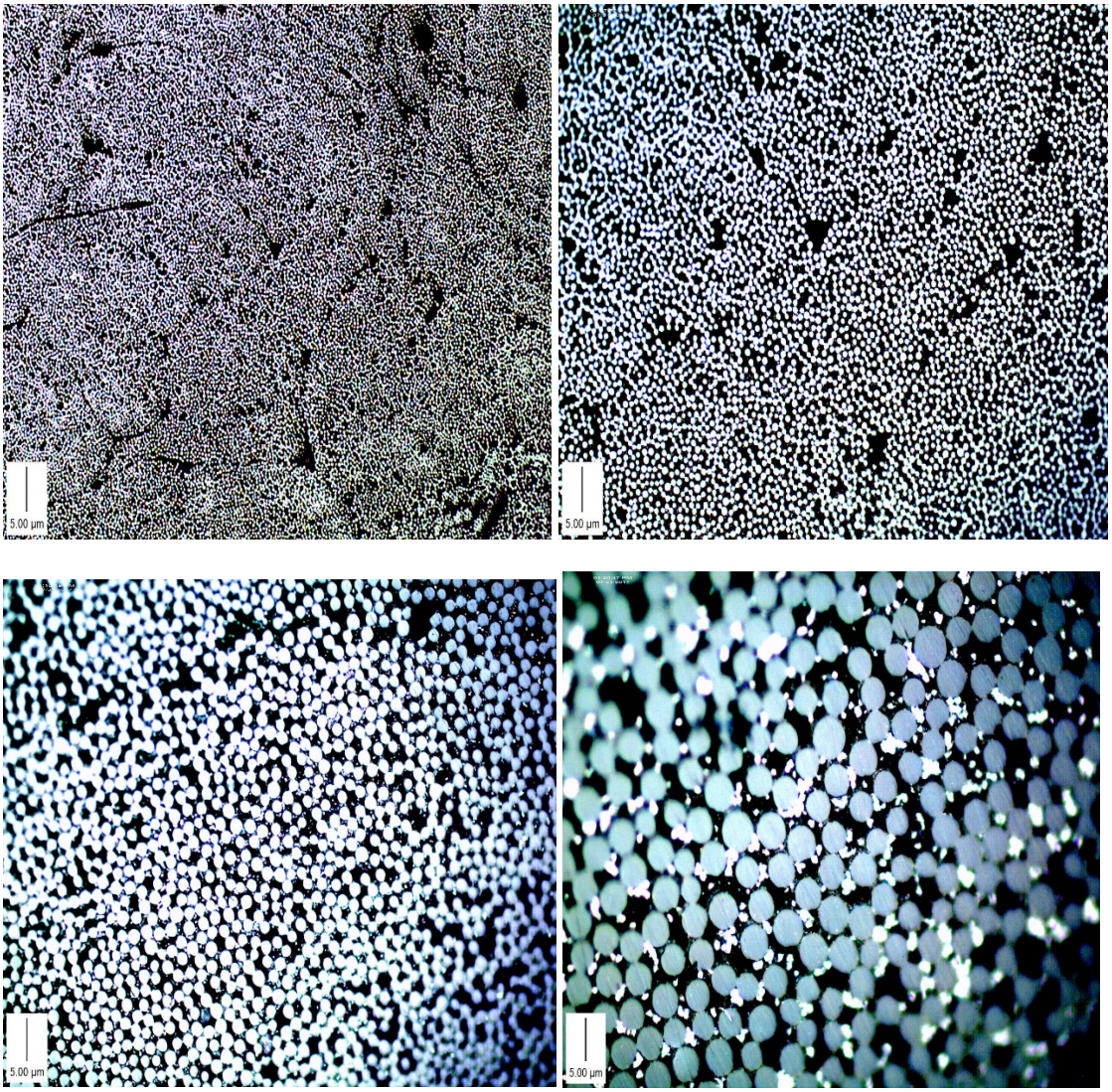

Figure B-27: D-S-5 x50 Magnification (top left). x100 Magnification (top right) x200 Magnification (bottom left), x500 Magnification (bottom right)

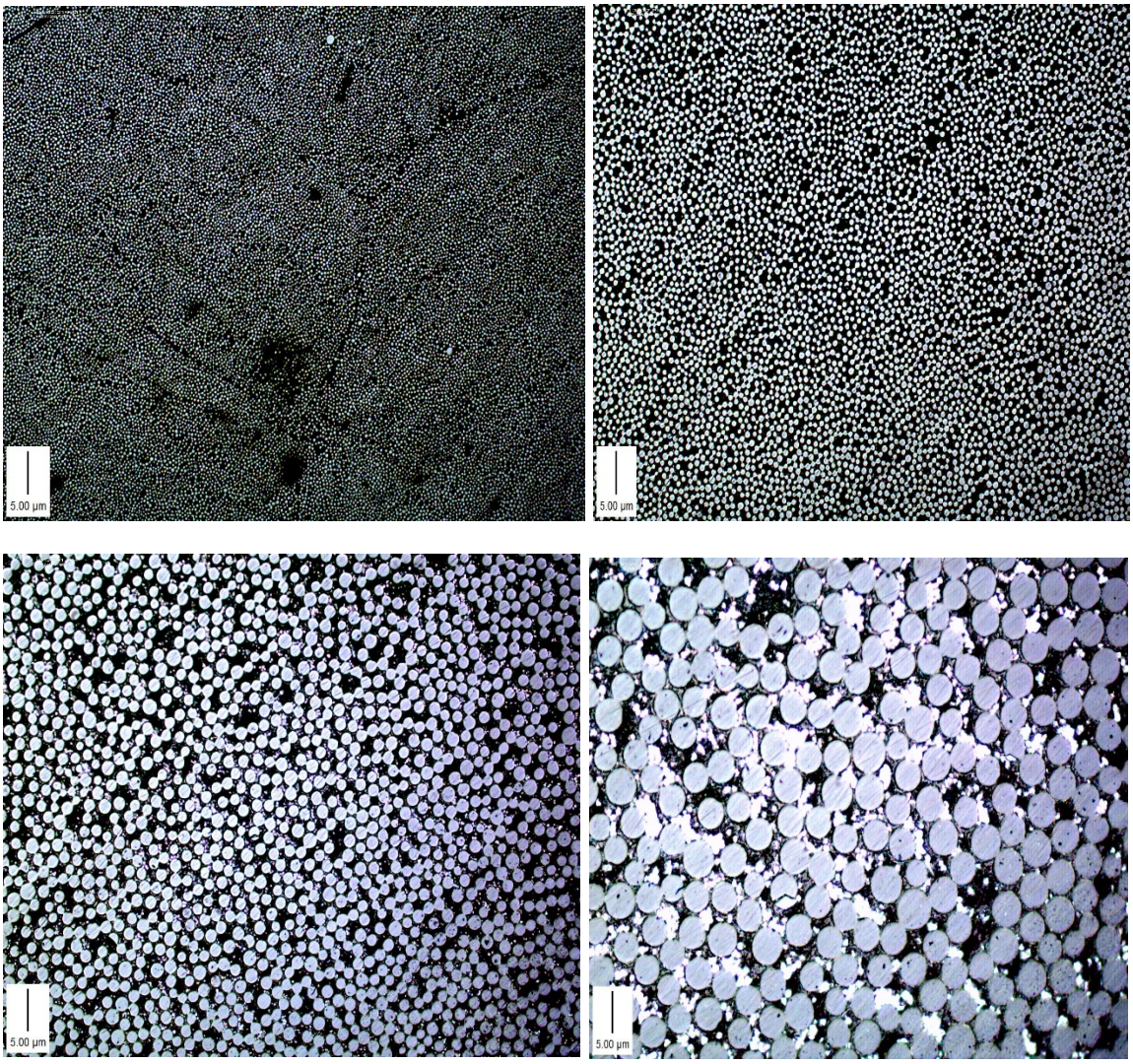

Figure B-28: P-S-1 x50 Magnification (top left). x100 Magnification (top right) x200 Magnification (bottom left), x500 Magnification (bottom right)

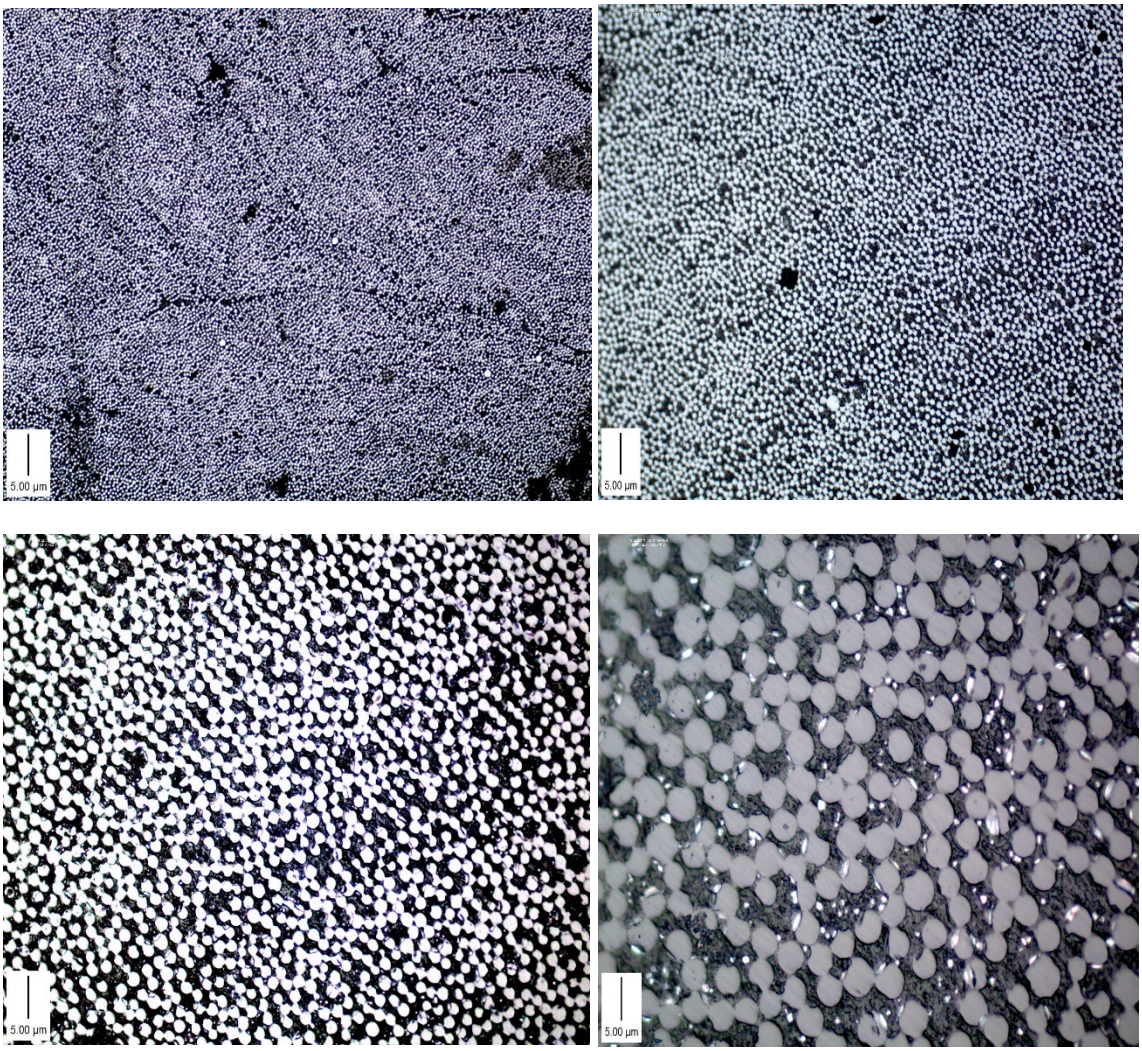

Figure B-29: P-S-2 x50 Magnification (top left). x100 Magnification (top right) x200 Magnification (bottom left), x500 Magnification (bottom right)

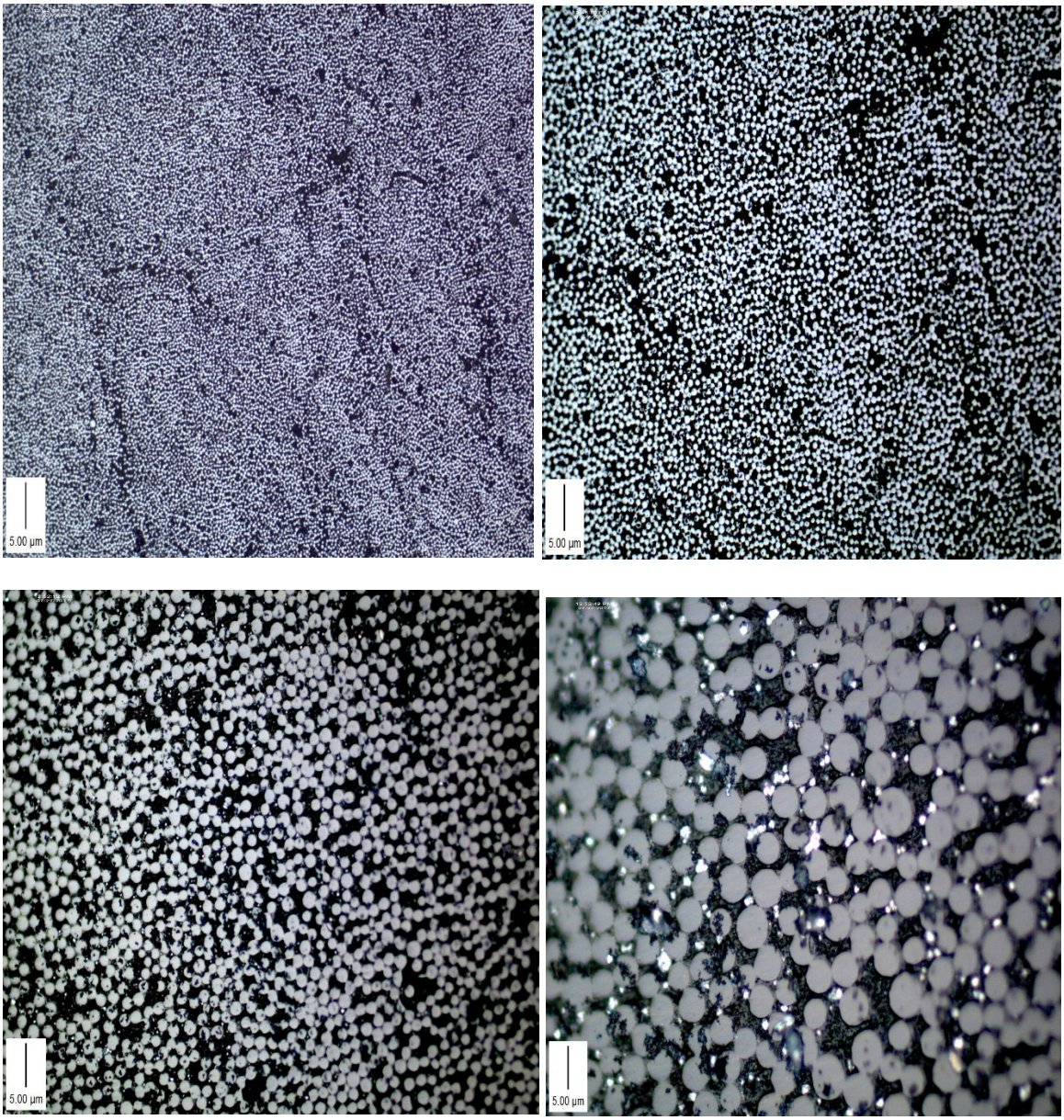

Figure B-30: P-S-3 x50 Magnification (top left). x100 Magnification (top right) x200 Magnification (bottom left), x500 Magnification (bottom right)

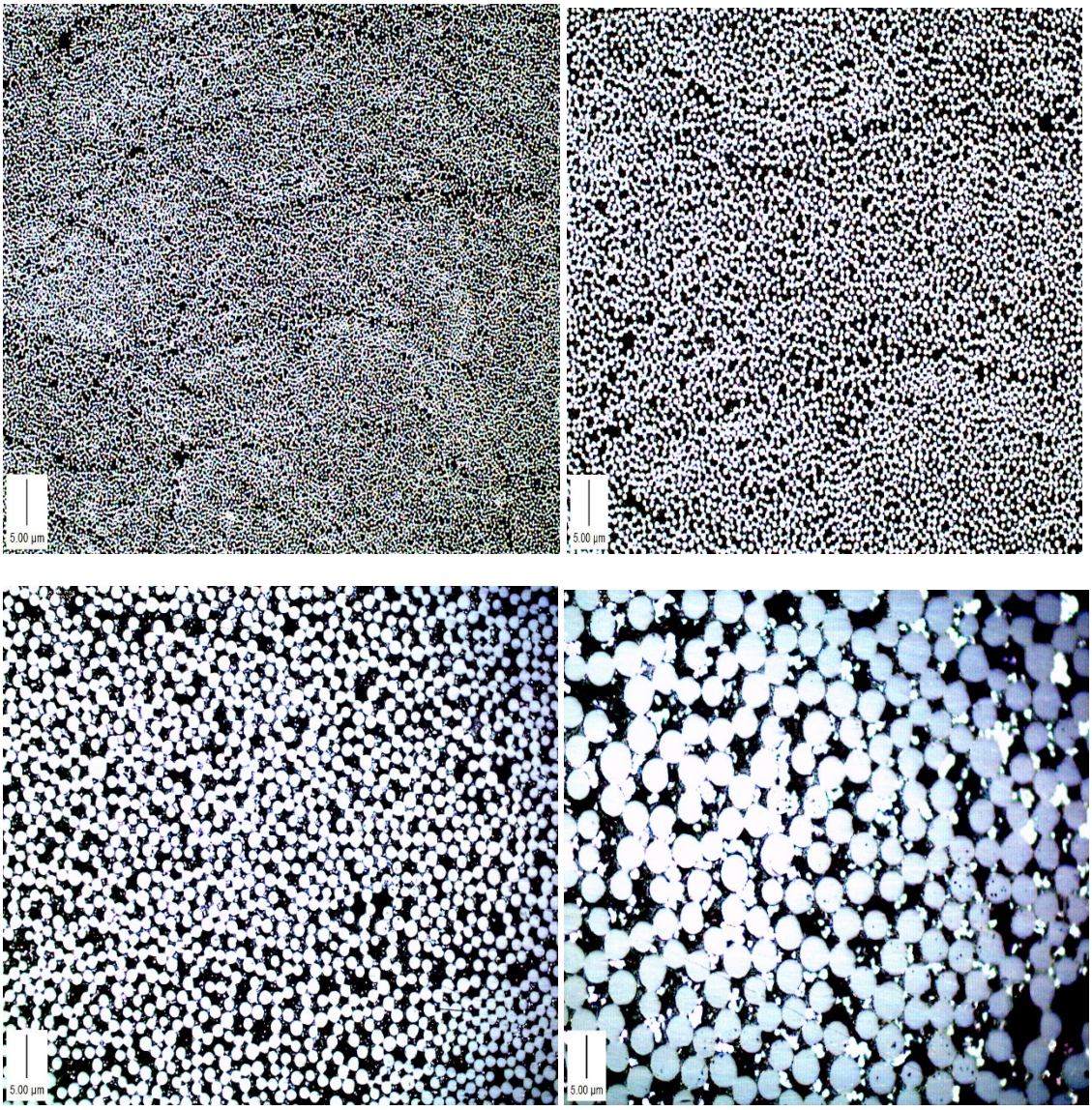

Figure B-30: P-S-4 x50 Magnification (top left). x100 Magnification (top right) x200 Magnification (bottom left), x500 Magnification (bottom right)

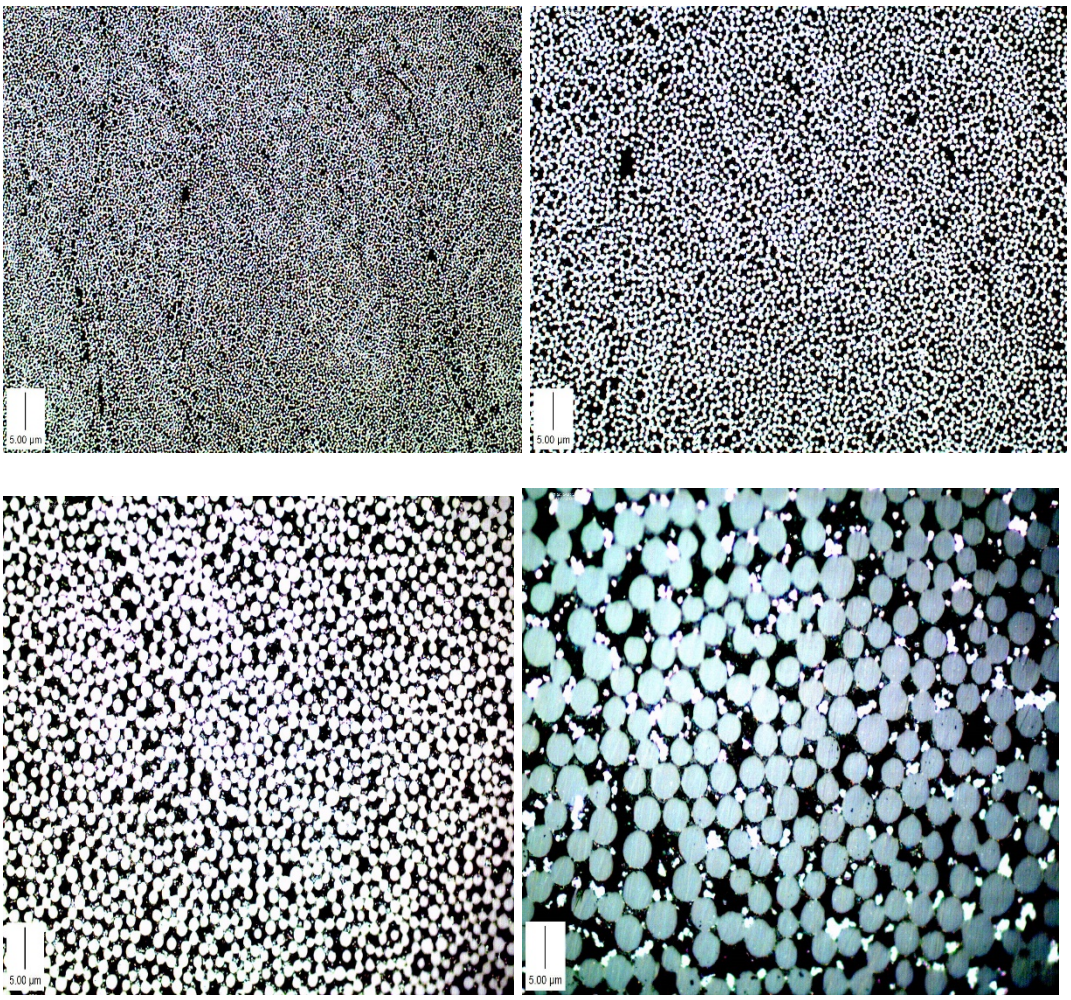

Figure B-31: P-S-5 x50 Magnification (top left). x100 Magnification (top right) x200 Magnification (bottom left), x500 Magnification (bottom right)

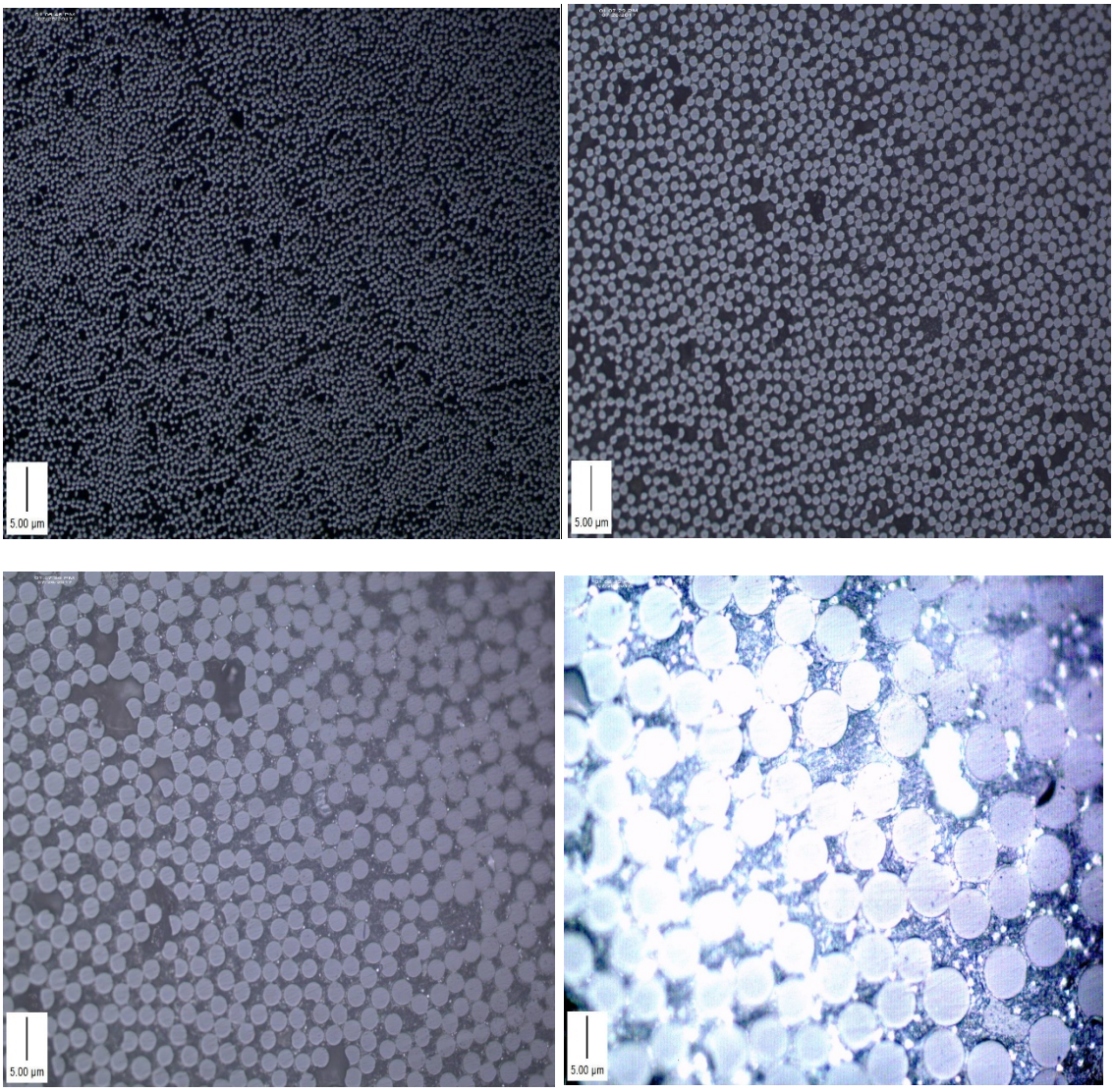

Figure B-31: C-1 x50 Magnification (top left). x100 Magnification (top right) x200 Magnification (bottom left), x500 Magnification (bottom right)

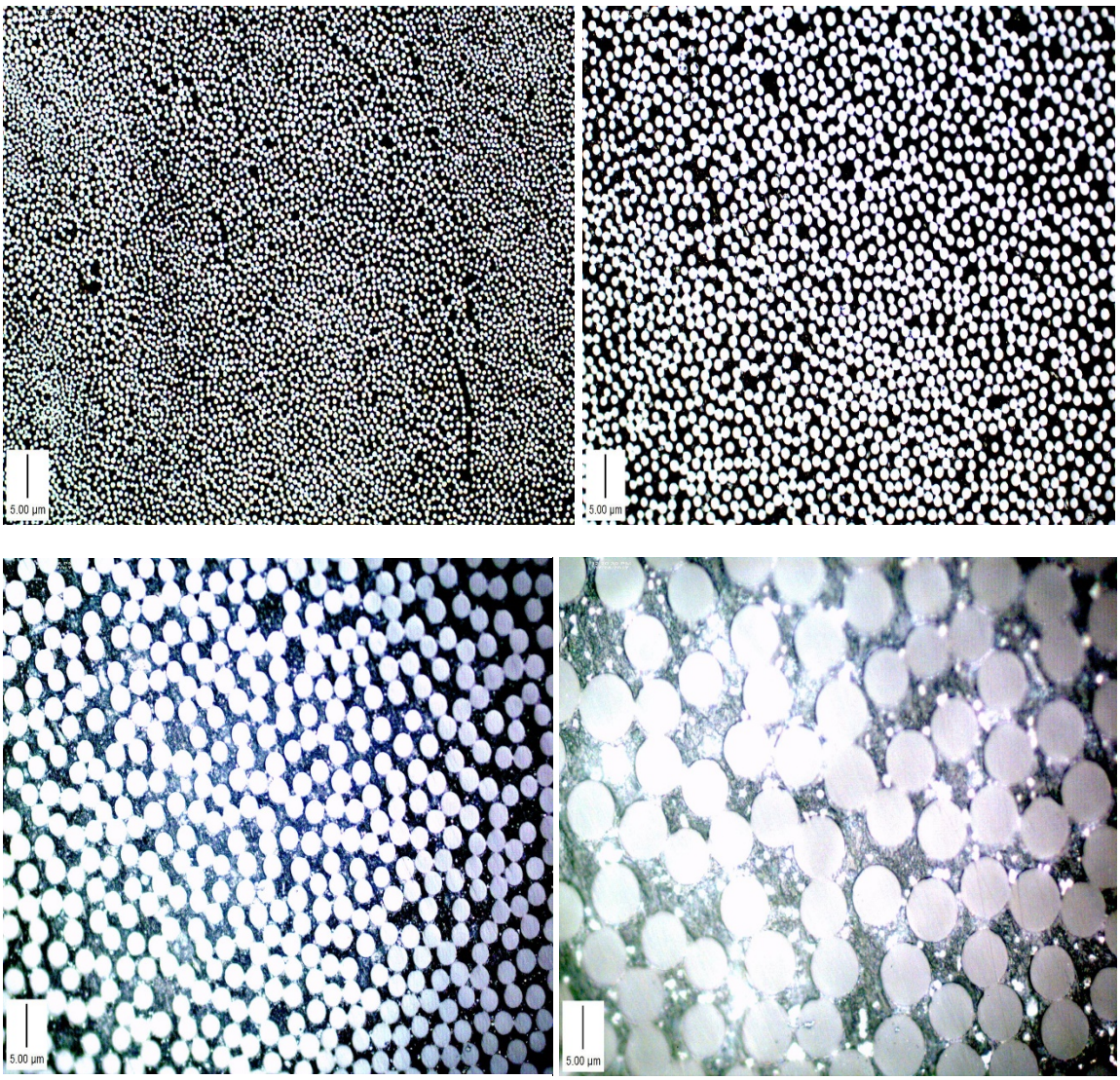

Figure B-31: C-2 x50 Magnification (top left). x100 Magnification (top right) x200 Magnification (bottom left), x500 Magnification (bottom right)

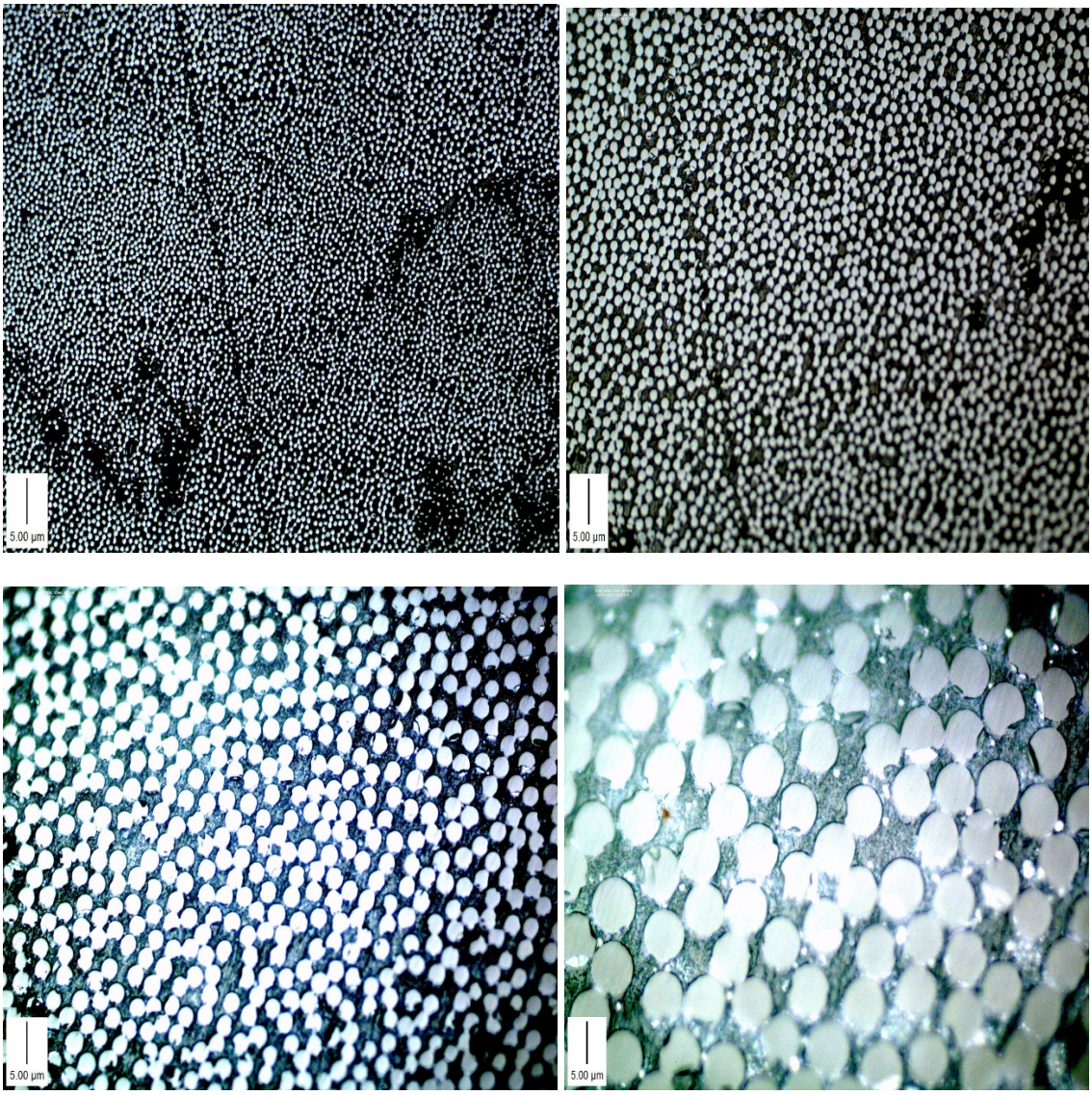

Figure B-31: C-3 x50 Magnification (top left). x100 Magnification (top right) x200 Magnification (bottom left), x500 Magnification (bottom right)

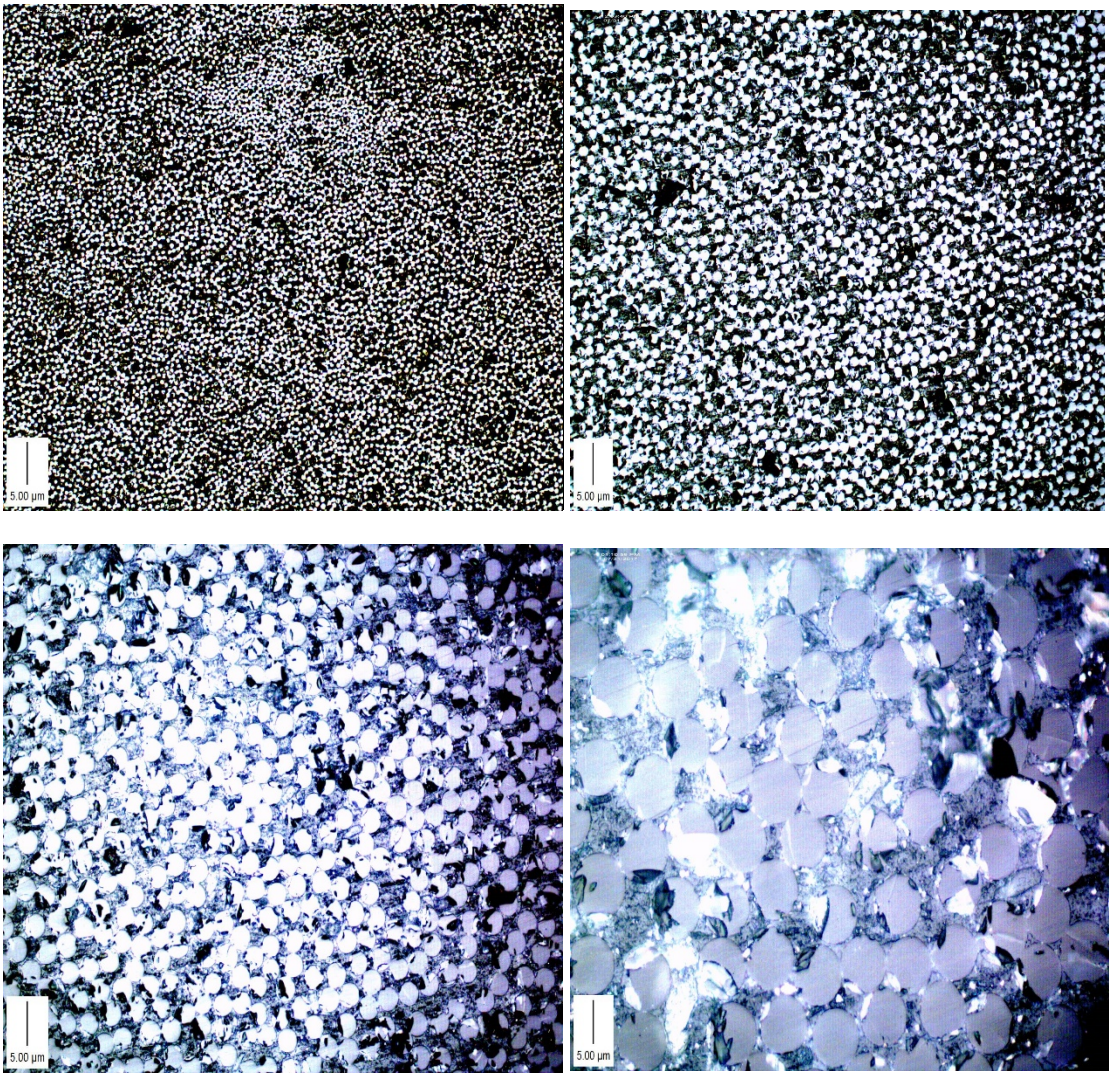

Figure B-31: C-4 x50 Magnification (top left). x100 Magnification (top right) x200 Magnification (bottom left), x500 Magnification (bottom right)

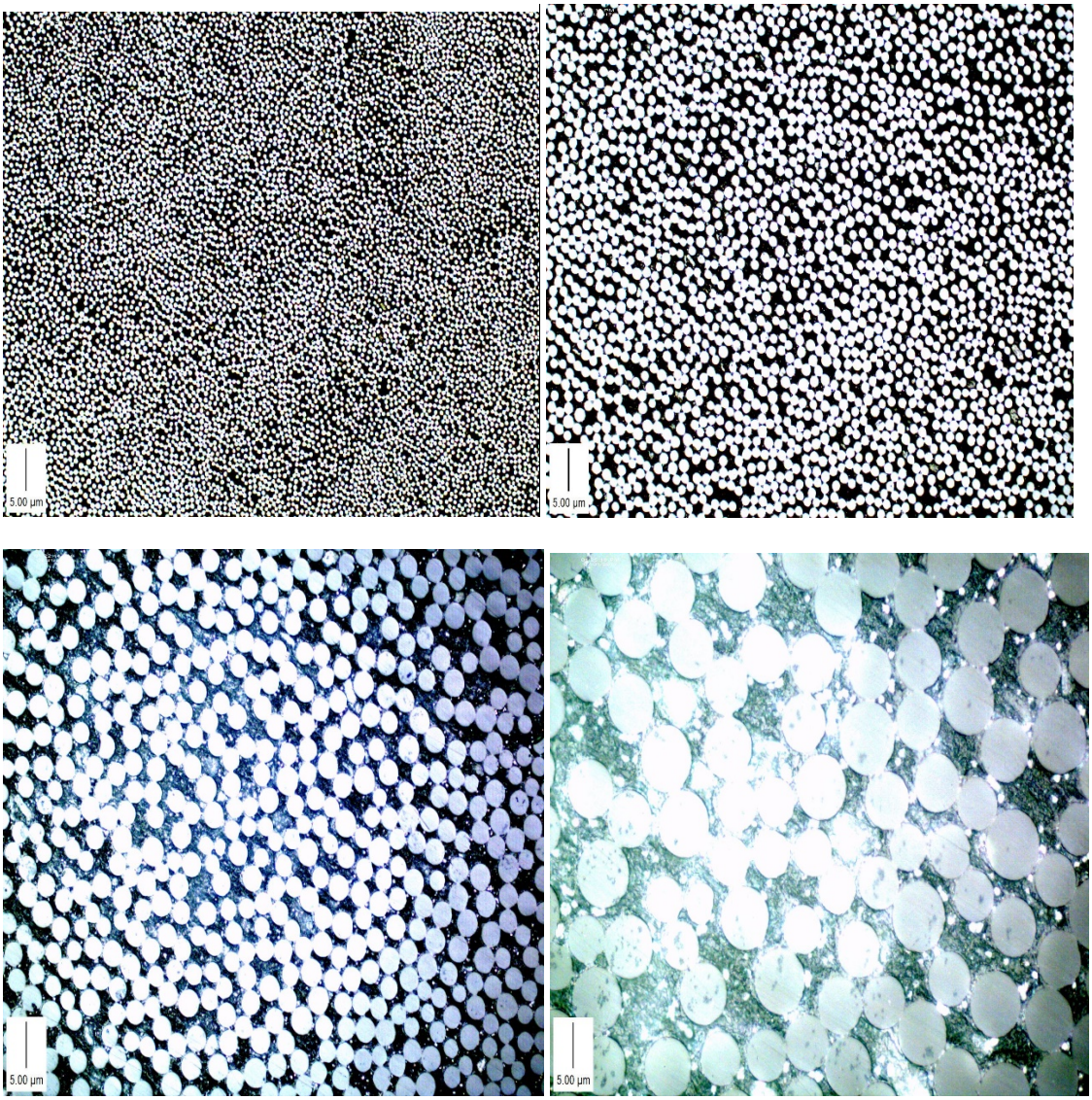

Figure B-32: C-5 x50 Magnification (top left). x100 Magnification (top right) x200 Magnification (bottom left), x500 Magnification (bottom right)

APPENDIX C. INLINE OVEN AND FRAME DRAWINGS

This section shows CADD drawings of the inline oven and cable pully frame that were submitted for fabrication.

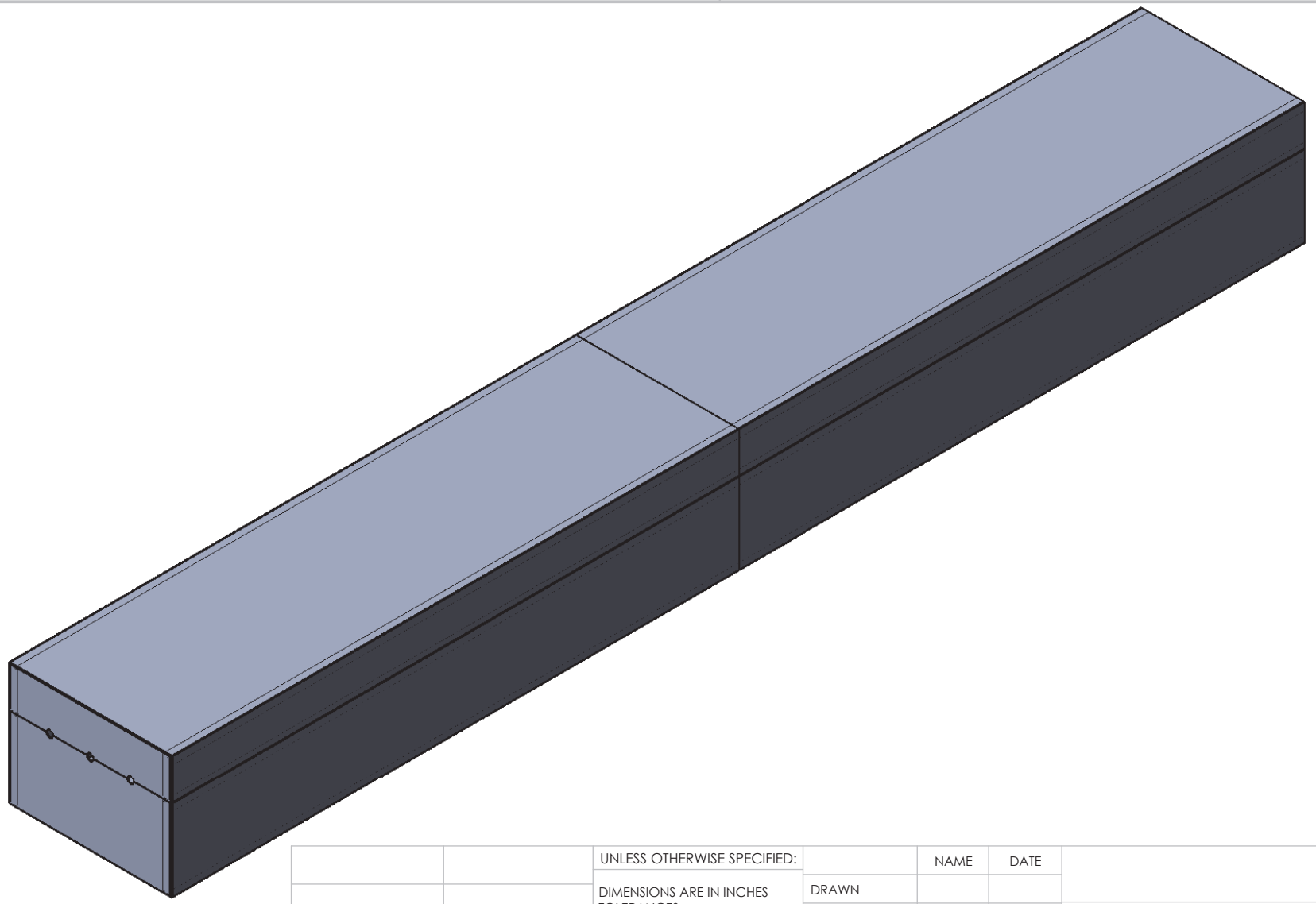

		UNLESS OTHERWISE SPECIFIED:		NAME	DATE
		DIMENSIONS ARE IN INCHES TOLERANCES: FRACTIONAL ± ANGULAR: MACH ± BEND ± TWO PLACE DECIMAL ± THREE PLACE DECIMAL ±	DRAWN		
			CHECKED		
			ENG APPR.		
			MFG APPR.		
		INTERPRET GEOMETRIC TOLERANCING PER:	Q.A.		
		MATERIAL	COMMENTS:		
NEXT ASSY	USED ON	FINISH			
APPLICATION		DO NOT SCALE DRAWING			

TITLE:

SIZE	DWG. NO.	REV
A	oven	
SCALE: 1:48	WEIGHT:	SHEET 1 OF 1

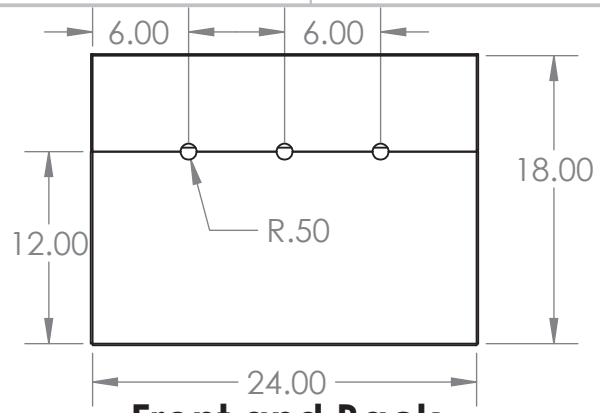

Front and Back

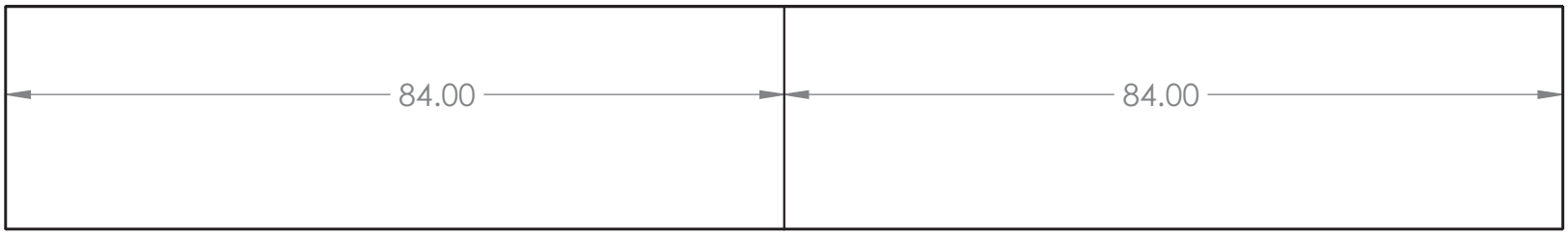

Top and Bottom

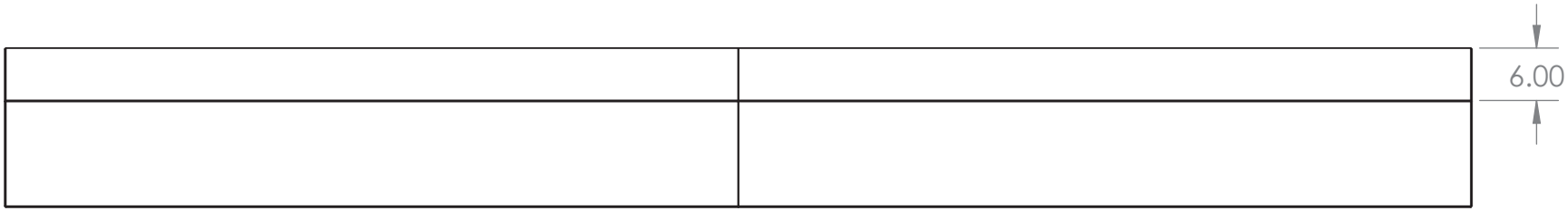

Side View

		UNLESS OTHERWISE SPECIFIED:		NAME	DATE
		DIMENSIONS ARE IN INCHES TOLERANCES: FRACTIONAL ± ANGULAR: MACH ± BEND ± TWO PLACE DECIMAL ± THREE PLACE DECIMAL ±	DRAWN		
			CHECKED		
			ENG APPR.		
			MFG APPR.		
		INTERPRET GEOMETRIC TOLERANCING PER:	Q.A.		
		MATERIAL	COMMENTS:		
NEXT ASSY	USED ON	FINISH			
APPLICATION		DO NOT SCALE DRAWING			

TITLE:

SIZE	DWG. NO.	REV
A	oven	
SCALE: 1:48	WEIGHT:	SHEET 1 OF 1

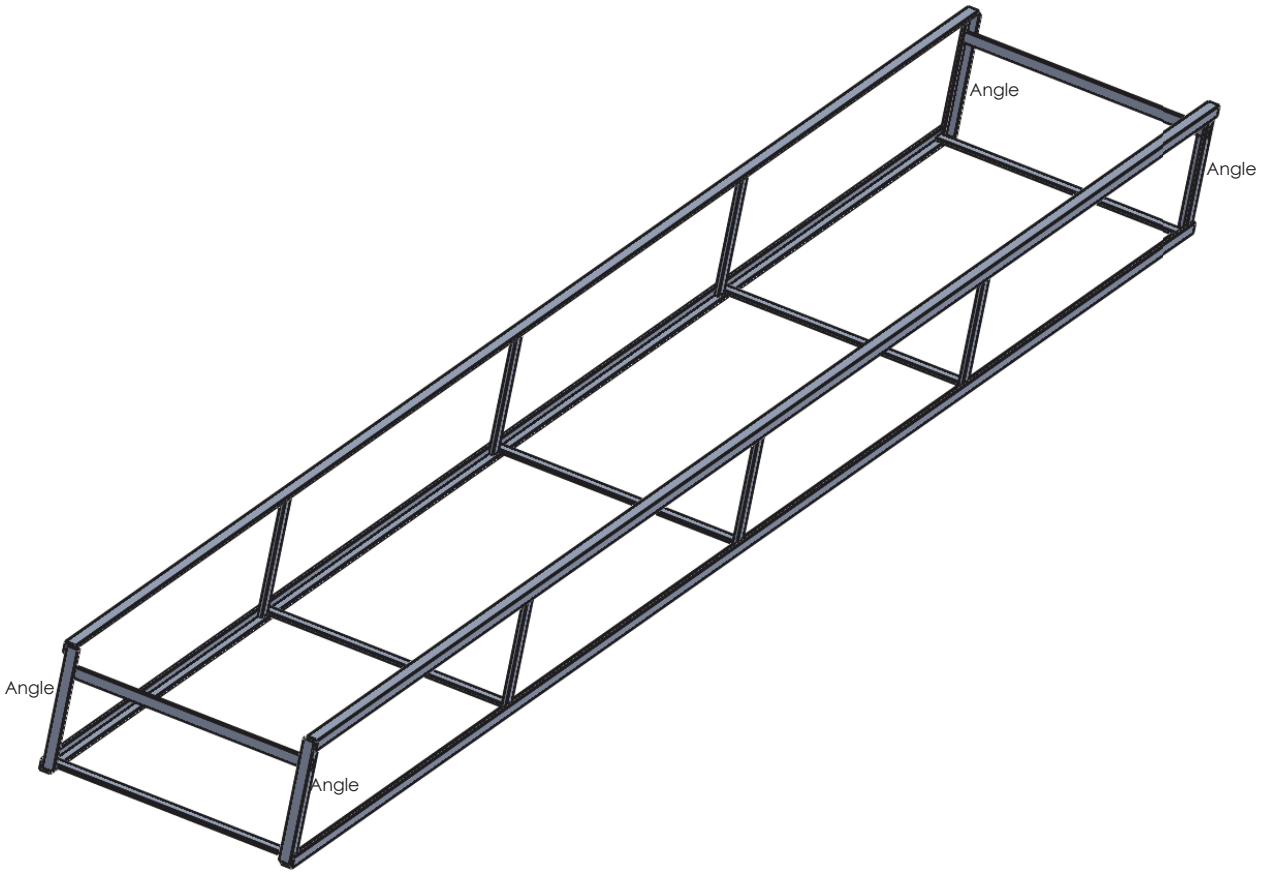

Stiffeners:
Angles x 4, The outside vertical stiffeners are angles
Flat Bars - Everything else

		UNLESS OTHERWISE SPECIFIED:		NAME	DATE
		DIMENSIONS ARE IN INCHES TOLERANCES: FRACTIONAL ± ANGULAR: MACH ± BEND ± TWO PLACE DECIMAL ± THREE PLACE DECIMAL ±	DRAWN		
			CHECKED		
			ENG APPR.		
			MFG APPR.		
		INTERPRET GEOMETRIC TOLERANCING PER:	Q.A.		
		MATERIAL	COMMENTS:		
NEXT ASSY	USED ON	FINISH			
APPLICATION		DO NOT SCALE DRAWING			

TITLE:

SIZE	DWG. NO.	REV
A	Bottom Frame	
SCALE: 1:48	WEIGHT:	SHEET 1 OF 1

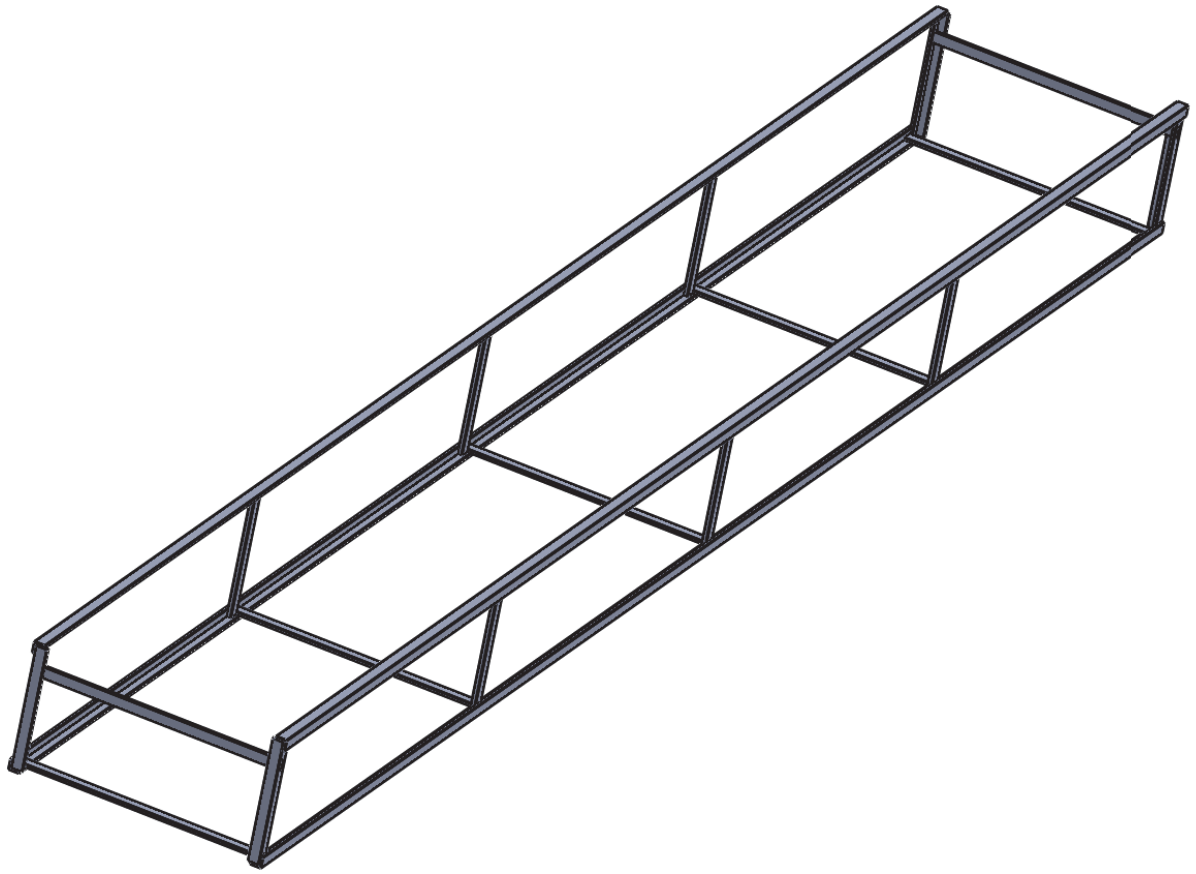

		UNLESS OTHERWISE SPECIFIED:		NAME	DATE
		DIMENSIONS ARE IN INCHES TOLERANCES: FRACTIONAL ± ANGULAR: MACH ± BEND ± TWO PLACE DECIMAL ± THREE PLACE DECIMAL ±	DRAWN		
			CHECKED		
			ENG APPR.		
			MFG APPR.		
		INTERPRET GEOMETRIC TOLERANCING PER:	Q.A.		
		MATERIAL	COMMENTS:		
NEXT ASSY	USED ON	FINISH			
APPLICATION		DO NOT SCALE DRAWING			

TITLE:

SIZE	DWG. NO.	REV
A	BottomFrame	
SCALE: 1:48	WEIGHT:	SHEET 1 OF 1

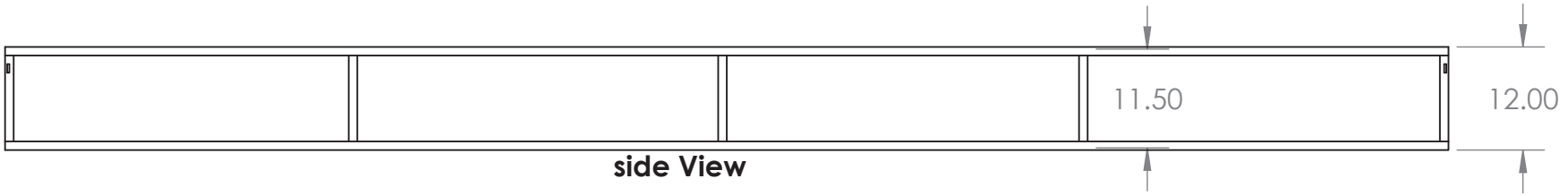

side View

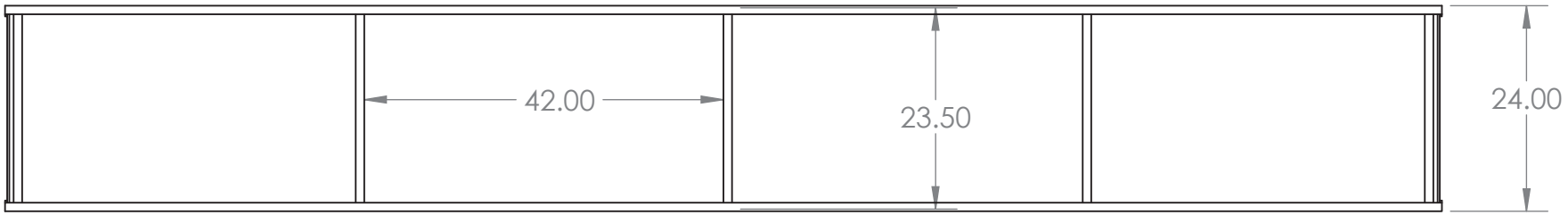

Top/Bottom View

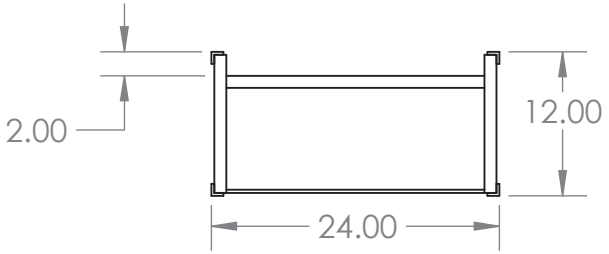

Front/Back View

Frame
Angle 1x1x1/4 Stiffeners-
1x1/4 flat bar
Vertical stiffeners 11.5"
Horizontal stiffeners 23.5"

		UNLESS OTHERWISE SPECIFIED:		NAME	DATE
		DIMENSIONS ARE IN INCHES TOLERANCES: FRACTIONAL ± ANGULAR: MACH ± BEND ± TWO PLACE DECIMAL ± THREE PLACE DECIMAL ±	DRAWN		
			CHECKED		
			ENG APPR.		
			MFG APPR.		
		INTERPRET GEOMETRIC TOLERANCING PER:	Q.A.		
		MATERIAL	COMMENTS:		
NEXT ASSY	USED ON	FINISH			
APPLICATION		DO NOT SCALE DRAWING			

TITLE:

SIZE	DWG. NO.	REV
A	BottomFrame	
SCALE: 1:48	WEIGHT:	SHEET 1 OF 1

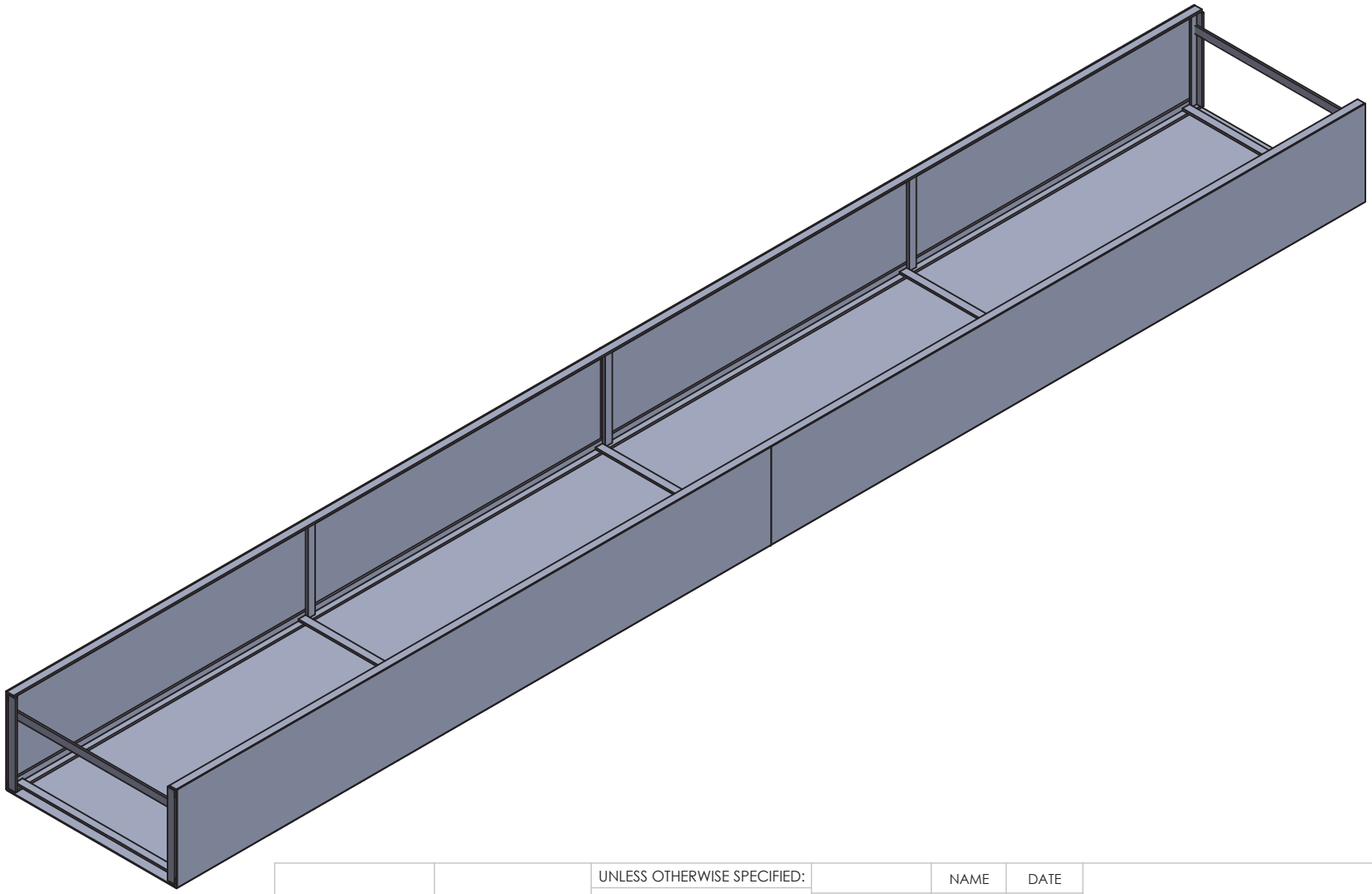

		UNLESS OTHERWISE SPECIFIED:		NAME	DATE
		DIMENSIONS ARE IN INCHES TOLERANCES: FRACTIONAL ± ANGULAR: MACH ± BEND ± TWO PLACE DECIMAL ± THREE PLACE DECIMAL ±	DRAWN		
			CHECKED		
			ENG APPR.		
			MFG APPR.		
		INTERPRET GEOMETRIC TOLERANCING PER:	Q.A.		
		MATERIAL	COMMENTS:		
NEXT ASSY	USED ON	FINISH			
APPLICATION		DO NOT SCALE DRAWING			

TITLE:

SIZE	DWG. NO.	REV
A	Bottom Piece	

SCALE: 1:48	WEIGHT:	SHEET 1 OF 1

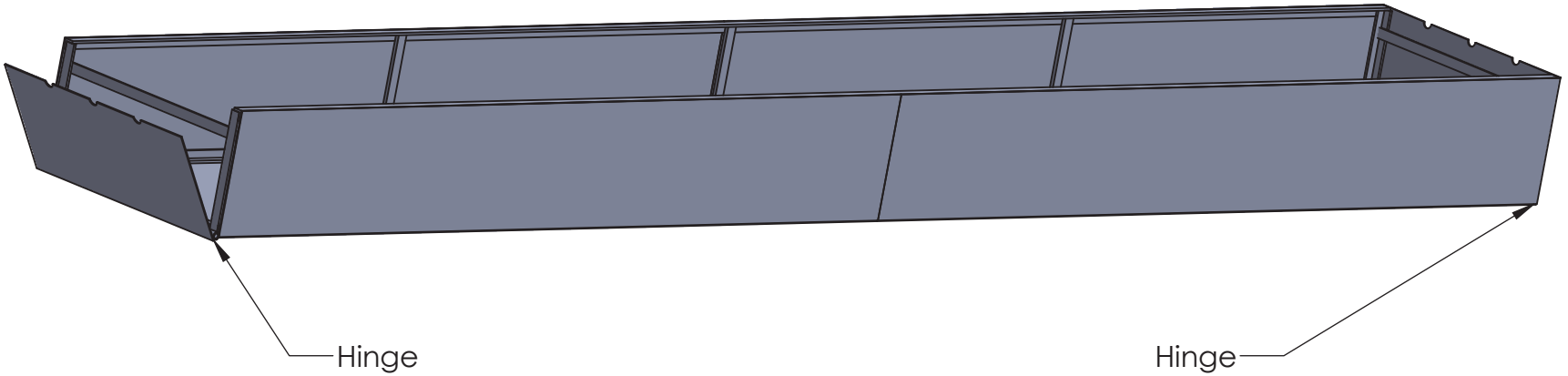

Front and back doors hinge down

		UNLESS OTHERWISE SPECIFIED:		NAME	DATE
		DIMENSIONS ARE IN INCHES TOLERANCES: FRACTIONAL ± ANGULAR: MACH ± BEND ± TWO PLACE DECIMAL ± THREE PLACE DECIMAL ±	DRAWN		
			CHECKED		
			ENG APPR.		
			MFG APPR.		
		INTERPRET GEOMETRIC TOLERANCING PER:	Q.A.		
		MATERIAL	COMMENTS:		
NEXT ASSY	USED ON	FINISH			
APPLICATION		DO NOT SCALE DRAWING			

TITLE:

SIZE	DWG. NO.	REV
A	BottomPiece	
SCALE: 1:48	WEIGHT:	SHEET 1 OF 1

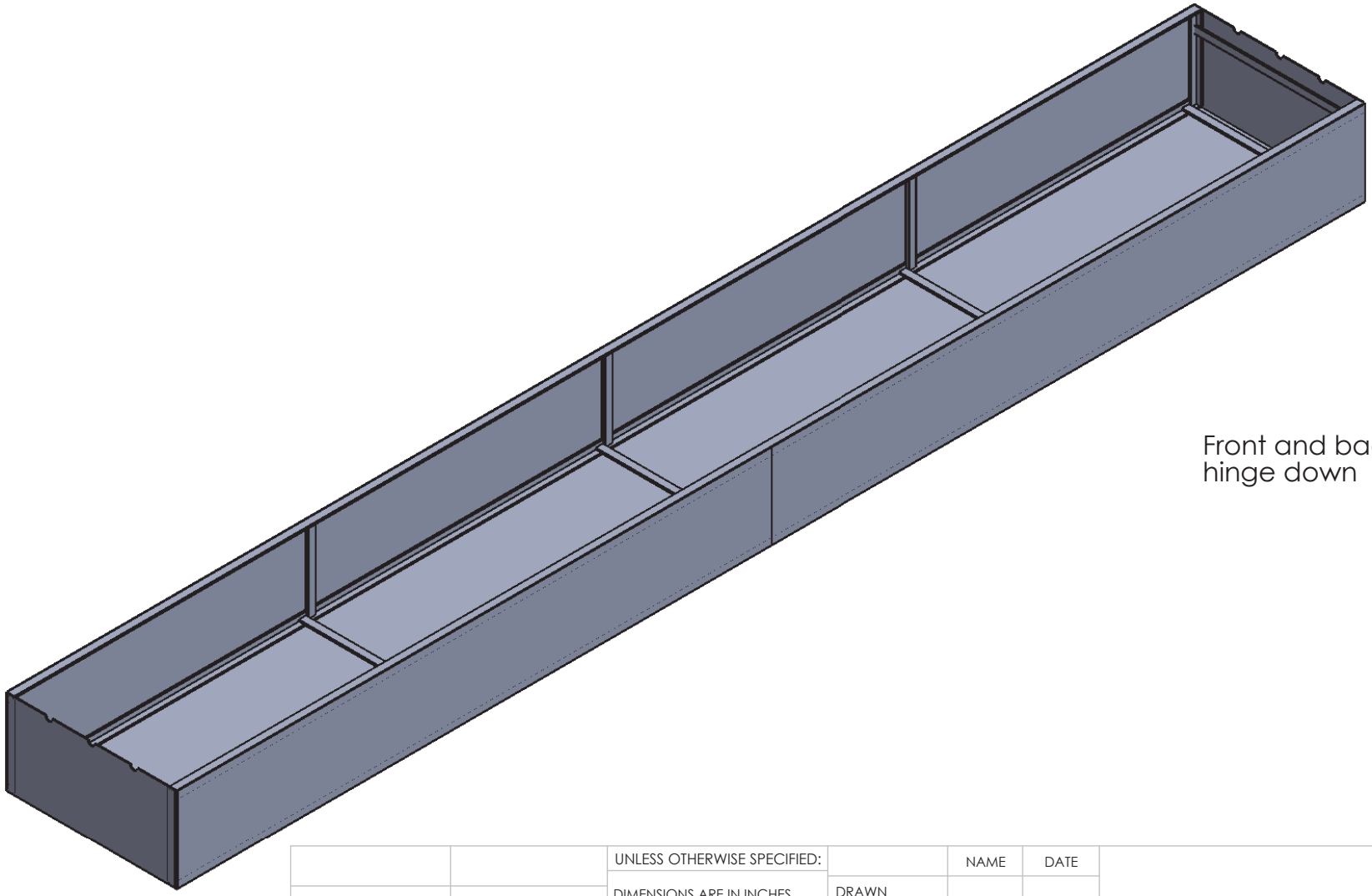

Front and back doors
hinge down

		UNLESS OTHERWISE SPECIFIED:		NAME	DATE
		DIMENSIONS ARE IN INCHES TOLERANCES: FRACTIONAL ± ANGULAR: MACH ± BEND ± TWO PLACE DECIMAL ± THREE PLACE DECIMAL ±	DRAWN		
			CHECKED		
			ENG APPR.		
			MFG APPR.		
		INTERPRET GEOMETRIC TOLERANCING PER:	Q.A.		
		MATERIAL	COMMENTS:		
NEXT ASSY	USED ON	FINISH			
APPLICATION		DO NOT SCALE DRAWING			

TITLE:

SIZE	DWG. NO.	REV
A	BottomPiece	

SCALE: 1:48	WEIGHT:	SHEET 1 OF 1

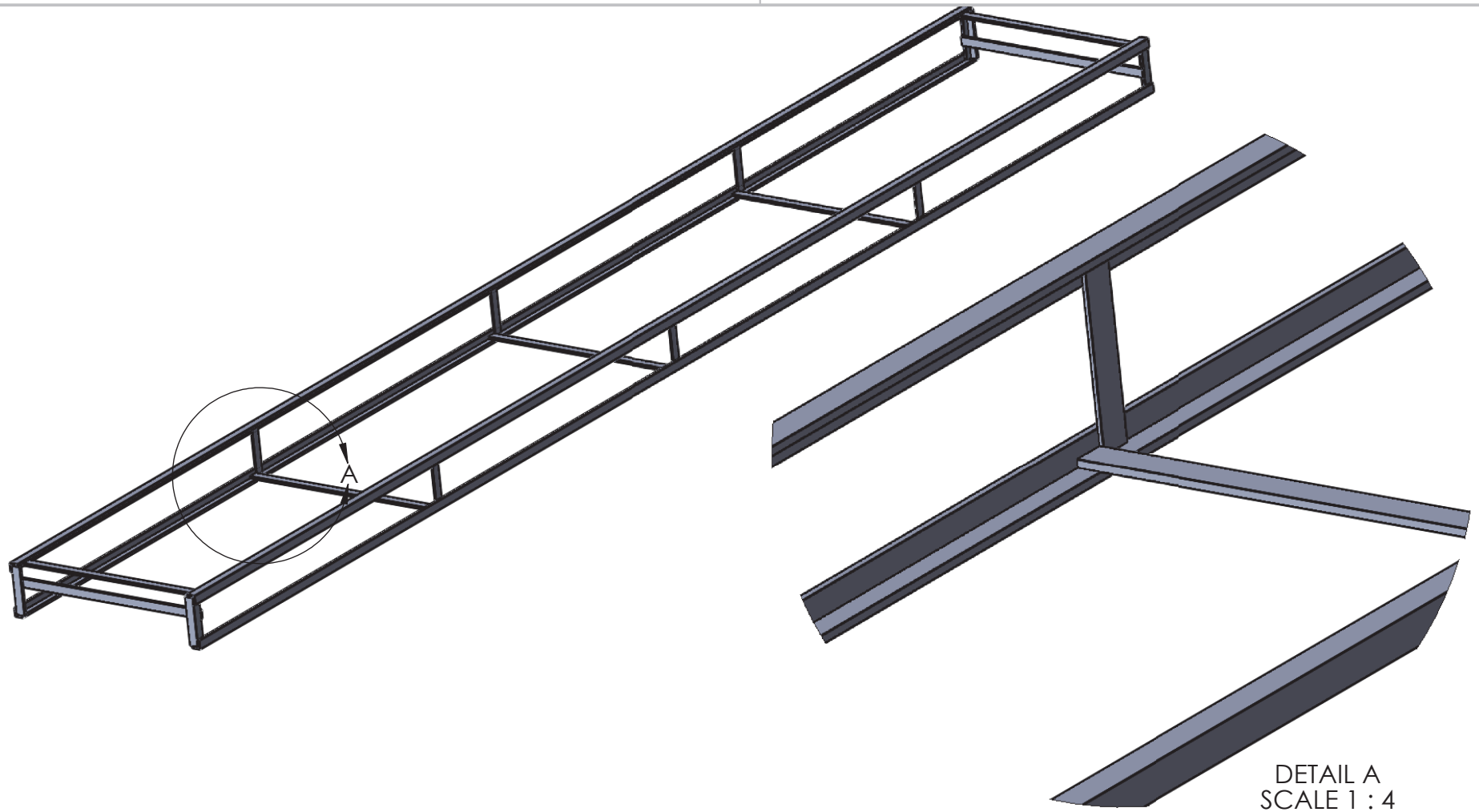

DETAIL A
SCALE 1 : 4

		UNLESS OTHERWISE SPECIFIED:		NAME	DATE
		DIMENSIONS ARE IN INCHES TOLERANCES: FRACTIONAL ± ANGULAR: MACH ± BEND ± TWO PLACE DECIMAL ± THREE PLACE DECIMAL ±	DRAWN		
			CHECKED		
			ENG APPR.		
			MFG APPR.		
		INTERPRET GEOMETRIC TOLERANCING PER:	Q.A.		
		MATERIAL	COMMENTS:		
NEXT ASSY	USED ON	FINISH			
APPLICATION		DO NOT SCALE DRAWING			

TITLE:

SIZE	DWG. NO.	REV
A	TopFrame	
SCALE: 1:48	WEIGHT:	SHEET 1 OF 1

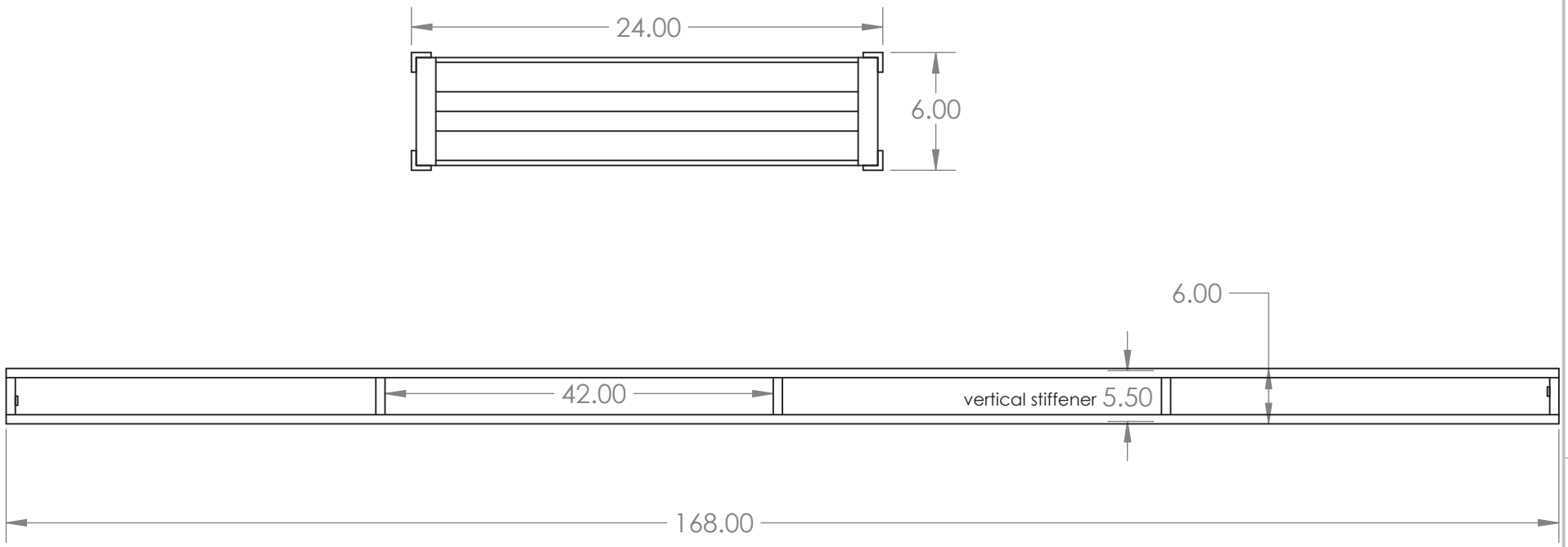

		UNLESS OTHERWISE SPECIFIED:		NAME	DATE
		DIMENSIONS ARE IN INCHES TOLERANCES: FRACTIONAL ± ANGULAR: MACH ± BEND ± TWO PLACE DECIMAL ± THREE PLACE DECIMAL ±	DRAWN		
			CHECKED		
			ENG APPR.		
			MFG APPR.		
		INTERPRET GEOMETRIC TOLERANCING PER:	Q.A.		
		MATERIAL	COMMENTS:		
NEXT ASSY	USED ON	FINISH			
APPLICATION		DO NOT SCALE DRAWING			

TITLE:

SIZE	DWG. NO.	REV
A	TopFrame	
SCALE: 1:48	WEIGHT:	SHEET 1 OF 1

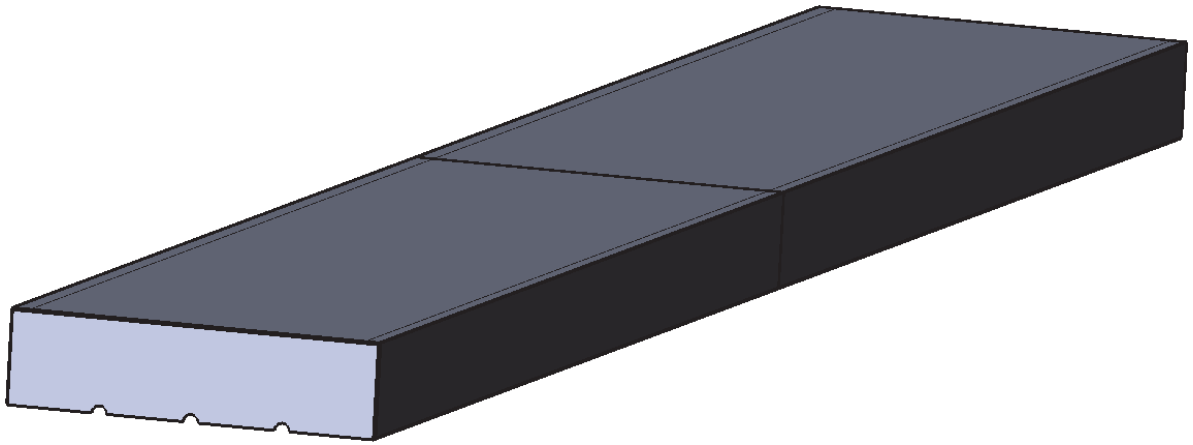

No hinges on top piece

		UNLESS OTHERWISE SPECIFIED:		NAME	DATE
		DIMENSIONS ARE IN INCHES TOLERANCES: FRACTIONAL ± ANGULAR: MACH ± BEND ± TWO PLACE DECIMAL ± THREE PLACE DECIMAL ±	DRAWN		
			CHECKED		
			ENG APPR.		
			MFG APPR.		
		INTERPRET GEOMETRIC TOLERANCING PER:	Q.A.		
		MATERIAL	COMMENTS:		
NEXT ASSY	USED ON	FINISH			
APPLICATION		DO NOT SCALE DRAWING			

TITLE:

SIZE	DWG. NO.	REV
A	TopPiece	
SCALE: 1:48	WEIGHT:	SHEET 1 OF 1

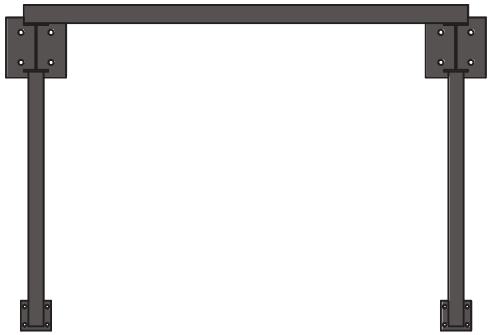

		UNLESS OTHERWISE SPECIFIED:		NAME	DATE
		DIMENSIONS ARE IN INCHES TOLERANCES: FRACTIONAL ± ANGULAR: MACH ± BEND ± TWO PLACE DECIMAL ± THREE PLACE DECIMAL ±	DRAWN		
			CHECKED		
			ENG APPR.		
			MFG APPR.		
		INTERPRET GEOMETRIC TOLERANCING PER:	Q.A.		
		MATERIAL	COMMENTS:		
NEXT ASSY	USED ON	FINISH			
APPLICATION		DO NOT SCALE DRAWING			

TITLE:

SIZE	DWG. NO.	REV
A	Framesystem	
SCALE: 1:32	WEIGHT:	SHEET 1 OF 1

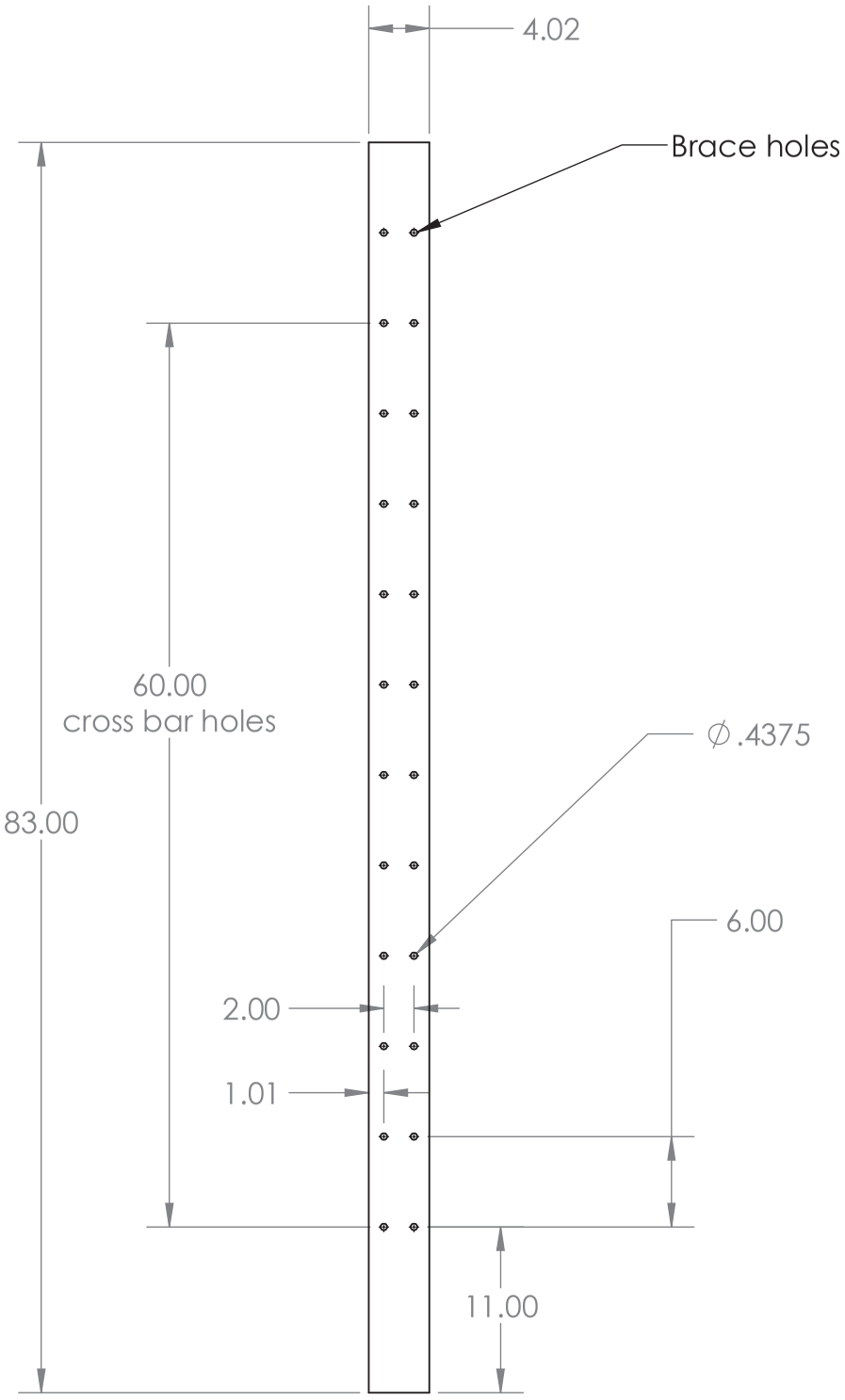

		DIMENSIONS ARE IN INCHES TOLERANCES: FRACTIONAL ± ANGULAR: MACH ± BEND ± TWO PLACE DECIMAL ± THREE PLACE DECIMAL ±		NAME	DATE
			DRAWN		
			CHECKED		
			ENG APPR.		
			MFG APPR.		
		MATERIAL	Q.A.		
			COMMENTS:		
NEXT ASSY	USED ON	FINISH			
APPLICATION		DO NOT SCALE DRAWING			

Upright, I-Beam

SIZE	DWG. NO.	REV.
A	Upright	
SCALE:1:16	WEIGHT:	SHEET 1 OF 1

CROSSBAR AND TOPBRACE

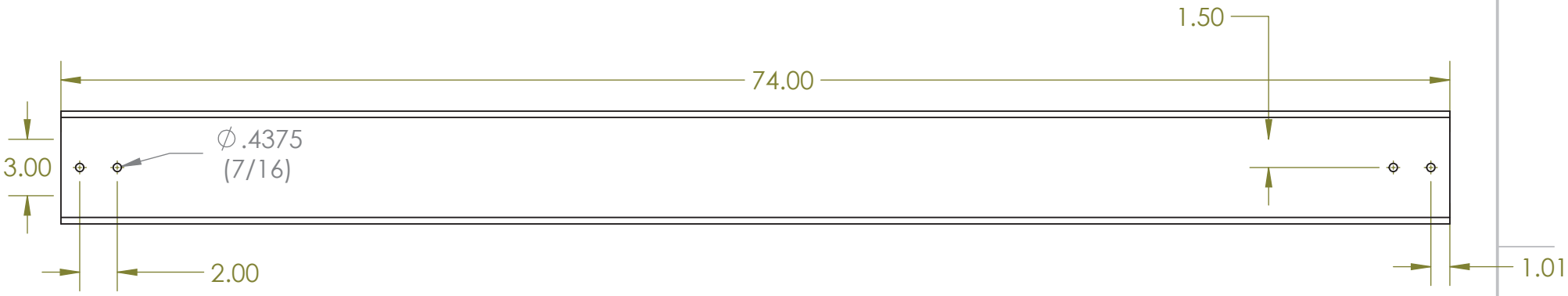

Machine gears span 60"
3" clearance on each side
4" to cover beam flanges
total length = 74"

		UNLESS OTHERWISE SPECIFIED:		NAME	DATE
		DIMENSIONS ARE IN INCHES TOLERANCES: FRACTIONAL ± ANGULAR: MACH ± BEND ± TWO PLACE DECIMAL ± THREE PLACE DECIMAL ±	DRAWN		
			CHECKED		
			ENG APPR.		
			MFG APPR.		
		INTERPRET GEOMETRIC TOLERANCING PER:	Q.A.		
		MATERIAL	COMMENTS:		
NEXT ASSY	USED ON	FINISH			
APPLICATION		DO NOT SCALE DRAWING			

TITLE:

SIZE	DWG. NO.	REV
A	crossbar	
SCALE: 1:16	WEIGHT:	SHEET 1 OF 1

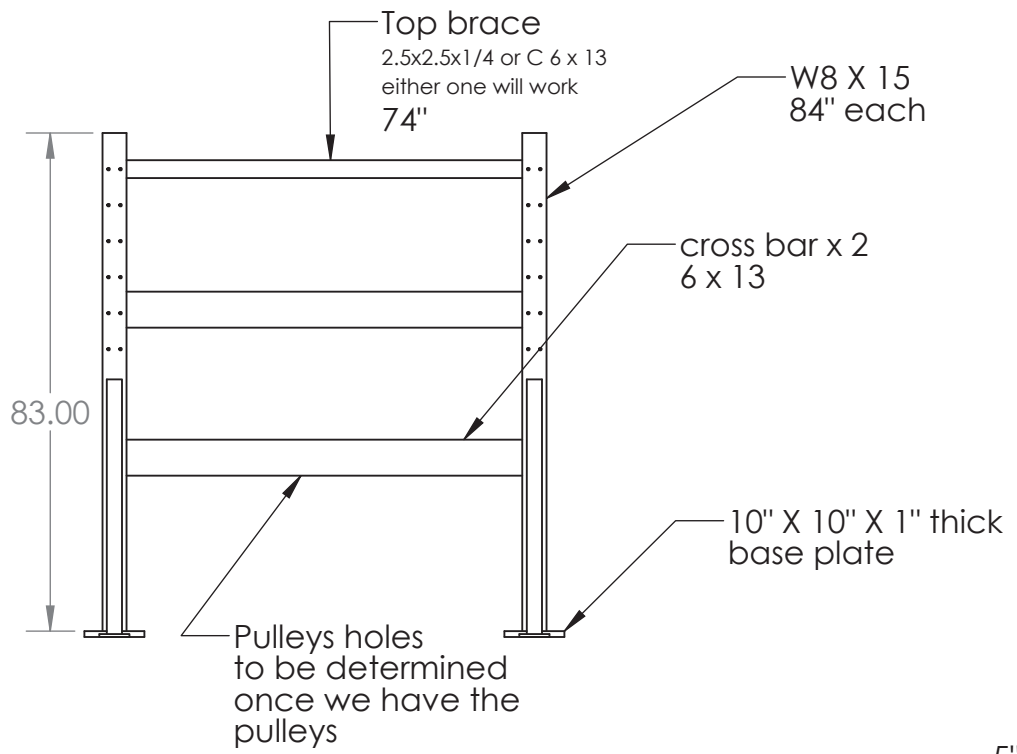

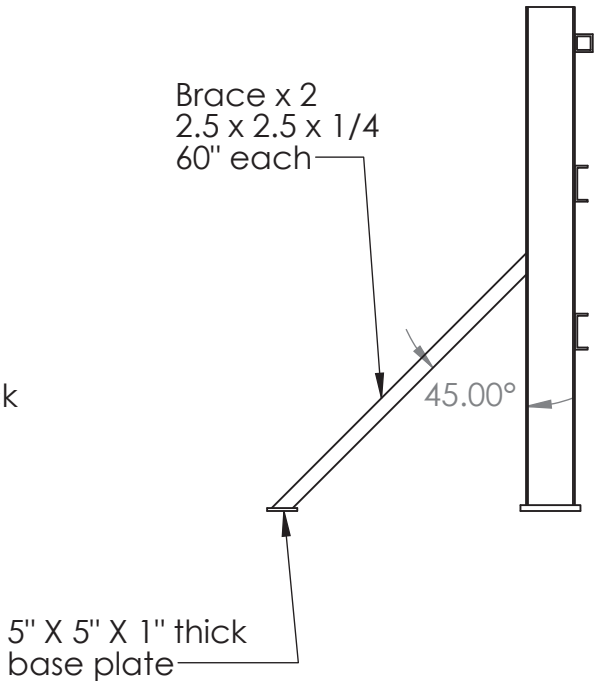

		UNLESS OTHERWISE SPECIFIED:		NAME	DATE
		DIMENSIONS ARE IN INCHES TOLERANCES: FRACTIONAL ± ANGULAR: MACH ± BEND ± TWO PLACE DECIMAL ± THREE PLACE DECIMAL ±	DRAWN		
			CHECKED		
			ENG APPR.		
			MFG APPR.		
		INTERPRET GEOMETRIC TOLERANCING PER:	Q.A.		
		MATERIAL	COMMENTS:		
NEXT ASSY	USED ON	FINISH			
APPLICATION		DO NOT SCALE DRAWING			

TITLE:

SIZE	DWG. NO.	REV
A	Framesystem	
SCALE: 1:32	WEIGHT:	SHEET 1 OF 1

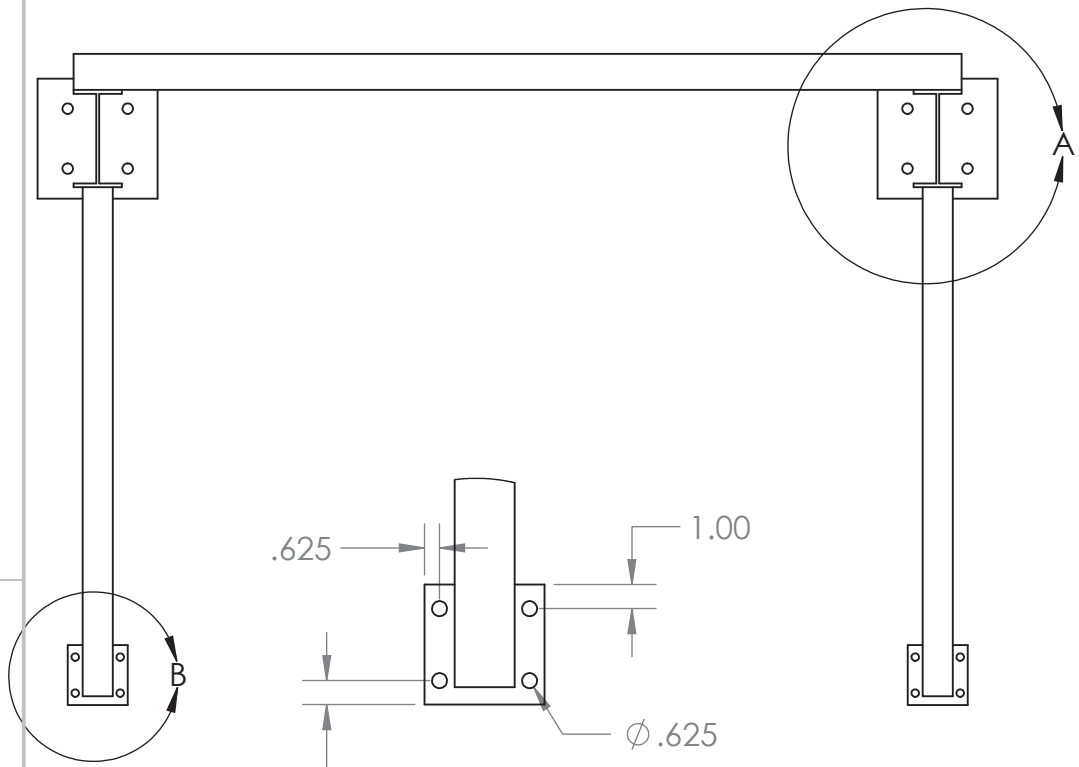

DETAIL B
SCALE 1 : 8

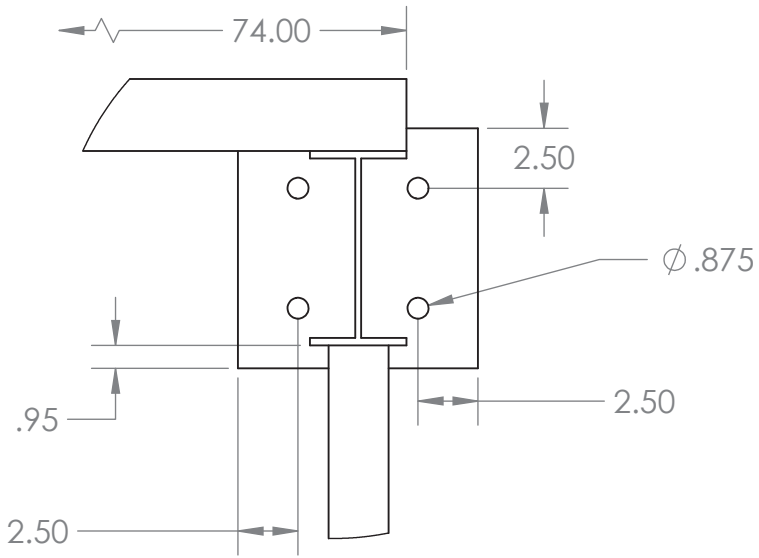

DETAIL A
SCALE 1 : 8

		UNLESS OTHERWISE SPECIFIED:		NAME	DATE
		DIMENSIONS ARE IN INCHES TOLERANCES: FRACTIONAL ± ANGULAR: MACH ± BEND ± TWO PLACE DECIMAL ± THREE PLACE DECIMAL ±	DRAWN		
			CHECKED		
			ENG APPR.		
			MFG APPR.		
		INTERPRET GEOMETRIC TOLERANCING PER:	Q.A.		
		MATERIAL	COMMENTS:		
NEXT ASSY	USED ON	FINISH			
APPLICATION		DO NOT SCALE DRAWING			

TITLE:

SIZE	DWG. NO.	REV
A4	Framesystem	
SCALE: 1:32	WEIGHT:	SHEET 1 OF 1

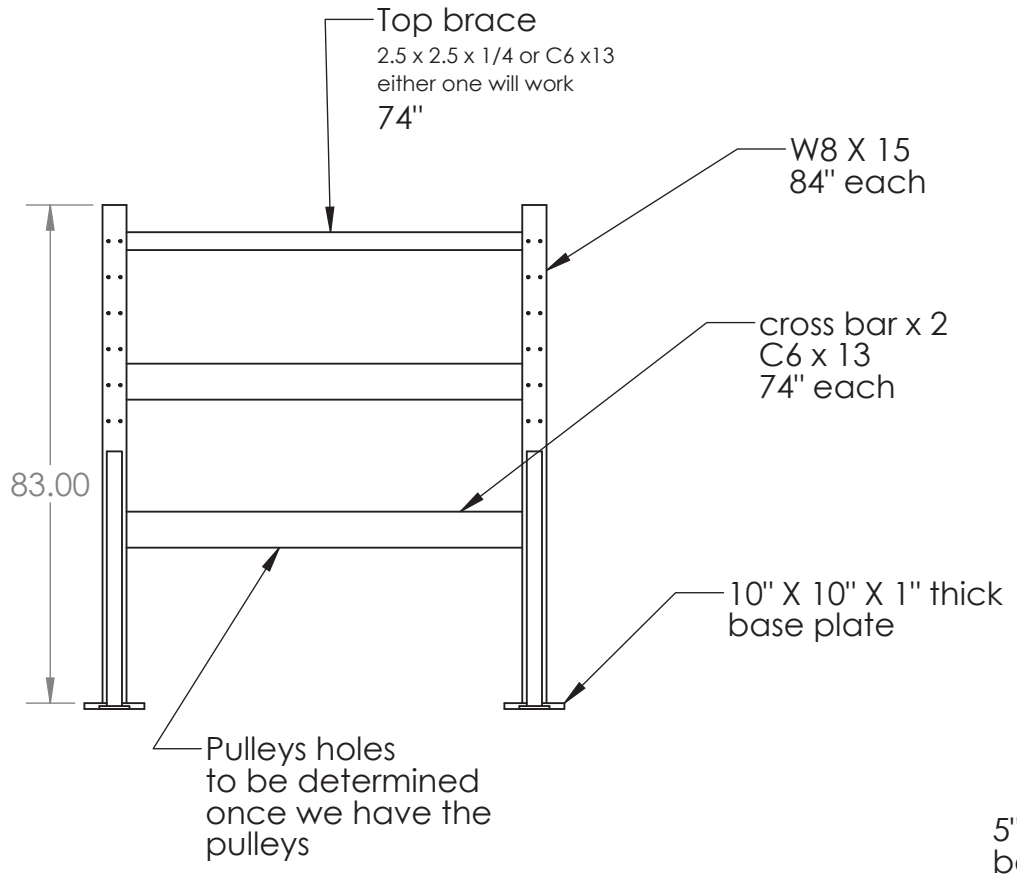

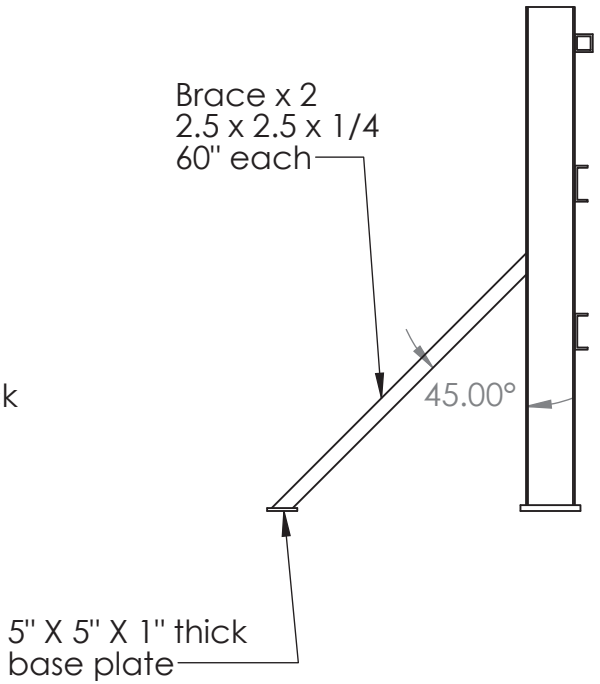

		UNLESS OTHERWISE SPECIFIED:		NAME	DATE
		DIMENSIONS ARE IN INCHES TOLERANCES: FRACTIONAL ± ANGULAR: MACH ± BEND ± TWO PLACE DECIMAL ± THREE PLACE DECIMAL ±	DRAWN		
			CHECKED		
			ENG APPR.		
			MFG APPR.		
		INTERPRET GEOMETRIC TOLERANCING PER:	Q.A.		
		MATERIAL	COMMENTS:		
NEXT ASSY	USED ON	FINISH			
APPLICATION		DO NOT SCALE DRAWING			

TITLE:

SIZE	DWG. NO.	REV
A	FrameSystem	
SCALE: 1:32	WEIGHT:	SHEET 1 OF 1